

Andrew Henry Cordes

**Optical Sources for High-Resolution Optical Coherence
Tomography**

Tese de Doutorado

Tese apresentada como requisito parcial para
obtenção do título de Doutor pelo Programa de
Pós-Graduação em Engenharia Elétrica da PUC-
Rio.

Orientador: Jean Pierre von der Weid

Rio de Janeiro
Janeiro de 2012



Andrew Henry Cordes

Optical Sources for High-Resolution Optical Coherence Tomography

Tese apresentada como requisito parcial para obtenção do título de Doutor pelo Programa de Pós-Graduação em Engenharia Elétrica da PUC-Rio. Aprovada pela Comissão Examinadora abaixo assinada.

Prof. Jean Pierre Von der Weid

Orientador

Centro de Estudos em Telecomunicações /PUC-Rio

Prof. Guilherme Barreto Xavier

CEFOP/UDEC – Chile

Prof. Rogério Passy

MLS-Wireless

Prof. Giancarlo Vilela de Faria

Centro de Estudos em Telecomunicações /PUC-Rio

Prof. Djeisson Hoffman Thomas

Centro de Estudos em Telecomunicações /PUC-Rio

Prof. Guilherme P. Temporão

Centro de Estudos em Telecomunicações /PUC-Rio

Prof. José Eugenio Leal

Coordenador Setorial do Centro

Técnico Científico - PUC-Rio

Rio de Janeiro, 27 de Janeiro de 2012

Todos os direitos reservados. É proibida a reprodução total ou parcial do trabalho sem autorização da universidade, do autor e do orientador.

Andrew Henry Cordes

Graduou-se em Engenharia Elétrica (Electrical and Computer Engineering), em 1984, na Universidade de Wisconsin em Madison. No mesmo ano, iniciou seu mestrado no mesmo lugar, o qual, concluiu em 1987 sob orientação do Prof. Bahaa Saleh. Trabalhou para Lawrence Livermore National Laboratory em Livermore, California por uns sete anos. Entrou New Focus em 1994 onde ficou até Julho de 2011 passando pelo Bookham, Oclaro e Newport. Em quanto disso, em 2005 mudou para o Brasil e iniciou o doutorado no Centro de Estudos em Telecomunicações da Pontifícia Universidade Católica do Rio de Janeiro.

Ficha Catalográfica

Cordes, Andrew Henry

Optical Sources for High-Resolution Optical Coherence Tomography/ Andrew Henry Cordes; orientador: Jean Pierre Von der Weid. – Rio de Janeiro PUC, Departamento de Engenharia Elétrica, 2012.

215 f. : Il. color. ; 30 cm

1. Tese (doutorado) – Pontifícia Universidade Católica do Rio de Janeiro, Departamento de Engenharia Elétrica, 2012.

Inclui referências bibliográficas

1. Engenharia Elétrica – Teses. 2. OCT. 3. SSOC. 4. Swept Source Optical Coherence Tomography. 5. Ultra-wideband. 6. Tunable laser. 7. OFDR. 8. Hilbert Transform. I. Weid, Jean Pierre von der II. Pontifícia Universidade Católica do Rio de Janeiro. Departamento de Engenharia Elétrica. III. Título.

CDD: 621.3

“Real knowledge is to know the extent of one's ignorance.”

Confúcio

Thanks mom.

Agradecimentos

To Prof. Jean Pierre, for inspiration, guidance, incentive and opportunity.

To Amalia and Monica and everyone in the lab - Gian, Djeisson, Janaina, Guilherme, Thiago, Temporao, Janaina, Guix and Douglas for companionship and help. Especially Gian, Djeisson and Amalia for all the help with Brazilian culture.

To everyone in CPTI and CETUC for all the friendship and all the beer.

To Patricia and Fernando and everyone of Andrew Coiffeur and Adam & Eve for all the unexpected and delightful.

In the USA to Rosie and Roberto who were steadfast in supporting me.

To my friends in the USA who gave me confidence that to get a PhD you don't need to leave your humanity nor your friendships behind.

To my sister Kathy and her family, Miles, Adair, Calvin and Elena for giving me the incentive to finish the PhD before someone else did first.

To my mother Gail who never wavered in support or confidence. And Duane for good advice and good cheer.

To Ormand who would have gotten his own PhD had not a son arrived on the scene.

To everyone at the Bar das Freiras, Fast Way, Coviflor, the Padaria and Casa de Empada where I spent so much time these last few years.

To Eduardo and his father and the Chinese Restaurant on Copacabana beach where I studied every night for years.

To all the professors and employees of CETUC and PUC-Rio for all the support, technical and academic.

To VRAC PUC-Rio for financial support.

Resumo

Cordes, Andrew Henry; Weid, Jean Pierre von der. **Fontes ópticas para tomografia de coerência óptica de alta resolução**. Rio de Janeiro, 2012. 215p. Tese de Doutorado - Departamento de Engenharia Elétrica, Pontifícia Universidade Católica do Rio de Janeiro.

Foram desenvolvidas fontes ópticas para obtenção de imagens por tomografia de coerência óptica com alta resolução. Dois tipos de abordagens foram realizados, uma com um laser contínuo sintonizável, que neste trabalho foi instrumentado com marcadores de frequência óptica, outra com uma fonte óptica pulsada de banda larga. Mediante um processo de calibração desenvolvido neste trabalho, a fonte contínua forneceu resoluções de 8 μm e alcances até 0,5 mm, enquanto que a fonte pulsada forneceu resoluções de 3 μm e alcances de 300 μm . A fonte pulsada permitiu ainda a obtenção de imagens em tempo real com capacidade de captura de movimento do objeto.

Palavras-chave

OC; SSOC; Swept Source Optical Coherence Tomography; Ultra-wideband; Tunable laser; OFDR; Hilbert Transform.

Abstract

Cordes, Andrew Henry; Weid, Jean Pierre von der. **Optical Sources for High-Resolution Optical Coherence Tomography**. Rio de Janeiro, 2012. 215p. Doctoral Thesis - Departamento de Engenharia Elétrica, Pontifícia Universidade Católica do Rio de Janeiro.

Optical sources to obtain images through high resolution optical coherence tomography were developed. Two approaches were taken, one with a continuously tunable external cavity laser which, in this work, was modified to produce optical frequency markers, the other with an ultra-wideband pulsed source. Using a calibration process we developed in this work the continuously tunable source continued to achieve resolutions 8 μm and ranges of 0.5 mm, while the pulsed source achieved resolutions of 3.3 μm and ranges of 300 μm .

The pulsed source has the capacity to capture real time images.

Keywords

OCT; SSOCT; Swept Source Optical Coherence Tomography; Ultra-wideband; Tunable laser; OFDR; Hilbert Transform.

Sumário

1 Introduction	30
1.1. Typical specs	35
2 Swept Source OCT	37
2.1. Incoherent beginnings	37
2.2. Coherent approach	37
2.3. Basic setup	38
3 Fourier Details	41
3.1. Non-integer number of cycles	41
3.2. Zero padding	50
3.3. Non-integer number of samples with zero padding	57
3.4. Windowing	66
3.5. Initial Phase	86
3.5.1. Derivation of initial phase	87
3.5.2. Apply the initial phase	97
3.5.3. Initial phase conclusions	103
4 Non-linear sweeps	105
4.1. Examples of non-linear sweeps	105
4.1.1. Example - Constant sweep rate (linear sweep)	105
4.1.2. Example - Square wave variation in sweep rate	106
4.1.3. Example – Triangle wave variation in sweep rate	108
4.1.4. Example – Sinusoidal wave variation in sweep rate	110
4.1.5. Example – 1000nm/s, a real world variation in sweep rate	111
4.2. Compensating for non-linear sweeps	116
4.3. Constant Optical Frequency Sampling	121
4.4. Optical Frequency Sampling	130
4.5. Distance scale	136
4.5.1. Perfect Standard	136
4.5.2. Differential Standard	137

4.5.3. Perfectly Known Sweep Rate	139
4.5.4. Perfectly Known Optical Frequency Extent	140
4.6. Distance Limitations	142
4.6.1. Bandwidth	142
4.6.2. Sampling rate	142
4.6.2.1. Reducing the number of samples to induce aliasing	143
4.6.2.2. Effects of aliasing on an A-line	148
4.6.3. Coherence length	150
4.7. Topologies	151
4.7.1. Laser provides optical frequency triggers	152
4.7.2. Optical frequency triggers derived from output of laser	152
4.7.3. Optical data resampled using sample numbers recalculated each sweep	154
4.7.4. Optical data resampled using sample numbers calculated once and reused	155
 5 Working systems	 158
5.1. New Focus Laser	158
5.2. Stretched Pulse Santec Laser	171
5.2.1. Components	171
5.2.2. Time and Spectrum	174
5.2.2.1. Output of the laser	175
5.2.2.2. After the dispersive fiber	177
5.2.2.3. After Filter 1	178
5.2.2.4. After Filter 2	179
5.2.2.5. At Reference / Measurement plane	180
5.2.2.6. At the detector	181
5.2.3. Calibration	183
5.2.3.1. Calibration of sweep	184
5.2.3.2. Applying the sweep calibration	189
5.2.3.3. Calibrating the distance scale	193
5.2.3.4. Application of distance calibration	194
5.2.4. Resolution	195
5.2.5. Handywrap scans	197

5.3. Comparison of the two systems	202
6 Model	205
7 Conclusion	209
7.1. Interesting things.	209
7.2. In the future	210
8 Referências bibliográficas	212

Lista de figuras

Figure 1.1 – Light traveling through air (yellow) incident on a sample made from two materials (blue and red) with different indices of refraction.	30
Figure 1.2 – As the light reaches the blue material some reflects from the air – blue material boundary or interface.	30
Figure 1.3 – As the light reaches the red material some reflects from the blue material – red material interface.	31
Figure 1.4 – As the light leaves the red material some reflects from the red material – blue material interface.	31
Figure 1.5 – Finally, as the light leaves the sample, some reflects from the blue material – air interface.	31
Figure 1.6 – OCT is able to discern how much reflected light comes from each interface and at what distance along the axis of the light the reflection occurred. The one dimensional plot of this information is called an A-scan or A-line.....	31
Figure 1.7 – A-scan of Handywrap. An A-scan is a simply XY plot. X locates the interface while Y indicates the amount of light received from that interface.	32
Figure 1.8 – B-line of Handywrap. Constructed of 200 A-lines separated by 10um laterally. A B-line is a 3D image where X and Y locate the interface and Z indicates the light received from that interface.	32
Figure 1.9 – C-line of Handywrap. Constructed of 200 B-lines separated by 10um laterally. A C-scan is a volume. X, Y and Z locate the interface. The amount of light received from the interface is indicated by varying color or intensity or opacity.	33
Figure 1.10 – Zeiss OCT machine for the imaging of retinal tissues at the back of the eye. A),B) show B-scan and C-scan images of the retinal tissue. C) shows the front door access OCT has to the retinal tissues. D) shows the machine itself with patient and diagnostic information on the machine. (1)(Liu, Y.-Y. et al. (2011))	34
Figure 1.11 – A) Eyeball and B),C) OCT B-scan images taken through the eyeball of the retinal tissues at the back of the eye. B) shows healthy tissue while C) shows diseased tissue. (2)(Harding; Yalin (2009))	34
Figure 2.1 – Interferometer portion of SSOCT showing the optical paths to and from the reference and from an interface at distance d within the sample.	38

Figure 2.2 – Sweep rate as a function of time. In this simple example the sweep speed is assumed to remain constant during the entire 100ms of sweep.....	39
Figure 2.3 – The detector sees a sinewave at the difference frequency between the optical frequency reflected by the reference and that reflected by the interface at distance d into the sample.....	39
Figure 2.4 – FFT of the sinewave seen by the detector.....	40
Figure 2.5 – The frequency scale of the FFT has been rescaled to distance using knowledge of the scan speed and the index of refraction of the sample. $d = f c / (2 n \text{ SweepRate})$	40
Figure 3.1 – Integer number of cycles. Time domain.	41
Figure 3.2 – Integer number of cycles. FFT is a single point.....	41
Figure 3.3 – Non-integer. 1/12 of a cycle extra. Time domain.	42
Figure 3.4 – Non-integer. 1/12 of a cycle extra. FFT.....	42
Figure 3.5 – Non-integer. 2/12 of a cycle extra. Time domain.	42
Figure 3.6 – Non-integer. 2/12 of a cycle extra. FFT starts to walk away from the initial bin.....	43
Figure 3.7 – Non-integer. 3/12 of a cycle extra. Time domain.	43
Figure 3.8 – Non-integer. 3/12 of a cycle extra. FFT.....	43
Figure 3.9 – Non-integer. 4/12 of a cycle extra. Time domain.	44
Figure 3.10 – Non-integer. 4/12 of a cycle extra. FFT.....	44
Figure 3.11 – Non-integer. 5/12 of a cycle extra. Time domain.	44
Figure 3.12 – Non-integer. 5/12 of a cycle extra. FFT.....	45
Figure 3.13 – Non-integer. 6/12 of a cycle extra. Time domain.	45
Figure 3.14 – Non-integer. 6/12 of a cycle extra. FFT.....	45
Figure 3.15 – Non-integer. 7/12 of a cycle extra. Time domain.	46
Figure 3.16 – Non-integer. 7/12 of a cycle extra. FFT.....	46
Figure 3.17 – Non-integer. 8/12 of a cycle extra. Time domain.	46
Figure 3.18 – Non-integer. 8/12 of a cycle extra. FFT.....	47
Figure 3.19 – Non-integer. 9/12 of a cycle extra. Time domain.	47
Figure 3.20 – Non-integer. 9/12 of a cycle extra. FFT.....	47
Figure 3.21 – Non-integer. 10/12 of a cycle extra. Time domain.	48
Figure 3.22 – Non-integer. 10/12 of a cycle extra. FFT.....	48
Figure 3.23 – Non-integer. 11/12 of a cycle extra. Time domain.	48
Figure 3.24 – Non-integer. 11/12 of a cycle extra. FFT.....	49

Figure 3.25 – Integer. One full cycle extra. Time domain.	49
Figure 3.26 – Integer. One full cycle extra. The FFT once again is a single point.	49
Figure 3.27 – No zero padding. Time domain.....	50
Figure 3.28 – No-zero padding. FFT.....	51
Figure 3.29 – Zero-padding to 2x. Time domain.	51
Figure 3.30 – Zero-padding to 2x. FFT.....	51
Figure 3.31 – Zero-padding to 3x. Time domain.	52
Figure 3.32 – Zero-padding to 3x. FFT.....	52
Figure 3.33 – Zero-padding to 4x. Time domain.	52
Figure 3.34 – Zero-padding to 4x. FFT.....	53
Figure 3.35 – Zero-padding to 5x. Time domain.	53
Figure 3.36 – Zero-padding to 5x. FFT.....	53
Figure 3.37 – Zero-padding to 6x. Time domain.	54
Figure 3.38 – Zero-padding to 6x. FFT.....	54
Figure 3.39 – Zero-padding to 7x. Time domain.	54
Figure 3.40 – Zero-padding to 7x. FFT.....	55
Figure 3.41 – Zero-padding to 8x. Time domain.	55
Figure 3.42 – Zero-padding to 8x. FFT.....	55
Figure 3.43 – Zero-padding to 9x. Time domain.	56
Figure 3.44 – Zero-padding to 9x. FFT.....	56
Figure 3.45 – Zero-padding to 10x. Time domain.	56
Figure 3.46 – Zero-padding to 10x. FFT.....	57
Figure 3.47 – Integer number of cycles with zero-padding. Time domain.	57
Figure 3.48 – Integer number of cycles with zero-padding. FFT.....	58
Figure 3.49 – Non-integer. 1/12 of a cycle extra with zero-padding. Time domain.	58
Figure 3.50 – Non-integer. 1/12 of a cycle extra with zero-padding. FFT.....	58
Figure 3.51 – Non-integer. 2/12 of a cycle extra. Zero padding. Time domain.	59
Figure 3.52 – Non-integer. 2/12 of a cycle extra. Zero-padding. FFT.	59
Figure 3.53 – Non-integer. 3/12 of a cycle extra. Zero-padding. Time domain.	59
Figure 3.54 – Non-integer. 3/12 of a cycle extra. Zero-padding. FFT.	60
Figure 3.55 – Non-integer. 4/12 of a cycle extra. Zero-padding. Time domain.	60
Figure 3.56 – Non-integer. 4/12 of a cycle extra. Zero-padding. FFT.	60

Figure 3.57 – Non-integer. 5/12 of a cycle extra. Zero-padding. Time domain.	61
Figure 3.58 – Non-integer. 5/12 of a cycle extra. Zero-padding. FFT.	61
Figure 3.59 – Non-integer. 6/12 of a cycle extra. Zero-padding. Time domain.	61
Figure 3.60 – Non-integer. 6/12 of a cycle extra. Zero-padding. FFT.	62
Figure 3.61 – Non-integer. 7/12 of a cycle extra. Zero-padding. Time domain.	62
Figure 3.62 – Non-integer. 7/12 of a cycle extra. Zero-padding. FFT.	62
Figure 3.63 – Non-integer. 8/12 of a cycle extra. Zero-padding. Time domain.	63
Figure 3.64 – Non-integer. 8/12 of a cycle extra. Zero-padding. FFT.	63
Figure 3.65 – Non-integer. 9/12 of a cycle extra. Zero-padding. Time domain.	63
Figure 3.66 – Non-integer. 9/12 of a cycle extra. Zero-padding. FFT.	64
Figure 3.67 – Non-integer. 10/12 of a cycle extra. Zero-padding. Time domain.	64
Figure 3.68 – Non-integer. 10/12 of a cycle extra. Zero-padding. FFT.	64
Figure 3.69 – Non-integer. 11/12 of a cycle extra. Zero-padding. Time domain.	65
Figure 3.70 – Non-integer. 11/12 of a cycle extra. Zero-padding. FFT.	65
Figure 3.71 – Integer number of cycles with zero padding. One complete cycle more than in Figure 3.47. Time domain.	65
Figure 3.72 – Integer number of cycles with zero padding. One complete cycle more than in Figure 3.48. FFT.	66
Figure 3.73 – Window: Rectangular. A) Time domain, B) FFT linear scale, C) FFT log scale	67
Figure 3.74 – Window: Hanning. A) Time domain, B) FFT linear scale, C) FFT log scale	68
Figure 3.75 – Window: Hamming. A) Time domain, B) FFT linear scale, C) FFT log scale	69
Figure 3.76 – Window: Blackman-Harris. A) Time domain, B) FFT linear scale, C) FFT log scale	70
Figure 3.77 – Window: Exact Blackman. A) Time domain, B) FFT linear scale, C) FFT log scale	71
Figure 3.78 – Window: Blackman. A) Time domain, B) FFT linear scale, C) FFT log scale	72
Figure 3.79 – Window: Flat top. A) Time domain, B) FFT linear scale, C1 and C2) FFT log scale	73

Figure 3.80 – Window: 4-term Blackman-Harris. A) Time domain, B) FFT linear scale, C1 and C2) FFT log scale.....	74
Figure 3.81 – Window: 7-term Blackman-Harris. A) Time domain, B) FFT linear scale, C1 and C2) FFT log scale.....	75
Figure 3.82 – Window: Low Sidelobe. A) Time domain, B) FFT linear scale, C1 and C2) FFT log scale	76
Figure 3.83 – Window: Blackman Nuttall. A) Time domain, B) FFT linear scale, C1 and C2) FFT log scale.....	77
Figure 3.84 – Window: Triangle. A) Time domain, B) FFT linear scale, C) FFT log scale	78
Figure 3.85 – Window: Bartlett-Hanning. A) Time domain, B) FFT linear scale, C) FFT log scale	79
Figure 3.86 – Window: Bohman. A) Time domain, B) FFT linear scale, C1 and C2) FFT log scale	80
Figure 3.87 – Parzen. A) Time domain, B) FFT linear scale, C1 and C2) FFT log scale	81
Figure 3.88 – Window: Welch. A) Time domain, B) FFT linear scale, C) FFT log scale	82
Figure 3.89 – Window: Kaiser (Beta = 0.0). A) Time domain, B) FFT linear scale, C) FFT log scale	83
Figure 3.90 – Window: Dolph-Chebyshev. A) Time domain, B) FFT linear scale, C) FFT log scale	84
Figure 3.91 – Window: Gaussian. A) Time domain, B) FFT linear scale, C) FFT log scale.....	85
Figure 3.92 – FFT of SSOCT signals from two surfaces relatively far apart as the initial phases of each signal independently run through 360 degrees. The dots show the location of the peaks of the FFT's while the red vertical lines show the actual surface location. There is very little difference when the surfaces are far apart.	86
Figure 3.93 – FFT of SSOCT signals from two surfaces near to one another as the initial phases of each signal are independently run through 360 degrees. The dots show the location of the peaks while the red vertical bars show the actual location of the two surfaces. At close distances, depending on the initial phases, the results can vary and sometimes be misleading.	87

Figure 3.94 – Initial considerations of initial phase derivation	87
Figure 3.95 – Optical waveform travels from left to right.	88
Figure 3.96 – Optical frequency of the waveform at the moment of impacting the reference plane is defined as $\nu(0)$. The phase which it arrives with is termed ϕ_0 . ..	88
Figure 3.97 – During the roundtrip to the internal plane and back to the reference plane the optical frequency $\nu(0)$ accumulates phase of $\tau_{\text{inho}} * \nu(0)$	89
Figure 3.98 – The optical frequency incident at the reference plane has changed from $\nu(0)$ to $\nu(\tau_{\text{inho}})$ during the time τ_{inho}	89
Figure 3.99 – Accumulated phase is the integral of the optical frequency over the time period τ_{inho}	90
Figure 3.100 – The accumulated phase of the incident waveform is the area under $\nu(t)$ from 0 to τ_{inho}	90
Figure 3.101 – We can approximate $\nu(t)$ as a straight line from 0 to τ_{inho} if $\nu(t)$ is sufficiently smooth and/or τ_{inho} is very small.	90
Figure 3.102 – The accumulated phase is the area under this new curve.....	91
Figure 3.103 – The accumulated phase of the incident waveform, ϕ_{inho2} , can be calculated from the trapazoidal rule.	91
Figure 3.104 – The frequency and the accumulated phase of the two reflected waveforms at the reference plane.	92
Figure 3.105 – The two waveforms will travel together to the detector. The time required to get to the detector from the reference plane is called τ_{ao}	92
Figure 3.106 – Each waveform accumulates phase depending on its optical frequency.	93
Figure 3.107 – The total accumulated phase for each waveform.	94
Figure 3.108 – Some terms drop out and others can be grouped to simplify the equation for ϕ_{initial}	95
Figure 3.109 – Terms that can be grouped again.	95
Figure 3.110 – Difference in optical frequency term that can be estimated by the sweep rate * τ_{inho}	96
Figure 3.111 – Recap of elements contributing to the initial phase.	96
Figure 3.112 – Beat frequency and initial phase showing the contributors to the initial phase; the sweep rate, the size of the interferometer and the patch cord length.	96
Figure 3.113 – Not much variation with initial phase for interfaces far apart.....	97

Figure 3.114 – A lot of variation with initial phase for interfaces close together.	97
Figure 3.115 – Perceived and actual separations of two interfaces far apart.	98
Figure 3.116 – The perceived separation can be much different than the actual separation for interfaces close together.	98
Figure 3.117 – Separation trail showing the data points for the close together and far apart interfaces.	99
Figure 3.118 – Laser specs used.....	99
Figure 3.119 – 124.9Thz/s sweep rate, no patch cord and Blackman-Harris window. The tail of the FFT of the Blackman-Harris window is known to be low so the very good agreement of Apparent to Actual distances is not a surprise at large separations. However the initial phase affects are clear at small separations under 28um.....	100
Figure 3.120 – 124.9 Thz/s sweep rate, no patch cord and Rectangular window. While the affects of the long tails of the FFT of the rectangular window can be seen in a ripple in the separation trail, the peaks come together into one at small separation like you intuitively think it should.	100
Figure 3.121 – 400m patchcord. No different from 0m patchcord. Blackman-Harris.	101
Figure 3.122 – 400m patchcord. No different from 0m patchcord. Rectangular.	101
Figure 3.123 – 287M Thz/s. No patch cord. Blackman-Harris window. Resembles the data for the slower laser.....	102
Figure 3.124 - 287M Thz/s. No patch cord. Rectangular window. Resembles the data for the slower laser.....	102
Figure 3.125 – 287M Thz/s. 400m patch cord. Blackman-Harris window. Note the multiple oscillations.....	103
Figure 3.126 – 287M Thz/s. 400m patch cord. Rectangular window. Multiple oscillations even for the rectangular window.	103
Figure 4.1 – Constant sweep rate. A linear sweep has a constant sweep rate. ...	105
Figure 4.2 – The beat signal from a single reflector and a reference. Constant sweep rate. Beat signal from a constant sweep rate applied to a single reflection is a perfect sinewave.	106

Figure 4.3 – The FFT after windowing and zero-padding. The FFT of the beat signal has a single peak showing the location of the single reflector relative to the reference.	106
Figure 4.4 – Square wave variation in the sweep rate. Sweep rate varies from 75% slower to 75% faster than the constant sweep rate in Figure 4.1 on page 106.	107
Figure 4.5 – The beat signal from a single reflector and a reference. Square wave variation in the sweep rate. The frequency of the beat signal follows the sweep rate.	107
Figure 4.6 – The FFT after windowing and zero-padding. The FFT of the beat signal has multiple peaks resulting from the square wave variation in sweep rate. The multiple peaks obscure the location of the single reflector relative to the reference.	108
Figure 4.7 – Triangle wave variation in the sweep rate. Sweep rate varies from 75% slower to 75% faster than the constant sweep rate in Figure 4.1 on page 106.	108
Figure 4.8 – The beat signal from a single reflector and a reference. Triangle wave variation in the sweep rate. The frequency of the beat signal follows the sweep rate.	109
Figure 4.9 – The FFT after windowing and zero-padding. The FFT of the beat signal has multiple peaks resulting from the triangle wave variation in sweep rate. The multiple peaks obscure the location of the single reflector relative to the reference.	109
Figure 4.10 – Sinusoidal wave variation in the sweep rate. Sweep rate varies from 75% slower to 75% faster than the constant sweep rate in Figure 4.1 on page 106.	110
Figure 4.11 – The beat signal from a single reflector and a reference. Sinusoidal wave variation in the sweep rate. The frequency of the beat signal follows the sweep rate.	110
Figure 4.12 – The FFT after windowing and zero-padding. The FFT of the beat signal has multiple peaks resulting from the sinusoidal wave variation in sweep rate. The multiple peaks obscure the location of the single reflector relative to the reference.	111

Figure 4.13 – Optical frequency sweep rate while sweeping at a constant wavelength sweep rate. Average value is the constant sweep rate in Figure 4.1 on page 106.....	112
Figure 4.14 - The beat signal from a single reflector and a reference. Constant wavelength sweep rate.....	112
Figure 4.15 - The FFT after windowing and zero-padding. The FFT of the beat signal has only a single peak and appears very similar to the result from the constant sweep rate shown in Figure 4.3 on page 107.	113
Figure 4.16 - FFT peaks as the measured interface is moved from 48um to 9mm. The sweep rate is a constant nm/s (wavelength rate) which produces a non-constant optical frequency sweep rate. The width of the peak widens and the amplitude shrinks with relative distance from the reference.....	114
Figure 4.17 - Excess spreading in A-line peaks as the measured interface is moved from 48um to 9mm. The sweep rate is a constant nm/s (wavelength rate) which produces a non-constant optical frequency sweep rate.	114
Figure 4.18 – Excess amplitude loss in A-line peaks as the measured interface is moved from 48um to 9mm. The sweep rate is a constant nm/s (wavelength rate) which produces a non-constant optical frequency sweep rate.....	115
Figure 4.19 – A-lines of interfaces at distances from 48um to 9mm. The sweep rate was a constant optical frequency rate. There will be no excess spreading or loss of amplitude.....	115
Figure 4.20 – SSOCT interferometer	116
Figure 4.21 – Idealized A-line.....	116
Figure 4.22 – Best A-line possible.	117
Figure 4.23 – Beat signal required to obtain the best possible A-line.....	117
Figure 4.24 – Beat signal from a non-linear sweep. Specifically the sweep rate with square wave variation.....	117
Figure 4.25 – Idealized beat signal had four cycles	118
Figure 4.26 – Beat signal from highly non-linear sweep also has four cycles....	118
Figure 4.27 – The number of samples in each cycle is constant when the laser is swept at a constant sweep rate.....	119
Figure 4.28 – The number of samples in each cycle varies depending on the sweep rate if the sweep rate is not constant.....	119

Figure 4.29 – Sampling the cycles using the same number of samples per cycle.	120
Figure 4.30 – Plotting the same data versus sample number rather than time. ...	120
Figure 4.31 – Windowing, zero-padding and FFT gives the A-line we desired. Note that the scale is no longer distance. We will need to set the distance scale later.	121
Figure 4.32 – The number of samples in each cycle depends on the sweep rate at the time.	121
Figure 4.33 – Phase vs time.	122
Figure 4.34 – Dividing the phase range into constant sized phase deltas.	122
Figure 4.35 – The phase vs time curve is used to map the constant phase deltas into time values at which they occurred.	123
Figure 4.36 – Resampling at the times corresponding to the constant delta phase values gives us the constant number of samples per cycle we were looking for.	123
Figure 4.37 – Replotting the data vs sample number rather than vs time gives us a clean sine wave.	124
Figure 4.38 – FFT of the new sinewave is an unambiguous peak. The scale is not a distance scale yet.	124
Figure 4.39 – Once again the beat signal from the square wave sweep rate.	125
Figure 4.40 – Phase versus time.	125
Figure 4.41 – Optical frequency of source vs time.	126
Figure 4.42 – Phase versus optical frequency.	126
Figure 4.43 – Best linear fit of optical frequency versus time.	127
Figure 4.44 - Once again the beat signal from the square wave sweep rate.	127
Figure 4.45 – Optical frequency as a function of time.	128
Figure 4.46 – Equally spaced optical frequency intervals.	128
Figure 4.47 – The optical frequency versus time curve is used to find the times associate with the equally spaced optical frequencies.	129
Figure 4.48 – Resampling at the times corresponding to the equally spaced optical frequencies puts equal numbers of samples on each of the cycles of the beat signal.	129
Figure 4.49 – The data is replotted versus sample number giving a clean sinewave.	130

Figure 4.50 - FFT of the new sinewave is an unambiguous peak. The X-scale is not a distance.	130
Figure 4.51 – Brinkmeyer critereon vs dv/dt (sweep rate or velocity) and τ . The green / black demarkation is at the $\ll 1$ being set to 100u (one part in 10,000).	133
Figure 4.52 – From above the green area shows sweep rate and τ combinations which are acceptable. The black area is not allowable by the Brinkmeyer critereon.	134
Figure 4.53 – The new critereon, plotted at 1500nm (200Thz), expands the acceptable sweep rates and τ 's to include the new laser.	135
Figure 4.54 – After compensating for the non-linear sweep the A-line has only FFT bins to which need to be assigned distances.	136
Figure 4.55 – A perfect standard has a distance d which is known.	136
Figure 4.56 – The differential standard requires exact knowledge of neither of the two distances, only of the difference in distances.	137
Figure 4.57 – FFT data from two measurement planes. One mapped to bin 2 and the other to bin 10.	138
Figure 4.58 – Beat signal a calibration surface.	139
Figure 4.59 – FFT of beat signal showing 40hz.	140
Figure 4.60 – Distance scale calculated from the frequency.	140
Figure 4.61 – T_{bin1} is the time taken for one complete cycle of the beat signal... ..	141
Figure 4.62 – FFT of fundamental beat signal (in this case 10Hz).	141
Figure 4.63 – Sampling rate 25 samples/cycle. Time domain.	143
Figure 4.64 – Sampling rate 25 samples/cycle. FFT domain.	144
Figure 4.65 – Sampling rate 12 samples/cycle. Time domain.	144
Figure 4.66 - Sampling rate 12 samples/cycle. FFT domain.	145
Figure 4.67 – Sampling rate 6 samples/cycle. Time domain. Note that the straight line interpolation in green between samples starts to visually deviate from the actual signal in blue.	145
Figure 4.68 – Sampling rate 6 samples/cycle. FFT domain. The distance domain still shows the correct location. Some 'noise' in the sidebands is starting to become apparent.	146
Figure 4.69 – Sampling rate 3 samples/cycle. Time domain. The straight line interpolation is now obviously different than the blue signal.	146

Figure 4.70 – Sampling rate 3 samples/cycle. FFT domain. Despite being sampled at barely above Nyquist the FFT still clearly marks the correct distance.	147
Figure 4.71 - Sampling rate 1.75 samples/cycle. Time domain. This is just under the 2 samples/cycle Nyquist limit. The straight line interpolation between points completely misses whole half cycles and no longer represents the actual signal in blue.	147
Figure 4.72 – Sampling rate 12 samples/cycle. FFT domain. The time domain being undersampled results in aliasing - the FFT has shifted away from the true location.	148
Figure 4.73 – A-line of 10 interfaces separated by 1mm each. The further the distance the higher the frequency and the higher the sampling rate has to be maintained to avoid aliasing.	148
Figure 4.74 - FFT domain of measurement planes at various distances. The further the distance the higher the frequency and the higher the sampling rate has to be maintained to avoid aliasing. The dashed line shows one half the sampling rate that will be applied.	149
Figure 4.75 – Effect of aliasing on the A-line with interfaces more distant than the Nyquist rate allows folded back into the good data. This mixing of good and bad in an unseparable manner is what makes aliasing such a dangerous issue.....	150
Figure 4.76 – Topology 1. Laser provides equally spaced optical frequency triggers to the A/D.	152
Figure 4.77 – Topology 2. Equally spaced optical frequency triggers are created by passing a portion of the output of the laser through an etalon. The resulting periodic waveform is detected and trigger pulses for the A/D generated from zero crossings in the mean of the AC coupled detected signal.	153
Figure 4.78 – Topology 3. The OCT optical data is oversampled along with data from an optical reference. The sample numbers associated with equally spaced optical frequencies are calculated from the optical reference data and used to resample the OCT data.	155
Figure 4.79 – Topology 4. Calibration step. A fixed distance is used to generate a periodic optical signal. The constant phase sample number are stored away. ...	156
Figure 4.80 – Topology 4. Runtime. The constant phase sample numbers are used to resample the data from the actual measurement.	157

Figure 5.1 – New Focus 8700 External Cavity Tunable Diode Laser.....	159
Figure 5.2 – The optical cavity is a Littmann-Metcalf external cavity. The pivot point is specially chosen so that only a single mode is supported as the cavity changes size. [Liu, K.; Littman (1981)].....	160
Figure 5.3 – Topology for the 8700 based SS OCT system. Trig A outputs triggers for the A/D.	160
Figure 5.4 – The standard New Focus laser Trig A outputs triggers at 0.1nm intervals – constant wavelength intervals. The effect of constant wavelength sampling on the A-line is spreading and attenuation of the peaks.	161
Figure 5.5 – The modified laser Trig A puts out triggers at constant Optical Frequency intervals. The effect on the A-line data is to preserve sharp peaks with distance.	161
Figure 5.6 – Software to control optical frequency sweeps.	162
Figure 5.7 – Software to enable Trig A.	163
Figure 5.8 – Sync signals in red show the extent of a sweep. Trig A optical frequency markers are in green. Only a few show due to the limitations of the scope. In black are a periodic optical element.....	164
Figure 5.9 – One sweep cycle. Sync in red shows extent of the sweep. Trig A optical frequency markers are in green. The optical element is in black.	164
Figure 5.10 – The first 23 optical frequency markers (TrigA).....	165
Figure 5.11 – The last 23 optical frequency markers (TrigA).....	165
Figure 5.12 – The first optical frequency marker. The rising edge comes as the start optical frequency is reached and lasts for 1uS.....	166
Figure 5.13 – The last optical frequency marker. The rising edge comes as the stop optical frequency is reached and lasts for 1uS.....	166
Figure 5.14 – Multiple scans of a gas-cell line using 1pm wavelength markers to clock the data acquisition. One sigma deviation of 12 – 20 MHz indicates 1.7ppm repeatability across the 12THz sweep range.	167
Figure 5.15 – Data at various distances measured with standard wavelength markers. Note the characteristic broadening.	168
Figure 5.16 – Data at various distances measured with optical frequency markers. Note that the peaks remain sharp across the range.	168
Figure 5.17 - A-scan for plastic tape glued to microscope dioptre. Distance calibrated in glass. [Cordes, A.H. et al. (2010)]	169

Figure 5.18 - B-scan for plastic tape and dioptré. Light enters from bottom. Spacing between tape and glass surface on left hand side of tape due to presence of hair strand indicated by arrow creating air bubble to the left. Position of Figure 5.17 A-scan is also indicated. [Cordes, A.H. et al. (2010)]	170
Figure 5.19 – C-scan of multiple slide dioptrés with scotch tap covering the majority of the area scanned.....	170
Figure 5.20 – Components.	172
Figure 5.21 – Santec Ultra-wideband Source.....	172
Figure 5.22 – DS fiber. Used for dispersion.....	173
Figure 5.23 – Filter 1	173
Figure 5.24 – Filter 2	174
Figure 5.25 – Dispersion curve for DS fiber. Zero dispersion is at 1550nm.....	175
Figure 5.26 – Output of the laser	176
Figure 5.27 – Output of the laser. Time domain (drawing).....	176
Figure 5.28 – Output of the laser. Spectrum. It covers an enormous range including optical frequencies above the turnaround point of the DS dispersion curve (dashed line at 1550nm).....	176
Figure 5.29 – After the fiber.....	177
Figure 5.30 – After the fiber. Time domain. The pulse has been stretched out.	177
Figure 5.31 – After the fiber. Spectrum. There has been loss through the fiber and some Raman amplification moving energy from the 1500nm region to higher wavelengths.	178
Figure 5.32 – After filter 1.....	178
Figure 5.33 – After filter 1. Time domain.	178
Figure 5.34 – After filter 1. Spectrum.	179
Figure 5.35 – After filter 2.....	179
Figure 5.36 – After filter 2. Time domain.	179
Figure 5.37 – After filter 2. Spectrum.	180
Figure 5.38 – At reference / measurement.	180
Figure 5.39 – At reference / measurement. Time domain.	181
Figure 5.40 – At reference / measurement. Spectrum.	181
Figure 5.41 – At the detector.....	182
Figure 5.42 – At the detector. Reference reflection only. Time domain.	182
Figure 5.43 – At the detector. Reference reflection only. Spectrum.	182

Figure 5.44 – At the detector. Beat signal. Time domain.....	183
Figure 5.45 – At the detector. Beat signal. Spectrum.....	183
Figure 5.46 – Raw data.....	184
Figure 5.47 – Selected section. This same selection needs to be made on the actual data in order for the calibration to remain valid.	185
Figure 5.48 – Cut-data only with sample scale.	185
Figure 5.49 – FFT of cut-data.....	186
Figure 5.50 – Chosen area of FFT (choice is mirrored to the other data area)....	186
Figure 5.51 – Windowed with Hamming window	187
Figure 5.52 – IFFT	187
Figure 5.53 – Hilbert transform.....	188
Figure 5.54 – Zoom of IFFT and Hilbert transform together.....	188
Figure 5.55 – ATAN(Hilbert / IFFT)	189
Figure 5.56 – Unwrapped phase	189
Figure 5.57 – The raw measurement data must be taken in the same way as the calibration – same triggering, same number of samples, same samplerate.	190
Figure 5.58 – The data must be cut in the same way as the calibration.	190
Figure 5.59 – The cut-data.....	190
Figure 5.60 – Now we use the phase / time data we generated in the calibration phase to cast the time scale to phase (or optical frequency if you prefer).....	191
Figure 5.61 – Hilbert scale	191
Figure 5.62 – The scale must have equally spaced samples for the FFT so we resample to a convenient number of points.	192
Figure 5.63 – The FFT gives us the A-line with the single peak expected. However the scale is not yet calibrated to distance.	193
Figure 5.64 – A differential calibration will be used.....	193
Figure 5.65 – Two measurements with a differential distance of 150um. Peak detection tells us that the two peaks are separated by 64.21 bins. The scale calibration is thus 2.34um/bin.	194
Figure 5.66 – Applying the distance scale to the previously measured data gives the final A-line.	194
Figure 5.67 – Zoom into the peak to measure the width	195
Figure 5.68 – On a linear scale the full width half max can be seen to be 4.95um air (3.3um glass).	195

Figure 5.69 – Unlinearized peak.....	196
Figure 5.70 – FWHM of unlinearized peak is 44.4um air (29.6um glass).....	196
Figure 5.71 – Linearized and un-linearized data together.	197
Figure 5.72 – Handywrap. 10um to 14um thick.....	197
Figure 5.73 – A-line of handywrap. The two peaks are separated by 10um.	198
Figure 5.74 – B-scan of Handywrap. 2mm long.	199
Figure 5.75 – C-scan of Handywrap. 2 x 2 mm ²	200
Figure 5.76 – Peaks from B-line of unstressed handywrap and delta showing thickness.	201
Figure 5.77 – Peaks from B-line of handywrap starting near puncture. Stress points can be seen where the two peaks combine into one.	202
Figure 5.78 – One reflection, rectangular window.....	203
Figure 5.79 – One reflection, Blackman-Harris window.	203
Figure 5.80 - Handywrap as seen by both systems – Rectangular windows. Again the slight difference in positions is due to temperature and vibration. The higher resolution data shows the actual separation (8um – 10um). The lower resolution data also has two peaks due to phase effects in the beat signals.	204
Figure 5.81 – Handywrap as seen by both systems – Blackman-Harris windows. Again the slight difference in positions is due to temperature and vibration. The higher resolution data shows the actual separation (8um – 10um). The lower resolution data also has two peaks due to phase effects in the beat signals.	204

Lista de tabelas

Table 1 – Typical specifications for OCT systems.	35
Table 2 – Brinkmeyer critereon for Brinkmeyer’s laser, our New Focus laser and our Stretched Pulse Santec laser. The critereon still is reasonable for the New Focus laser as despite the sweep rate increasing by a factor of 1000 the time scale has decreased. The stretched pulse Santec laser on the other hand is so fast that the critereon breaks down despite the smaller time scale.....	132
Table 3 – The new critereon – under which all three lasers are acceptable.	135
Table 4 – Separation required to achieve a desired %error if encoder has 67nm resolution.	138
Table 5 – Percentage error in distance scale from not knowing index of refraction	138
Table 6 – Four topologies for realizing a basic Swept Source OCT system.	151
Table 7 – New commands for modified 8700	162

1

Introduction

Optical Coherent Tomography (OCT) is a powerful tool for the non-contact, non-destructive micrometer scale imaging of materials [Huang et al. (1991)].

OCT uses partial reflections of light from interfaces between dissimilar materials inside a sample under test to determine not only some character of each interface but also of where in the sample the interface resides.

As illustrated in Figure 1.6, light incident on a sample will partially reflect at each interface due to the change in index of refraction between the two materials on each side of the interface. The larger the change in index of refraction, the more light which is reflected [Saleh; Teich (2007)].

OCT uses coherence properties to determine where each interface lies relative to one another. The combination of strength of reflection and location of interface is known as a reflectogram or axial scan or A-scan as in Figure 1.6 to Figure 1.6.

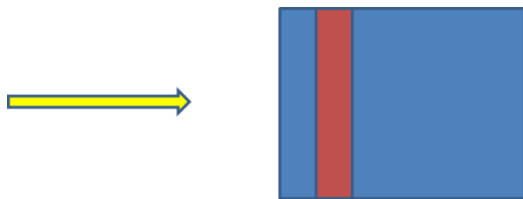


Figure 1.1 – Light traveling through air (yellow) incident on a sample made from two materials (blue and red) with different indices of refraction.

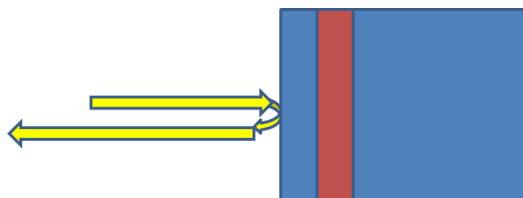


Figure 1.2 – As the light reaches the blue material some reflects from the air – blue material boundary or interface.

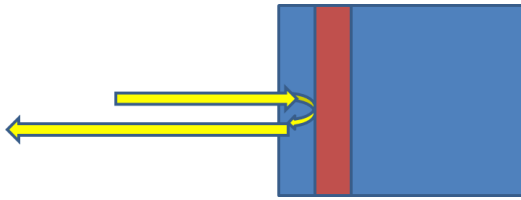


Figure 1.3 – As the light reaches the red material some reflects from the blue material – red material interface.

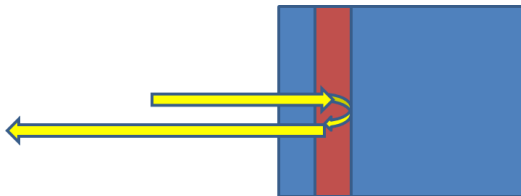


Figure 1.4 – As the light leaves the red material some reflects from the red material – blue material interface.

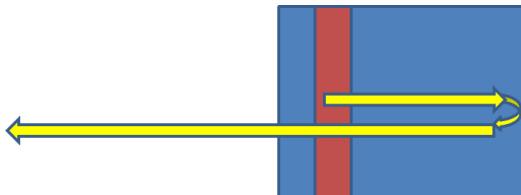


Figure 1.5 – Finally, as the light leaves the sample, some reflects from the blue material – air interface.

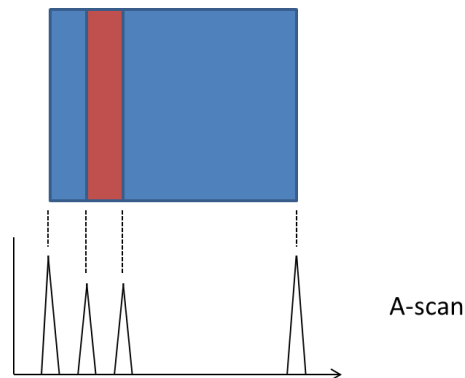
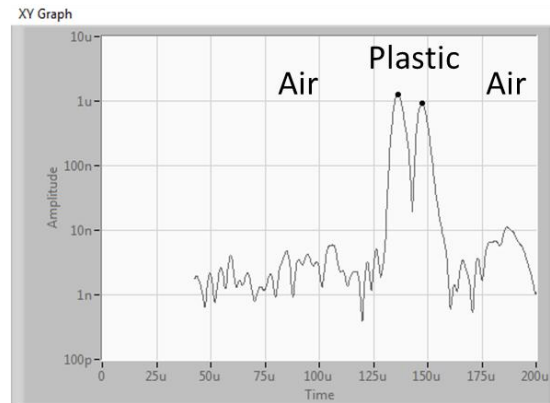


Figure 1.6 – OCT is able to discern how much reflected light comes from each interface and at what distance along the axis of the light the reflection occurred. The one dimensional plot of this information is called an A-scan or A-line.

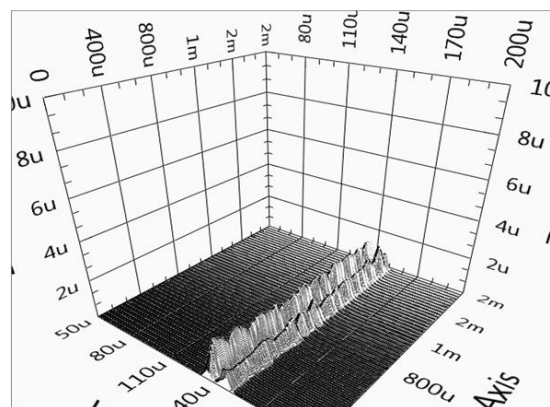
Figure 1.7 has a simple example; plastic handywrap and its OCT A-scan showing two interfaces – Air to plastic as the light enters the handywrap and plastic to air as the light leaves.



A-scan

Figure 1.7 – A-scan of Handywrap. An A-scan is a simply XY plot. X locates the interface while Y indicates the amount of light received from that interface.

Figure 1.8 shows a B-scan of the handywrap which is a collection of A-scans as the point of scan is moved laterally.

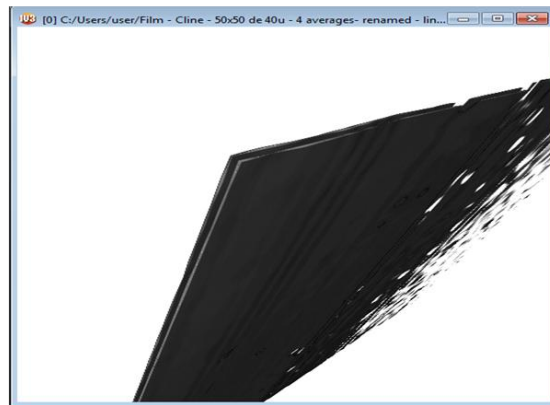


B-scan

Figure 1.8 – B-line of Handywrap. Constructed of 200 A-lines separated by 10um laterally. A B-line is a 3D image where X and Y locate the interface and Z indicates the light received from that interface.

Finally, Figure 1.9 shows a C-scan which is a collection of B-scans separated along the other lateral axis.

As X, Y and Z are all involved in locating the point in space the amount of light reflected has to be indicated in another manner. A combination of opacity (zero or negligible reflection being transparent) and color or intensity of color is used. The result is a volume image. As OCT identifies a material by the intensity of reflection from interfaces, it acts in a similar way to edge detection. A more representative volume image of the original material would be formed from integrated A-scans.



C-scan

Figure 1.9 – C-line of Handywrap. Constructed of 200 B-lines separated by 10um laterally. A C-scan is a volume. X, Y and Z locate the interface. The amount of light received from the interface is indicated by varying color or intensity or opacity.

A very important application of OCT is in the area of opthamology. OCT has the ability to gather information about the retinal tissues at the back of the eye without resorting to surgery (Figure 1.10 and Figure 1.11). This has led to an industry built around OCT machines for the imaging of the retinal tissues through the eye (1) (Liu, Y.-Y. et al. (2011)). These images aid the doctor in the evaluation of the nerves at the back of the eye for health or in the case of disease,

early detection, identification and guidance of treatment. (2) (Harding; Yalin (2009))

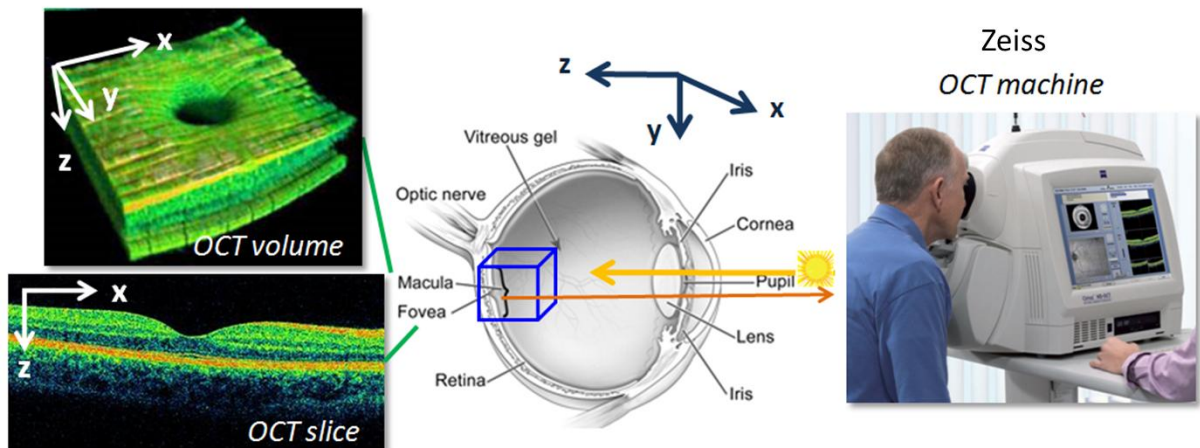


Figure 1.10 – Zeiss OCT machine for the imaging of retinal tissues at the back of the eye. A),B) show B-scan and C-scan images of the retinal tissue. C) shows the front door access OCT has to the retinal tissues. D) shows the machine itself with patient and diagnostic information on the machine. (1)(Liu, Y.-Y. et al. (2011))

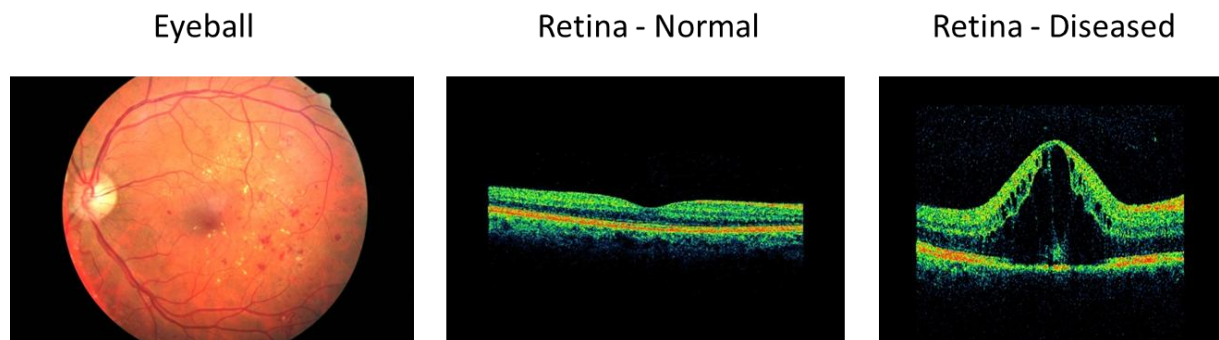


Figure 1.11 – A) Eyeball and B),C) OCT B-scan images taken through the eyeball of the retinal tissues at the back of the eye. B) shows healthy tissue while C) shows diseased tissue. (2)(Harding; Yalin (2009))

1.1. Typical specs

Typical specifications of OCT systems are shown in Table 1. Two commercial systems are shown as well as two systems built up around our lasers which are discussed in detail in section 5 beginning on page 158.

Table 1 – Typical specifications for OCT systems.

System	Axial Resolution (tissue)	Scan Speed (A-scans/s)	Wavelength (nm)
Zeiss Cirrus HD-OCT (Commercial)	5um	27,000	840
Thorlabs OCS 1300SS (Commercial)	9.2um	16,000	1275 - 1375
New Focus Laser	8.6um	5	1500 – 1600
Stretched Pulse Santec Laser	3.6um	6,000,000	1300 - 1500

In this work we will discuss swept sources for the OFDR based technique.

Section 1 is this introduction.

Section 2 describes Swept Source OCT in general.

Section 3 illustrates the Fourier concepts necessary for SSOCT.

Section 4 deals with non-linear sweeps and other source details.

Section 5 describes our work with a modified New Focus Littman-Metcalf external cavity tunable laser source and a swept source created by stretching an ultra-wideband impulse laser from Santec.

Section 6 describes our SSOCT model

Section 7 holds our conclusions

That which the author considers to the best of his knowledge to be new:

1. A methodology which separates the calibration of a Swept Source OCT system into two pieces; first, linearization of the sweep and second, calibration of the distance domain. The common approach is to use a single known reference which accomplishes both steps at the same time. However, by treating the two steps separately the overall process can be simplified.
2. A calibration method for the distance domain which is differential and does not require an absolute reference.
3. An adjustment to the criterion proposed in 1993 [Glombitza; Brinkmeyer (1993)] which allowed the mathematical substitution of optical frequency for the phase of the beat signal. The criterion was revisited in light of our source no longer falling under the original criterion. A new less restrictive yet sufficient criterion was proposed.
4. A derivation of the initial phase of the beat signal.
5. An improvement to a patent pending wavelength marker system developed by New Focus for spectroscopic applications [Pritchett et al. (Pending)]. The improvement is to produce optical frequency markers for use in interferometric applications such as Swept Source OCT.
6. The use of non-linear effects (Raman) and a two-stage cladding filter to shape the spectrum of the ultra-wideband impulse laser.

2 Swept Source OCT

2.1. Incoherent beginnings

When OCT was originally developed as a reflectometric technique for the inspection of optical devices, the technique was based on the measurement of the interference fringes of backscattered light originated from a low coherence source, launched on a Michelson interferometer and recombined on a detector [Huang et al. (1991) e Takada et al. (1987) e Danielson; Whittenberg (1987)].

The location of the coherence spike as the reference mirror is scanned locates each individual reflection from the test arm.

The axial resolution of the technique is given by the coherence length of the source, the broader the spectrum, the sharper the coherence spike.

Once the axial reflectogram (or A-scan) is obtained, two dimensional (B-scans) or three dimensional (C-scans) images are obtained by coupling the reflectometer to a transversal positioning device.

2.2. Coherent approach

A different approach than the original incoherent technique was Optical Frequency Domain Reflectometry (OFDR), in which a high coherence optical source is launched on the Michaelson interferometer and recombined on a detector. The source has its frequency swept over a certain spectral range and the low frequency beat signal coming from the beat of delayed replicas of the signal at the detector is measured with a Fast Fourier Transform (FFT) spectrometer [Eickhoff; Ulrich (1981) e Glombitza; Brinkmeyer (1993) e Passy et al. (1994) e Von der Weid et al. (1997) e Chinn et al. (1997) e Golubovic et al. (1997)].

This scheme has the advantage of having no moving parts in the interferometer and improved SNR [Passy et al. (1994) e Choma et al. (2003)].

As in the original scheme, the resolution is given by the total width of the spectral range covered by the source.

And again once the A-scan is obtained, two dimensional (B-scans) or three dimensional (C-scans) images are obtained by coupling the reflectometer to a transversal positioning device.

2.3. Basic setup

The basic setup for Swept Source OCT is shown in Figure 2.1. Light from the swept source enters the interferometer at the top left and is split between the reference and sample outputs. Reflections from the reference and a distance d into the sample are recombined in the splitter and passed on to the detector.

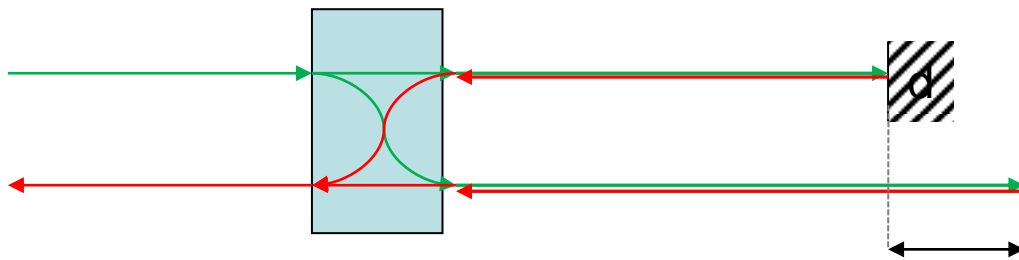


Figure 2.1 – Interferometer portion of SSOCT showing the optical paths to and from the reference and from an interface at distance d within the sample.

For simplicity let's consider a source which sweeps at a constant rate as shown in Figure 2.2. Real world sources are not able to perfectly sweep at a constant rate and we will consider the implications of this later but the essence of SSOCT is illustrated by this simplified case.

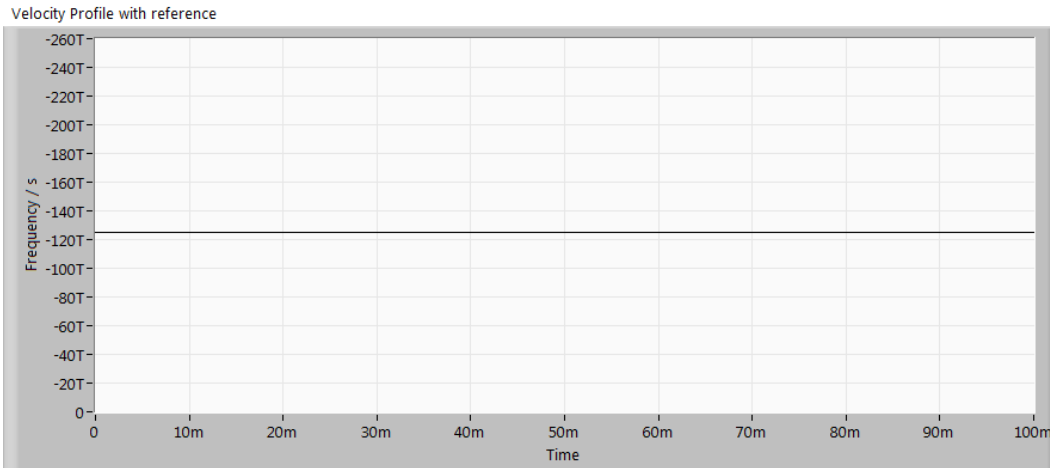


Figure 2.2 – Sweep rate as a function of time. In this simple example the sweep speed is assumed to remain constant during the entire 100ms of sweep.

Since the source is sweeping, the optical frequencies reflected by the reference and by the interface at depth d inside the sample which recombine in the splitter will be different. The difference is the sweep rate times the time spent entering the sample, reflecting from depth d and returning as shown in Eq. 2.2. This difference frequency is what is seen by the detector as shown in Figure 2.3.

$$f = \text{Sweep Rate} * 2 n d / c \quad \text{Eq. 2.1}$$

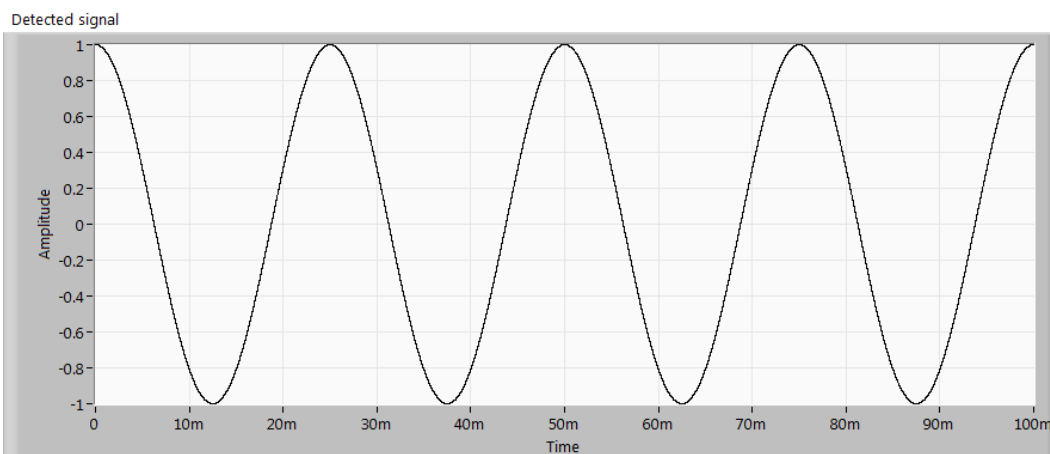


Figure 2.3 – The detector sees a sinewave at the difference frequency between the optical frequency reflected by the reference and that reflected by the interface at distance d into the sample.

An FFT of the detected signal produces a peak at the detected frequency
Figure 2.4.

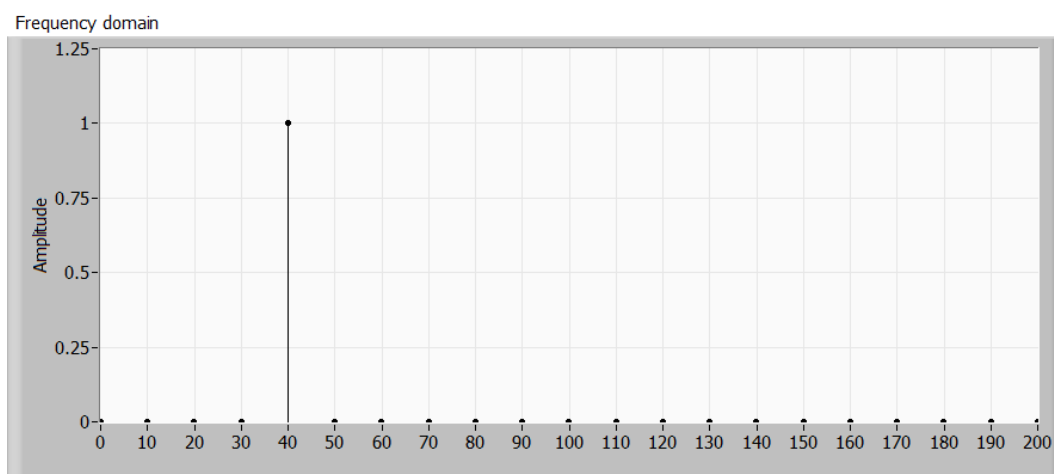


Figure 2.4 – FFT of the sinewave seen by the detector.

Finally, the distance scale can be applied using the inverse of Eq. 2.2.

$$d = f * c / (\text{Sweep Rate} * 2n) \quad \text{Eq. 2.2}$$

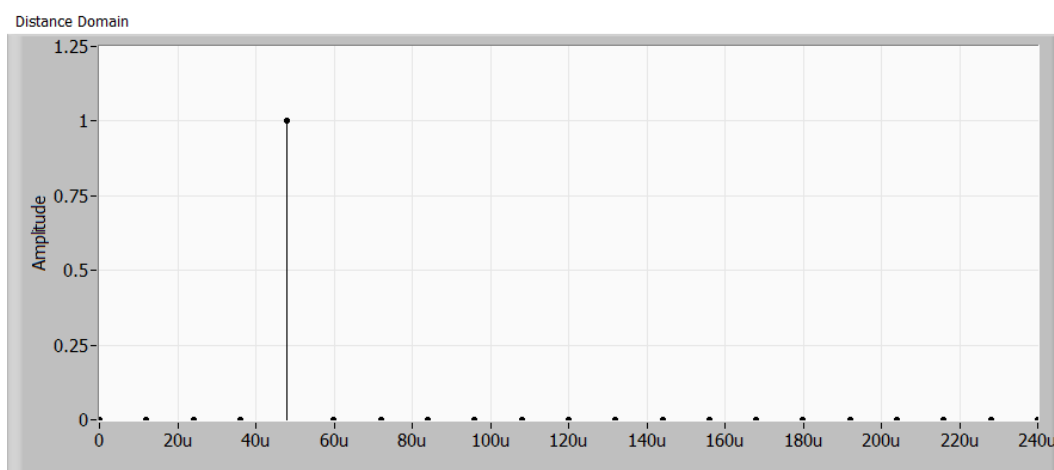


Figure 2.5 – The frequency scale of the FFT has been rescaled to distance using knowledge of the scan speed and the index of refraction of the sample. $d = f c / (2 n \text{ SweepRate})$.

3 Fourier Details

Swept Source OCT relies on the FFT. It is useful to be conversant in the techniques of using the FFT.

3.1. Non-integer number of cycles

The FFT of an integer number of cycles of a sinewave is a single point as shown in Figure 3.2.

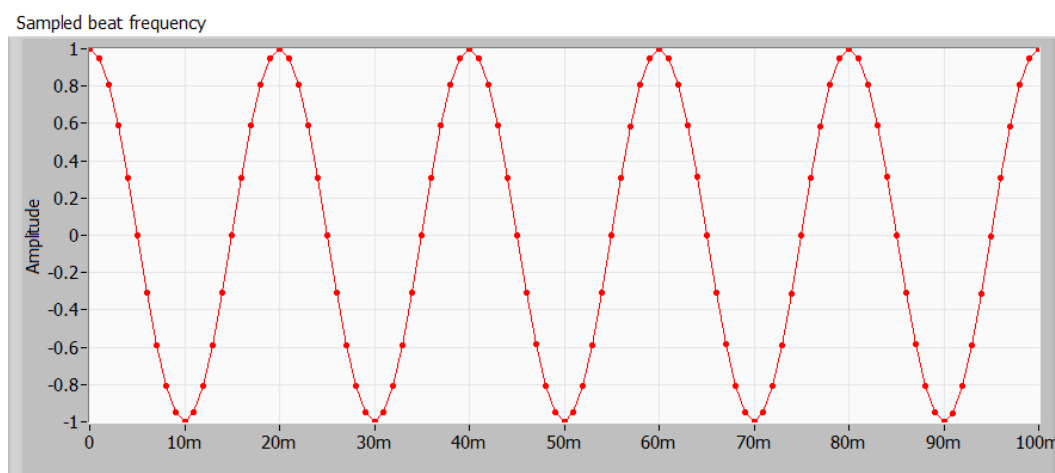


Figure 3.1 – Integer number of cycles. Time domain.

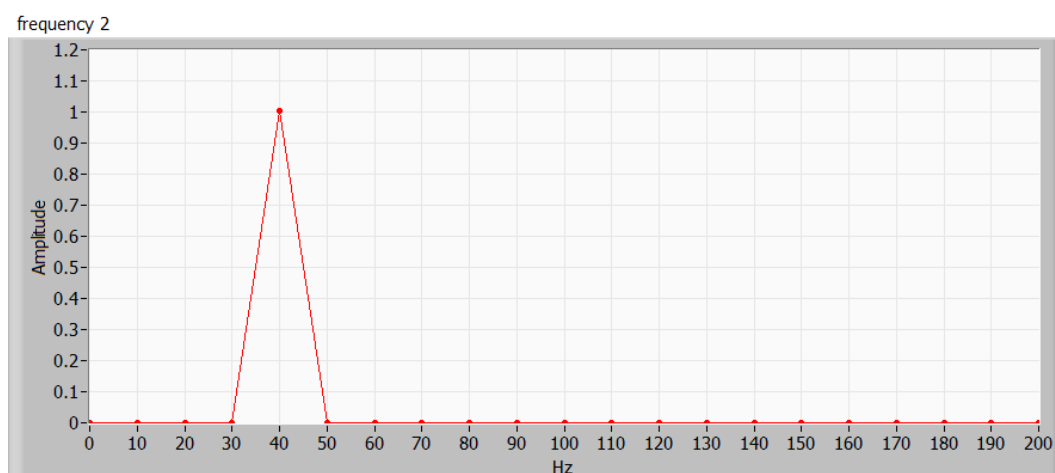


Figure 3.2 – Integer number of cycles. FFT is a single point.

If the number of cycles is not exactly an integer number then the FFT will not be a single point, rather it will be a jumble across several points (Figure 3.4 - Figure 3.24).

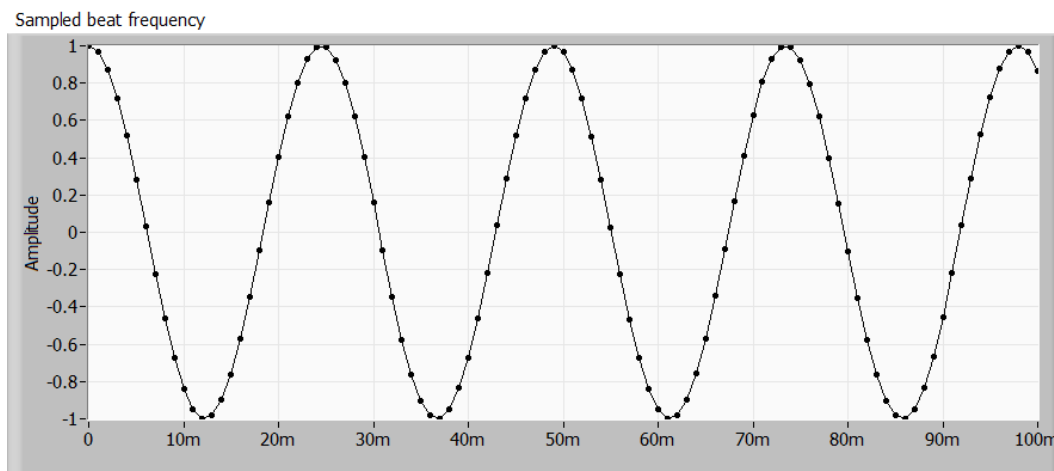


Figure 3.3 – Non-integer. 1/12 of a cycle extra. Time domain.

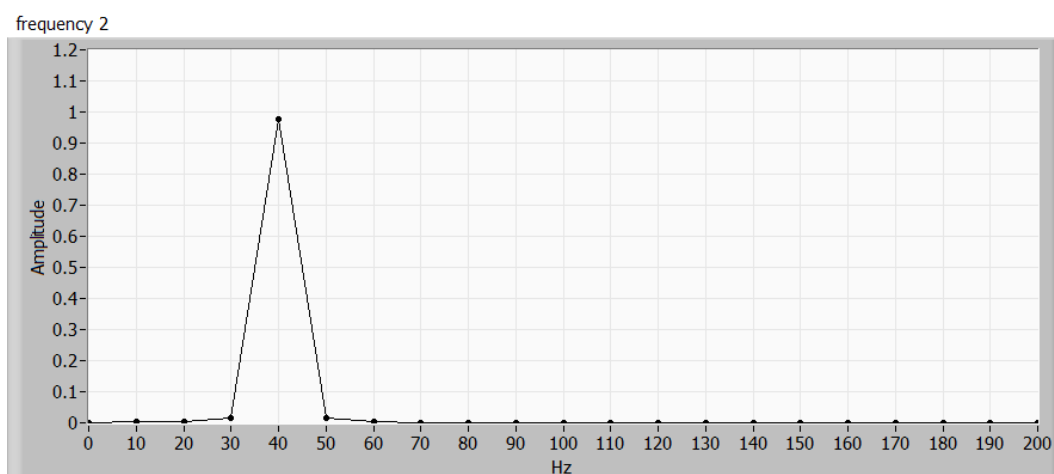


Figure 3.4 – Non-integer. 1/12 of a cycle extra. FFT.

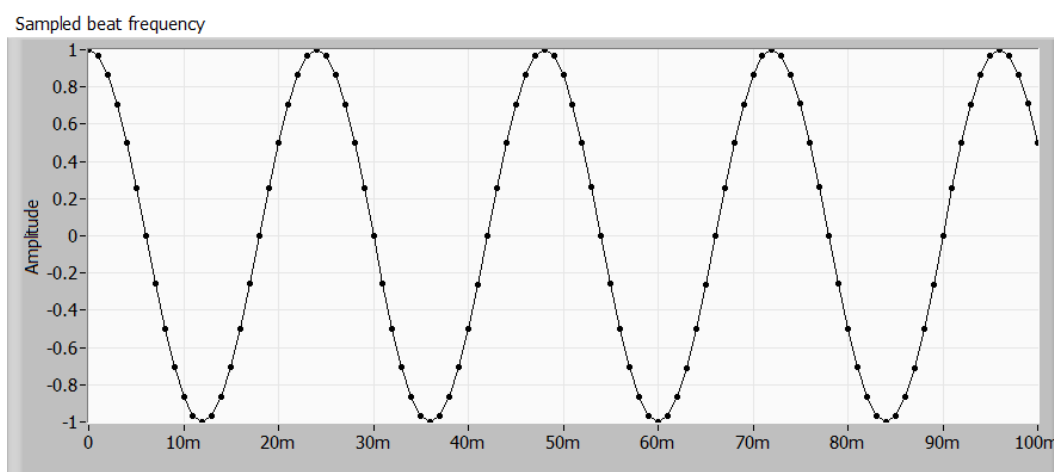


Figure 3.5 – Non-integer. 2/12 of a cycle extra. Time domain.

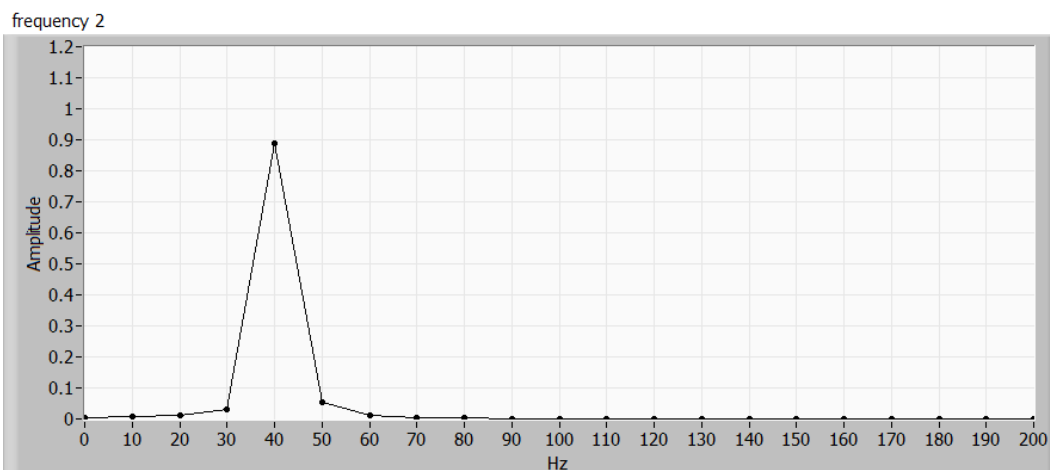


Figure 3.6 – Non-integer. 2/12 of a cycle extra. FFT starts to walk away from the initial bin.

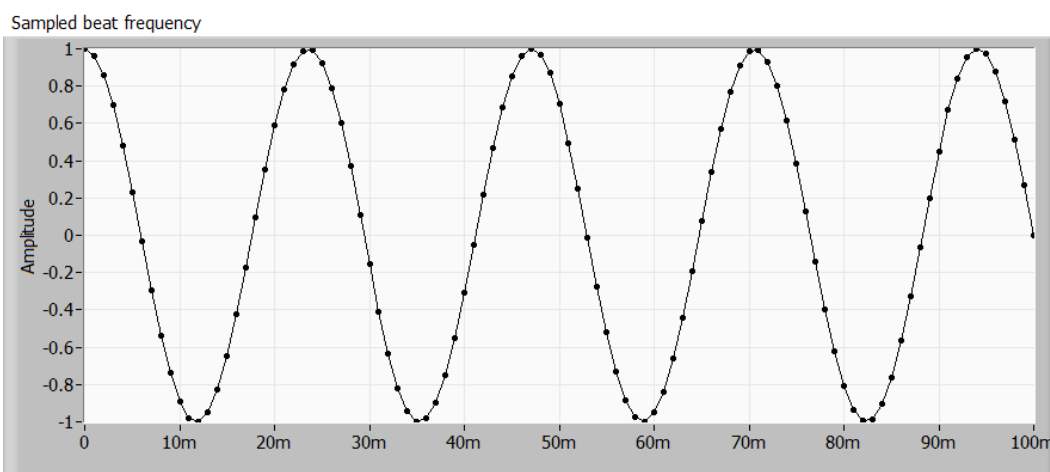


Figure 3.7 – Non-integer. 3/12 of a cycle extra. Time domain.

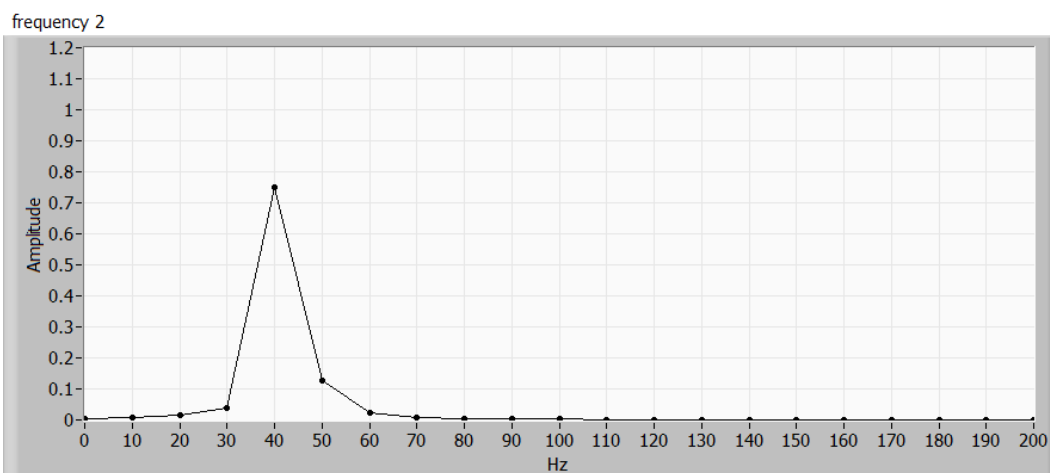


Figure 3.8 – Non-integer. 3/12 of a cycle extra. FFT.

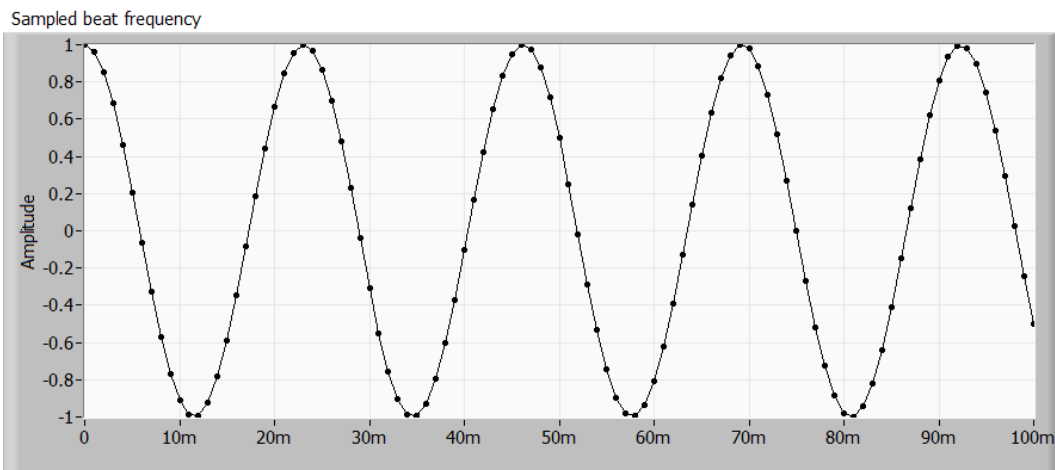


Figure 3.9 – Non-integer. 4/12 of a cycle extra. Time domain.

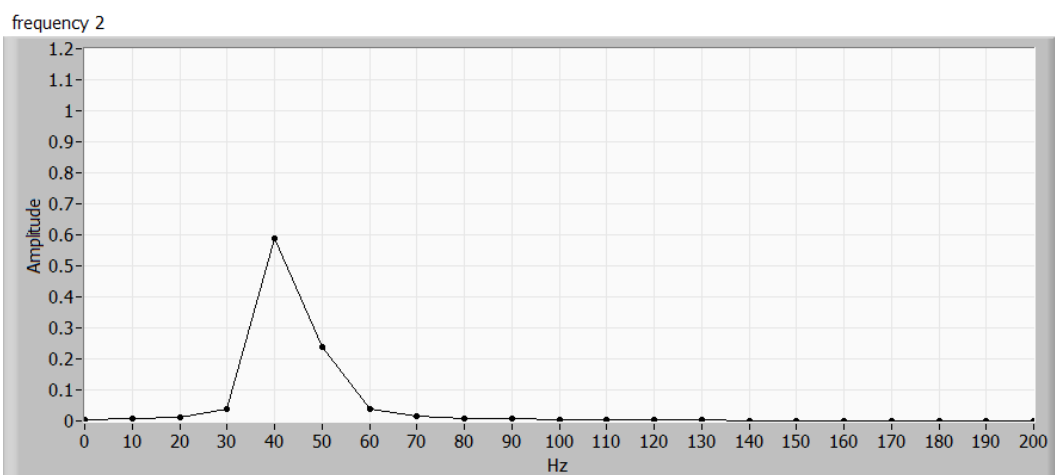


Figure 3.10 – Non-integer. 4/12 of a cycle extra. FFT.

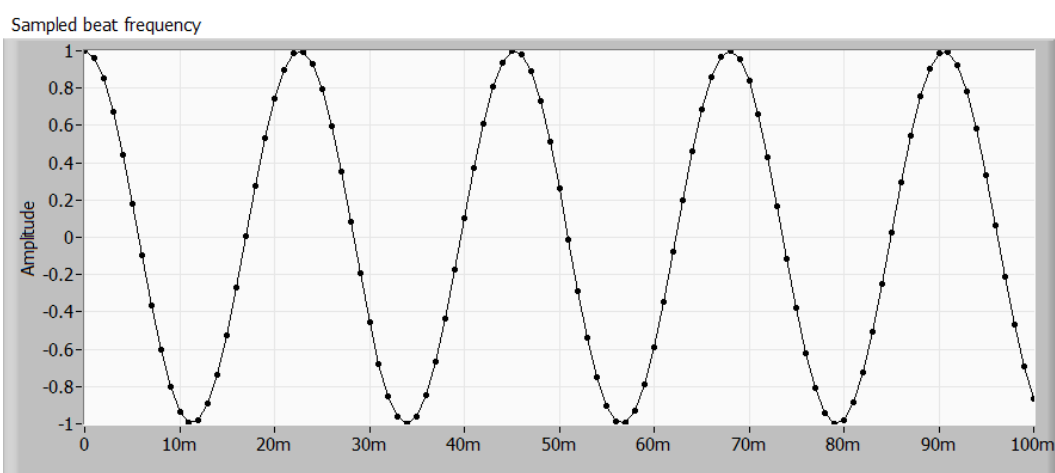


Figure 3.11 – Non-integer. 5/12 of a cycle extra. Time domain.

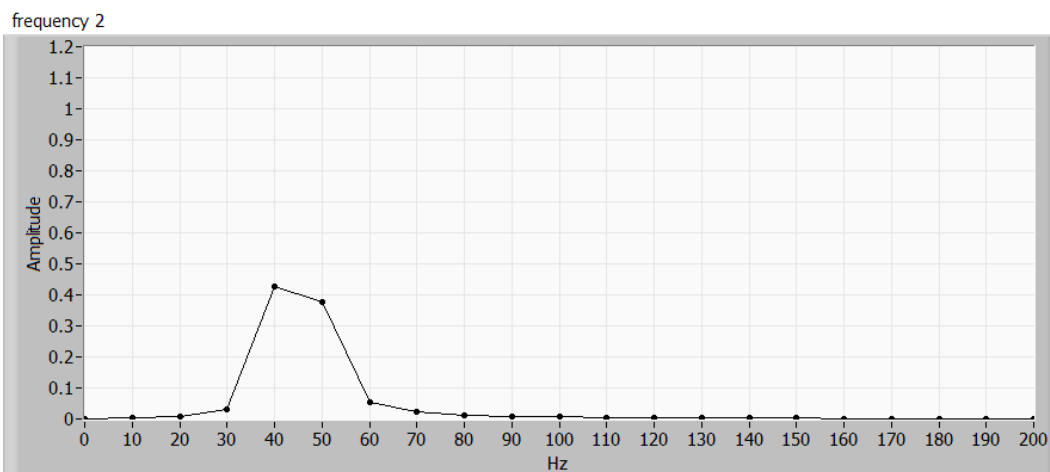


Figure 3.12 – Non-integer. 5/12 of a cycle extra. FFT.

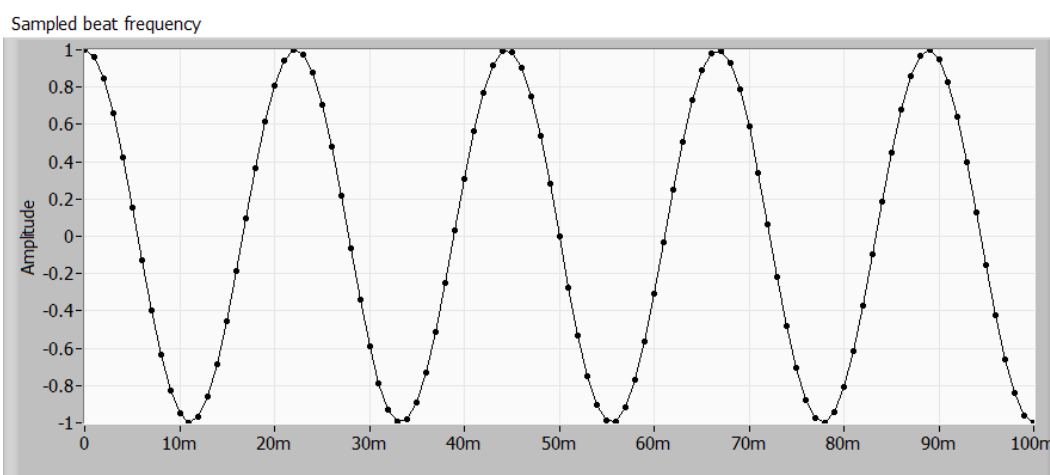


Figure 3.13 – Non-integer. 6/12 of a cycle extra. Time domain.

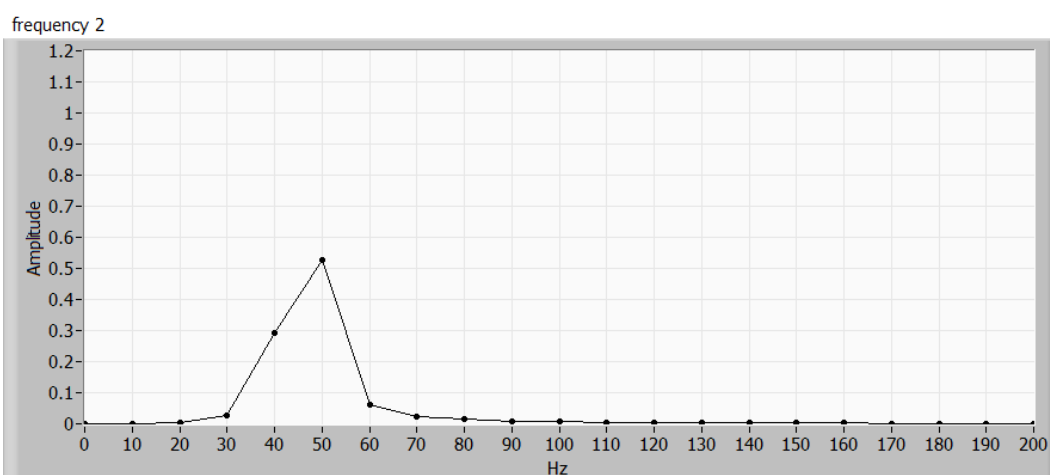


Figure 3.14 – Non-integer. 6/12 of a cycle extra. FFT.

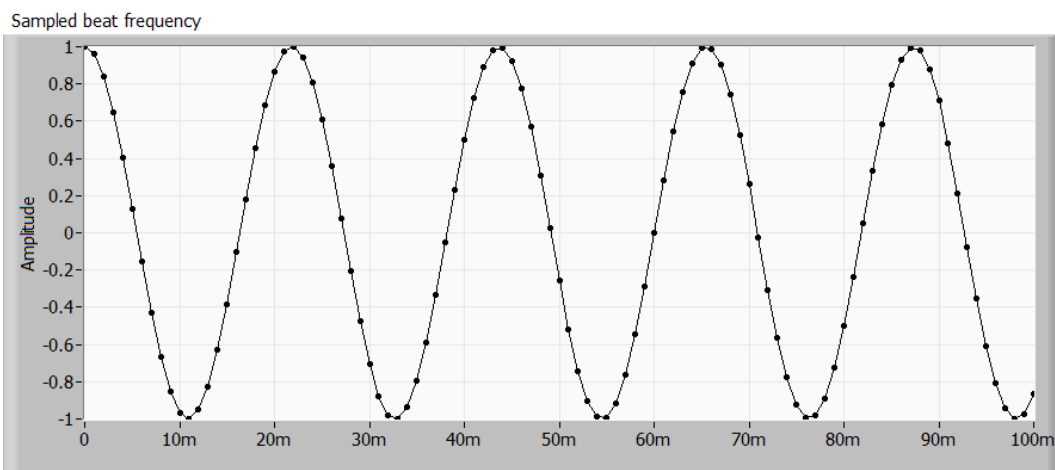


Figure 3.15 – Non-integer. 7/12 of a cycle extra. Time domain.

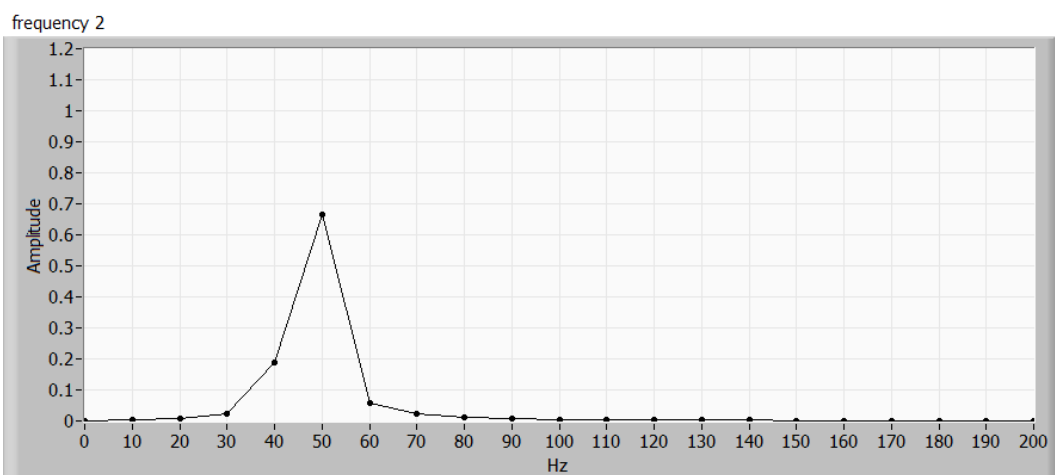


Figure 3.16 – Non-integer. 7/12 of a cycle extra. FFT.

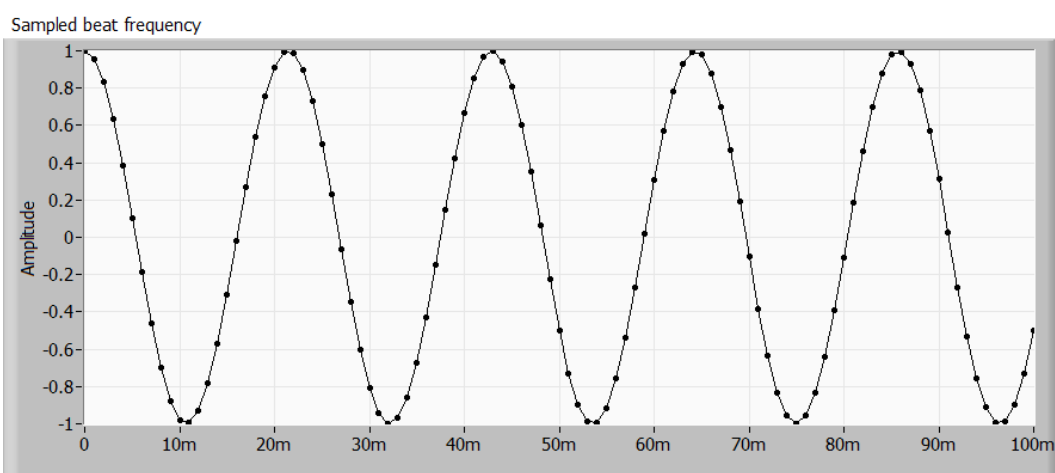


Figure 3.17 – Non-integer. 8/12 of a cycle extra. Time domain.

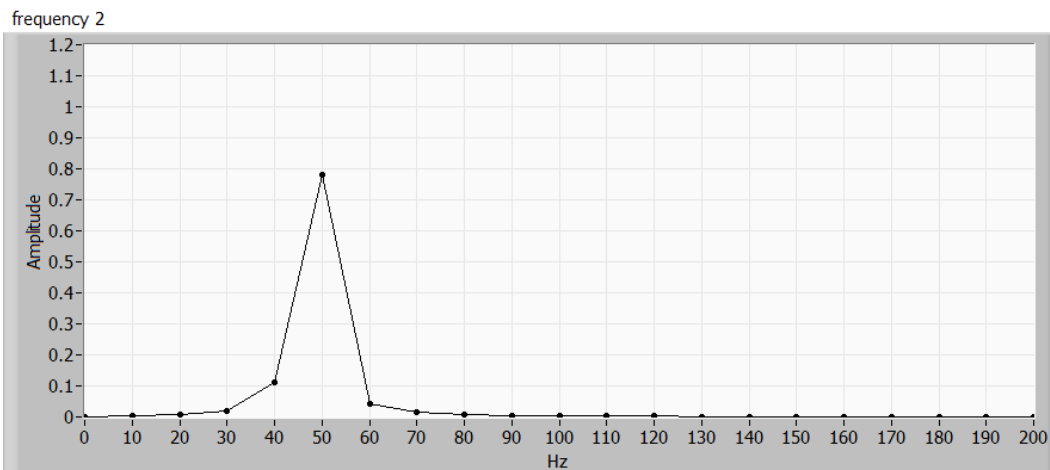


Figure 3.18 – Non-integer. 8/12 of a cycle extra. FFT.

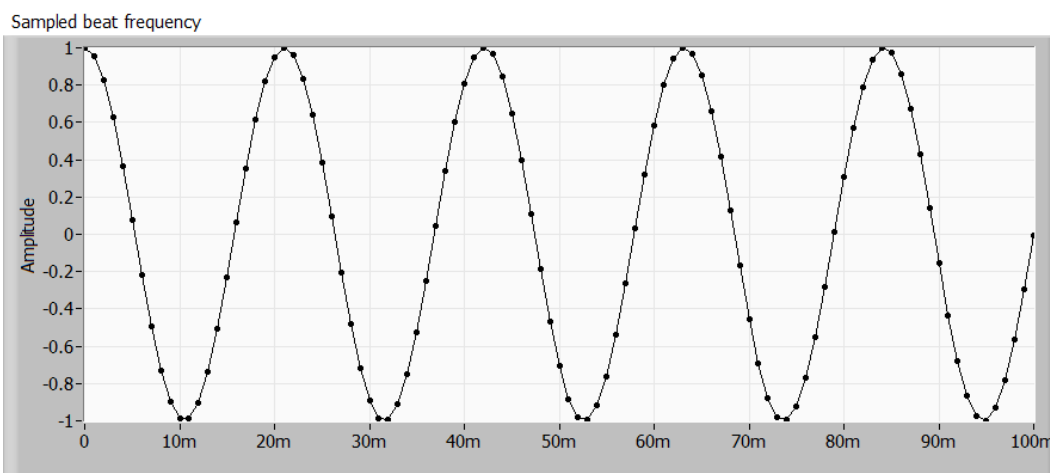


Figure 3.19 – Non-integer. 9/12 of a cycle extra. Time domain.

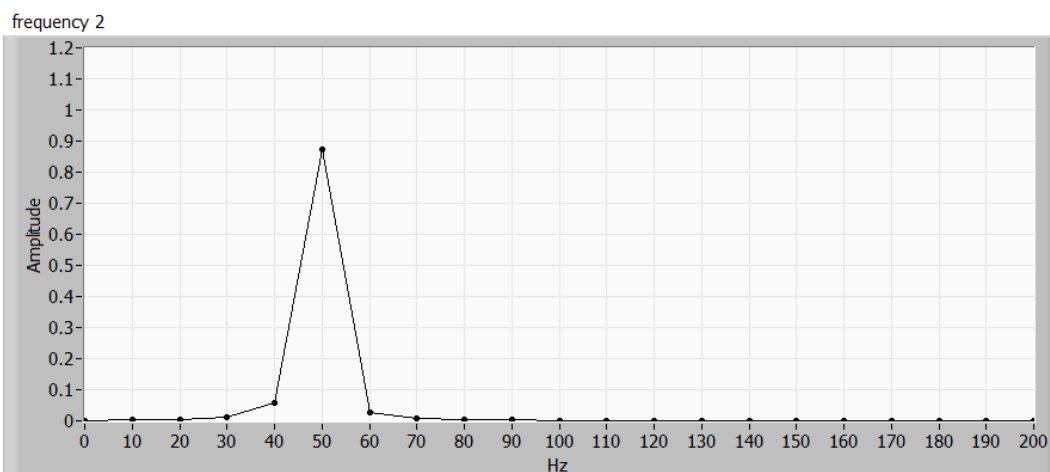


Figure 3.20 – Non-integer. 9/12 of a cycle extra. FFT.

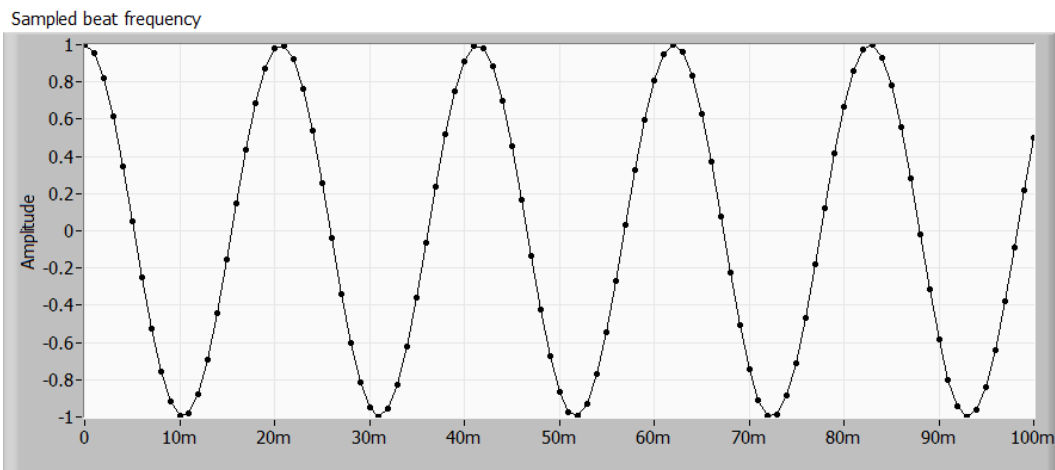


Figure 3.21 – Non-integer. 10/12 of a cycle extra. Time domain.

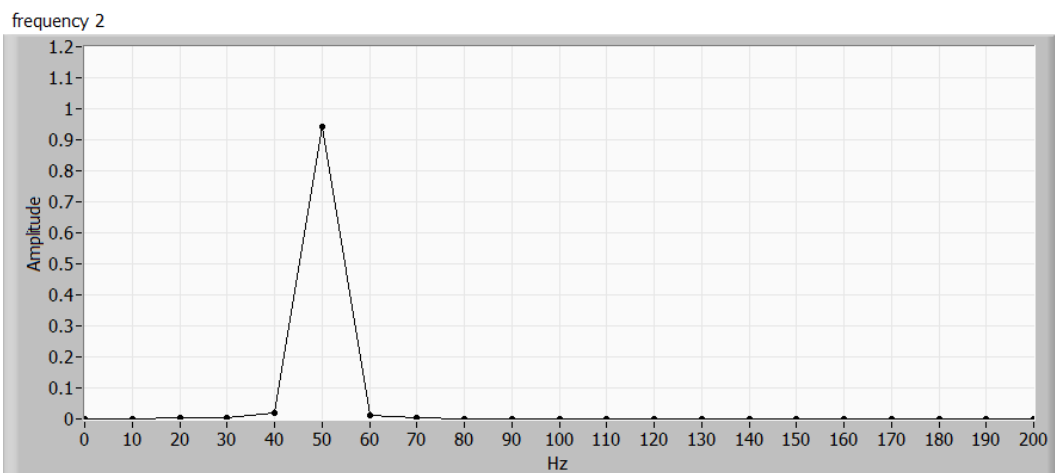


Figure 3.22 – Non-integer. 10/12 of a cycle extra. FFT.

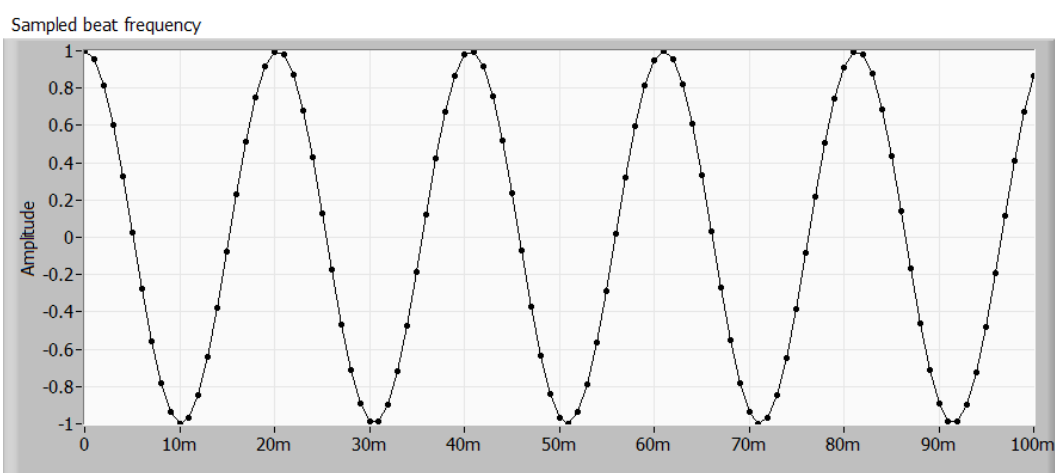


Figure 3.23 – Non-integer. 11/12 of a cycle extra. Time domain.

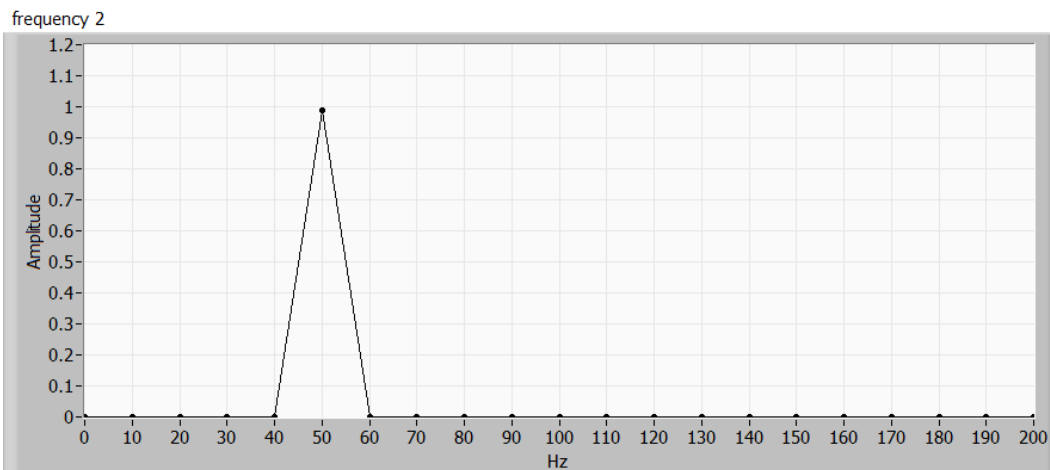


Figure 3.24 – Non-integer. 11/12 of a cycle extra. FFT

Finally, when the number of cycles is an integer number again, the FFT will resolve to a single point again as in Figure 3.26.

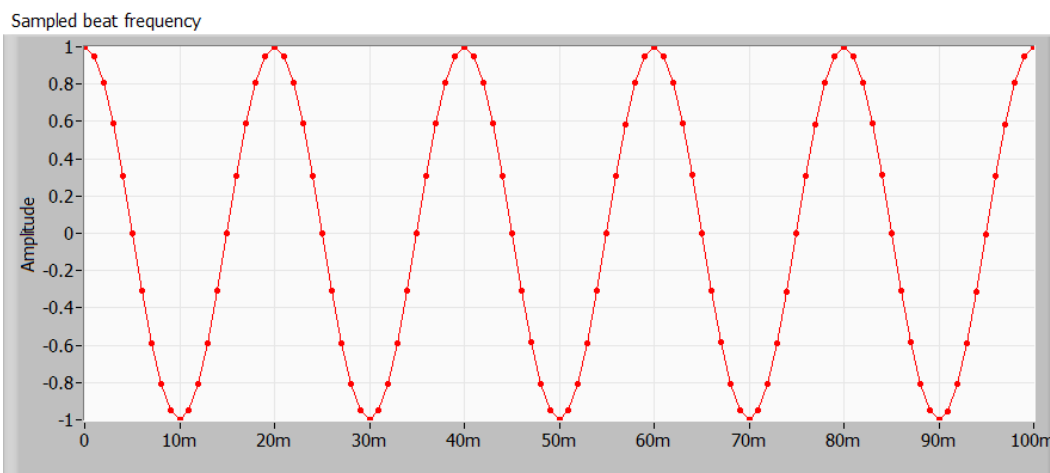


Figure 3.25 – Integer. One full cycle extra. Time domain.

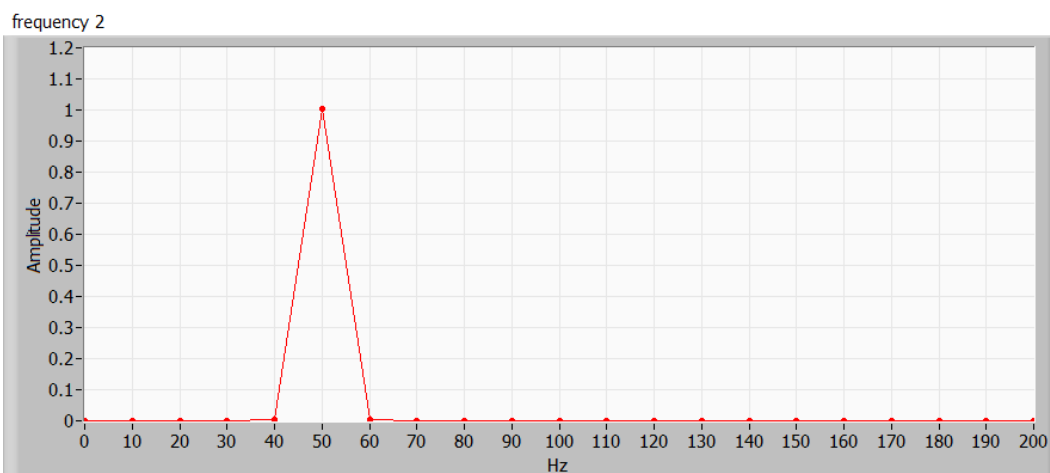


Figure 3.26 – Integer. One full cycle extra. The FFT once again is a single point.

If we were always to work with integer numbers of cycles then we would be very satisfied. However, in general we will not have control over this. The fact that the shape of the FFT then is variable and indistinct is a problem.

3.2. Zero padding

One solution is to use zero-padding to interpolate between the natural data points in the transform domain [Smith (2007)]. This has the effect of making the FFT the same irregardless of whether there an integer number of cycles or not.

Zero padding is adding zeros to the end of a waveform before taking the FFT. We always multiply by a window of some sort before taking an FFT, either implicitly (a rectangular window is the effect of using no window at all) or explicitly (choosing a Hanning or Hamming or other window), so the data is forced to zero at the endpoints. This is discussed in section 3.4 starting on page 66. Adding more zeros at the beginning or the end then does not change the signal content. However it does add more points to the FFT as the minimum FFT spacing is $1/T$ where T is the total time span.

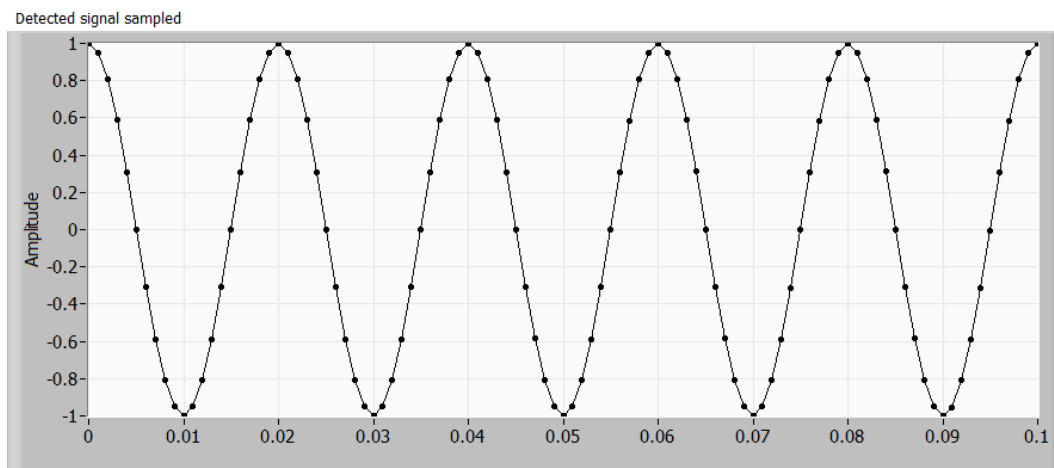


Figure 3.27 – No zero padding. Time domain.

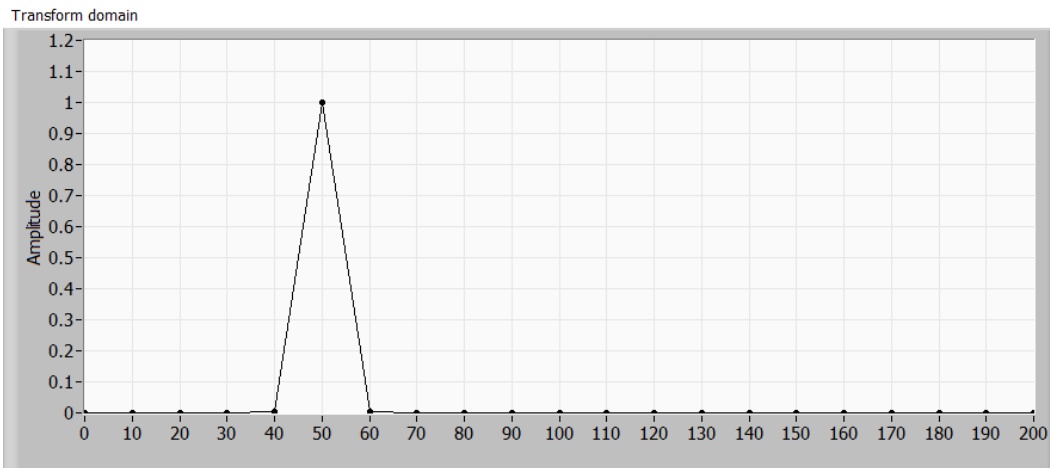


Figure 3.28 – No-zero padding. FFT.

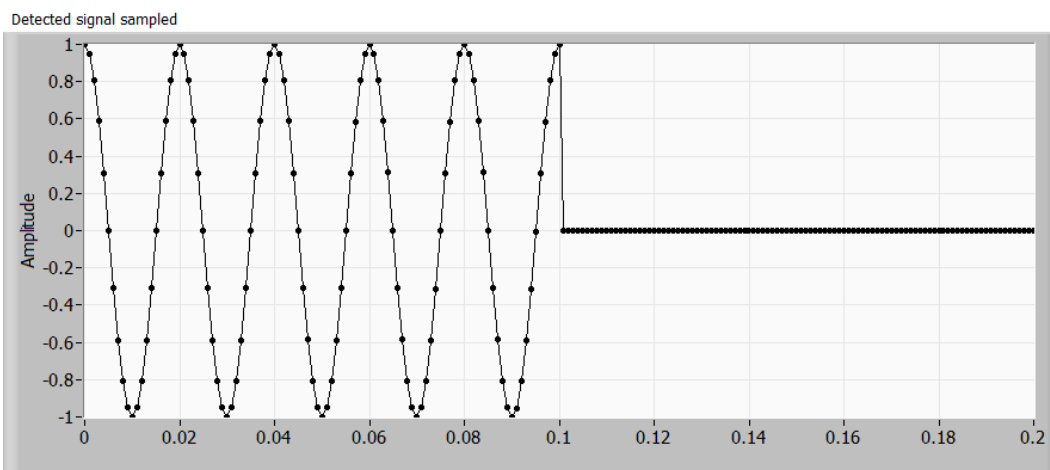


Figure 3.29 – Zero-padding to 2x. Time domain.

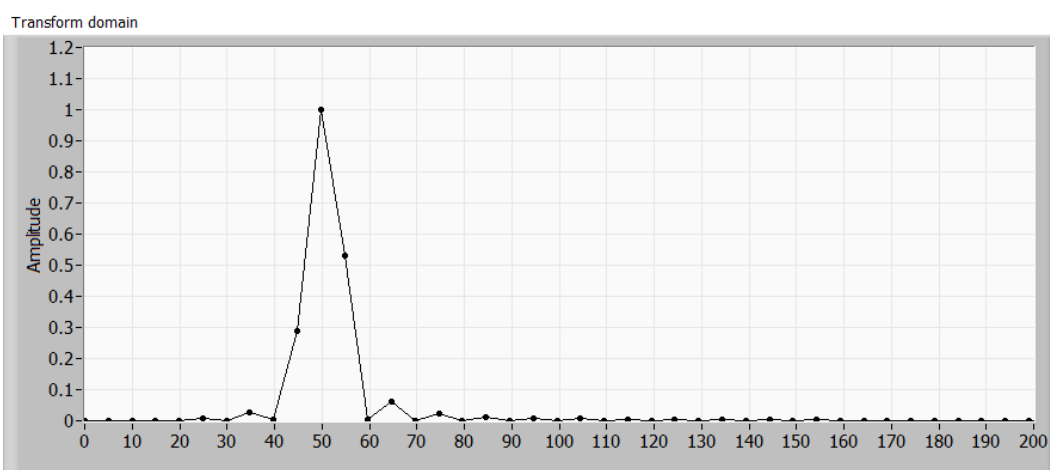


Figure 3.30 – Zero-padding to 2x. FFT.

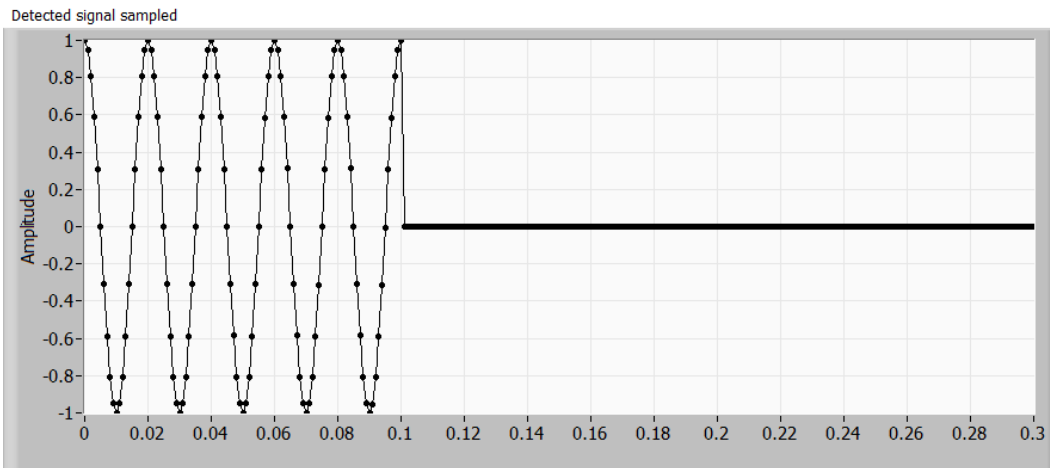


Figure 3.31 – Zero-padding to 3x. Time domain.

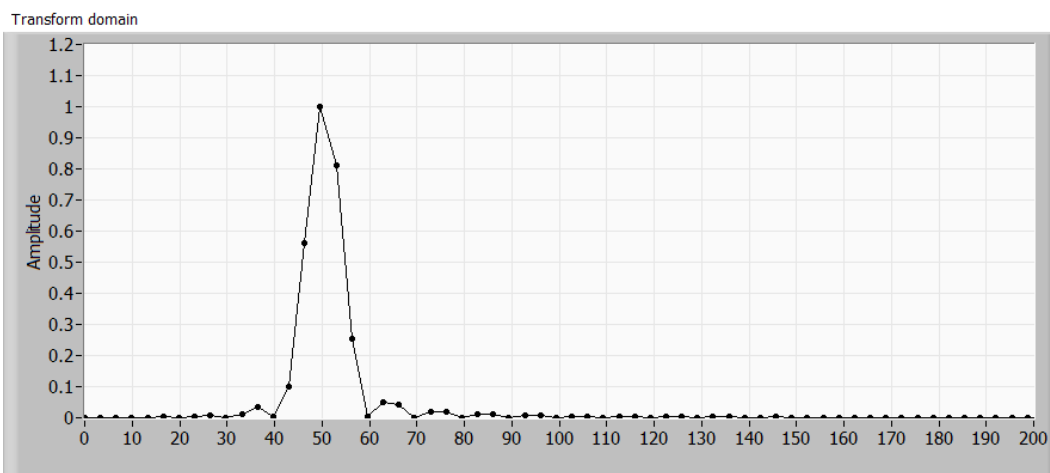


Figure 3.32 – Zero-padding to 3x. FFT.

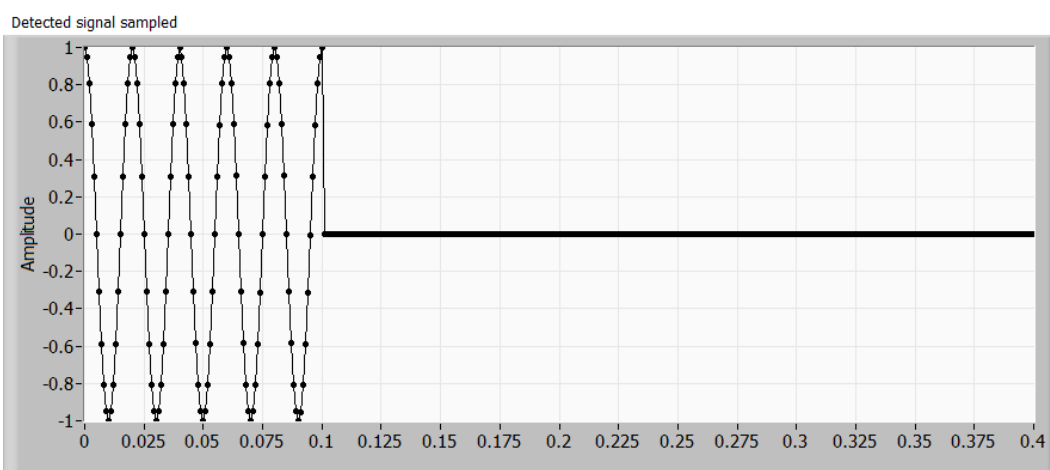


Figure 3.33 – Zero-padding to 4x. Time domain.

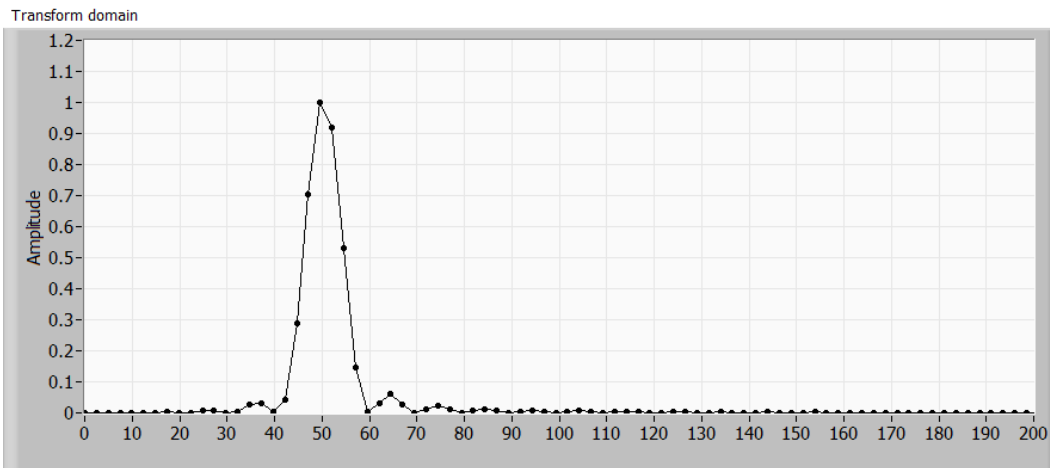


Figure 3.34 – Zero-padding to 4x. FFT.

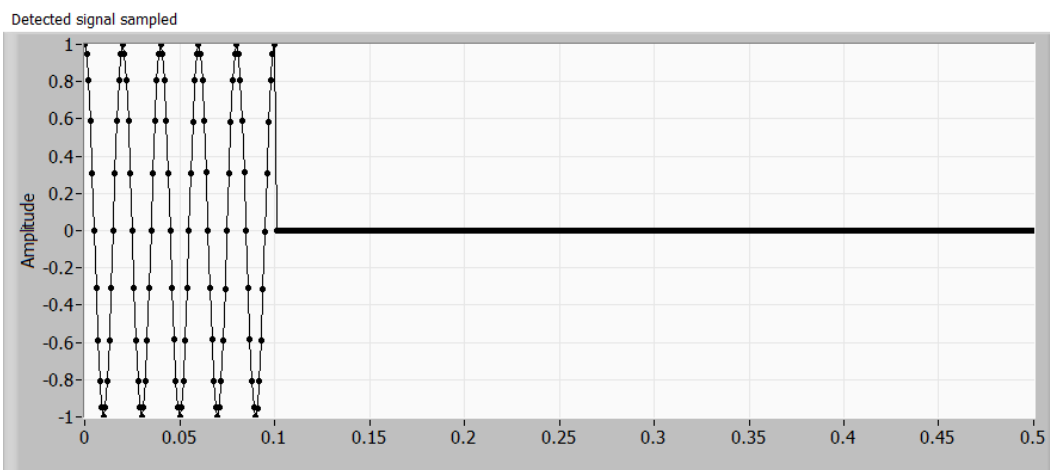


Figure 3.35 – Zero-padding to 5x. Time domain.

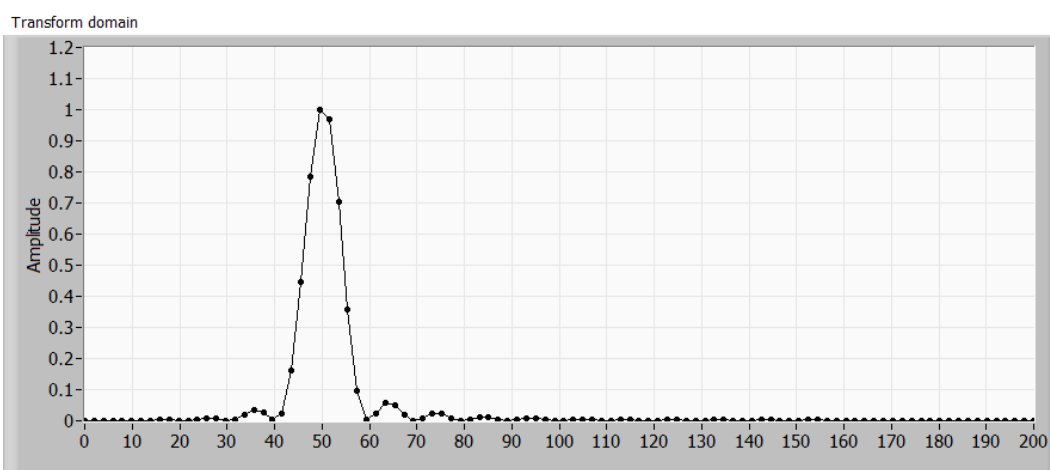


Figure 3.36 – Zero-padding to 5x. FFT.

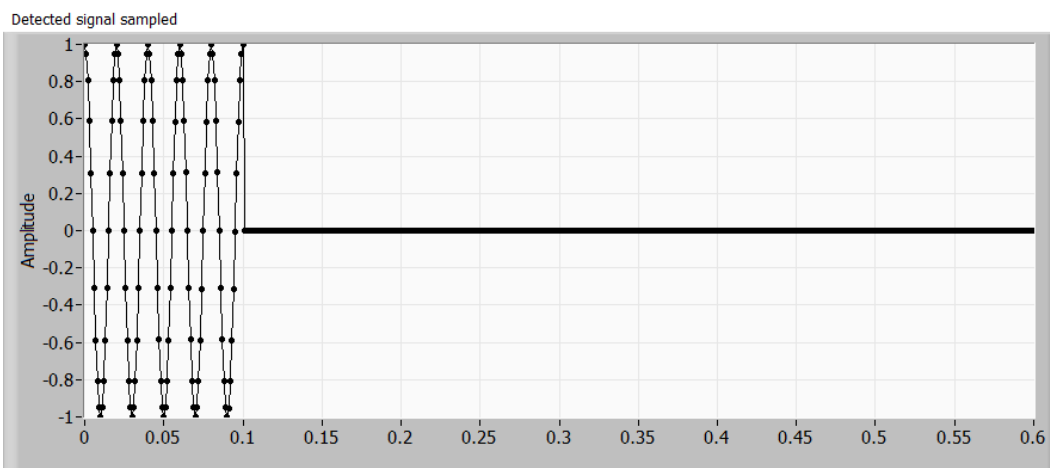


Figure 3.37 – Zero-padding to 6x. Time domain.

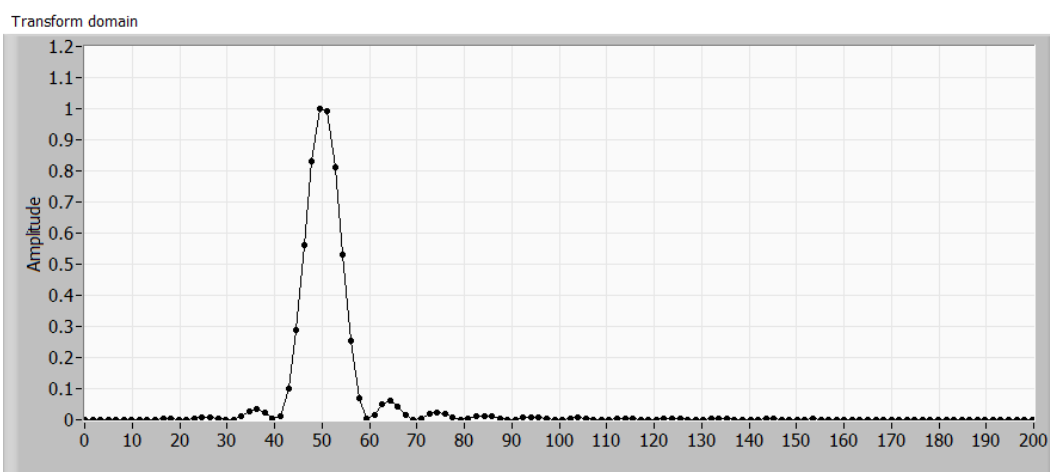


Figure 3.38 – Zero-padding to 6x. FFT.

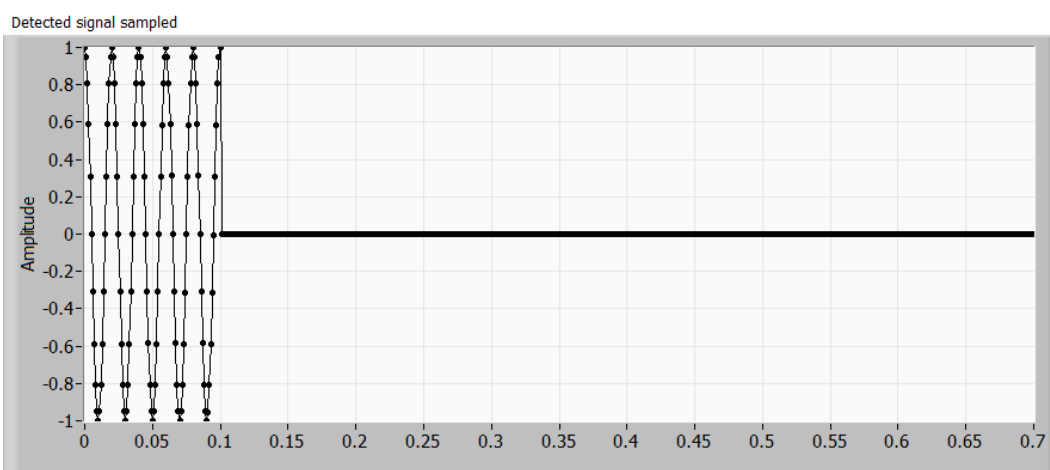


Figure 3.39 – Zero-padding to 7x. Time domain.

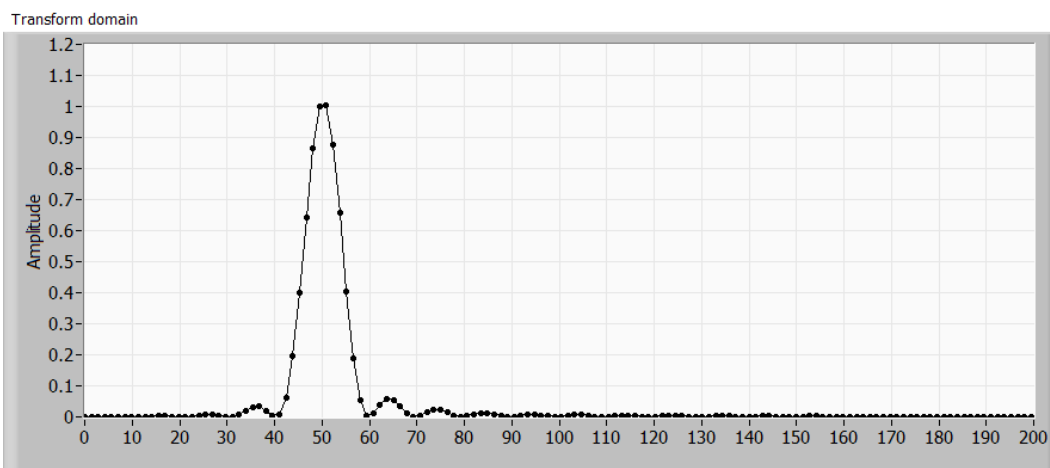


Figure 3.40 – Zero-padding to 7x. FFT.

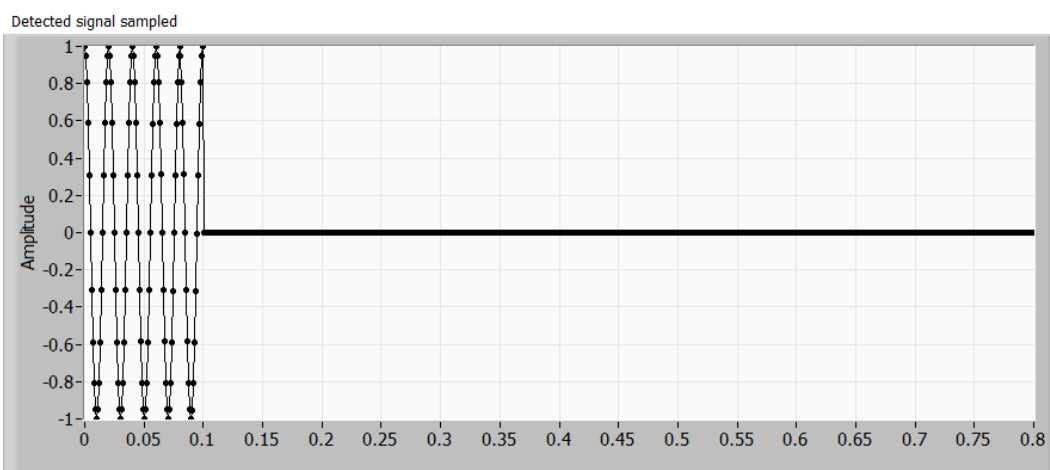


Figure 3.41 – Zero-padding to 8x. Time domain.

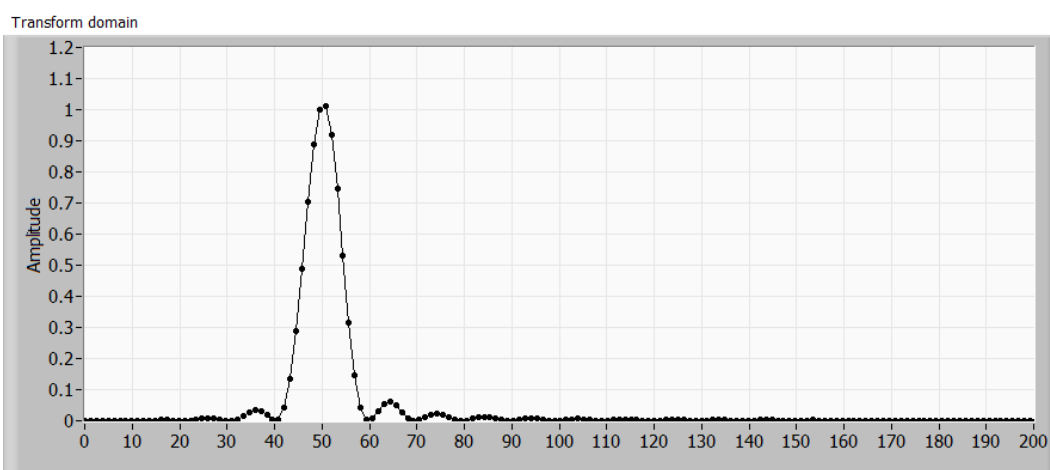


Figure 3.42 – Zero-padding to 8x. FFT.

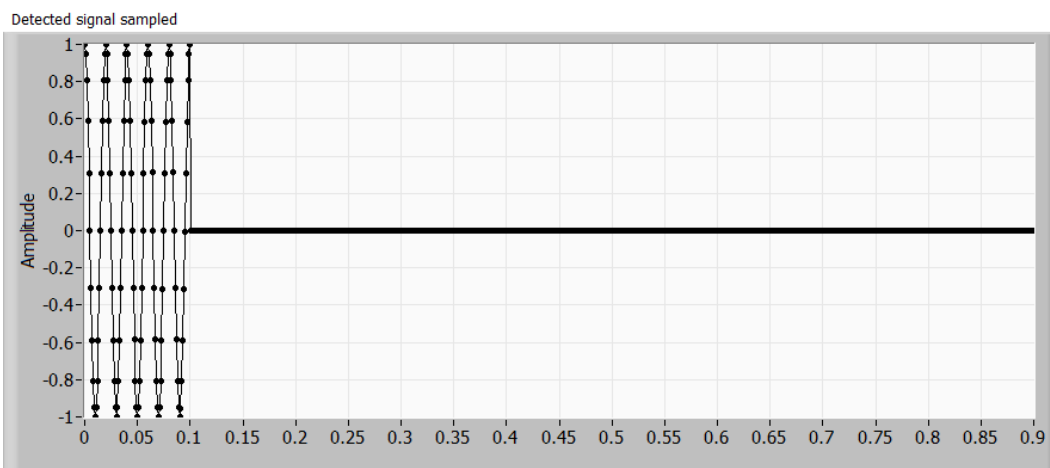


Figure 3.43 – Zero-padding to 9x. Time domain.

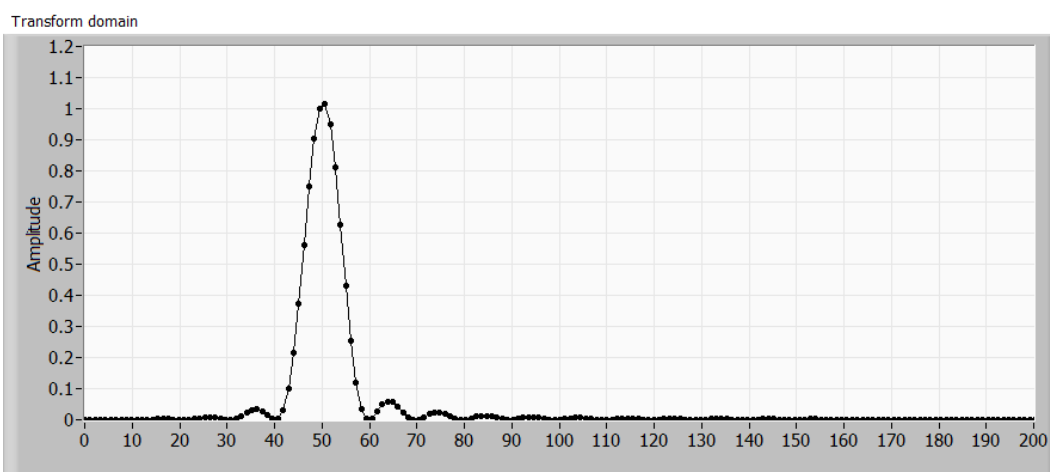


Figure 3.44 – Zero-padding to 9x. FFT.

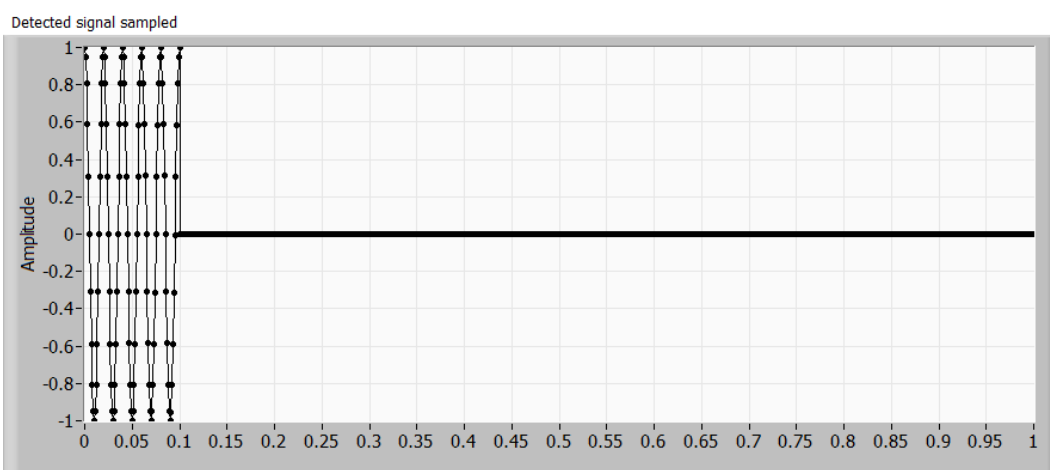


Figure 3.45 – Zero-padding to 10x. Time domain.

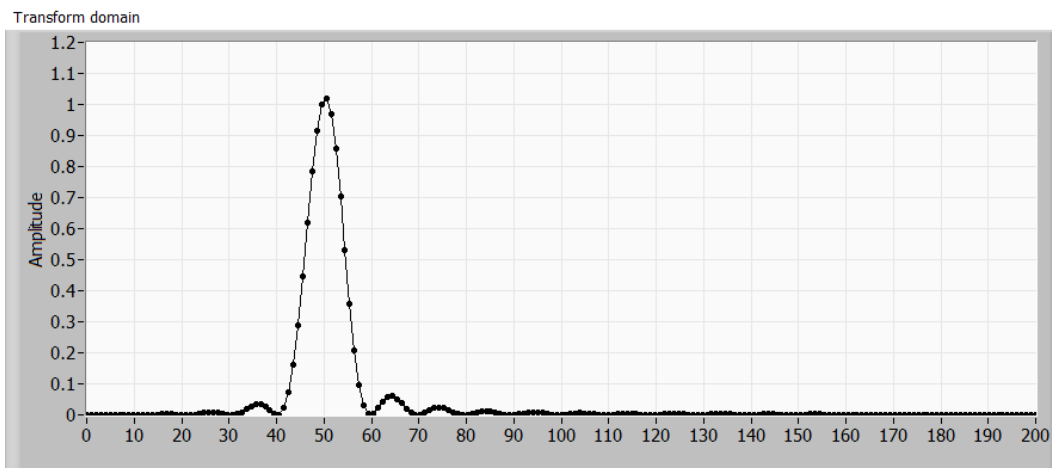


Figure 3.46 – Zero-padding to 10x. FFT.

3.3.

Non-integer number of samples with zero padding

If we revisit the integer and non-integer number of cycle data and apply a 10x zero padding we will see that the FFT is now consistent and allows a much more precise determination of location.

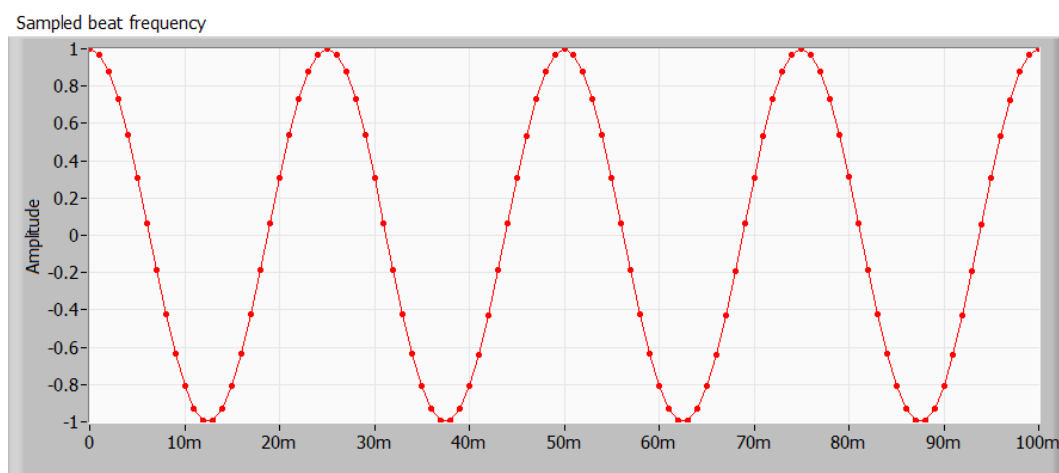


Figure 3.47 – Integer number of cycles with zero-padding. Time domain.

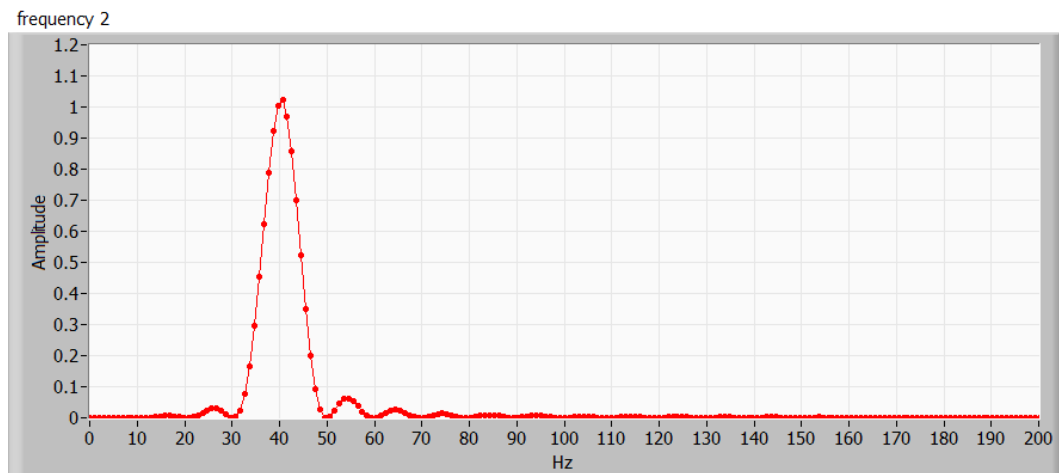


Figure 3.48 – Integer number of cycles with zero-padding. FFT.

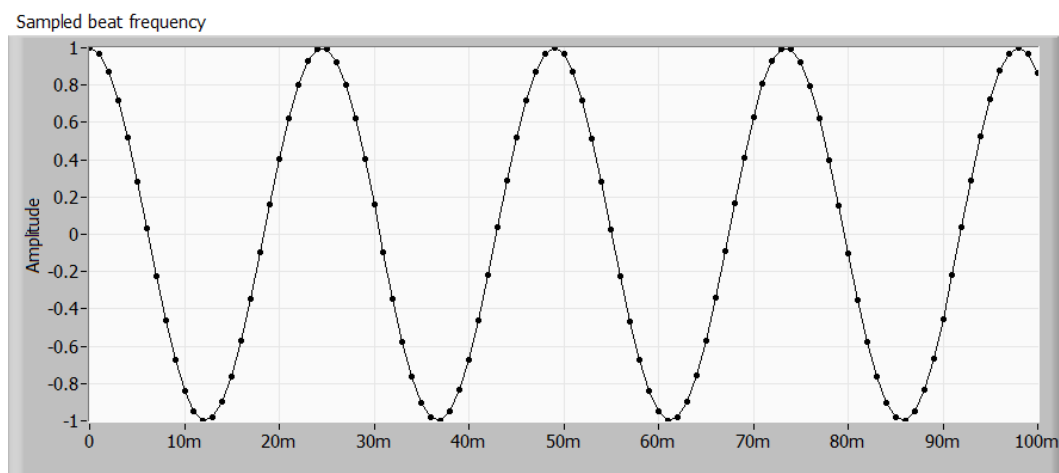


Figure 3.49 – Non-integer. 1/12 of a cycle extra with zero-padding.

Time domain.

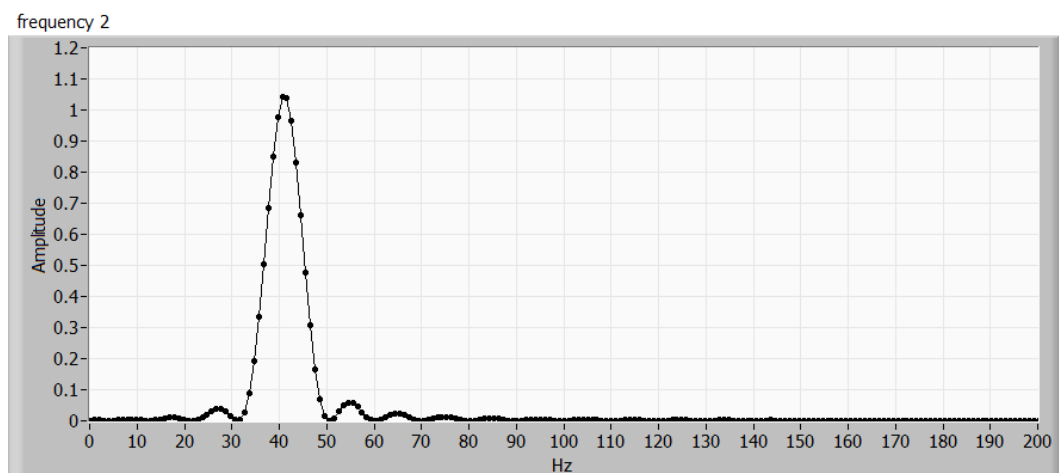


Figure 3.50 – Non-integer. 1/12 of a cycle extra with zero-padding.

FFT.

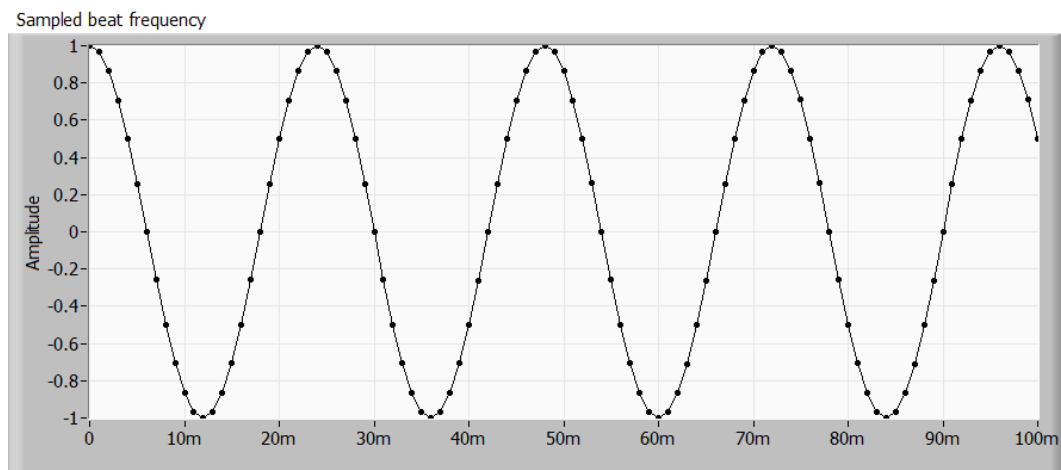


Figure 3.51 – Non-integer. $2/12$ of a cycle extra. Zero padding. Time domain.

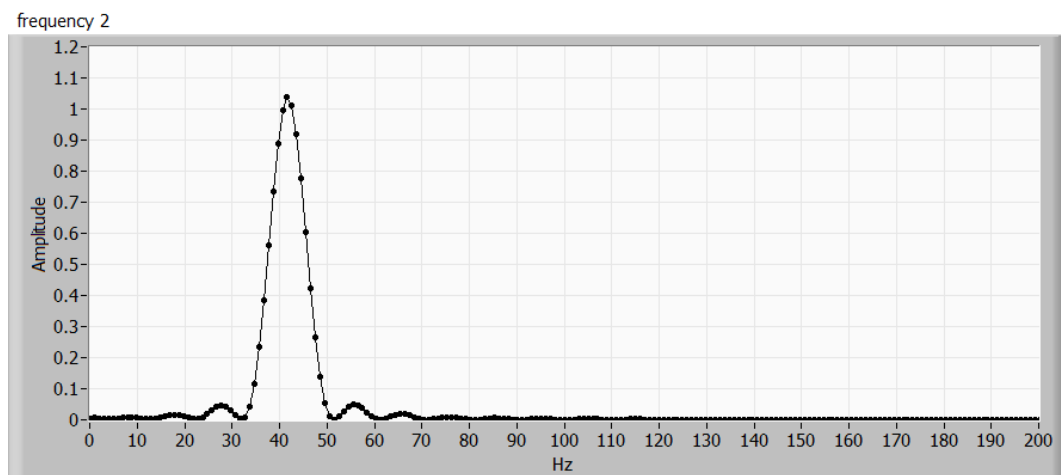


Figure 3.52 – Non-integer. $2/12$ of a cycle extra. Zero-padding. FFT.

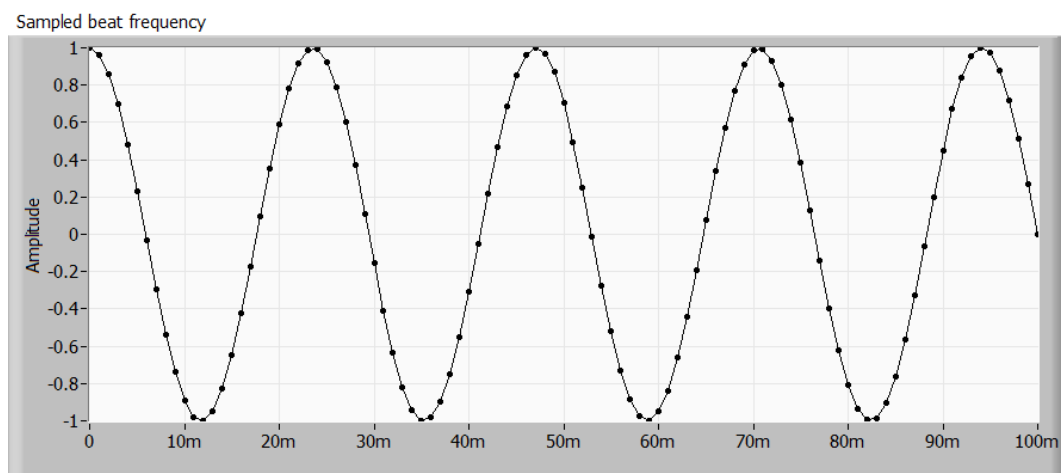


Figure 3.53 – Non-integer. $3/12$ of a cycle extra. Zero-padding. Time domain.

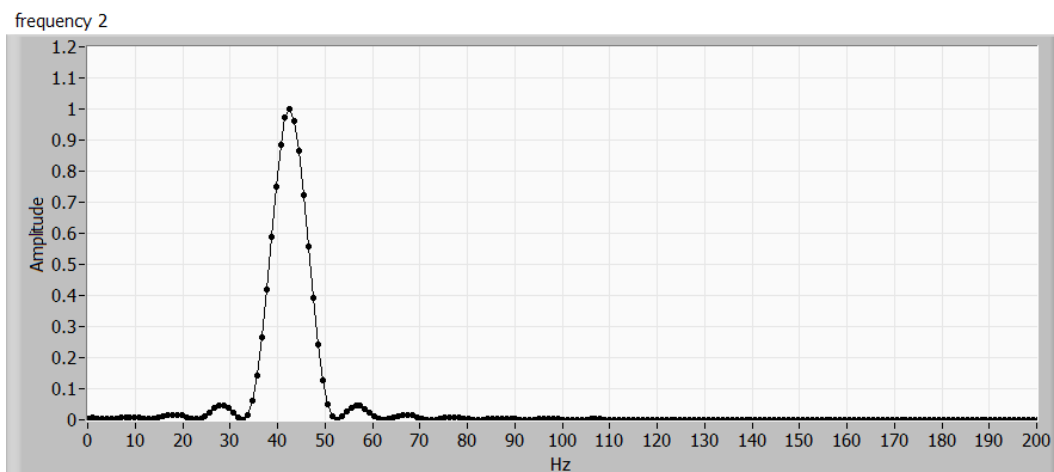


Figure 3.54 – Non-integer. $3/12$ of a cycle extra. Zero-padding. FFT.

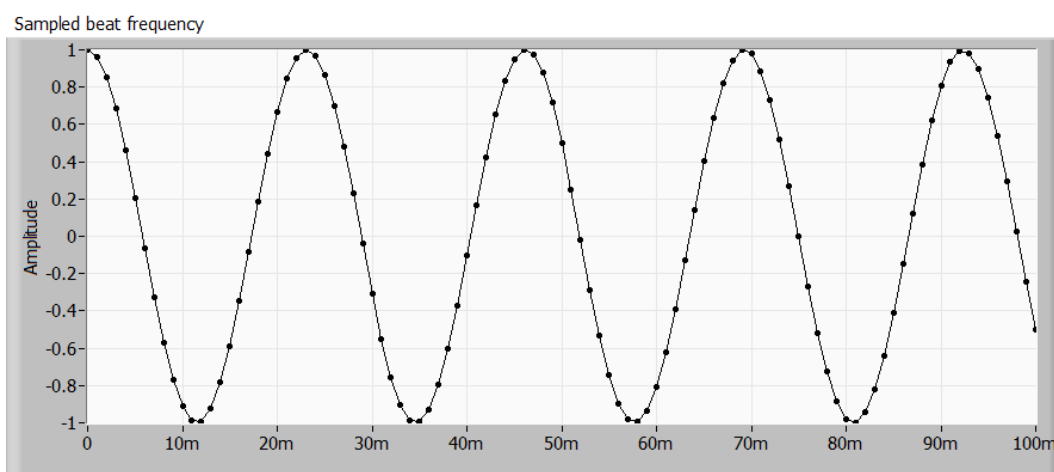


Figure 3.55 – Non-integer. $4/12$ of a cycle extra. Zero-padding. Time domain.

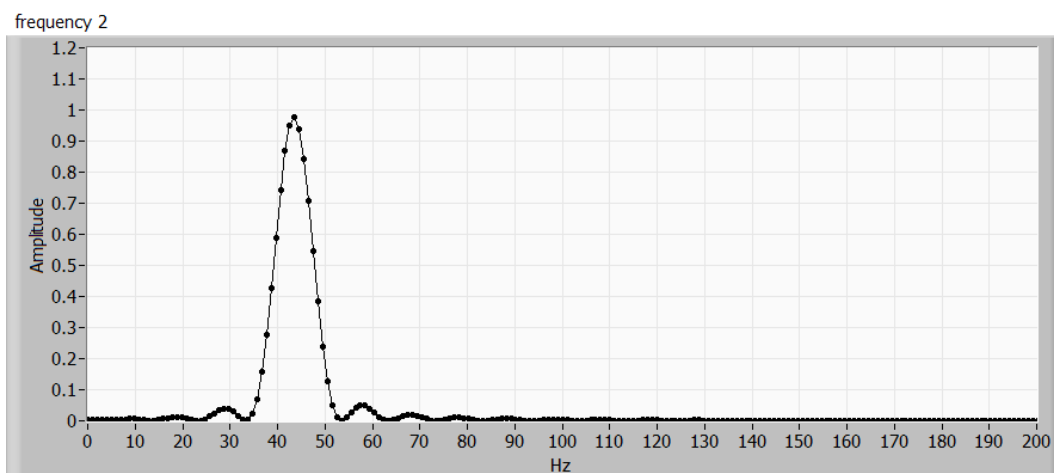


Figure 3.56 – Non-integer. $4/12$ of a cycle extra. Zero-padding. FFT.

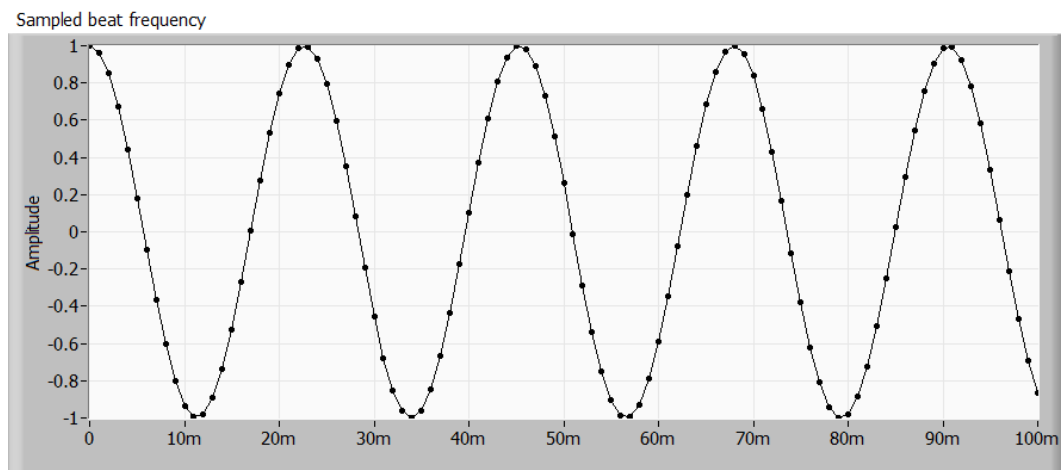


Figure 3.57 – Non-integer. $5/12$ of a cycle extra. Zero-padding. Time domain.

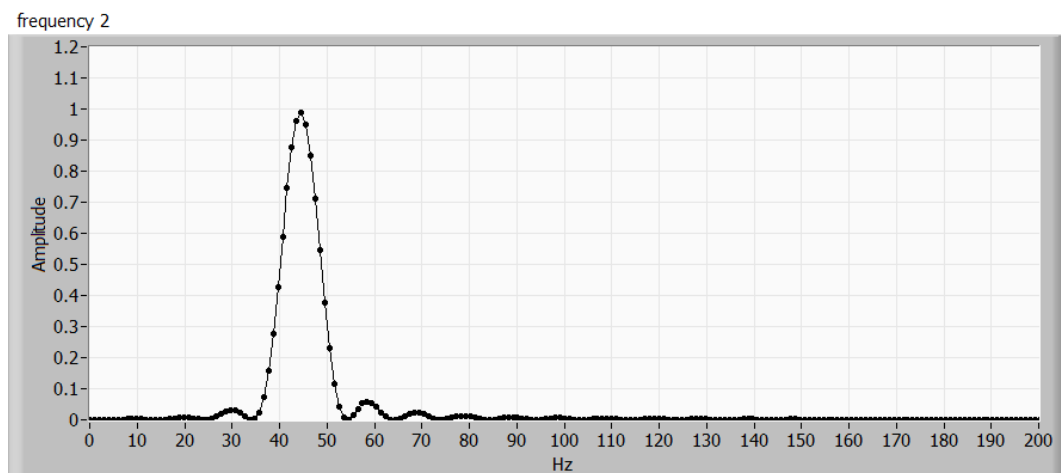


Figure 3.58 – Non-integer. $5/12$ of a cycle extra. Zero-padding. FFT.

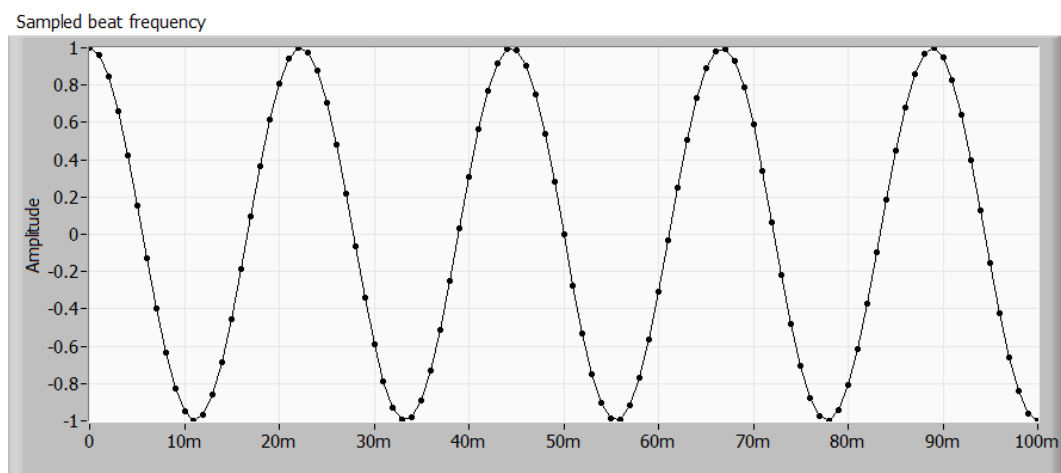


Figure 3.59 – Non-integer. $6/12$ of a cycle extra. Zero-padding. Time domain.

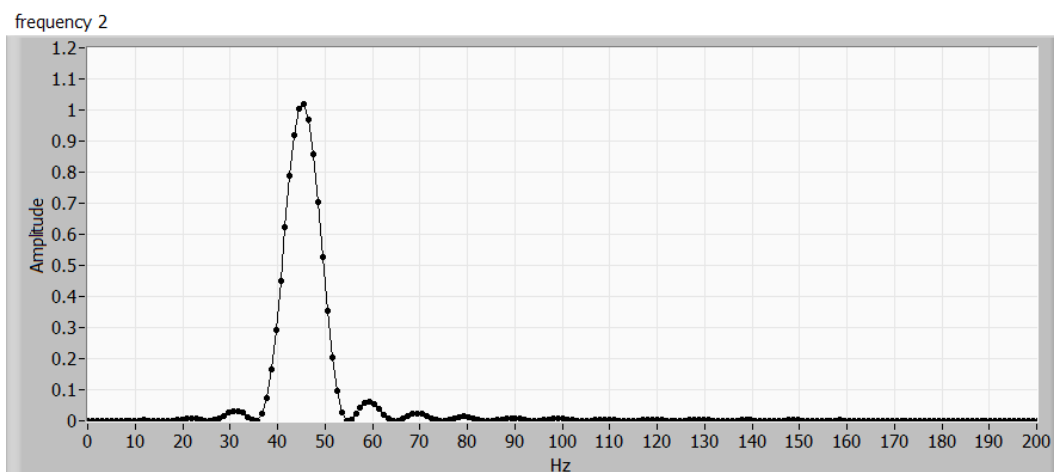


Figure 3.60 – Non-integer. 6/12 of a cycle extra. Zero-padding. FFT.

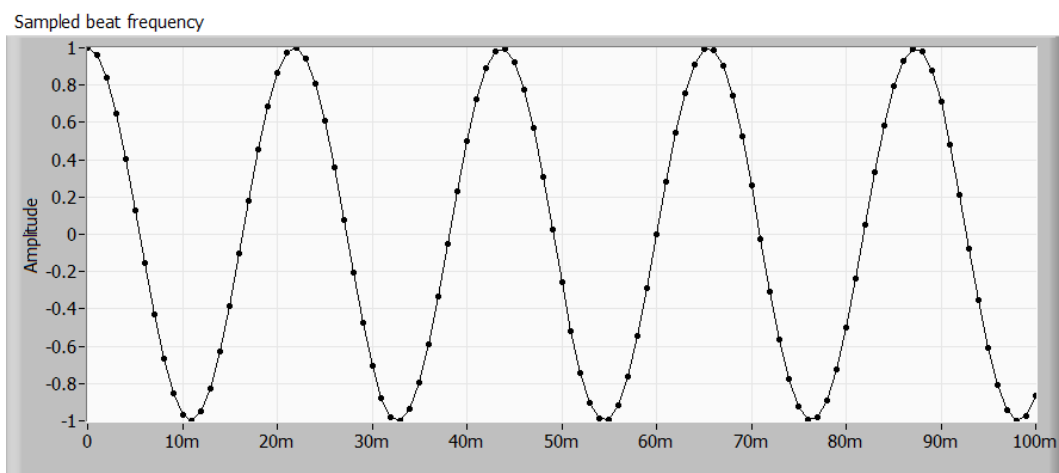


Figure 3.61 – Non-integer. 7/12 of a cycle extra. Zero-padding. Time domain.

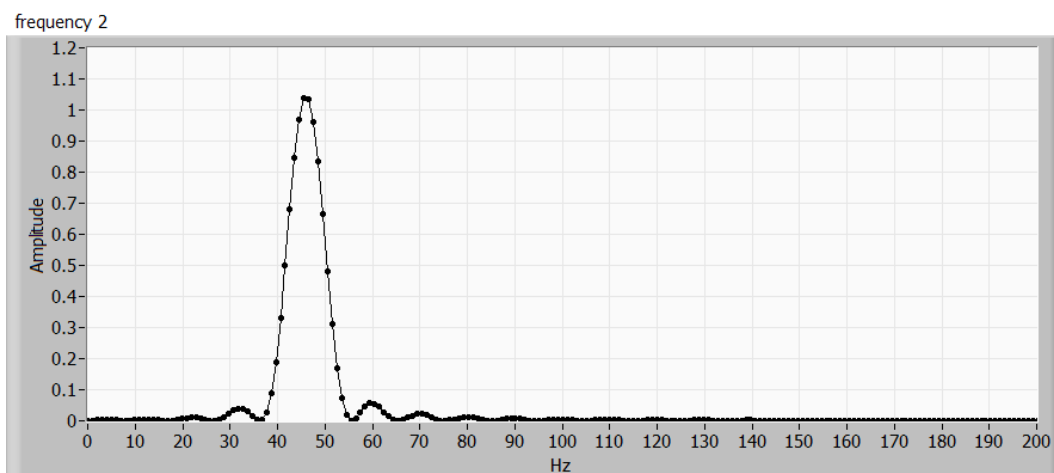


Figure 3.62 – Non-integer. 7/12 of a cycle extra. Zero-padding. FFT.

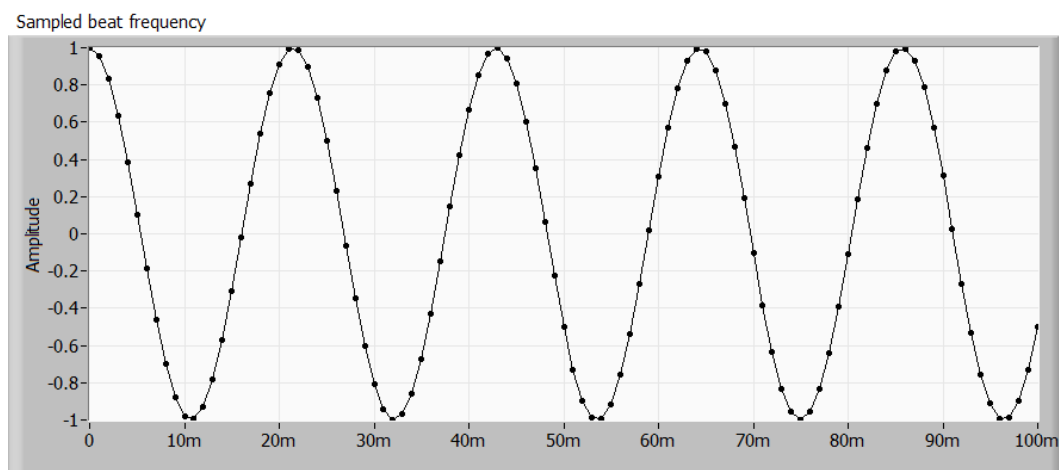


Figure 3.63 – Non-integer. 8/12 of a cycle extra. Zero-padding. Time domain.

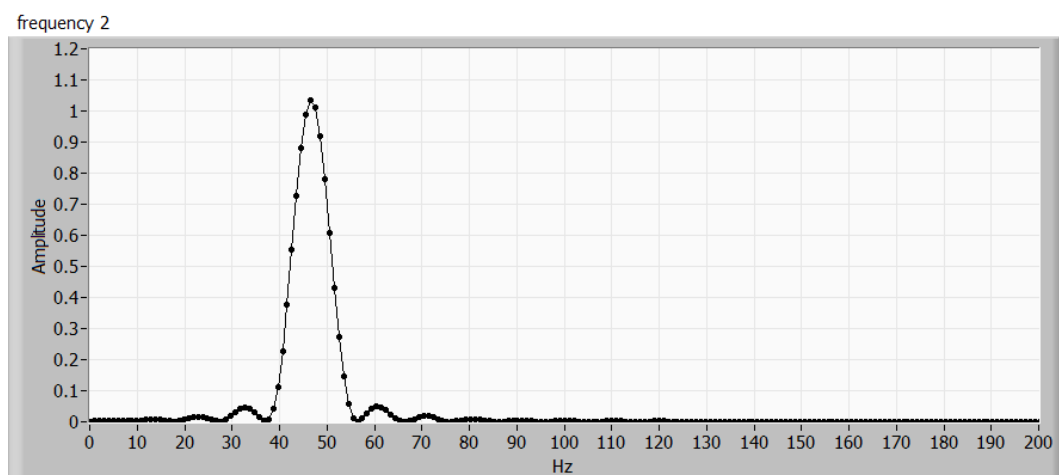


Figure 3.64 – Non-integer. 8/12 of a cycle extra. Zero-padding. FFT.

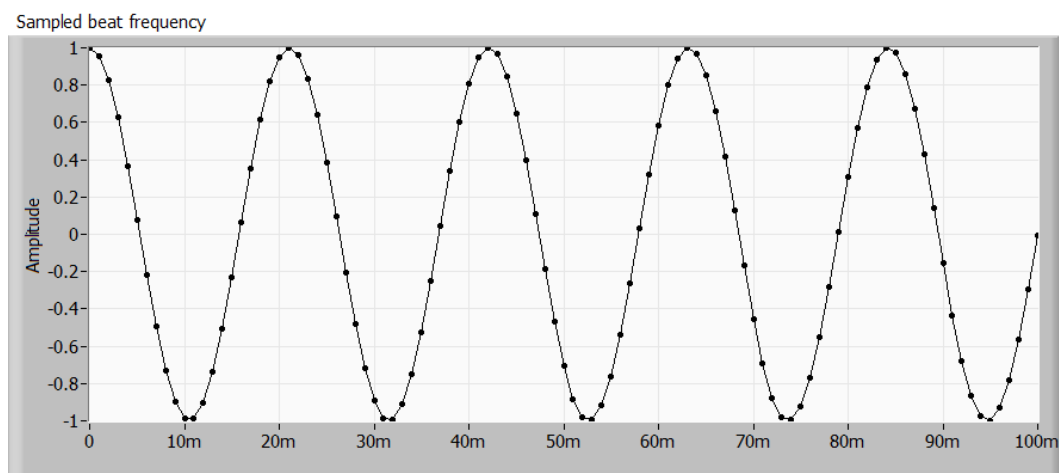


Figure 3.65 – Non-integer. 9/12 of a cycle extra. Zero-padding. Time domain.

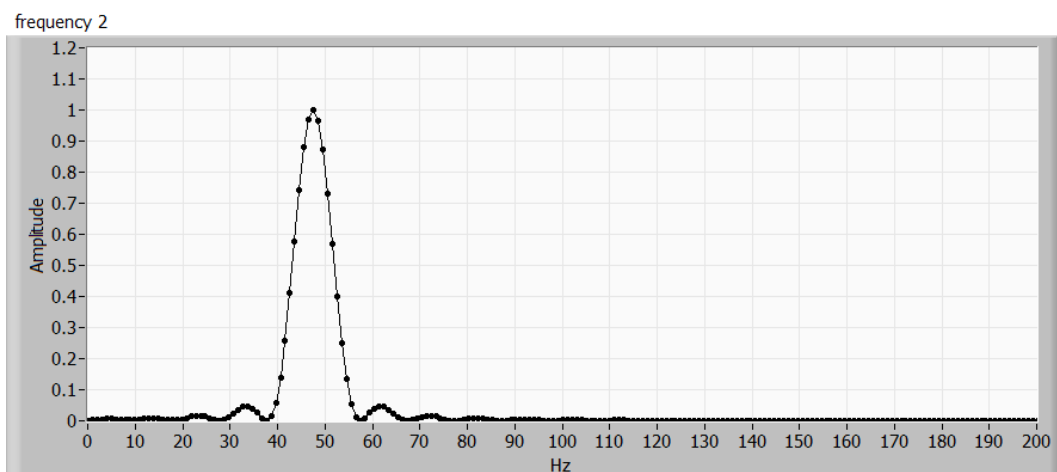


Figure 3.66 – Non-integer. 9/12 of a cycle extra. Zero-padding. FFT.

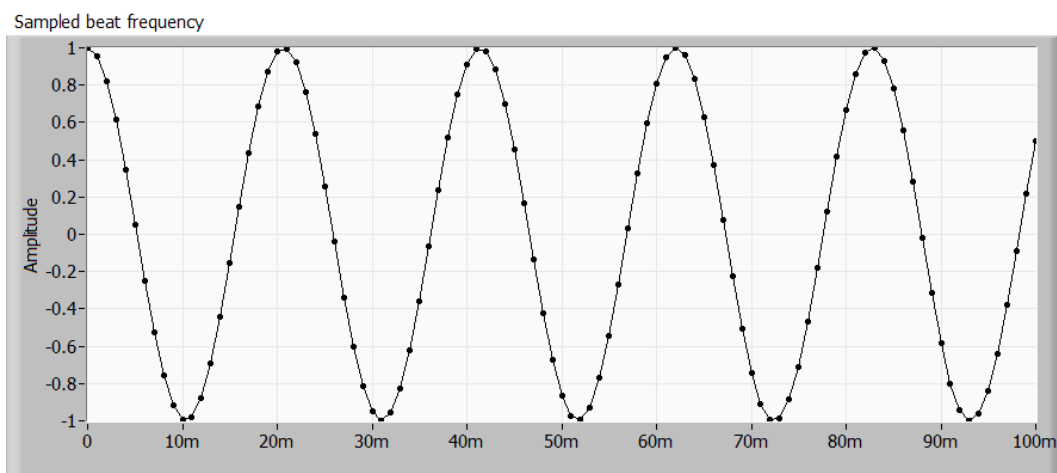


Figure 3.67 – Non-integer. 10/12 of a cycle extra. Zero-padding. Time domain.

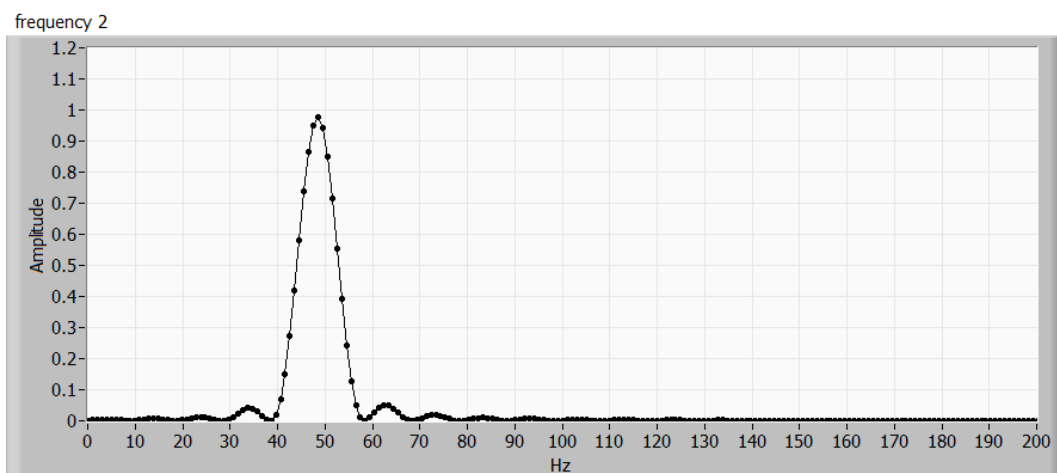


Figure 3.68 – Non-integer. 10/12 of a cycle extra. Zero-padding. FFT.

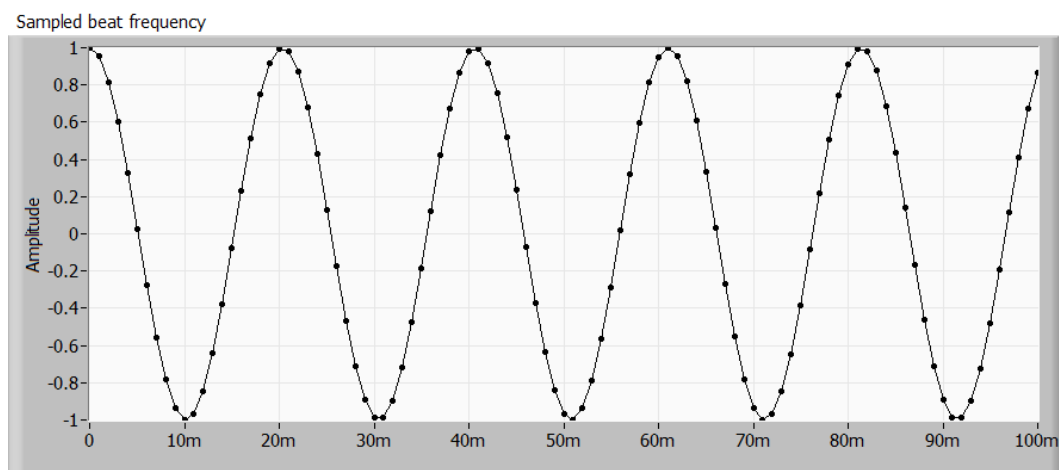


Figure 3.69 – Non-integer. 11/12 of a cycle extra. Zero-padding. Time domain.

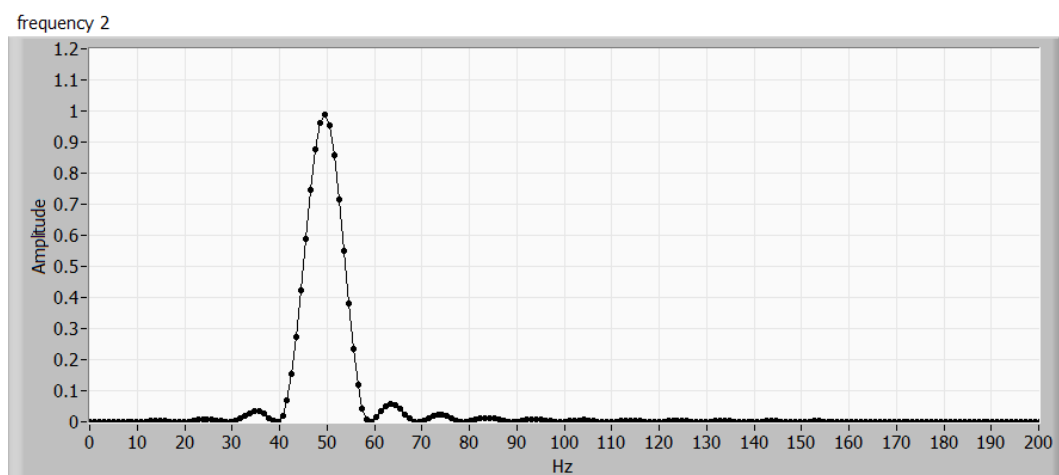


Figure 3.70 – Non-integer. 11/12 of a cycle extra. Zero-padding. FFT.

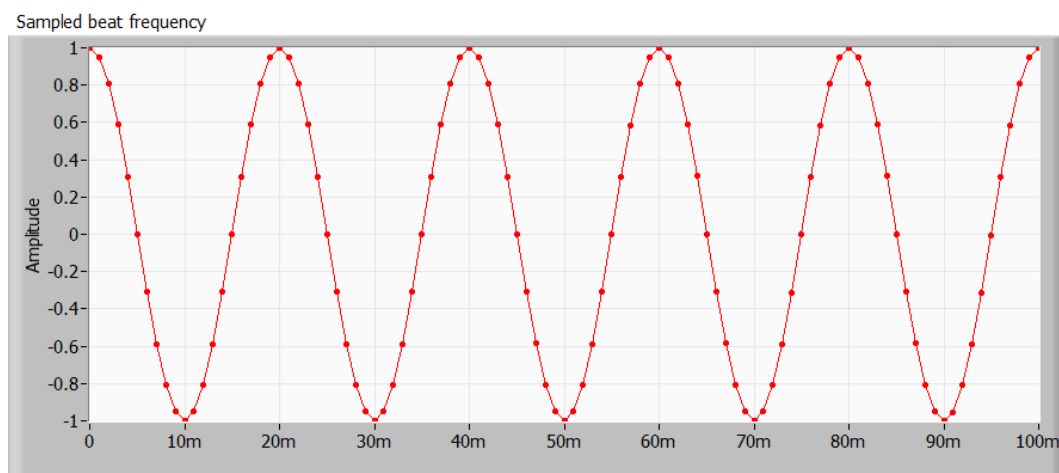


Figure 3.71 – Integer number of cycles with zero padding. One complete cycle more than in Figure 3.47. Time domain.

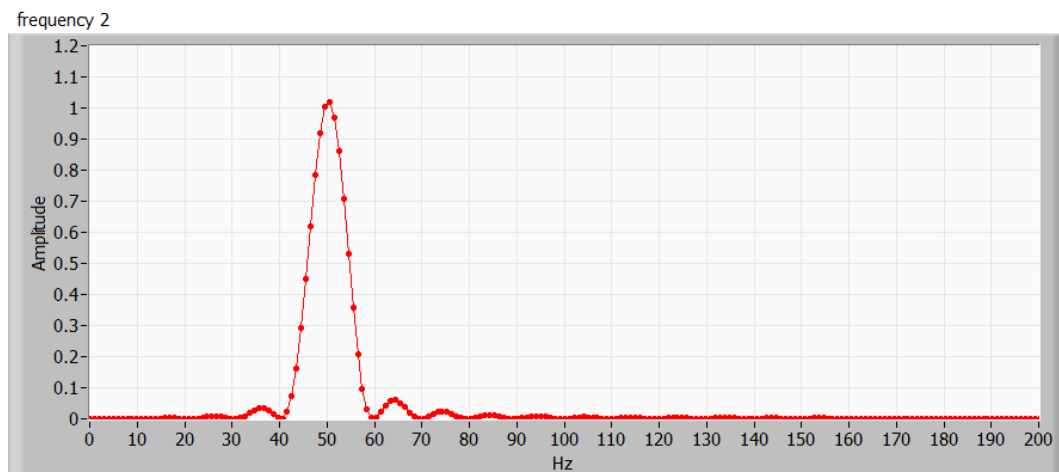


Figure 3.72 – Integer number of cycles with zero padding. One complete cycle more than in Figure 3.48. FFT.

3.4. Windowing

As mentioned earlier in section 3.2 on page 50, the data is usually multiplied by a window function before the FFT is applied. The purpose of the window is to take the endpoints of the data interval to zero in a smooth manner in order to reduce high frequency effects which affect neighboring signals. [Harris (1978)].

If no window is used the data still drops to zero but abruptly rather than smoothly. As we saw before, if the number of cycles is in integer number then this will not result in a excess FFT spreading, but in the general case one doesn't have control over this and so applying a window is a prudent idea.

The choice of the window must balance the full-width-half-max size (FWHM) of the FFT against the side-lobe amplitude; roughly a tradeoff between certainty in position and effect on more distant neighbors.

In order to get a sense of these two effects Figure 3.73 to Figure 3.91 show a windowed signal as well as its FFT in a linear and log scale. The linear scale is useful to see the FWHM while the reach side to side is more apparent in log scale

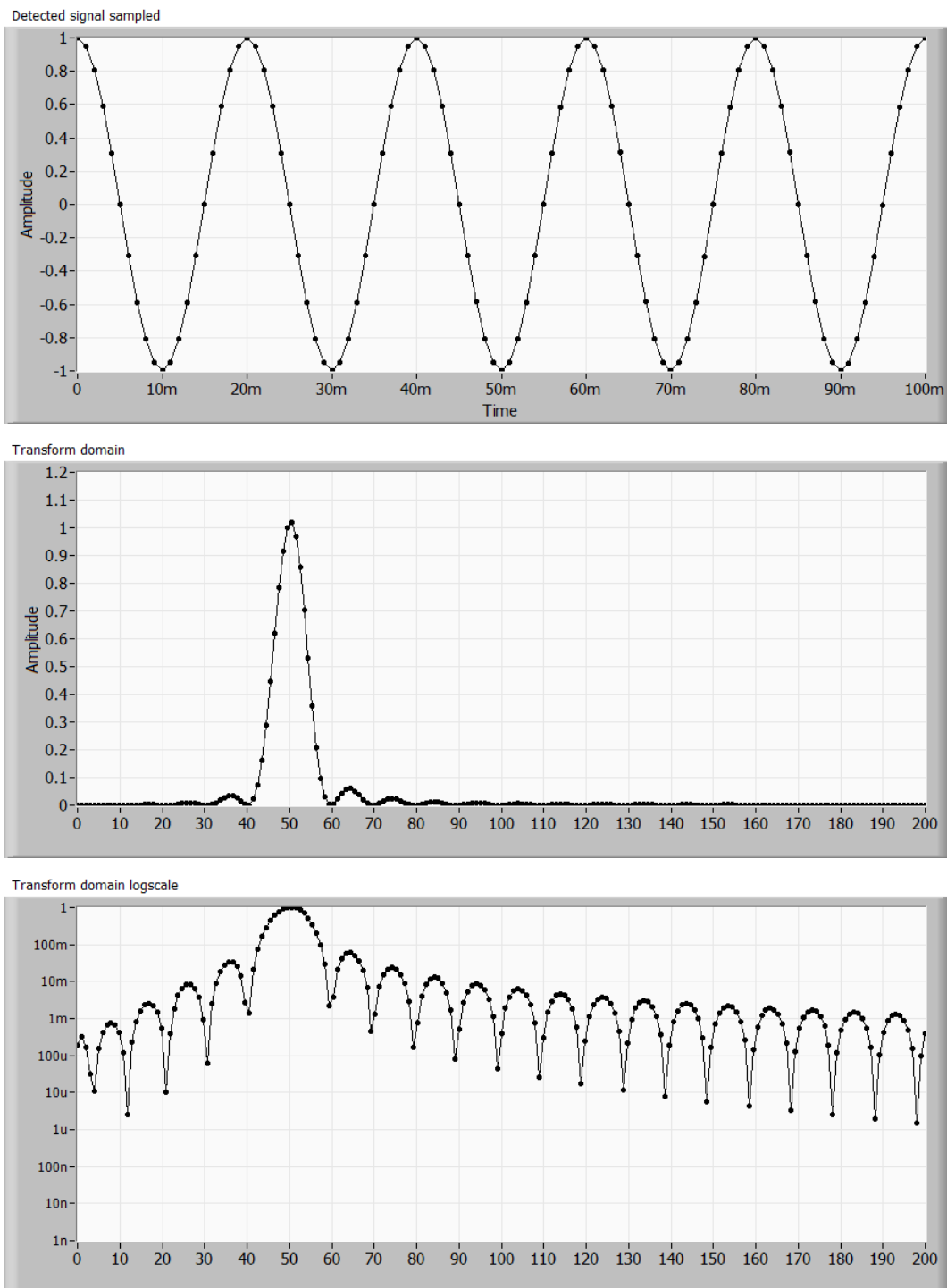


Figure 3.73 – Window: Rectangular. A) Time domain, B) FFT linear scale, C) FFT log scale

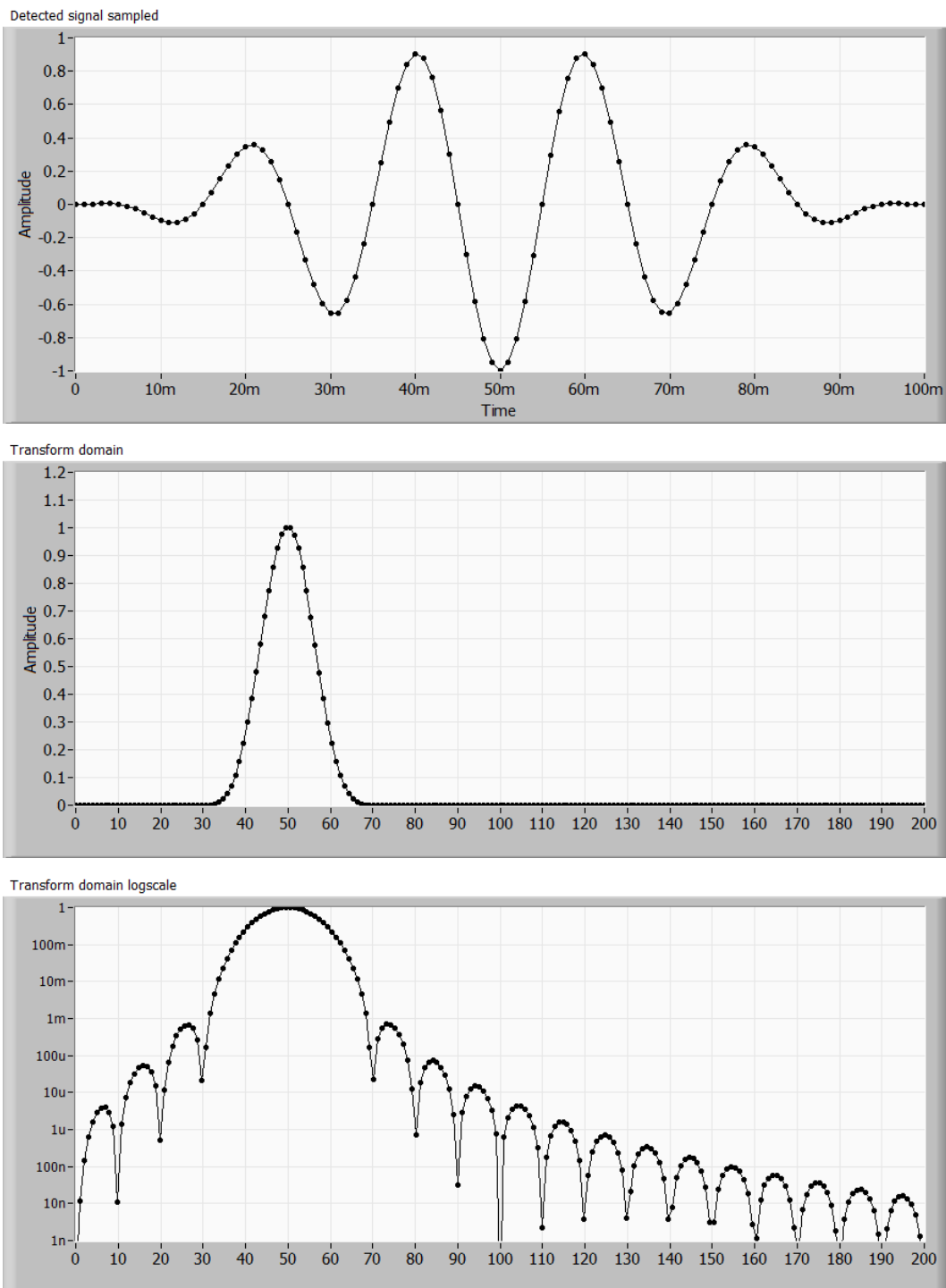


Figure 3.74 – Window: Hanning. A) Time domain, B) FFT linear scale, C) FFT log scale

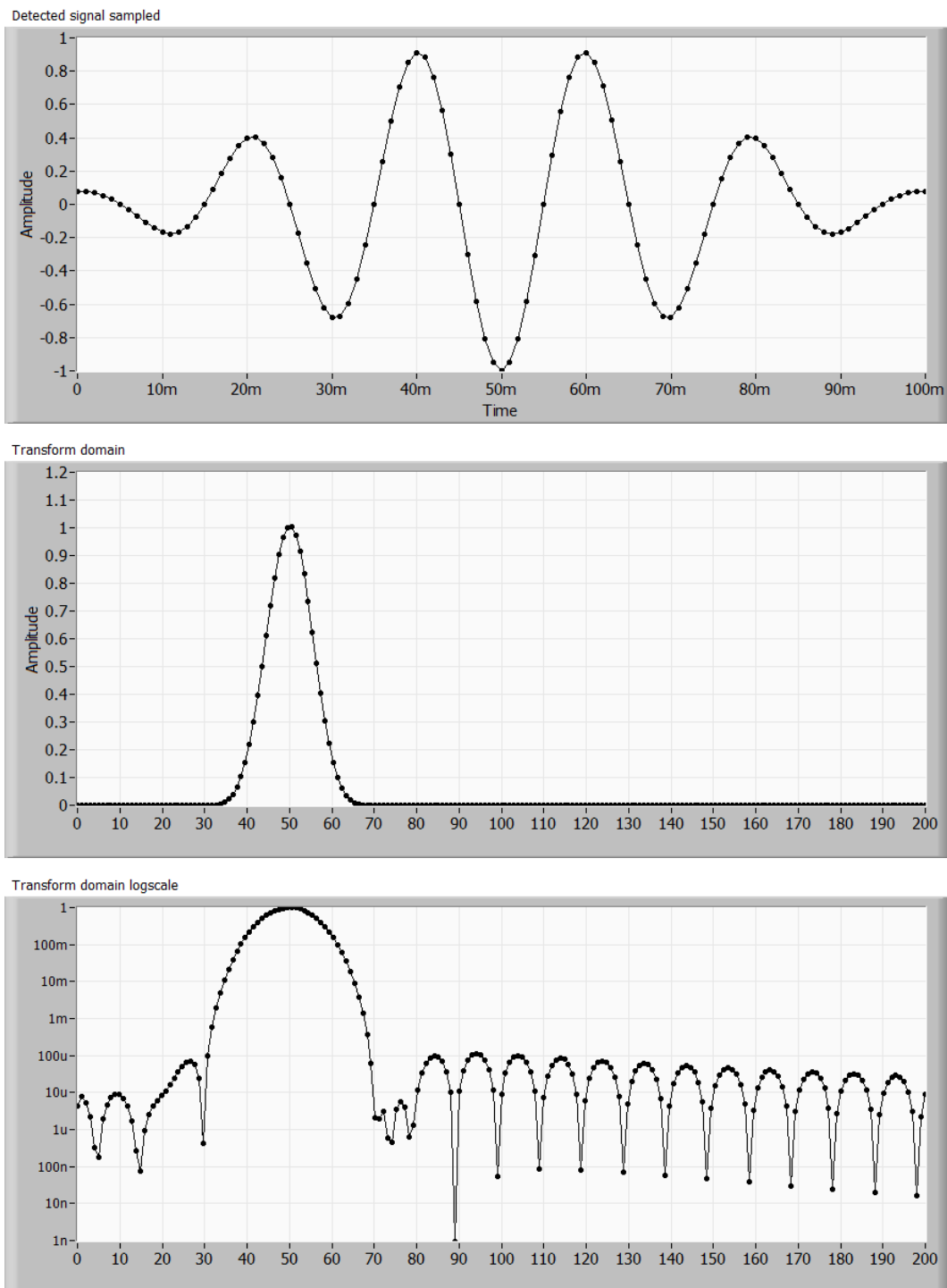


Figure 3.75 – Window: Hamming. A) Time domain, B) FFT linear scale, C) FFT log scale

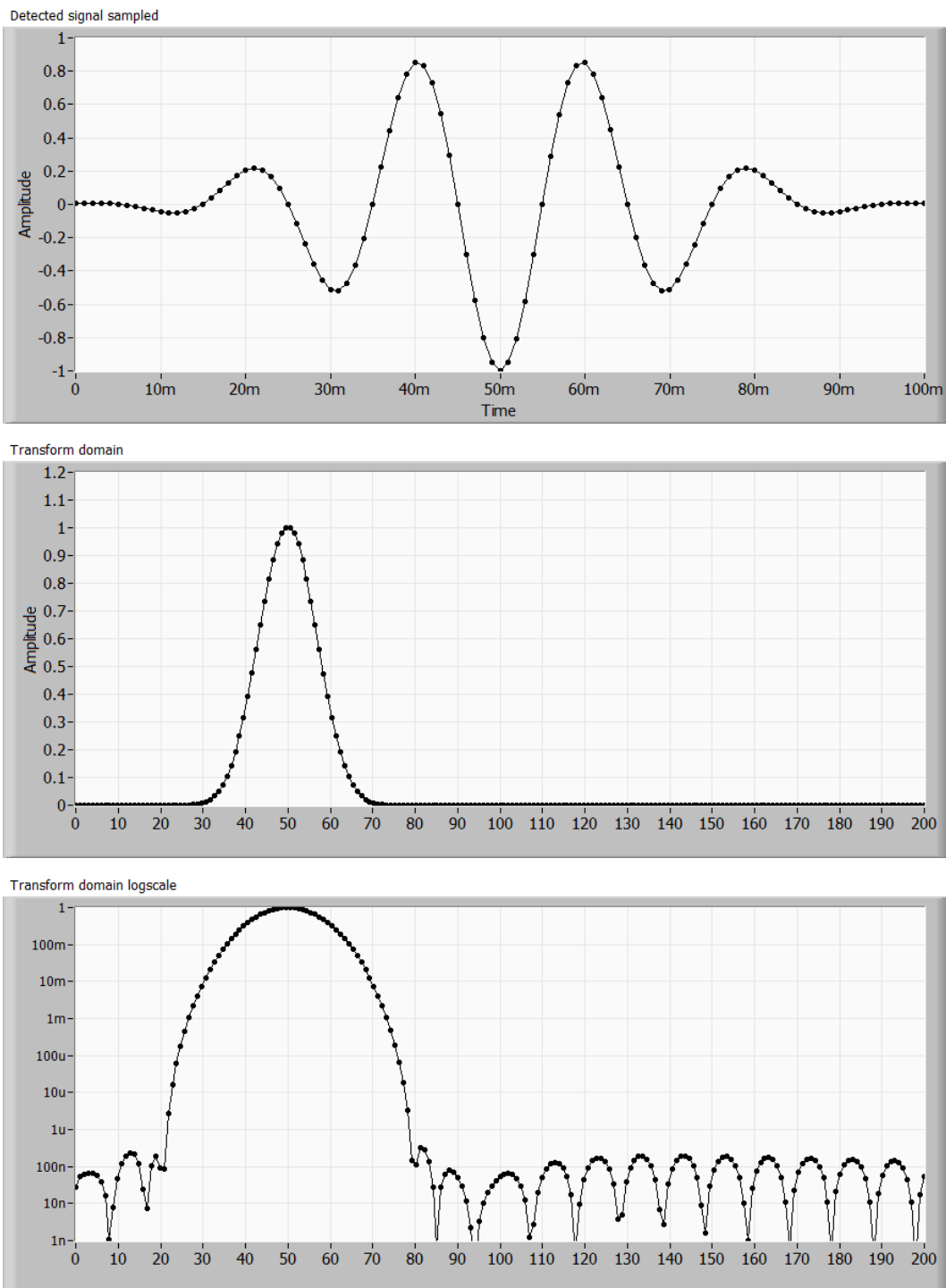


Figure 3.76 – Window: Blackman-Harris. A) Time domain, B) FFT linear scale, C) FFT log scale

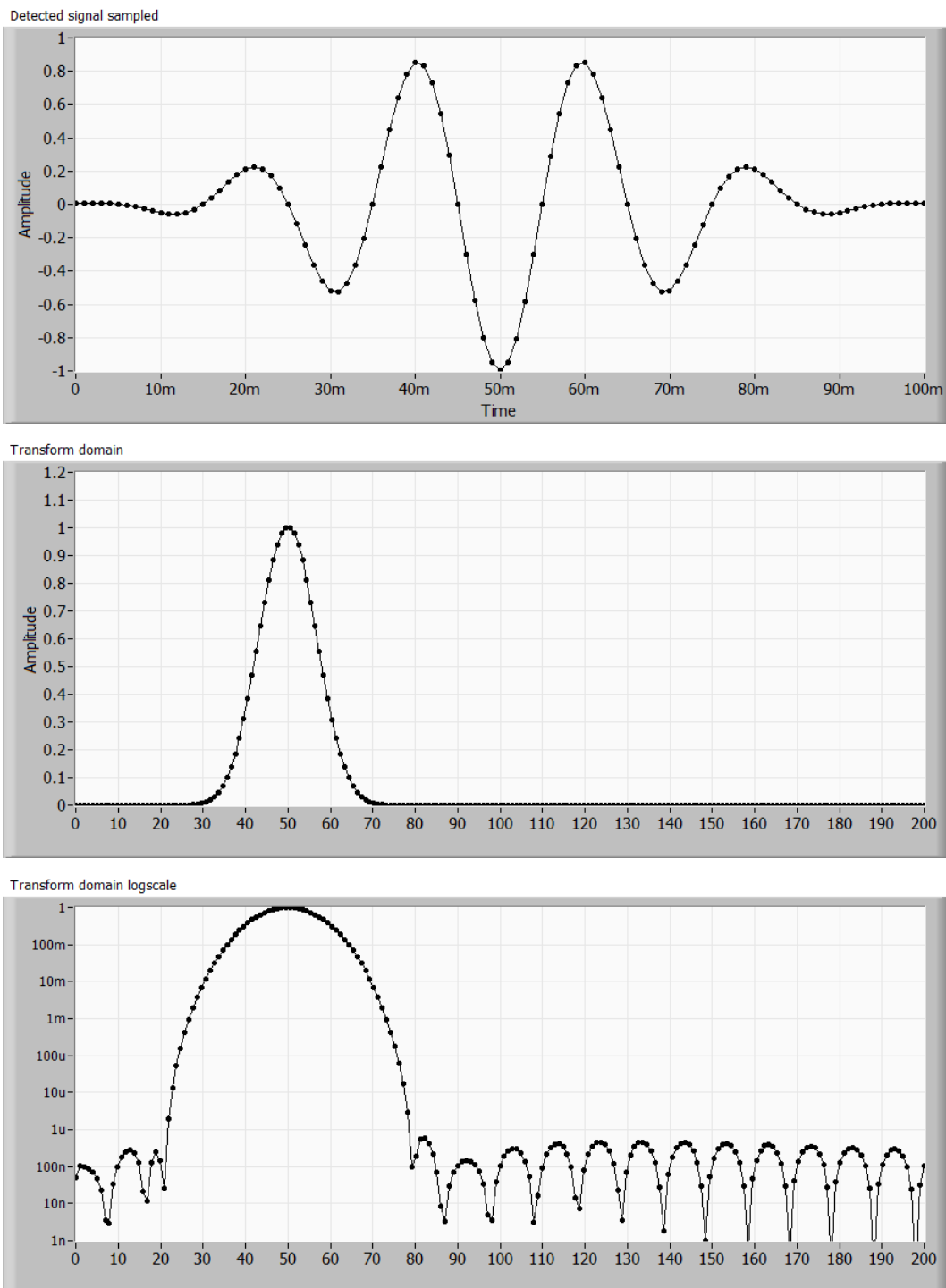


Figure 3.77 – Window: Exact Blackman. A) Time domain, B) FFT linear scale, C) FFT log scale

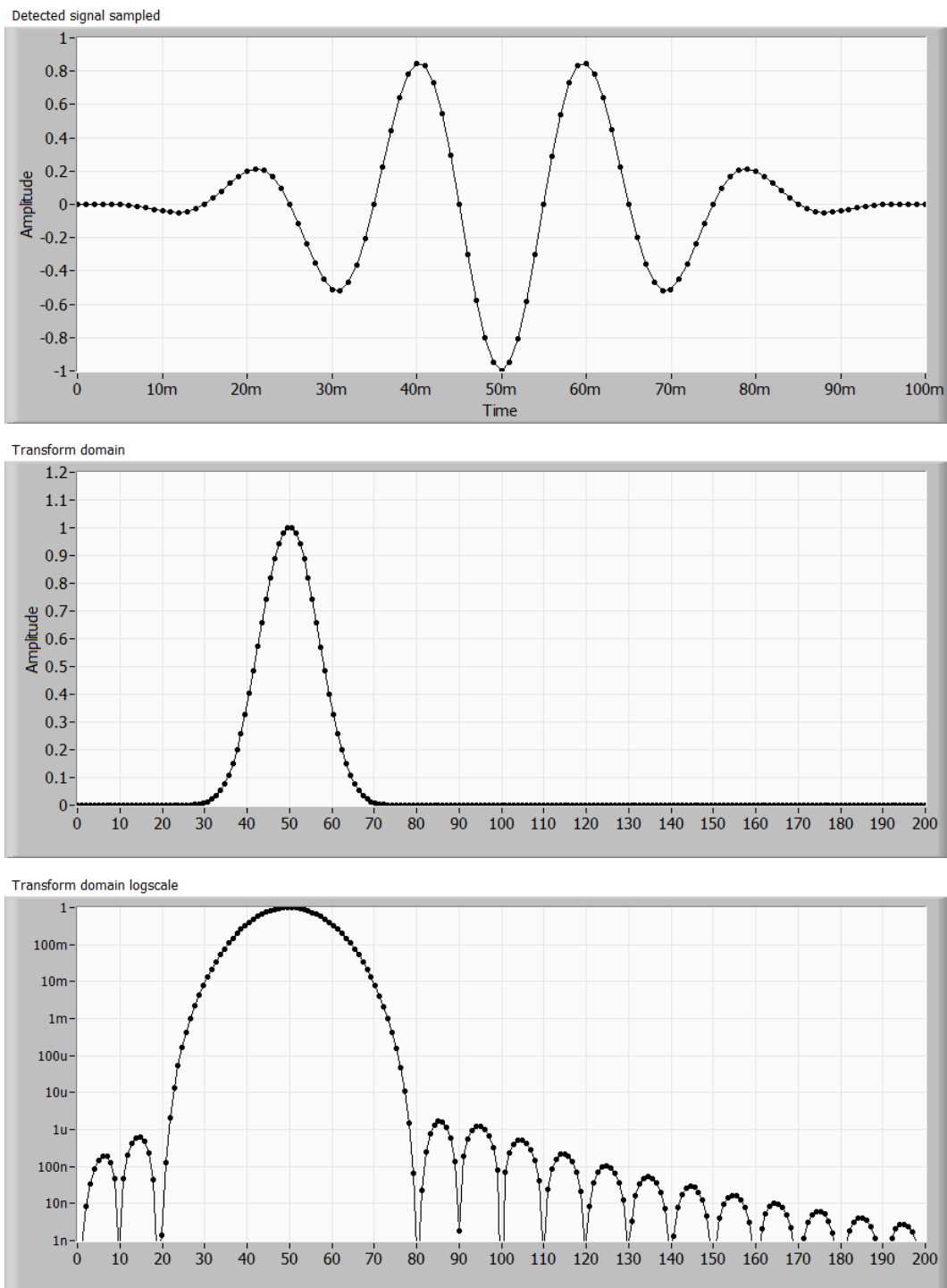


Figure 3.78 – Window: Blackman. A) Time domain, B) FFT linear scale, C) FFT log scale

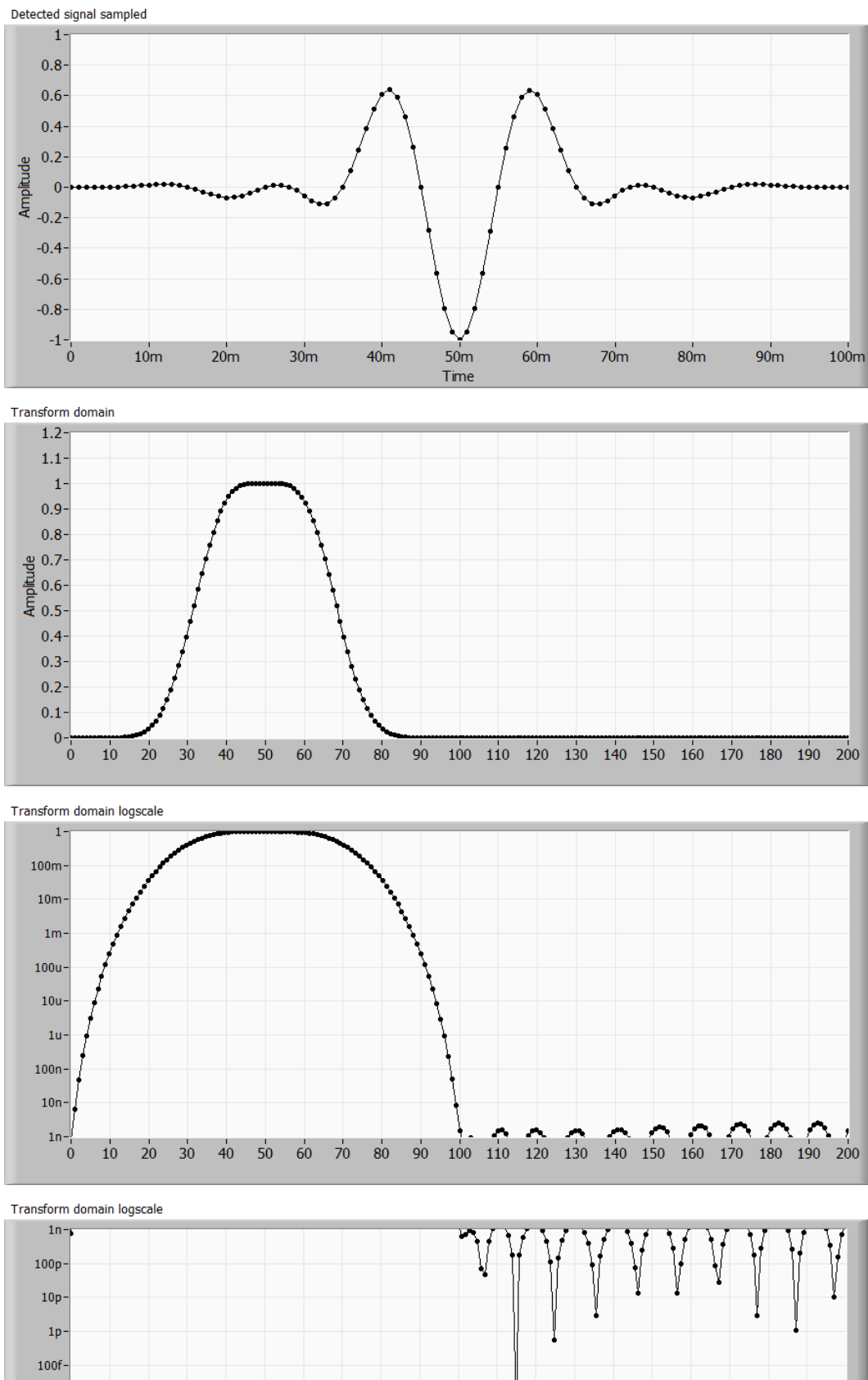


Figure 3.79 – Window: Flattop. A) Time domain, B) FFT linear scale, C1 and C2) FFT log scale

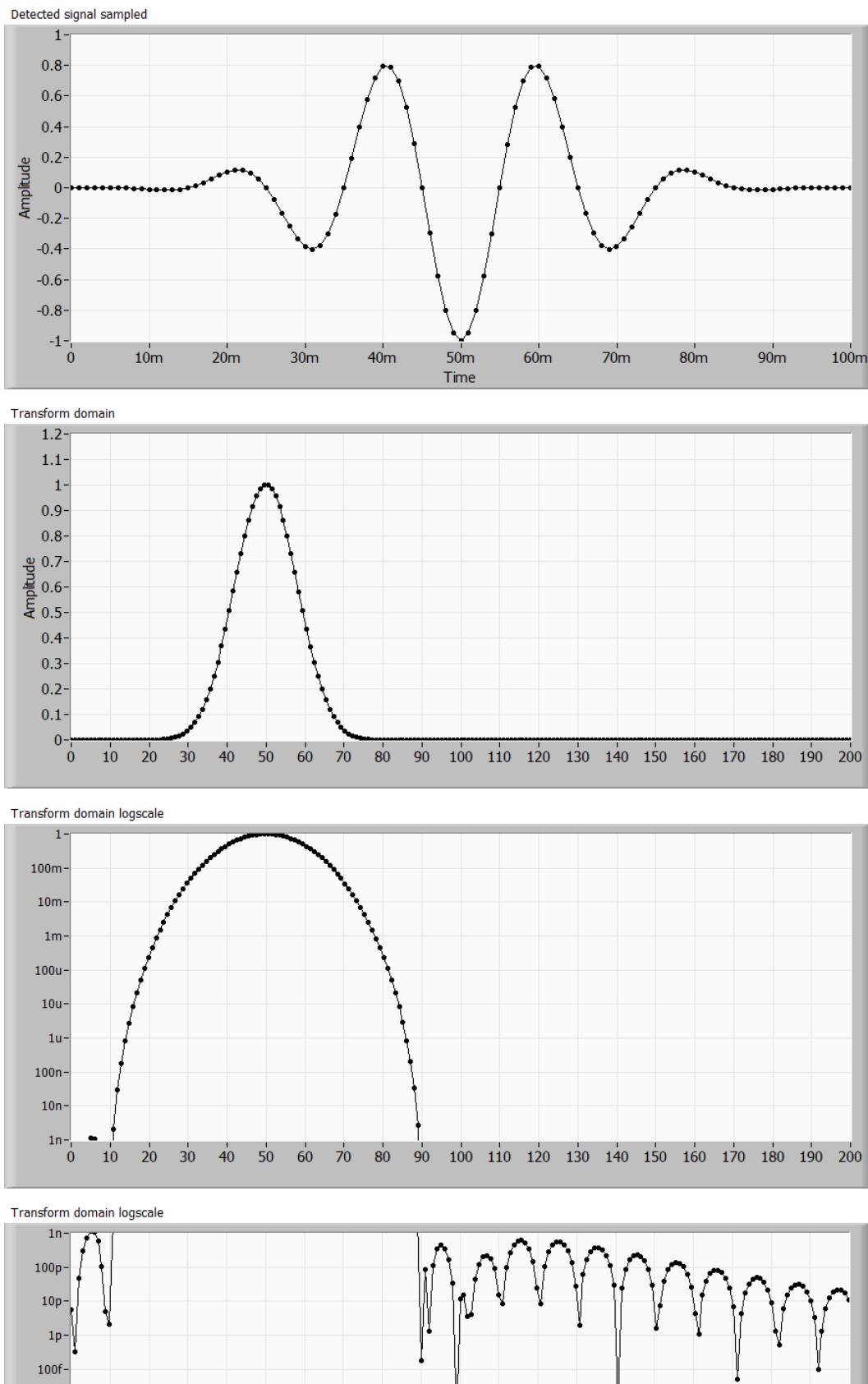


Figure 3.80 – Window: 4-term Blackman-Harris. A) Time domain, B) FFT linear scale, C1 and C2) FFT log scale

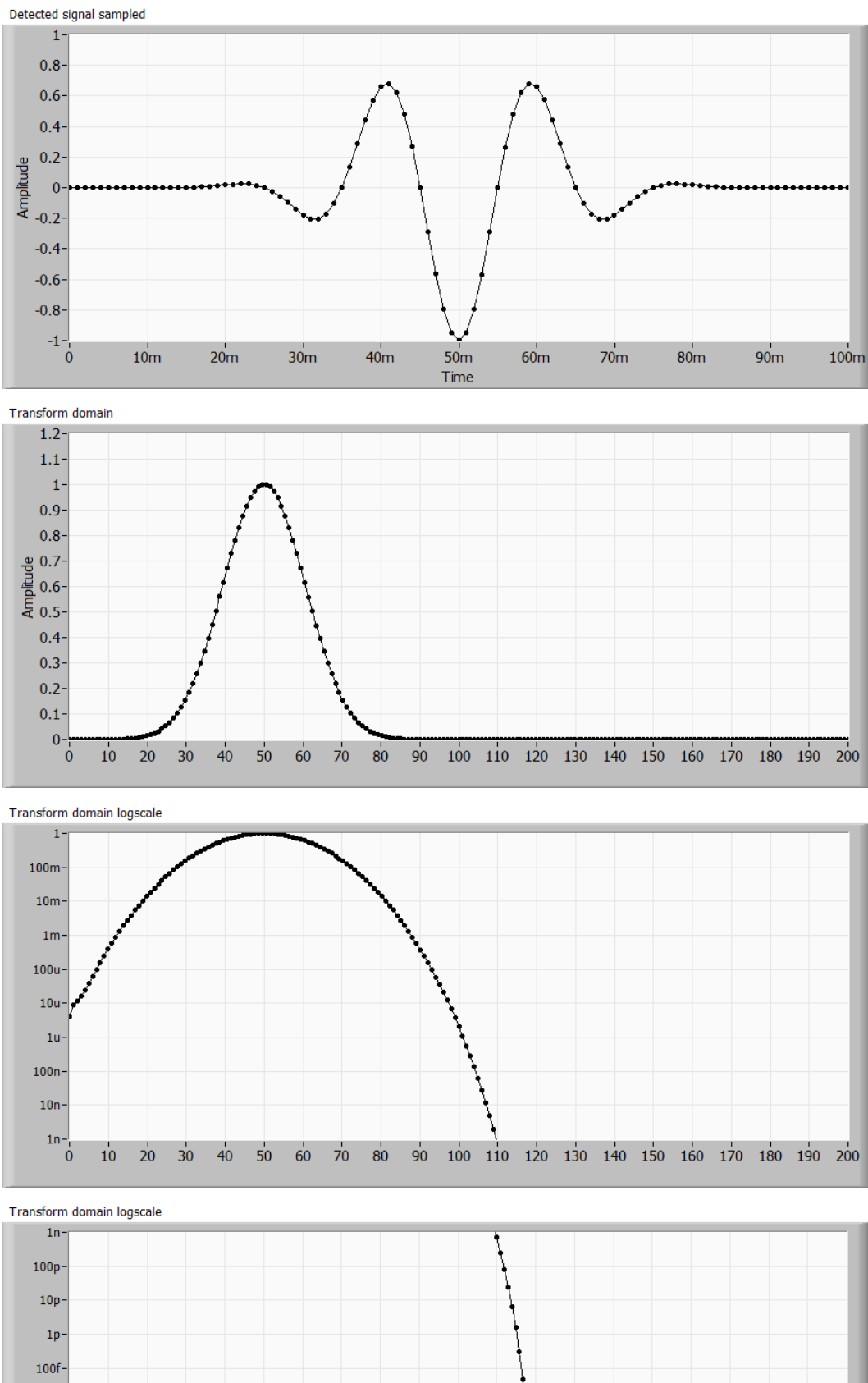


Figure 3.81 – Window: 7-term Blackman-Harris. A) Time domain, B) FFT linear scale, C1 and C2) FFT log scale

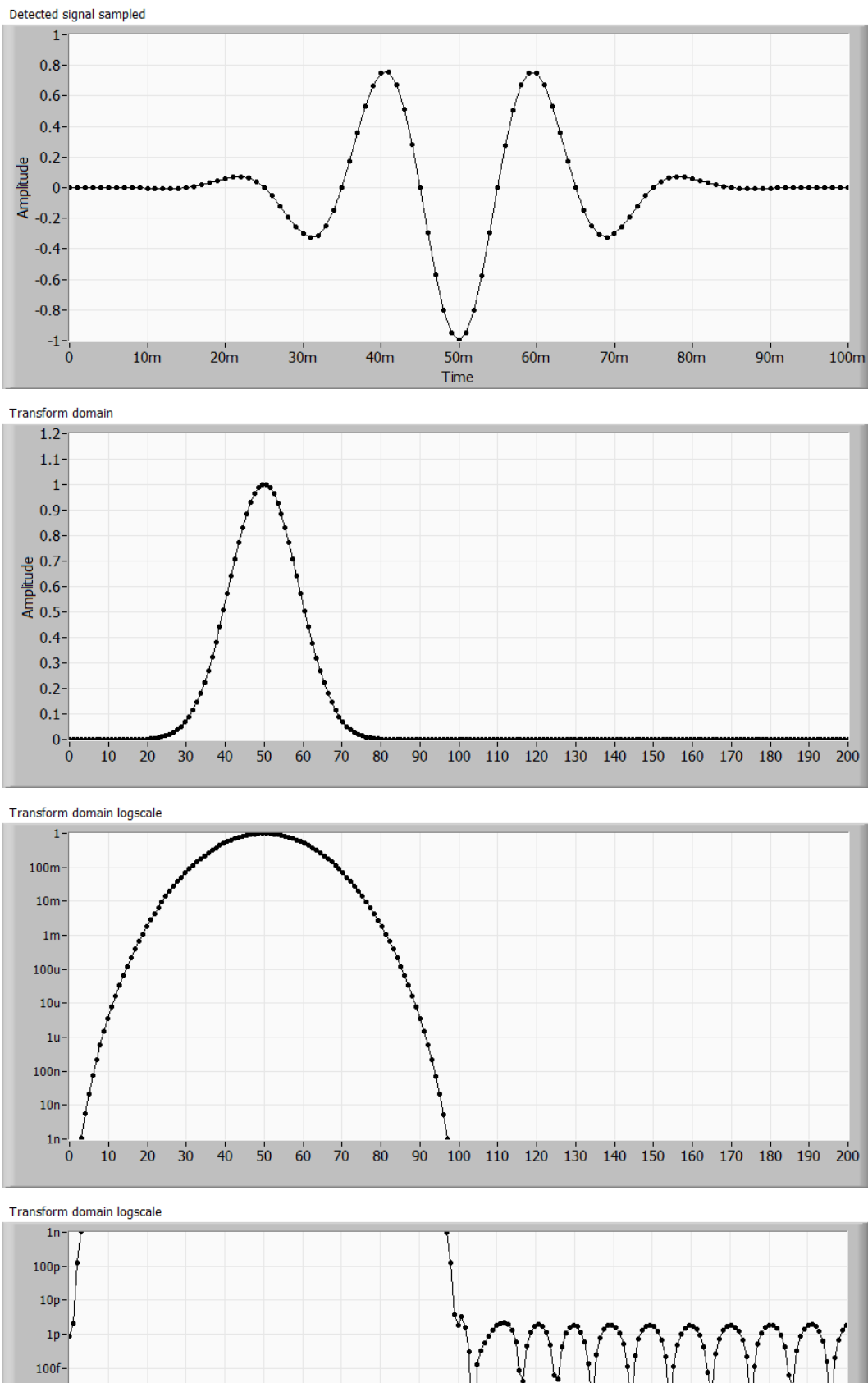


Figure 3.82 – Window: Low Sidelobe. A) Time domain, B) FFT linear scale, C1 and C2) FFT log scale

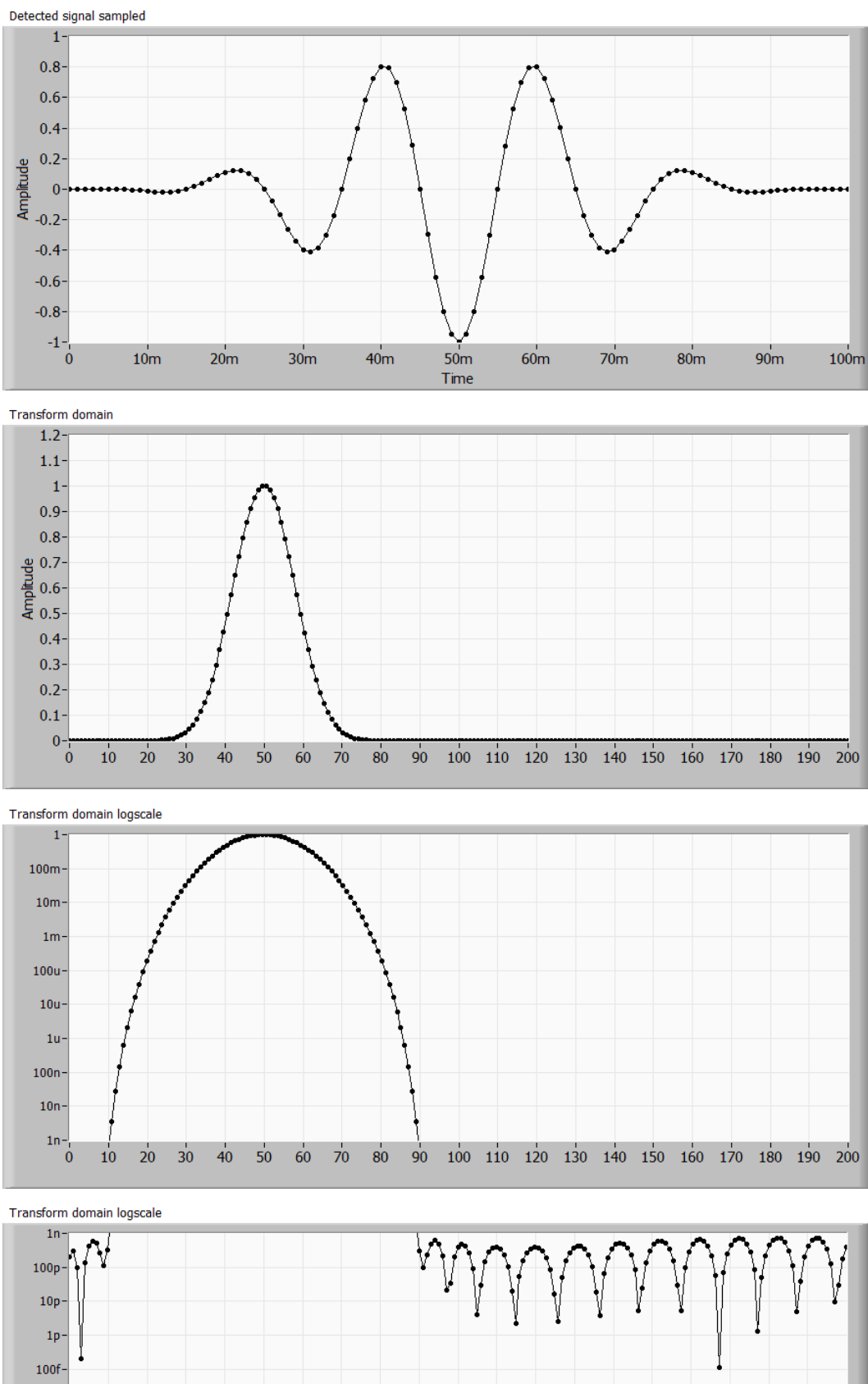


Figure 3.83 – Window: Blackman Nuttall. A) Time domain, B) FFT linear scale, C1 and C2) FFT log scale

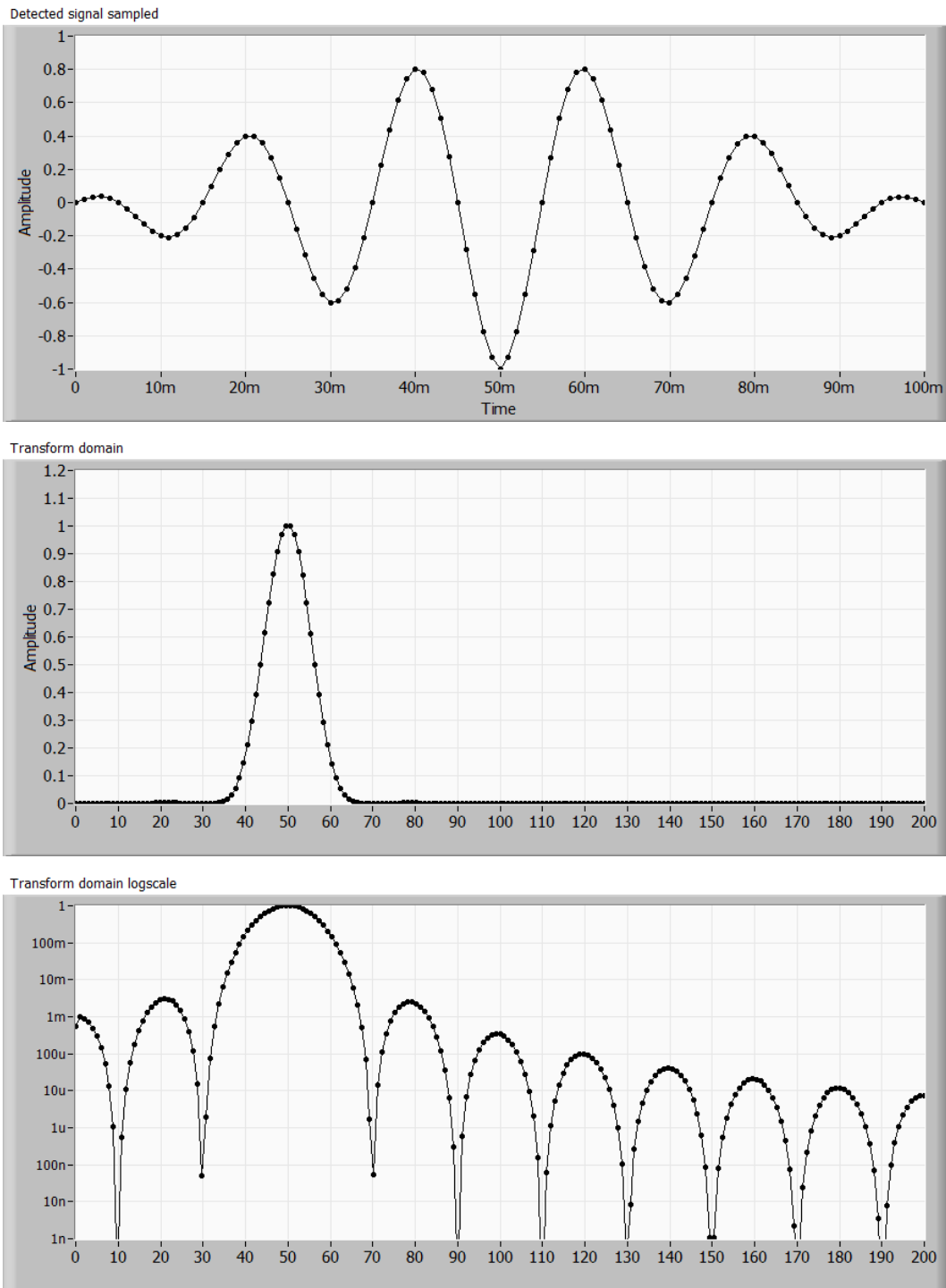


Figure 3.84 – Window: Triangle. A) Time domain, B) FFT linear scale, C) FFT log scale

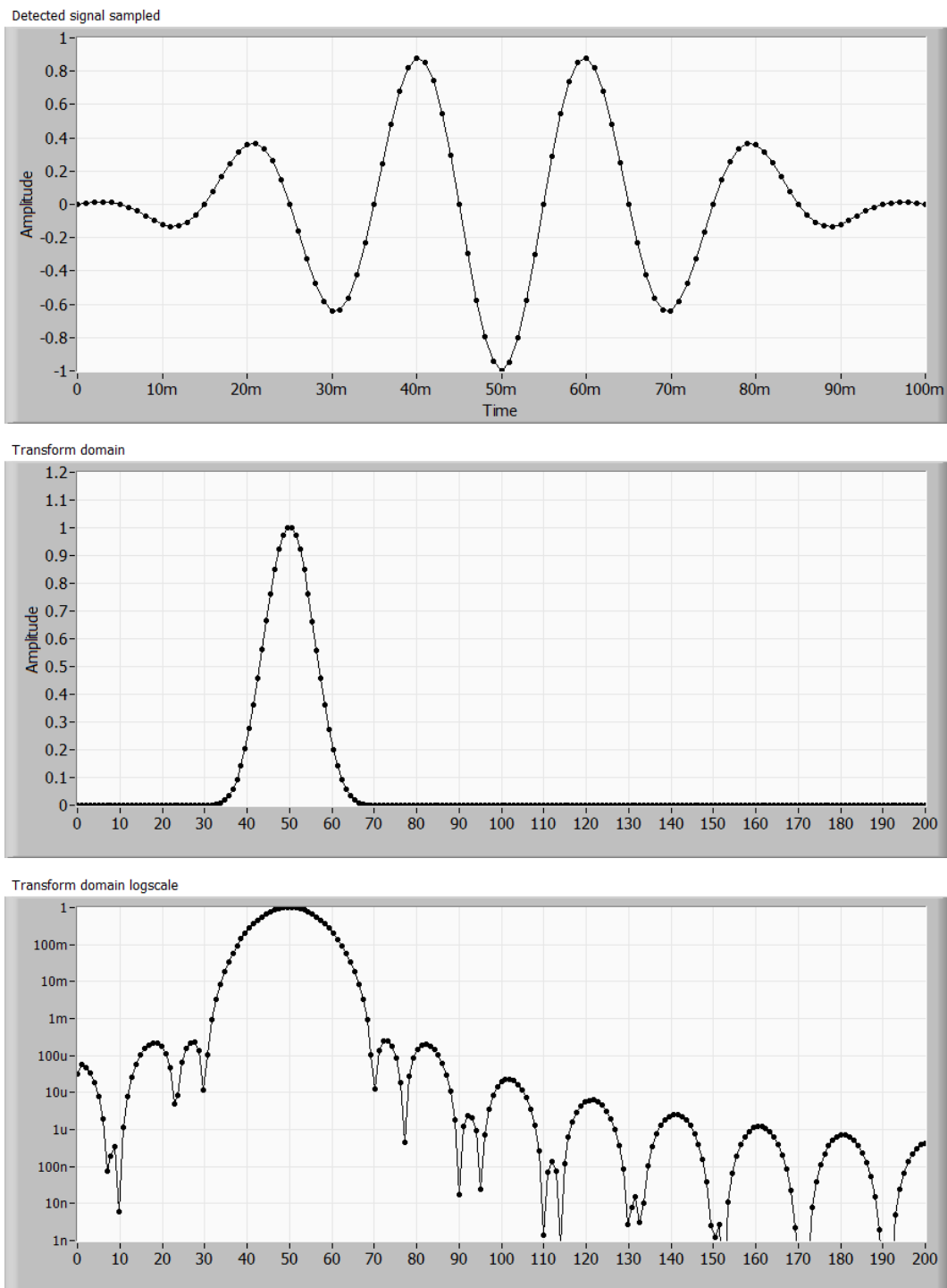


Figure 3.85 – Window: Bartlett-Hanning. A) Time domain, B) FFT linear scale, C) FFT log scale

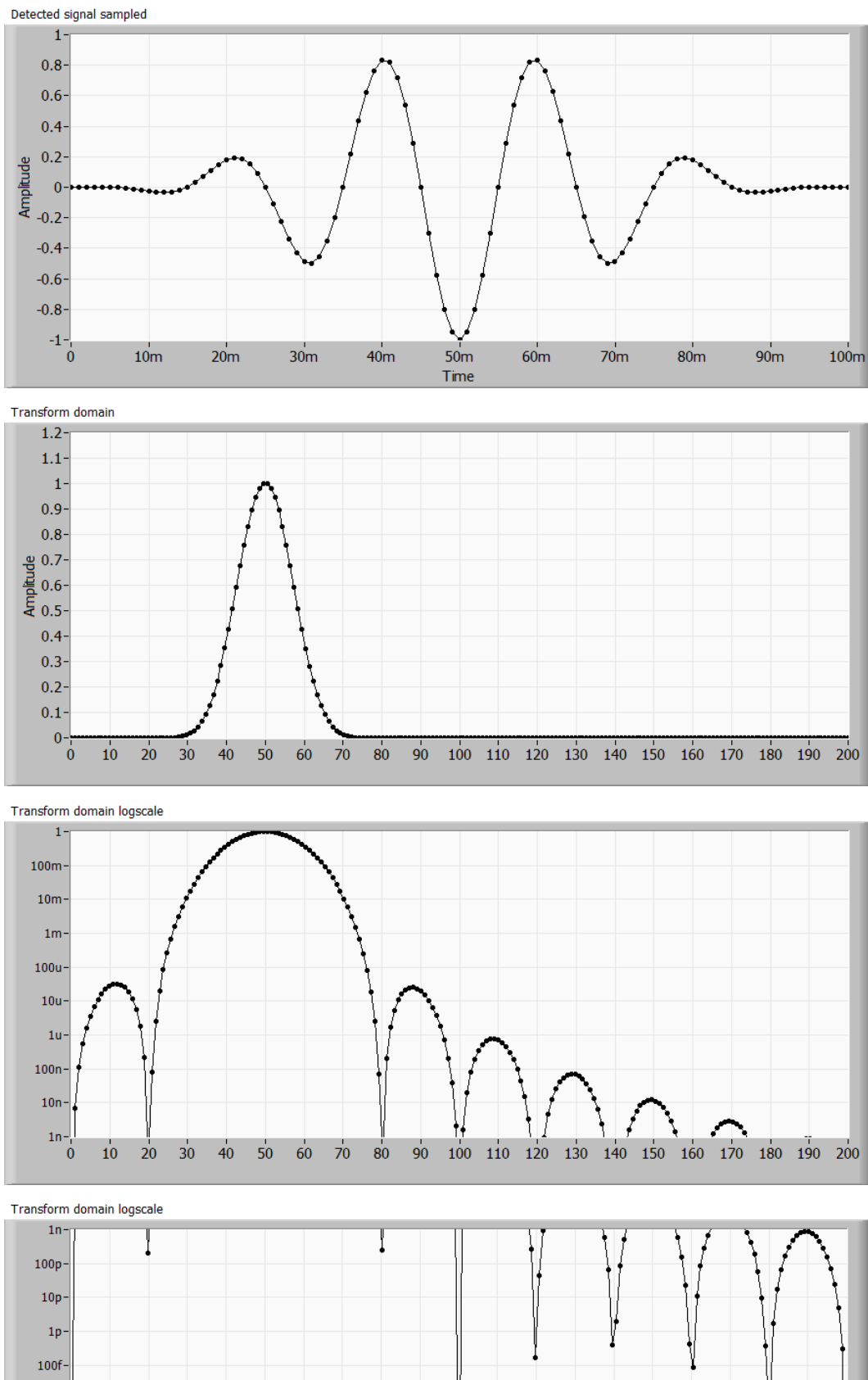


Figure 3.86 – Window: Bohman. A) Time domain, B) FFT linear scale, C1 and C2) FFT log scale

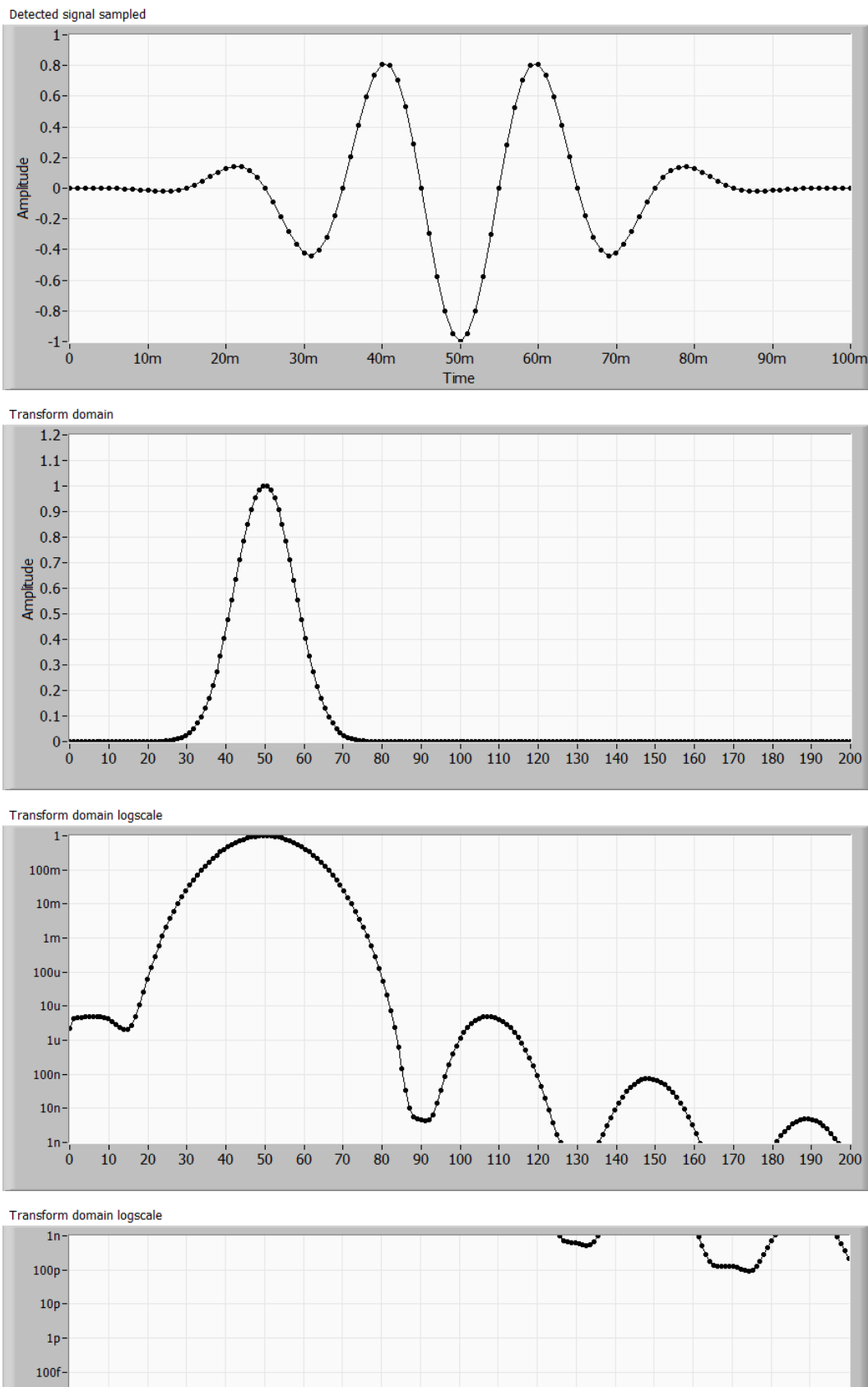


Figure 3.87 – Parzen. A) Time domain, B) FFT linear scale, C1 and C2) FFT log scale

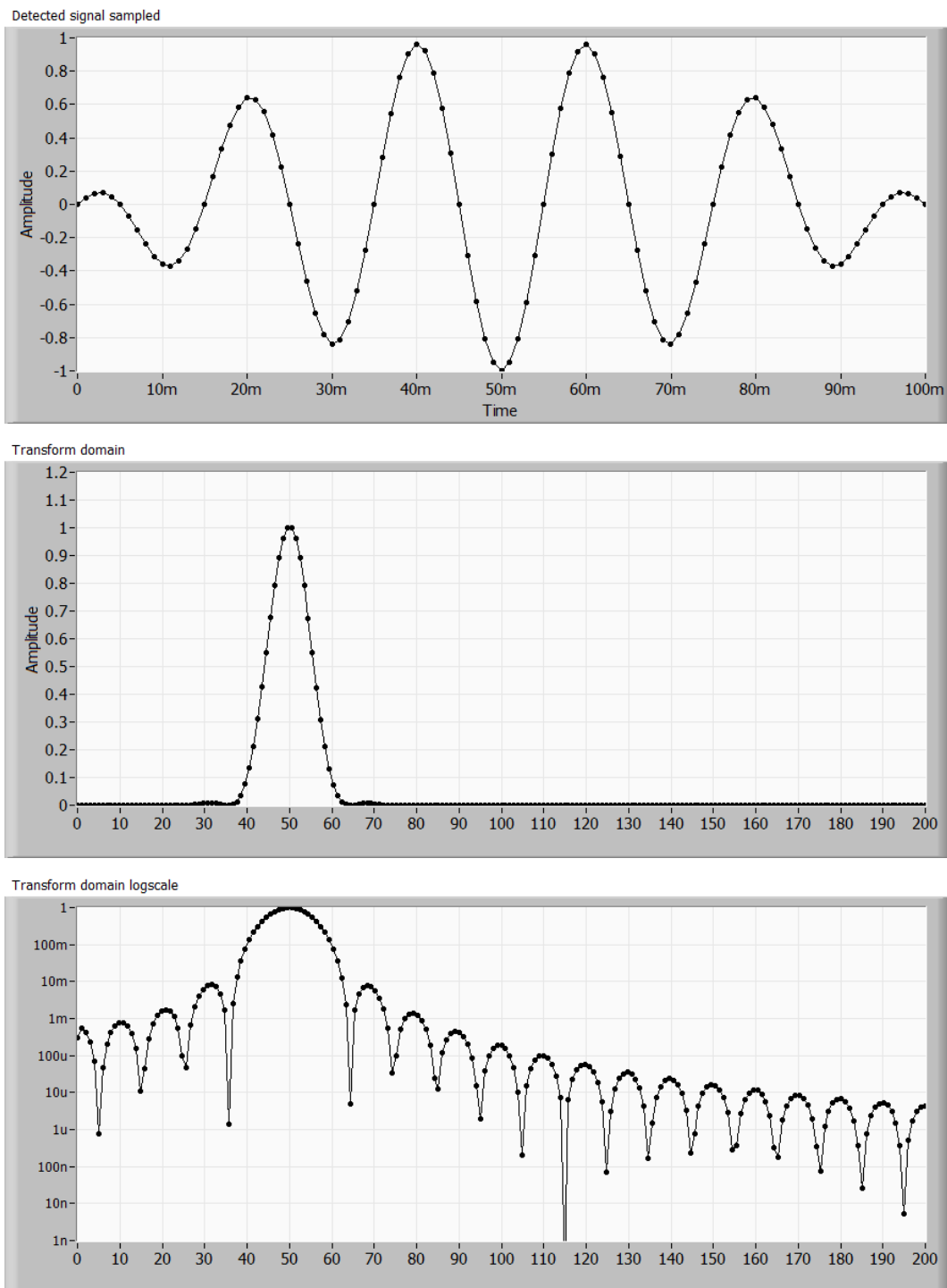


Figure 3.88 – Window: Welch. A) Time domain, B) FFT linear scale, C) FFT log scale

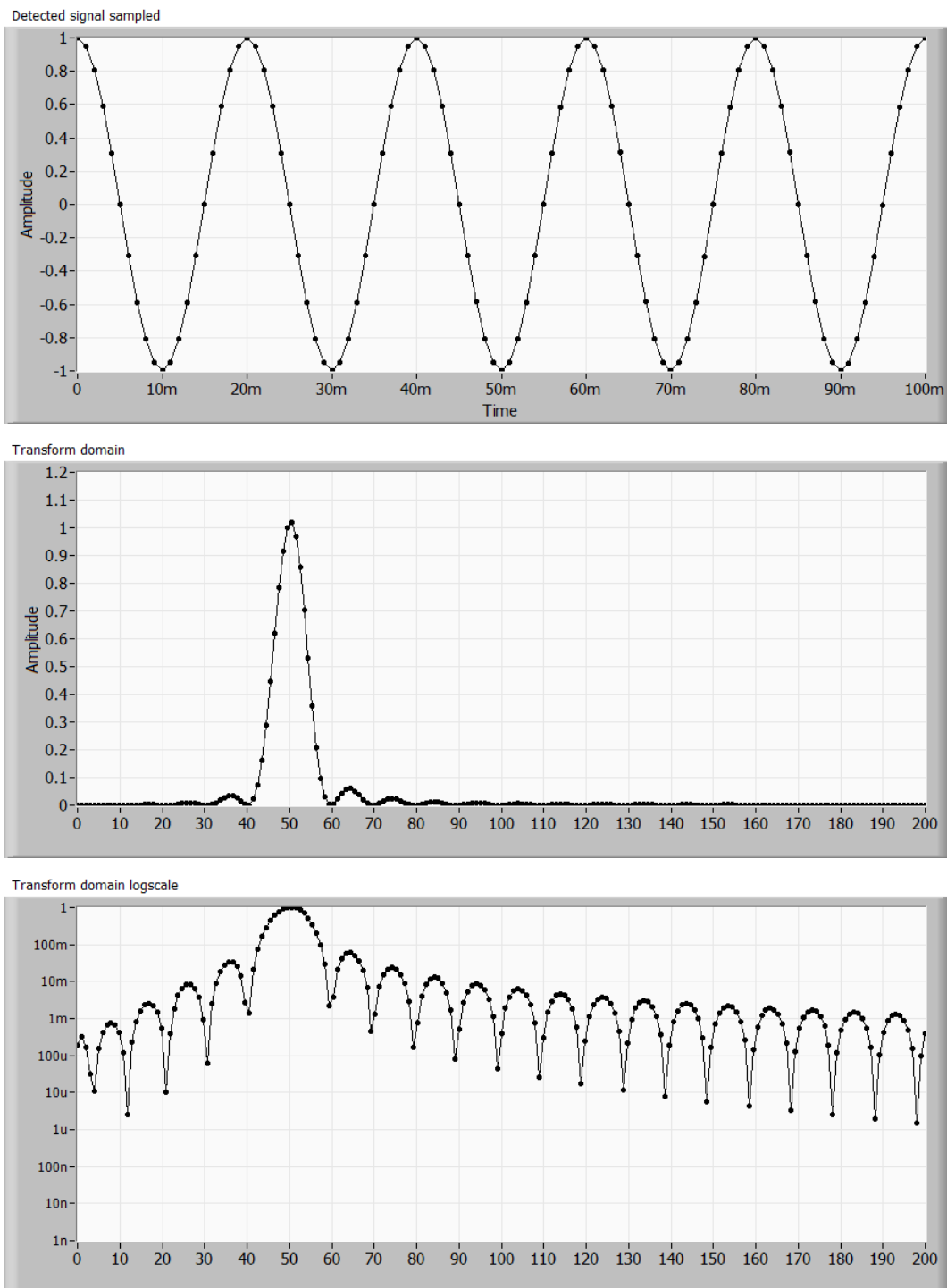


Figure 3.89 – Window: Kaiser (Beta = 0.0). A) Time domain, B) FFT linear scale, C) FFT log scale

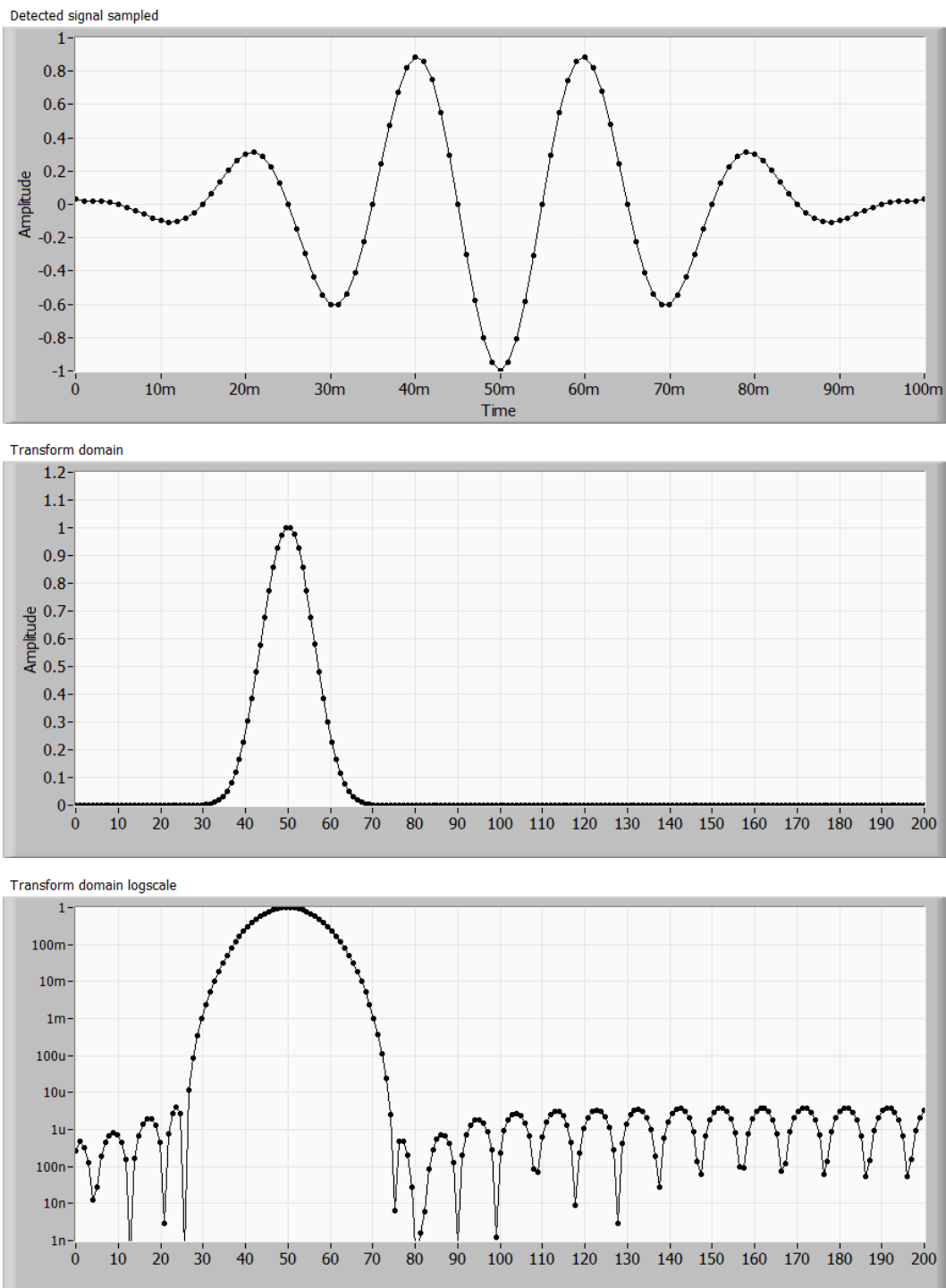


Figure 3.90 – Window: Dolph-Chebyshev. A) Time domain, B) FFT linear scale, C) FFT log scale

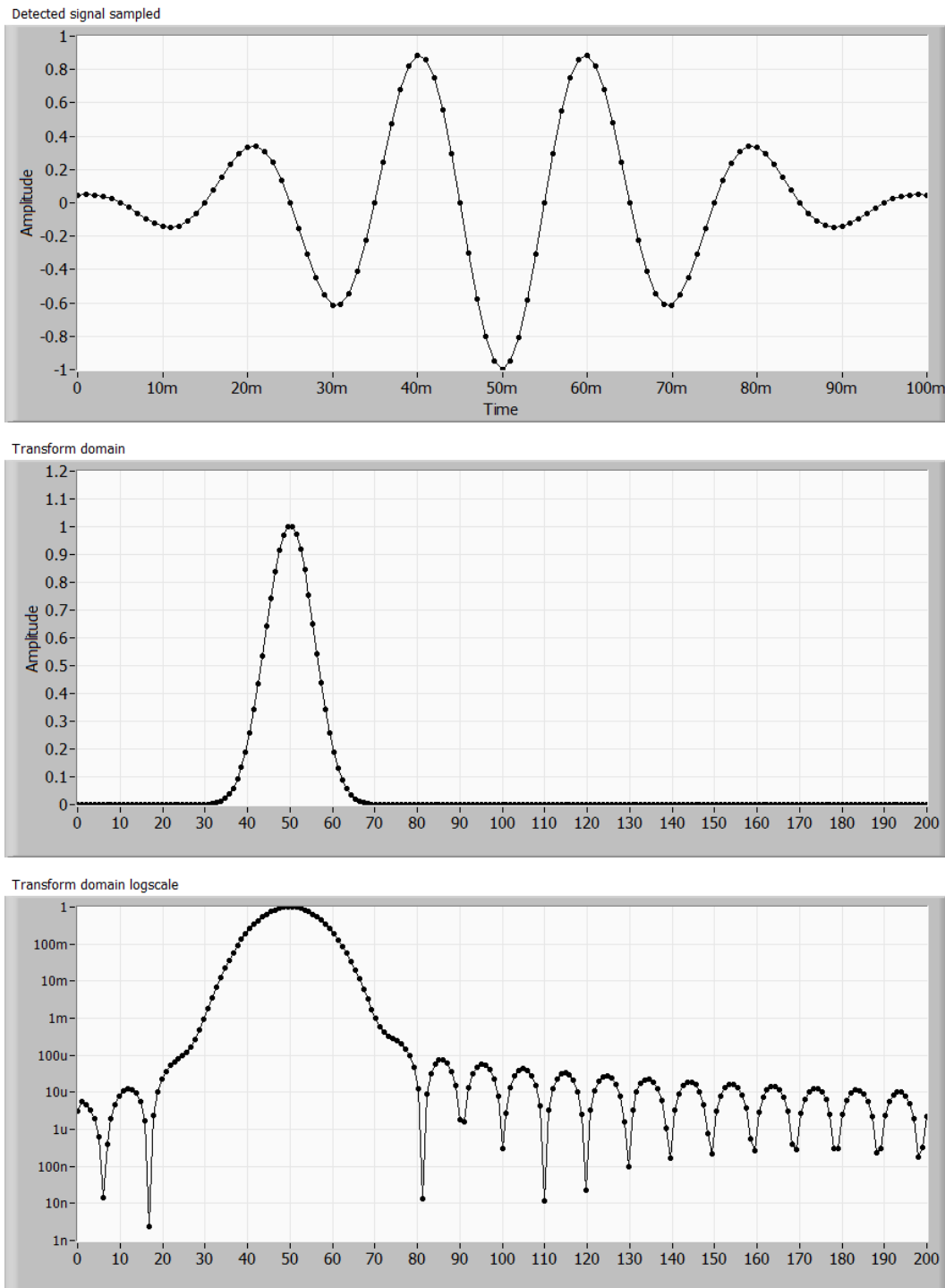


Figure 3.91 – Window: Gaussian. A) Time domain, B) FFT linear scale, C) FFT log scale

In general I use only two of these windows. Rectangular as shown in Figure 3.73 on page 67 for single reflections in order to minimize the spread of the main lobe of the FFT and Blackman-Harris as shown in Figure 3.76 on page 70 for multiple reflections to reduce the amplitude of the sidelobes to reduce their effects on neighboring reflections.

3.5. Initial Phase

The initial phase of the beat frequency is a term generally ignored in SSOCT. The basic theory is generally developed around a single reflecting surface and then extrapolated to more complicated structures (multiple reflecting surfaces) by invoking linearity.

One of the logical conclusions of the linearity invocation is the assumption of how the measurements of two surfaces will merge into one as the surfaces come together.

Common sense says that the FFT's of the two surfaces will start independent and far apart and as they come nearer and nearer, approaching the full-width half-max separation, start to merge into one single peak.

However, depending on the initial phases of each of the frequencies resulting from each surface the resulting FFT could take on one of many possible shapes. This effect only happens when two surfaces are quite close together.

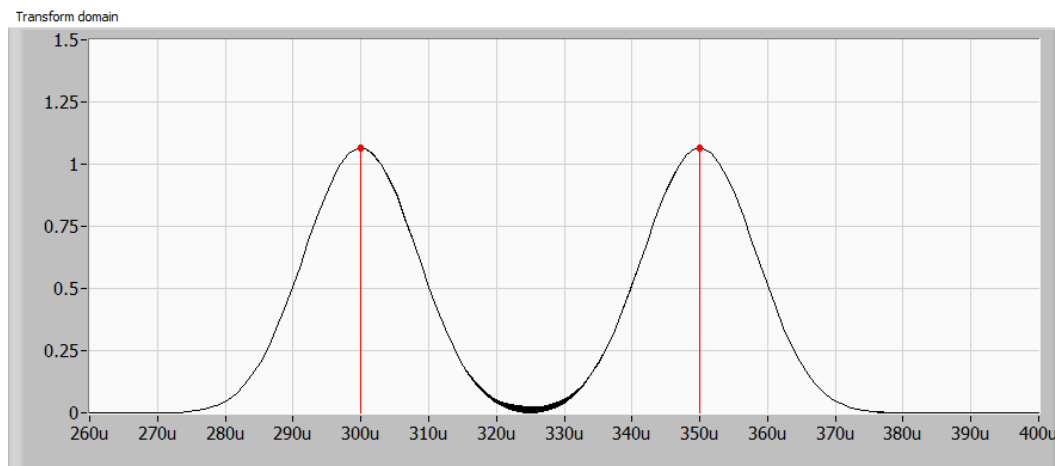


Figure 3.92 – FFT of SSOCT signals from two surfaces relatively far apart as the initial phases of each signal independently run through 360 degrees. The dots show the location of the peaks of the FFT's while the red vertical lines show the actual surface location. There is very little difference when the surfaces are far apart.

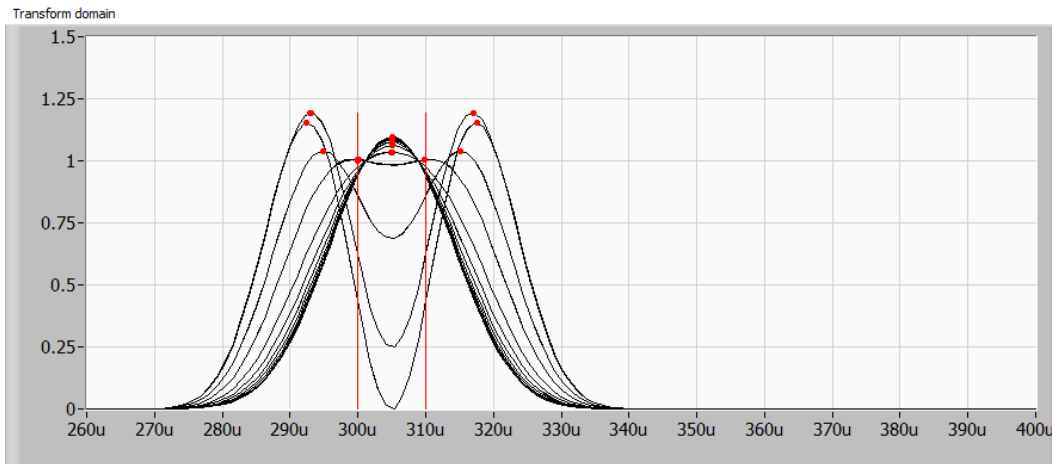


Figure 3.93 – FFT of SSOCT signals from two surfaces near to one another as the initial phases of each signal are independently run through 360 degrees. The dots show the location of the peaks while the red vertical bars show the actual location of the two surfaces. At close distances, depending on the initial phases, the results can vary and sometimes be misleading.

3.5.1. Derivation of initial phase

Let's start by considering an optical waveform at optical frequency $\nu(t)$ whose frequency is varying at a sweep rate of $d\nu/dt$. Also let's consider two planes separated in space, a reference plane and an internal plane.

		Reference	Internal
$\frac{d\nu}{dt}$	Sweep rate		
$\nu(t)$	Optical frequency		

Figure 3.94 – Initial considerations of initial phase derivation

The optical waveform is traveling from left to right and so impinges first on the reference plane.

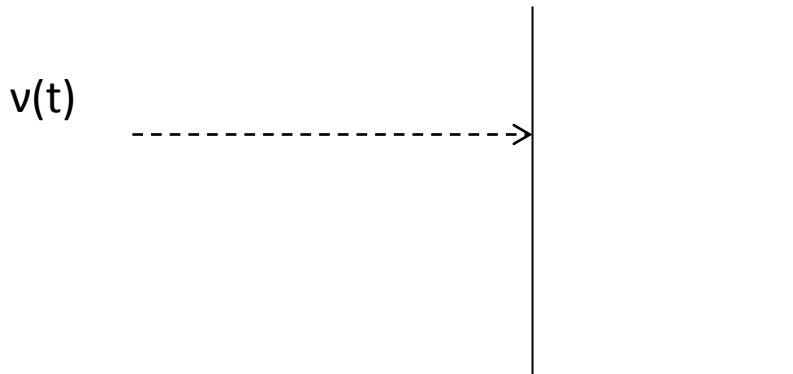


Figure 3.95 – Optical waveform travels from left to right.

Let's define $t=0$ as the moment the waveform hits the reference plane. That makes the optical frequency at that moment $v(0)$. The waveform arrives with a phase which we will call ϕ_0 .

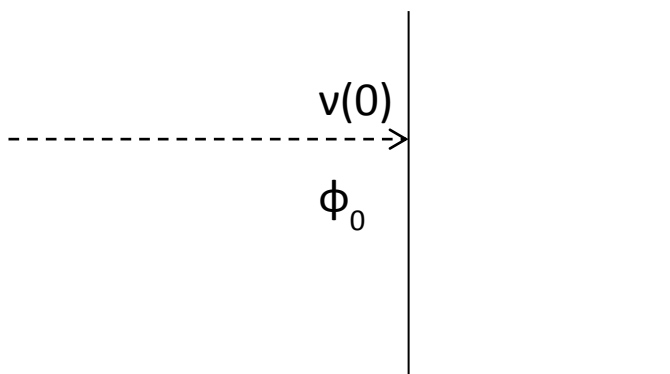


Figure 3.96 – Optical frequency of the waveform at the moment of impacting the reference plane is defined as $v(0)$. The phase which it arrives with is termed ϕ_0 .

This optical frequency continues on to the internal plane, reflects and returns to the reference plane. The roundtrip time taken to travel, reflect and return is we will call τ_{inho} as it is quite small. The additional phase accumulated by this optical frequency during this time is ϕ_{inho1} .

$$\phi_{\text{inho1}} = 2\pi v(0) * \tau_{\text{inho}}$$

Eq. 3.1

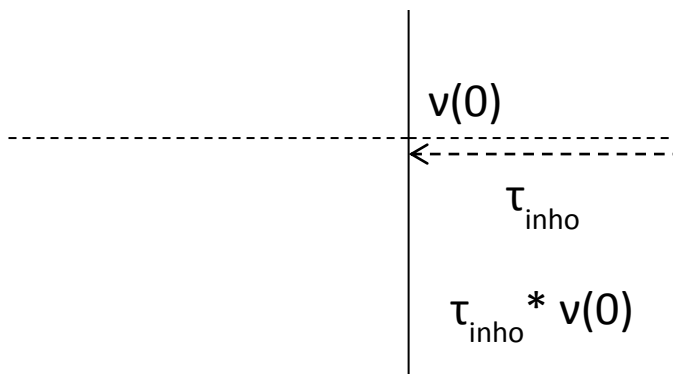


Figure 3.97 – During the roundtrip to the internal plane and back to the reference plane the optical frequency $v(0)$ accumulates phase of $2\pi (\tau_{incho} * v(0))$.

Meanwhile, back at the reference plane, the optical frequency of the incident waveform has not remained constant. During the time τ_{incho} that $v(0)$ took to reflect back from the internal plane it has changed from $v(0)$ to $v(\tau_{incho})$.

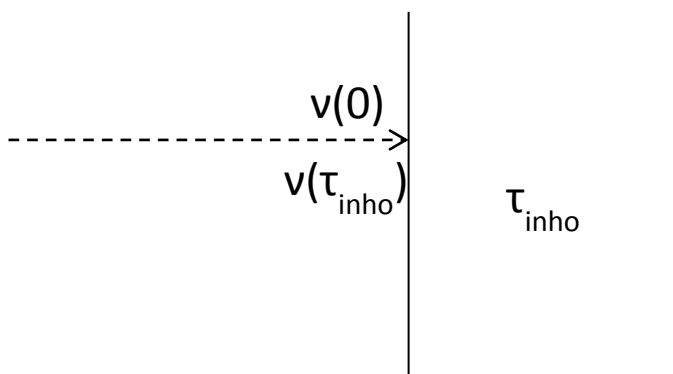


Figure 3.98 – The optical frequency incident at the reference plane has changed from $v(0)$ to $v(\tau_{incho})$ during the time τ_{incho} .

This point accumulates phase during the entire time as the optical frequency varies. The total accumulated phase will be the integral of the optical frequency over this time period τ_{incho} .

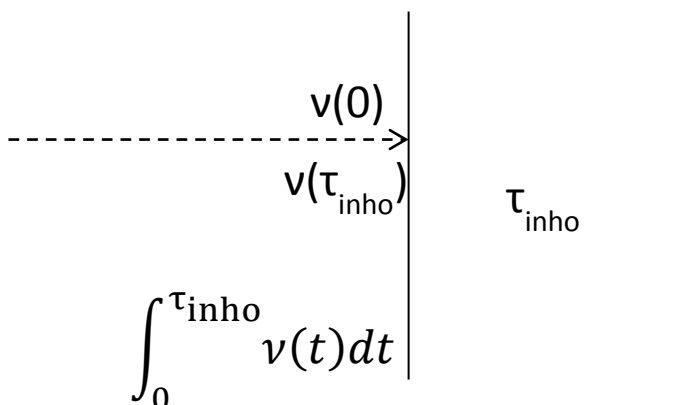


Figure 3.99 – Accumulated phase is the integral of the optical frequency over the time period τ_{incho} .

Which is the area under the curve of $v(t)$ from 0 to τ_{incho} .

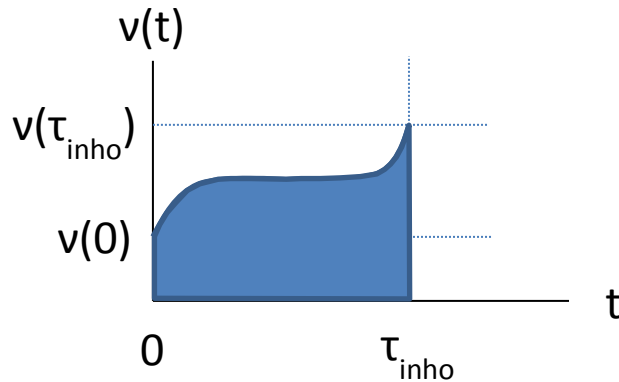


Figure 3.100 – The accumulated phase of the incident waveform is the area under $v(t)$ from 0 to τ_{incho} .

If $v(t)$ is changing smoothly and / or if τ_{incho} is very short then we can approximate the change in $v(t)$ as a straight line (which is the same as saying dv/dt is constant over this time period).

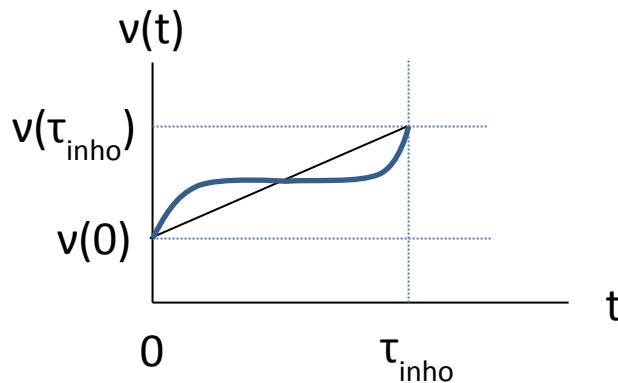


Figure 3.101 – We can approximate $v(t)$ as a straight line from 0 to τ_{incho} if $v(t)$ is sufficiently smooth and/or τ_{incho} is very small.

The accumulated phase then can be calculated by finding the area under this new curve.

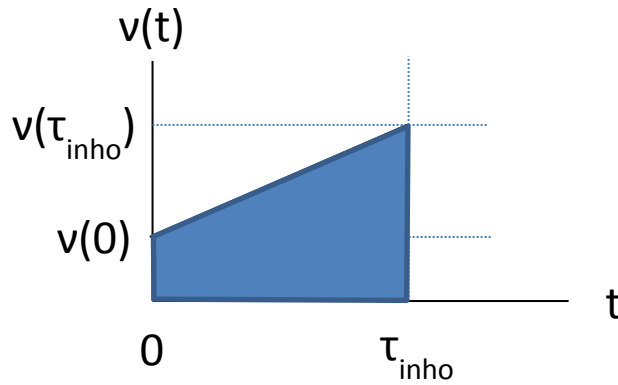


Figure 3.102 – The accumulated phase is the area under this new curve.

This new area is a trapazoid and the area can be easily calculated to give ϕ_{incho2} , the accumulated phase at this point.

$$\phi_{\text{incho2}} = 2\pi \tau_{\text{incho}} * (v(0) + v(\tau_{\text{incho}}))/2 \quad \text{Eq. 3.2}$$

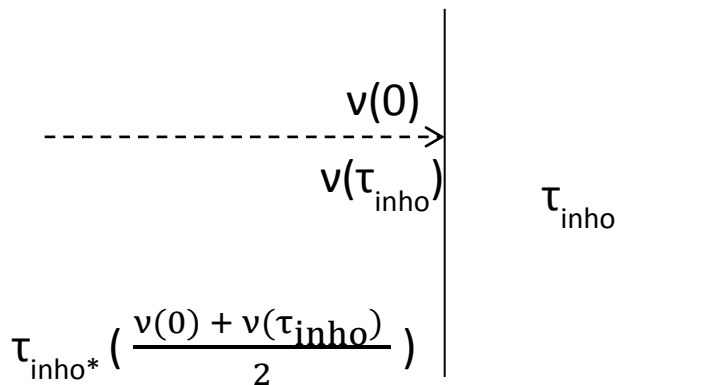
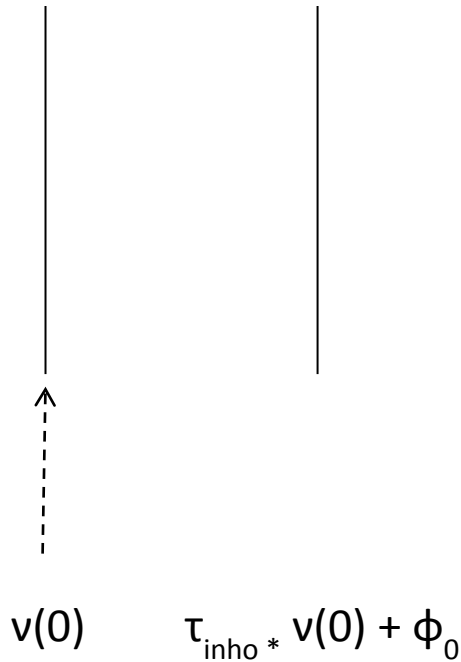


Figure 3.103 – The accumulated phase of the incident waveform, ϕ_{incho2} , can be calculated from the trapazoidal rule.

It is worth our while to pause for a moment and consider what we have. From the starting point of a single waveform incident on the reference plane we now have two reflected waveforms at the reference plane. Each waveform is at a different optical frequency and each has a different accumulated phase.



$$v(\tau_{incho}) = \tau_{incho} * \left(\frac{v(0) + v(\tau_{incho})}{2} \right) + \phi_0$$

Figure 3.104 – The frequency and the accumulated phase of the two reflected waveforms at the reference plane.

From here on out the two waveforms travel together to a detector. The time spent traveling to the detector will typically be much larger τ_{incho} and so we will refer to it as τ_{ao} .

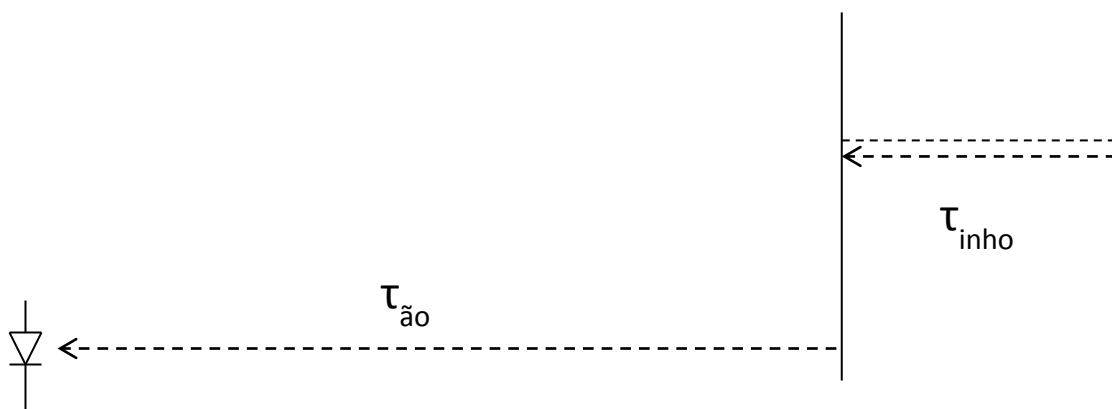
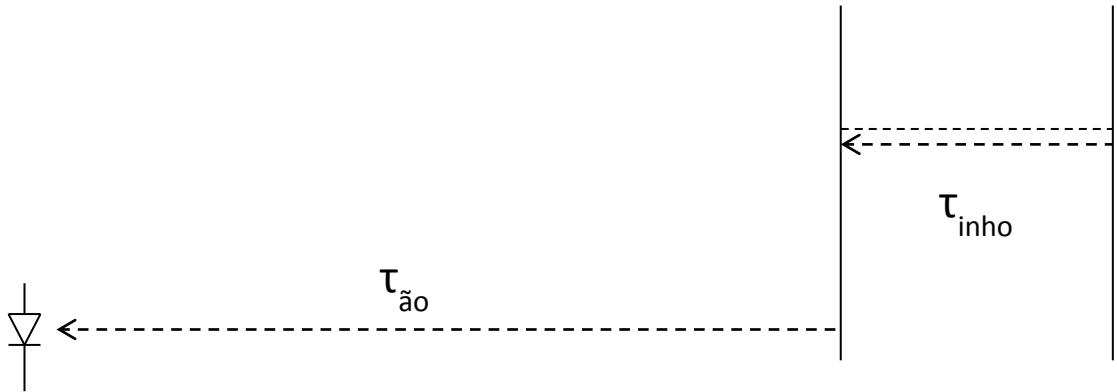


Figure 3.105 – The two waveforms will travel together to the detector. The time required to get to the detector from the reference plane is called τ_{ao} .

Each waveform will accumulate a different phase, depending on its optical frequency.

$$\varphi_{ao1} = 2\pi \tau_{ao} * v(0) \quad \text{Eq. 3.3}$$

$$\varphi_{ao2} = 2\pi \tau_{ao} * v(\tau_{incho}) \quad \text{Eq. 3.4}$$



$$v(0) \quad \tau_{\tilde{ao}} * v(0)$$

$$v(\tau_{incho}) \quad \tau_{\tilde{ao}} * v(\tau_{incho})$$

Figure 3.106 – Each waveform accumulates phase depending on its optical frequency.

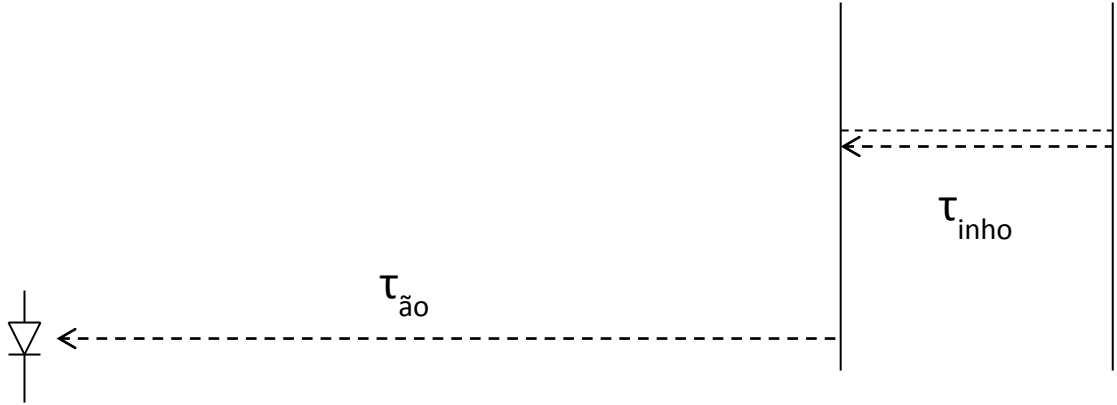
The total phase for each waveform is the sum of the phases φ_0 , φ_{incho} and φ_{ao} .

$$\varphi_1 = \varphi_{ao1} + \varphi_{incho1} + \varphi_0 \quad \text{Eq. 3.5}$$

$$= 2\pi \tau_{ao} * v(0) + 2\pi v(0) * \tau_{incho} + \varphi_0 \quad \text{Eq. 3.6}$$

$$\varphi_2 = \varphi_{ao2} + \varphi_{incho2} + \varphi_0 \quad \text{Eq. 3.7}$$

$$= 2\pi \tau_{ao} * v(\tau_{incho}) + 2\pi \tau_{incho} * (v(0) + v(\tau_{incho}))/2 + \phi_0 \quad \text{Eq. 3.8}$$



$$v(0) \quad \tau_{\tilde{ao}} * v(0) + \tau_{incho} * v(0) + \phi_0$$

$$v(\tau_{incho}) \quad \tau_{\tilde{ao}} * v(\tau_{incho}) + \tau_{incho} * \left(\frac{v(0) + v(\tau_{incho})}{2} \right) + \phi_0$$

Figure 3.107 – The total accumulated phase for each waveform.

Square law detection leaves us with a beat signal. The frequency of the signal is the difference in optical frequencies and the initial phase $\phi_{initial}$ is the difference in phase.

$$\phi_{initial} = \phi_2 - \phi_1 \quad \text{Eq. 3.9}$$

$$= 2\pi \tau_{ao} * v(\tau_{incho}) + 2\pi \tau_{incho} * (v(0) + v(\tau_{incho}))/2 + \phi_0 - 2\pi \tau_{ao} * v(0) - 2\pi v(0) * \tau_{incho} - \phi_0 \quad \text{Eq. 3.10}$$

The ϕ_0 terms drop out, τ_{incho} and τ_{ao} terms can combine to simplify the equation.

$$\phi_{initial} = 2\pi \tau_{ao} * (v(\tau_{incho}) - v(0)) + \frac{1}{2} 2\pi \tau_{incho} * (v(\tau_{incho}) - v(0)) \quad \text{Eq. 3.11}$$

$$v(\tau_{\text{incho}}) - v(0) \quad \text{Beat frequency}$$

$$\tau_{\text{ao}} * v(\tau_{\text{incho}}) + \tau_{\text{incho}} * \left(\frac{v(0) + v(\tau_{\text{incho}})}{2} \right) + \cancel{\phi_0} - \tau_{\text{ao}} * v(0) - \tau_{\text{incho}} * v(0) - \cancel{\phi_0} \quad \text{Initial phase}$$

Figure 3.108 – Some terms drop out and others can be grouped to simplify the equation for ϕ_{initial} .

Once again we can group terms to simplify the equation.

$$\phi_{\text{initial}} = 2\pi (\tau_{\text{ao}} + \frac{1}{2} \tau_{\text{incho}}) * (v(\tau_{\text{incho}}) - v(0)) \quad \text{Eq. 3.12}$$

$$v(\tau_{\text{incho}}) - v(0) \quad \text{Beat frequency}$$

$$\tau_{\text{ao}} * (v(\tau_{\text{incho}}) - v(0)) + \frac{1}{2} \tau_{\text{incho}} * (v(\tau_{\text{incho}}) - v(0)) \quad \text{Initial phase}$$

Figure 3.109 – Terms that can be grouped again.

Finally, we note that the one of the terms in the equation is the difference in optical frequency between 0 and τ_{incho} . The same assumption we made to estimate the integral with the trapazoidal rule ($v(t)$ smooth or τ_{incho} small) lets us estimate this difference in optical frequency with the $\tau_{\text{incho}} * dv/dt$, or in other words,

$$\phi_{\text{initial}} = 2\pi (\tau_{\text{ao}} + \frac{1}{2} \tau_{\text{incho}}) * (\tau_{\text{incho}} * dv/dt) \quad \text{Eq. 3.13}$$

$$v(\tau_{\text{incho}}) - v(0) \quad \text{Beat frequency}$$

$$(\tau_{\text{ao}} + \frac{1}{2} \tau_{\text{incho}}) * (v(\tau_{\text{incho}}) - v(0)) \quad \text{Initial phase}$$

Figure 3.110 – Difference in optical frequency term that can be estimated by the sweep rate * $\tau_{\text{in}}\hbar$.

To recap, starting with an optical waveform whose optical frequency was varying with a sweep rate of dv/dt , we have followed the the frequencies and phases as they accumulate during the journey to and from the reference and internal interfaces to the detector.

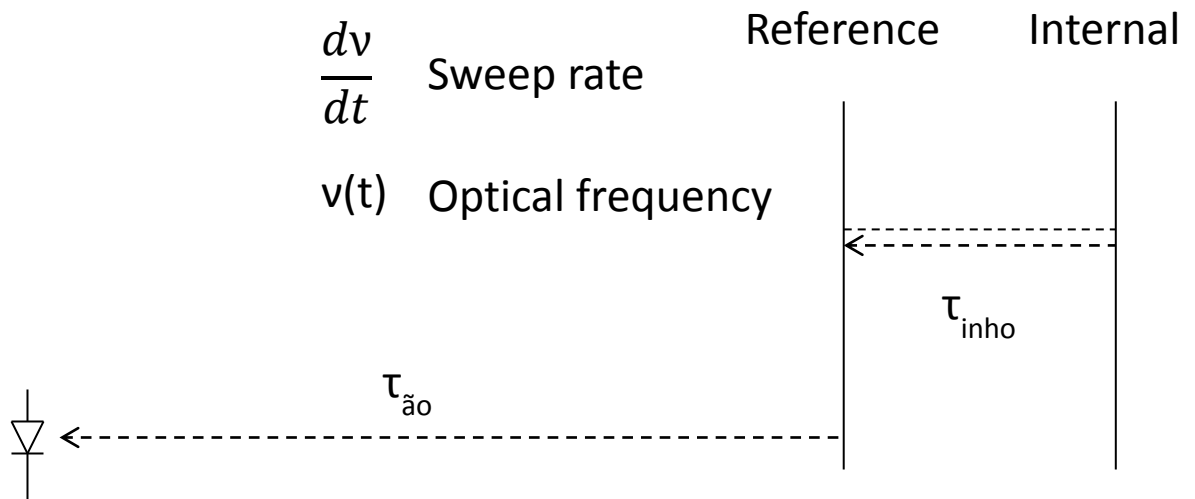


Figure 3.111 – Recap of elements contributing to the initial phase.

The initial phase was calculated from the difference in phase between the two waveforms arriving at the detector. The initial phase has

$$v(\tau_{\text{in}}\hbar) - v(0) \quad \text{Beat frequency}$$

$$(\tau_{\text{ao}} + \frac{1}{2} \tau_{\text{in}}\hbar) * (\tau_{\text{in}}\hbar * \frac{dv}{dt}) \quad \text{Initial phase}$$

Patch cord
Interferometer
Sweep rate

Figure 3.112 – Beat frequency and initial phase showing the contributors to the initial phase; the sweep rate, the size of the interferometer and the patch cord length.

3.5.2. Apply the initial phase

Now that we have the initial phase calculated, we can revisit the effects we saw in Figure 3.92 and Figure 3.93 (repeated below) where there were many possible outcomes to the FFT of two SSOCT signals depending on the initial phases and the distances between the interfaces.

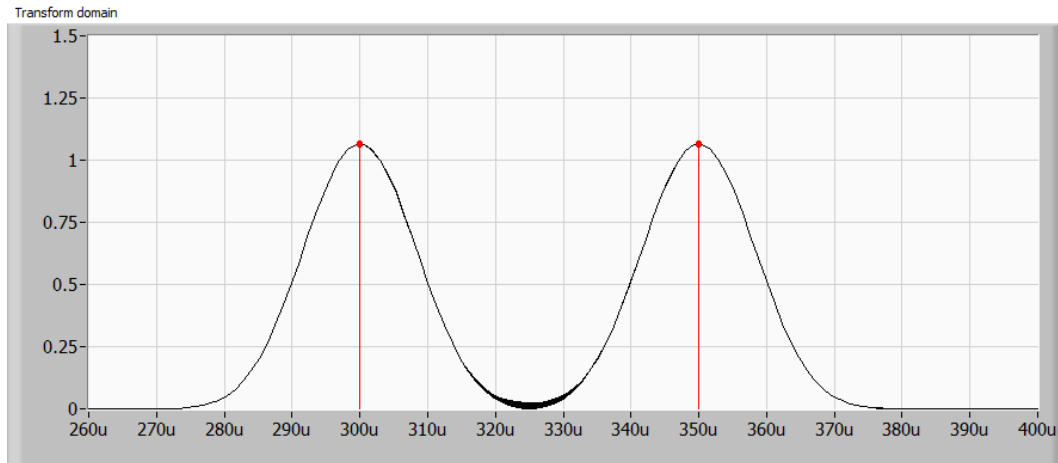


Figure 3.113 – Not much variation with initial phase for interfaces far apart.

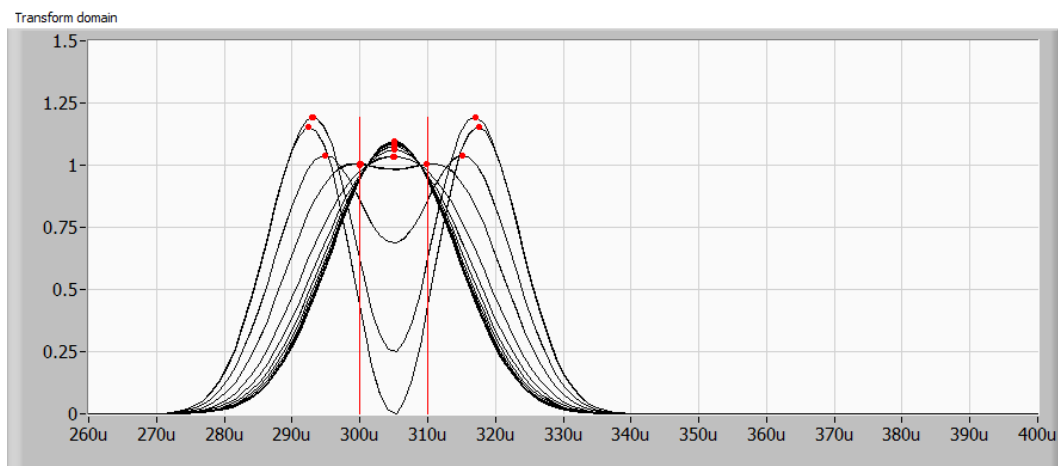


Figure 3.114 – A lot of variation with initial phase for interfaces close together.

Since the effects vary with separation, it is useful to have a means to track the effects with changing distance. Let's create a plot of the perceived separation of the two interfaces vs the actual separation. We can call this a separation trail.

For interfaces well separated, the actual and perceived separations will be the same.

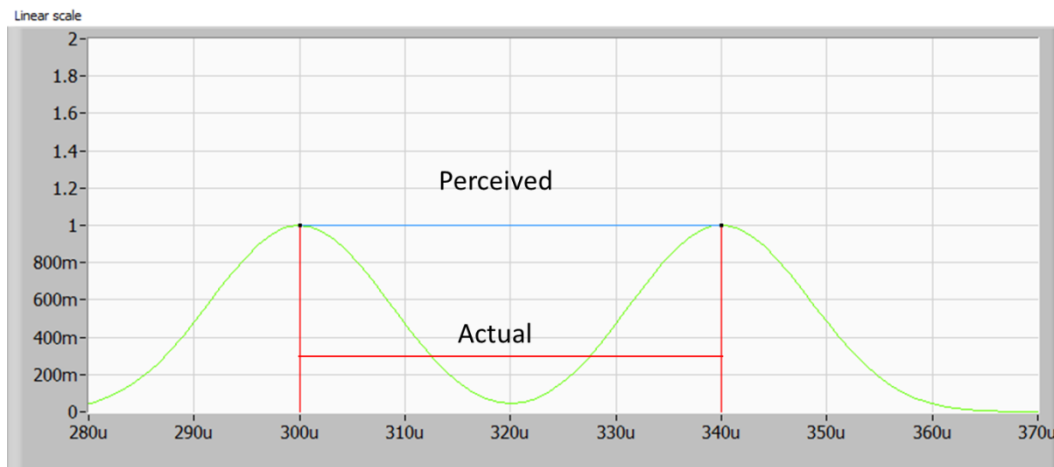


Figure 3.115 – Perceived and actual separations of two interfaces far apart.

For interfaces close together, the perceived separation can be much different than the actual separation.

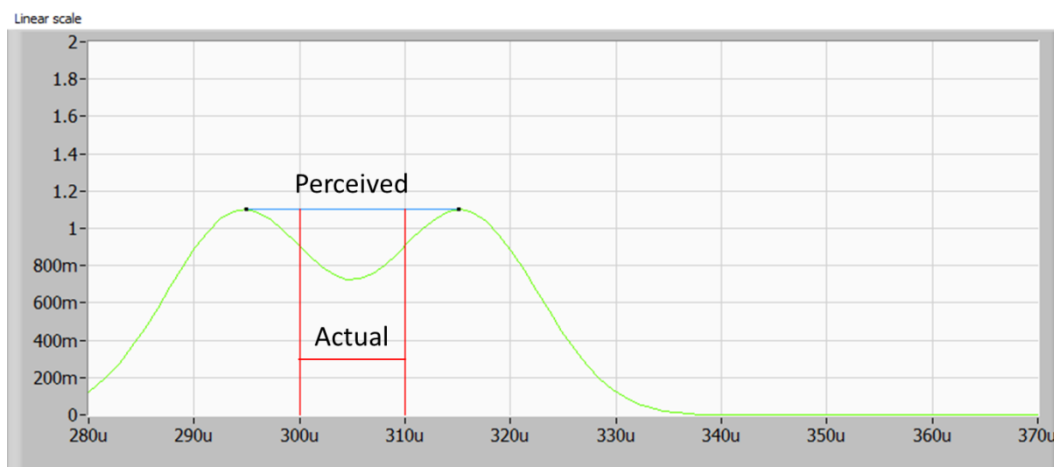


Figure 3.116 – The perceived separation can be much different than the actual separation for interfaces close together.

If we walk through a large number of separations and plot these perceived vs actual data points, the result is the separation trail shown in Figure 3.117.

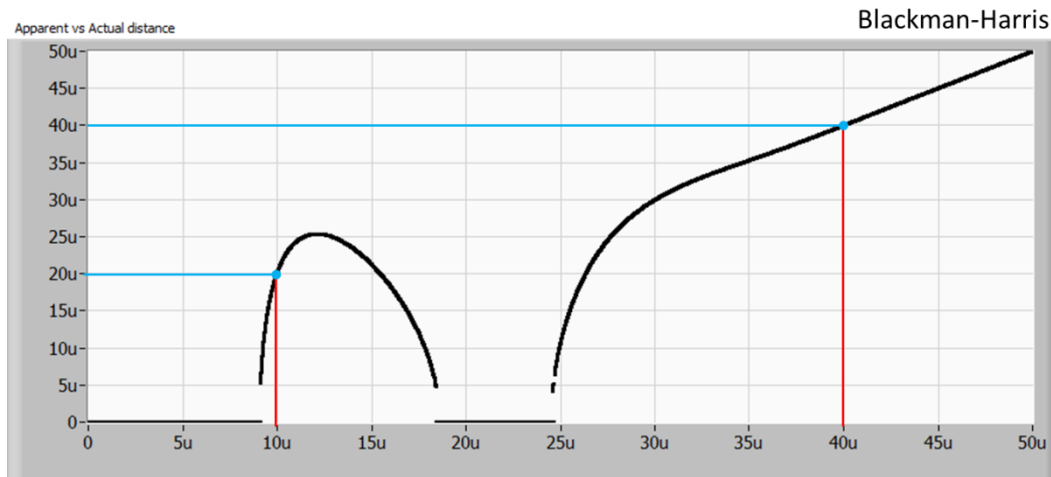


Figure 3.117 – Separation trail showing the data points for the close together and far apart interfaces.

The separation trail immediately shows at which scale the separation of two interfaces can be determined by the A-scan.

Now let's take a look at some different scenarios, scenarios based on the parameters that affect the initial phase.

The three parameters that affect the initial phase, as seen in Figure 3.112, are the separation between the interfaces (defines the size of the interferometer which defines $\tau_{\text{in}}h\omega$), the length of the patch cord (sets τ_{ao}) and the sweep rate (dv/dt).

The other parameter is the window which is used. We will look at two windows, the rectangular window and the Blackman-Harris window. Using the rectangular window is like using no window at all while the Blackman-Harris is a good representation for the behaviour all the other windows.

Laser	Brinkmeyer 1993	Laser 1	Laser 2
τ_{mgr}	1ns	66ps	66ps
dv/dt	100Ghz/s	124.9Thz/s	287M Thz/s
v	200T	200T	200T

Figure 3.118 – Laser specs used

First we will look at case for Laser 1 with a sweep rate on the order of 124.9Thz/s. We'll examine the case for no patchcord and the case of a 2us (400m) patchcord.

Figure 3.119 and Figure 3.120 show the separation trails at low speed with no patchcord

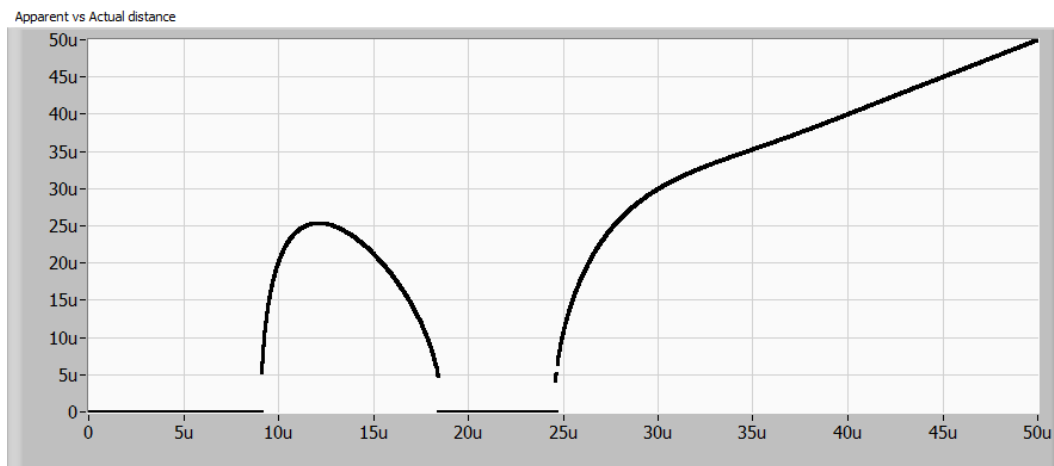


Figure 3.119 – 124.9Thz/s sweep rate, no patch cord and Blackman-Harris window. The tail of the FFT of the Blackman-Harris window is known to be low so the very good agreement of Apparent to Actual distances is not a surprise at large separations. However the initial phase affects are clear at small separations under 28um.

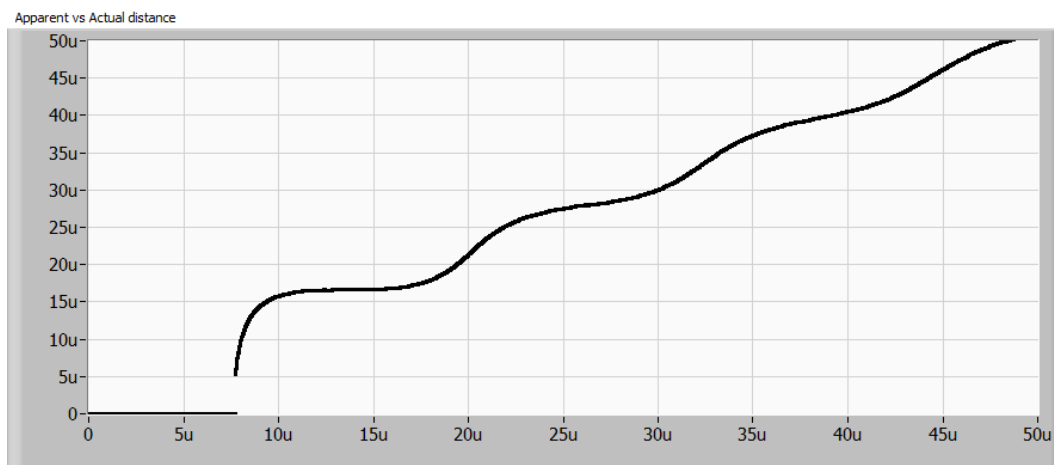


Figure 3.120 – 124.9 Thz/s sweep rate, no patch cord and Rectangular window. While the affects of the long tails of the FFT of the rectangular window can be seen in a ripple in the separation trail, the peaks come together into one at small separation like you intuitively think it should.

Figure 3.121 and Figure 3.122 show the separation trails at low speed but with the addition of a 400m patchcord.

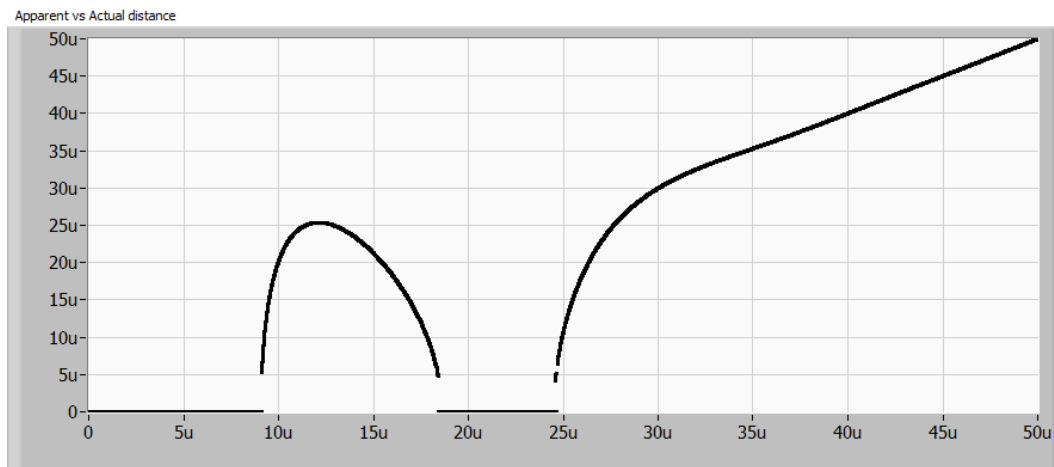


Figure 3.121 – 400m patchcord. No different from 0m patchcord. Blackman-Harris.

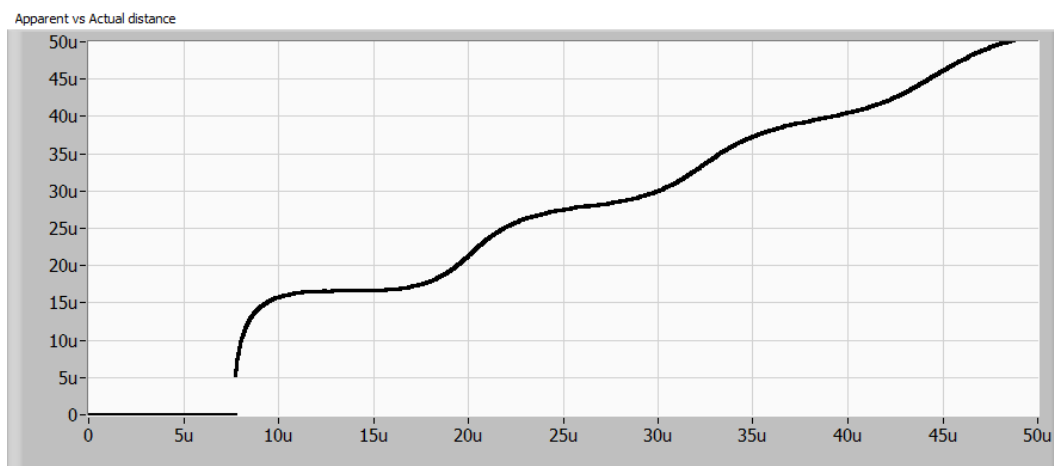


Figure 3.122 – 400m patchcord. No different from 0m patchcord. Rectangular.

We will now look at higher speeds. The Laser2 has a much higher sweep rate at 287M Thz/s.

Figure 3.123 and Figure 3.124 show the separation trails for high speed and with no patch cord.

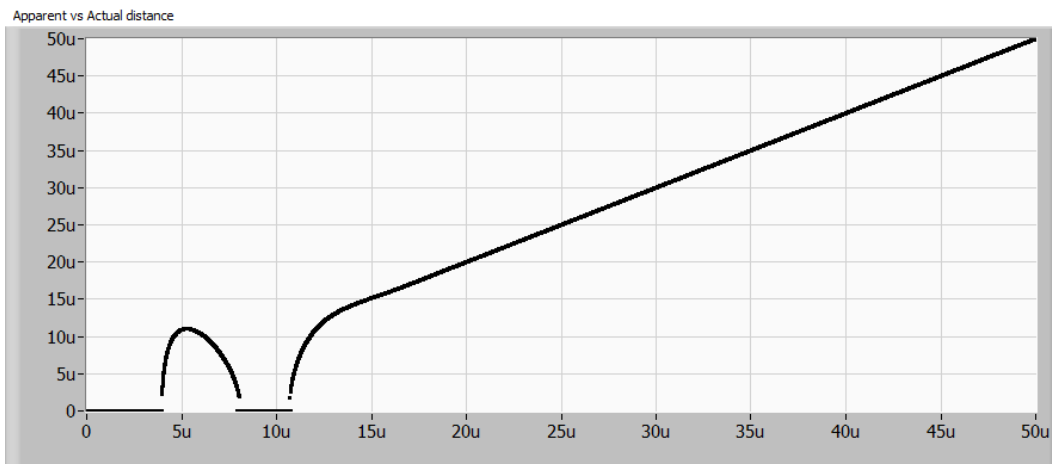


Figure 3.123 – 287M Thz/s. No patch cord. Blackman-Harris window.
Resembles the data for the slower laser.

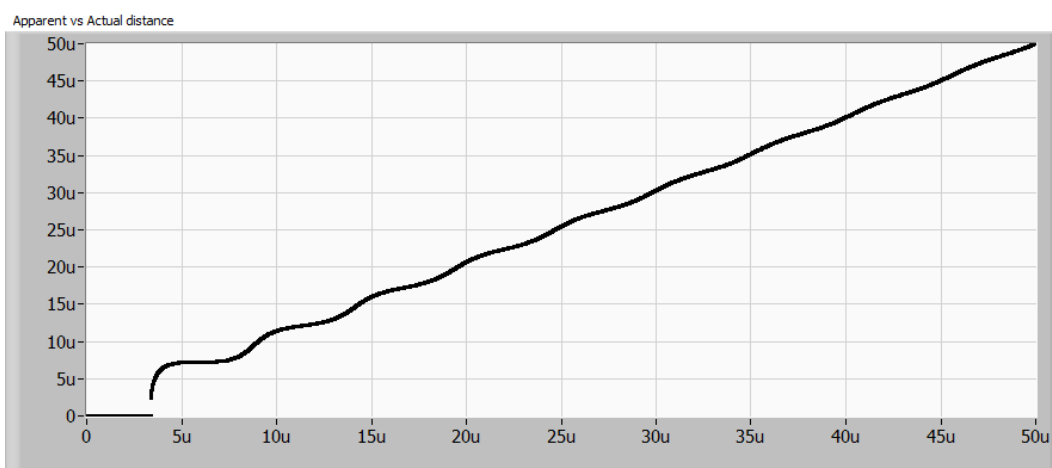


Figure 3.124 - 287M Thz/s. No patch cord. Rectangular window.
Resembles the data for the slower laser.

Now we add a patch cord.

Figure 3.125 and Figure 3.126 show the separation trails for high speed and a patch cord.

Here the extreme sweep rate has set up a difference in the two optical frequencies from any one of the interfaces. This difference in optical frequency accumulates as a difference in initial optical phase.

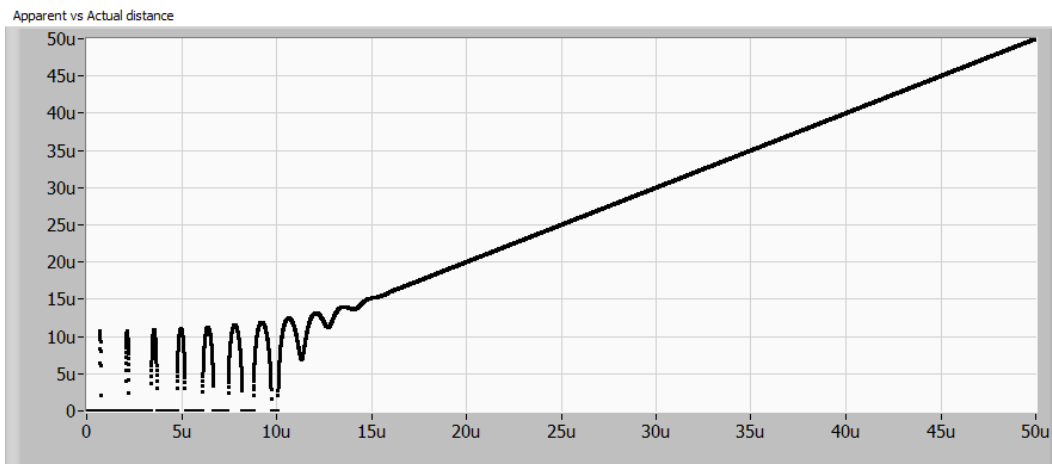


Figure 3.125 – 287M Thz/s. 400m patch cord. Blackman-Harris window. Note the multiple oscillations.

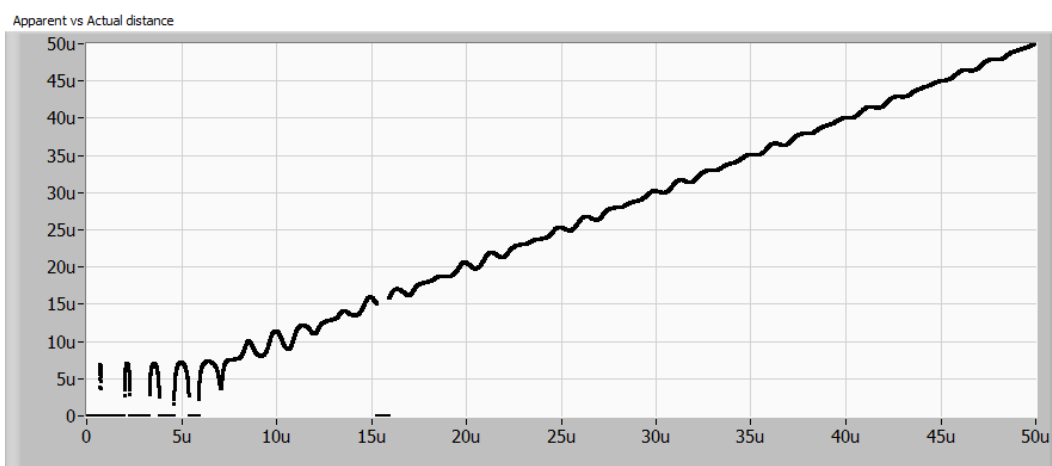


Figure 3.126 – 287M Thz/s. 400m patch cord. Rectangular window. Multiple oscillations even for the rectangular window.

3.5.3. Initial phase conclusions

Contrary to intuition, interfaces with sub-resolution separations can ‘appear’ to be resolved when non-rectangular windows are used, even at slow scan rates. Resolution in this case is as defined the window’s FFT width.

The locations do not reflect reality but do show sensitivity to those locations in a way that could be exploited.

In systems with slow scanning lasers, rectangular windows behave intuitively with sub-resolution interfaces merging into a single point. However the tradeoff is that there is significant error for distant interfaces.

For faster systems the sub-resolution effect becomes a function of patchcord length. One more sub-resolution window is added each time the initial phase walks through 360 degrees. The effect even appears in systems using rectangular windows.

4 Non-linear sweeps

It is almost impossible to sweep a laser at a constant sweep rate. It's necessary then to get a sense of the effect of a non-constant sweep rate or non-linear sweep and to develop a means to compensate for it.

4.1. Examples of non-linear sweeps

A non-linear sweep is characterized by a sweep rate which is not constant.

First, for contrast, section 4.1.1 reminds us of the linear sweep. Section 4.1.2 to 4.1.5 then show some non-linear sweeps and their effects.

4.1.1. Example - Constant sweep rate (linear sweep)

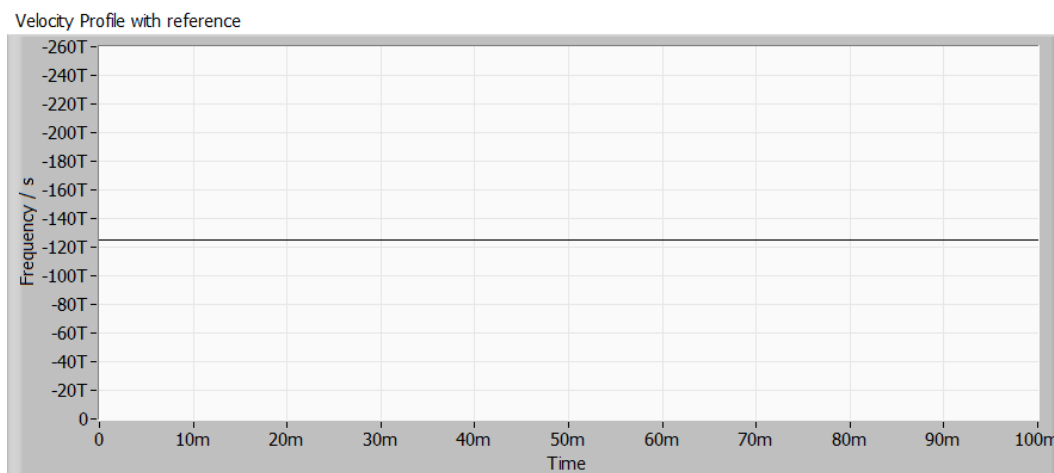


Figure 4.1 – Constant sweep rate. A linear sweep has a constant sweep rate.

As seen before, the beat signal seen at the detector will be a sinewave at a constant frequency for the entire duration of the sweep. The actual frequency will be determined by the separation between reference and signal interfaces.

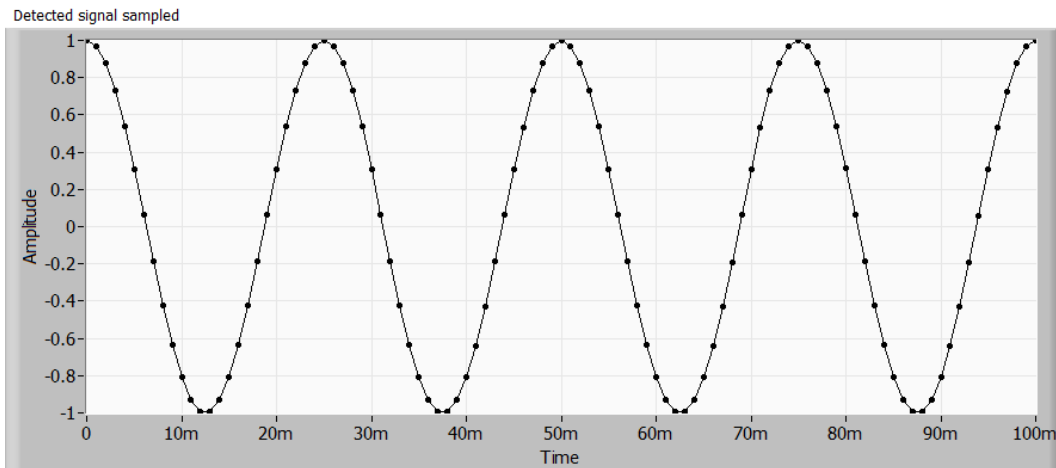


Figure 4.2 – The beat signal from a single reflector and a reference. Constant sweep rate. Beat signal from a constant sweep rate applied to a single reflection is a perfect sinewave.

The resulting A-line will be a single peak. The shape of the A-line is dependant on the window chosen and the amount of zero-padding. All the examples will use the same choices.

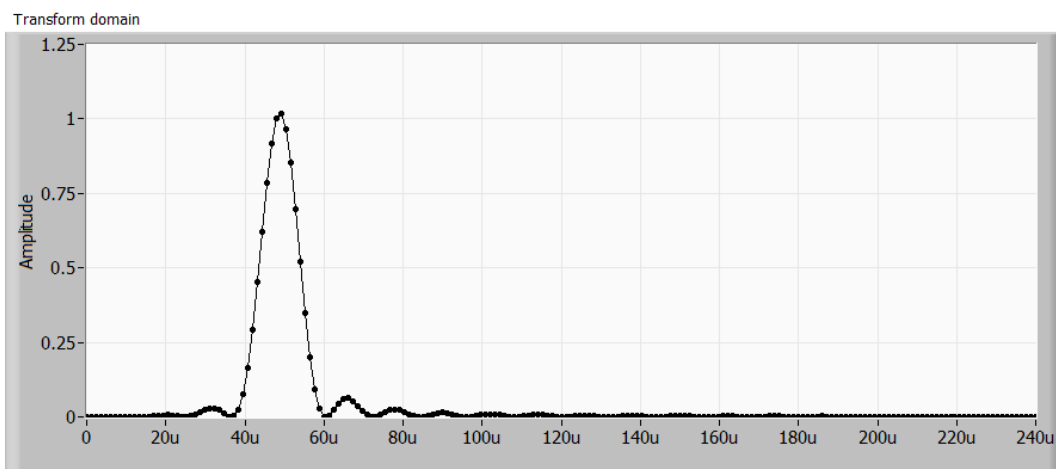


Figure 4.3 – The FFT after windowing and zero-padding. The FFT of the beat signal has a single peak showing the location of the single reflector relative to the reference.

4.1.2.

Example - Square wave variation in sweep rate

Here is an example of a non-linear sweep. The sweep rate varies from 75% slower to 75% faster than the constant sweep rate in Figure 4.1. This is a rather dramatic variation but it makes the effects very easy to follow.

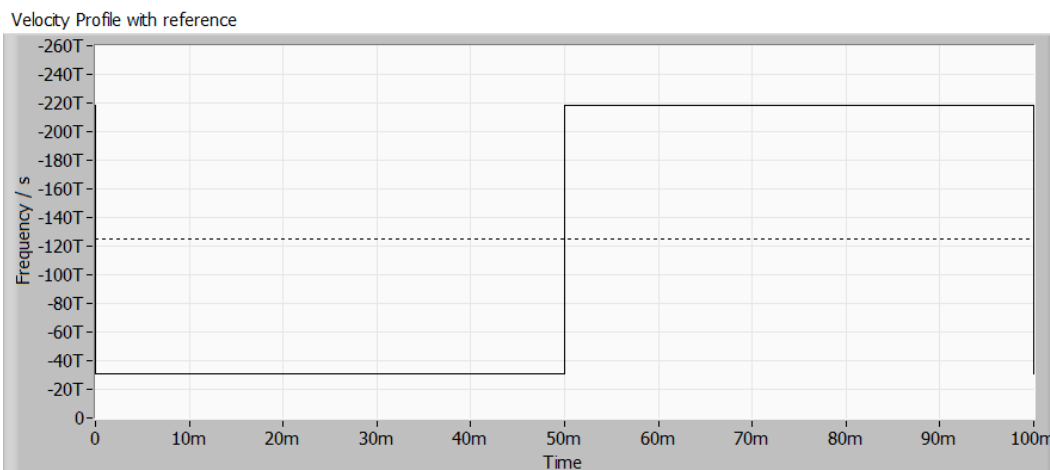


Figure 4.4 – Square wave variation in the sweep rate. Sweep rate varies from 75% slower to 75% faster than the constant sweep rate in Figure 4.1 on page 105.

The beat signal has two very obvious regions, the lower frequency region corresponding with the slower sweep rate and the higher frequency region corresponding with the higher sweep rate.

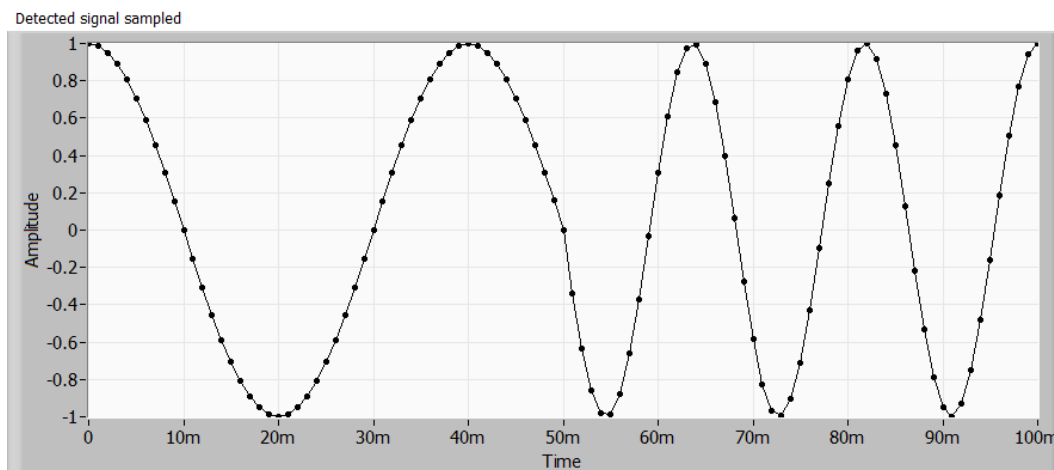


Figure 4.5 – The beat signal from a single reflector and a reference. Square wave variation in the sweep rate. The frequency of the beat signal follows the sweep rate.

The A-line is no longer a single peak but rather two, indicating the presence of the two frequencies in the beat signal.

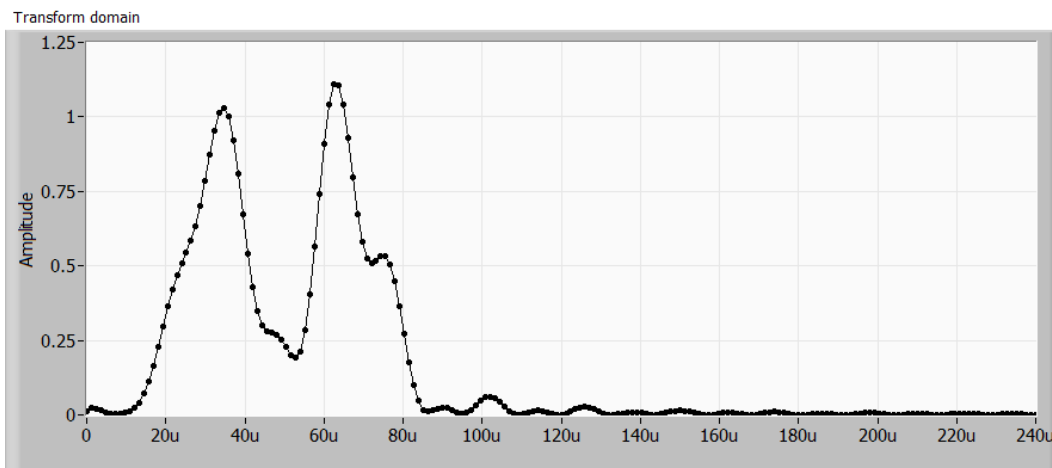


Figure 4.6 – The FFT after windowing and zero-padding. The FFT of the beat signal has multiple peaks resulting from the square wave variation in sweep rate. The multiple peaks obscure the location of the single reflector relative to the reference.

4.1.3.

Example – Triangle wave variation in sweep rate

In this case the sweep rate has the same average as before and even hits the same maximum and minimum sweep rates. However the variation is not abrupt, rather changing linearly.

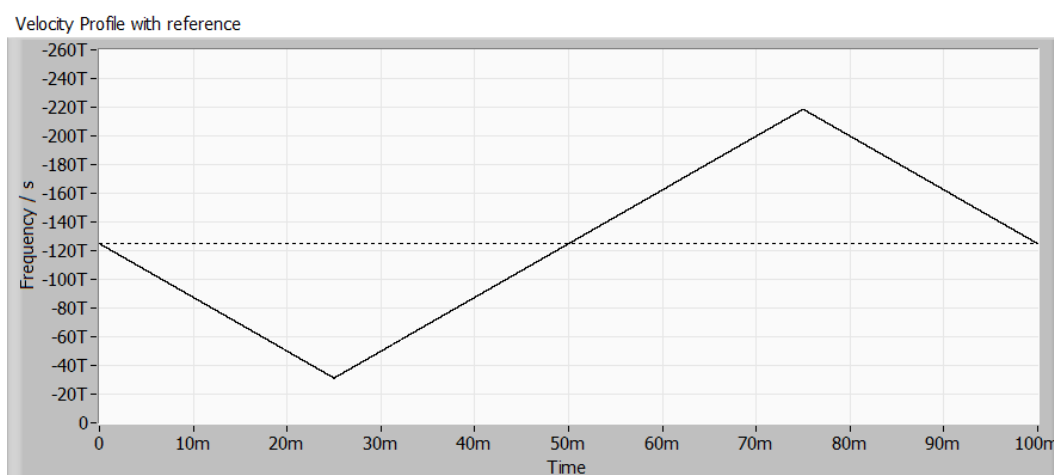


Figure 4.7 – Triangle wave variation in the sweep rate. Sweep rate varies from 75% slower to 75% faster than the constant sweep rate in Figure 4.1 on page 105.

The beat signal once again has lower frequencies and higher frequencies but they change more slowly from one to the next.

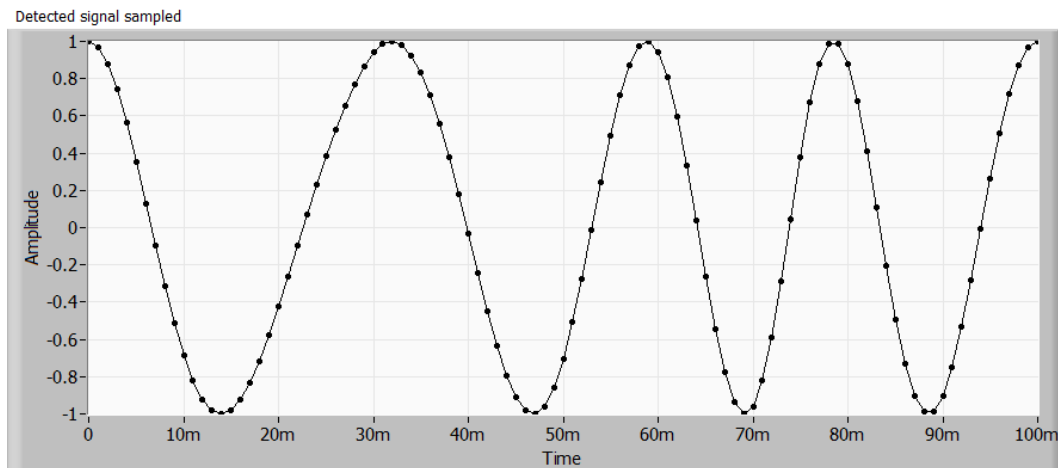


Figure 4.8 – The beat signal from a single reflector and a reference. Triangle wave variation in the sweep rate. The frequency of the beat signal follows the sweep rate.

The A-line is just as broad as before but now is more filled in, showing that more sweep rates were hit. More time was spent near the average rate than at the peak rates.

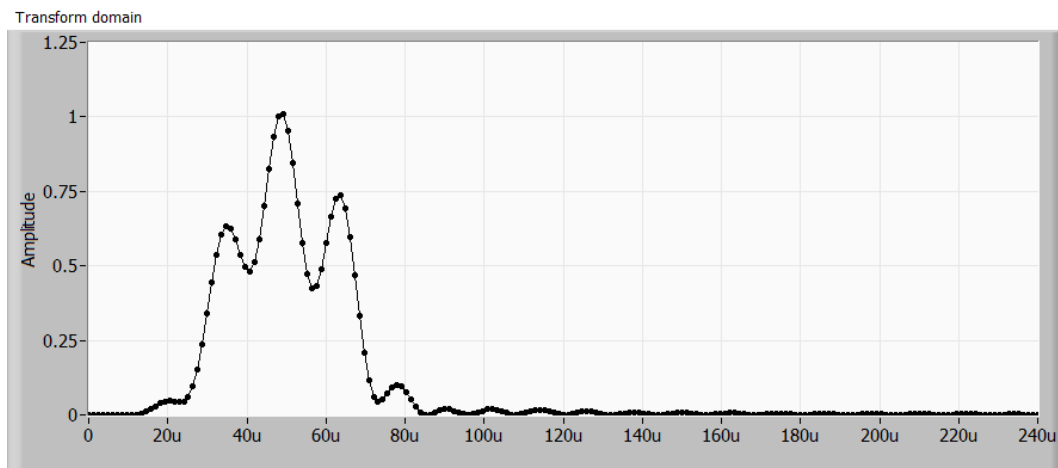


Figure 4.9 – The FFT after windowing and zero-padding. The FFT of the beat signal has multiple peaks resulting from the triangle wave variation in sweep rate. The multiple peaks obscure the location of the single reflector relative to the reference.

4.1.4.

Example – Sinusoidal wave variation in sweep rate

This time the sweep rate varies even more smoothly. The average, maximum and minimum sweep rates are still the same.

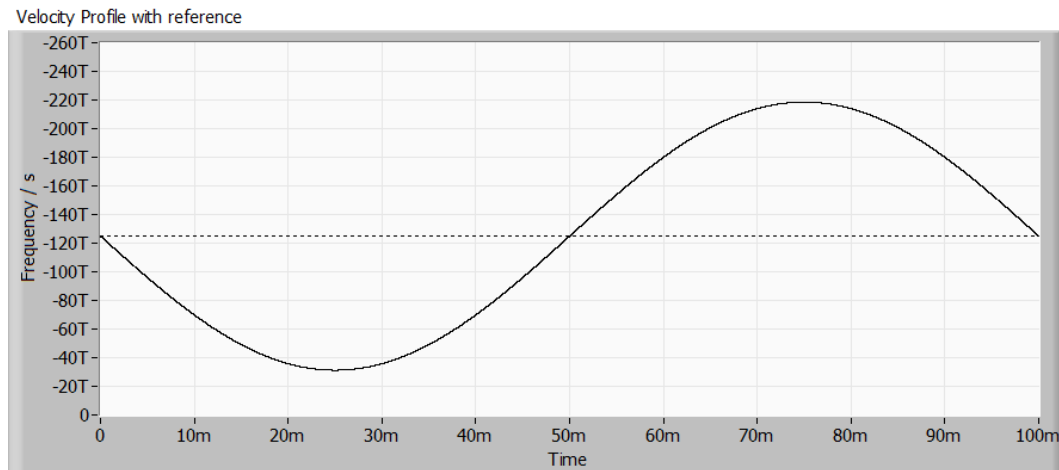


Figure 4.10 – Sinusoidal wave variation in the sweep rate. Sweep rate varies from 75% slower to 75% faster than the constant sweep rate in Figure 4.1 on page 105.

The beat signal consists of several frequencies again.

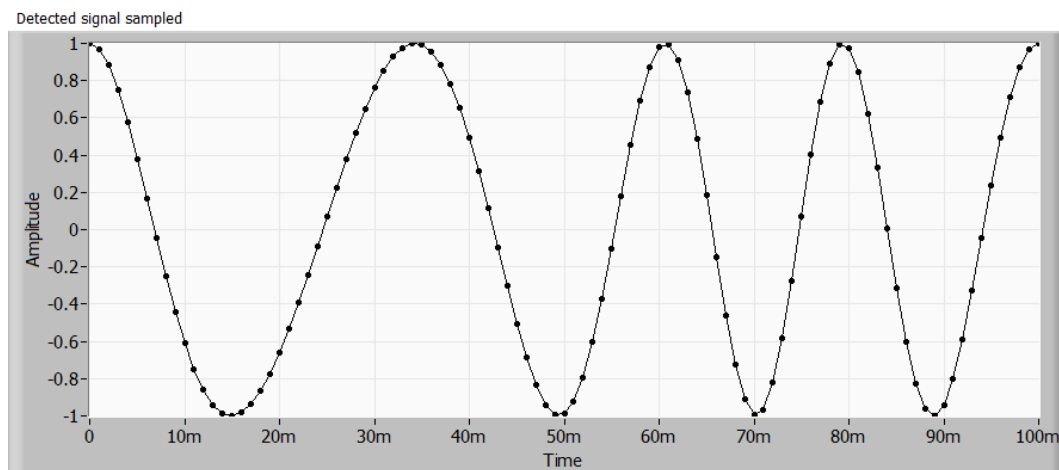


Figure 4.11 – The beat signal from a single reflector and a reference. Sinusoidal wave variation in the sweep rate. The frequency of the beat signal follows the sweep rate.

The A-line is spread across the same distances. More time was spent at lower and higher rates which is seen in the relative height of the peaks.

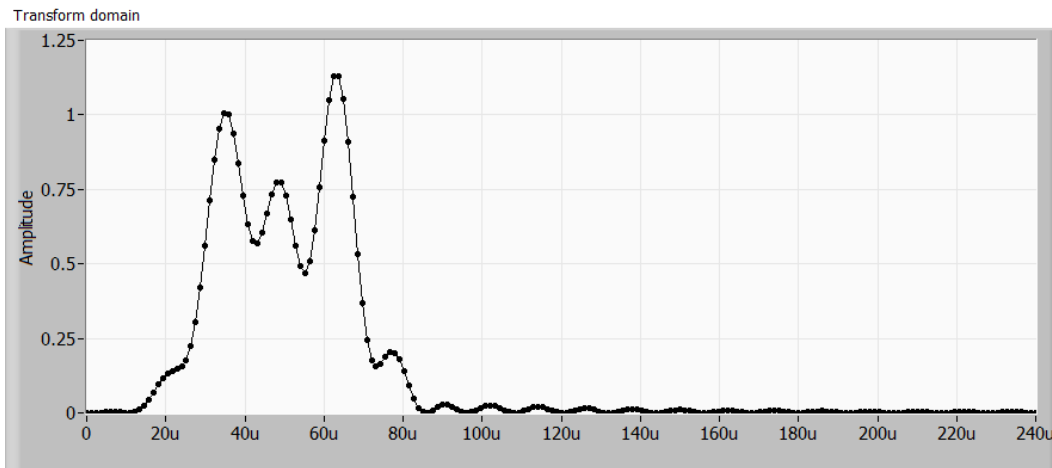


Figure 4.12 – The FFT after windowing and zero-padding. The FFT of the beat signal has multiple peaks resulting from the sinusoidal wave variation in sweep rate. The multiple peaks obscure the location of the single reflector relative to the reference.

4.1.5.

Example – 1000nm/s, a real world variation in sweep rate

A more realistic example is the subtle effect of sweeping at a constant wavelength rate rather than at a constant optical frequency rate.

Optical frequency and wavelength are inversely related.

$$\nu = c / \lambda \quad \text{Eq. 4.1}$$

Which means that the small changes in wavelength make changes in the optical frequency that change with the wavelength.

$$d\nu = -(c / \lambda^2) d\lambda \quad \text{Eq. 4.2}$$

Which means that the sweep rate in optical frequency will also be related to the sweep rate in wavelength as a function of wavelength.

$$d\nu/dt = -(c / \lambda^2) d\lambda/dt \quad \text{Eq. 4.3}$$

The optical frequency sweep rate seen while sweeping at a constant wavelength rate of 1000nm/s from 1500nm to 1600nm is shown in Figure 4.13. Note how small the difference is in comparison to the previous examples.

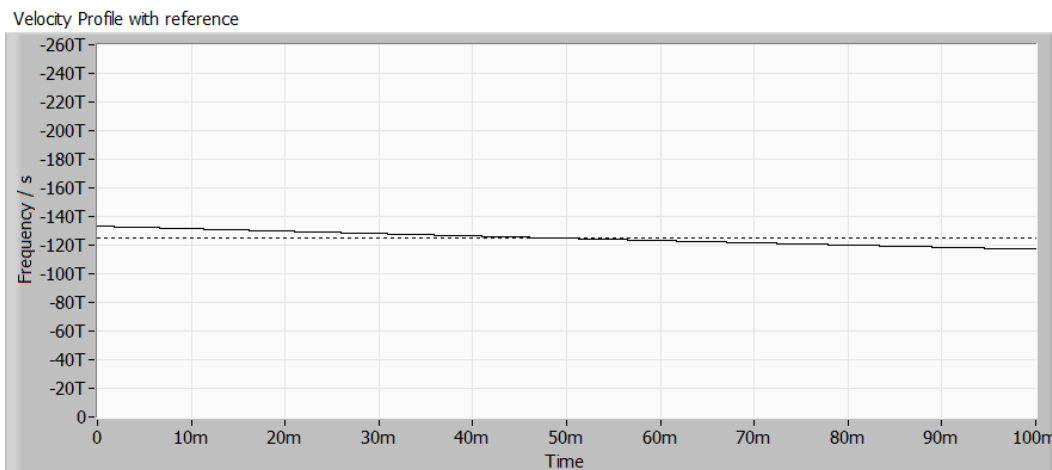


Figure 4.13 – Optical frequency sweep rate while sweeping at a constant wavelength sweep rate. Average value is the constant sweep rate in Figure 4.1 on page 105.

The change in optical frequency sweep rate is so slight that the frequency of the beat signal almost seems constant, at least to the naked eye.

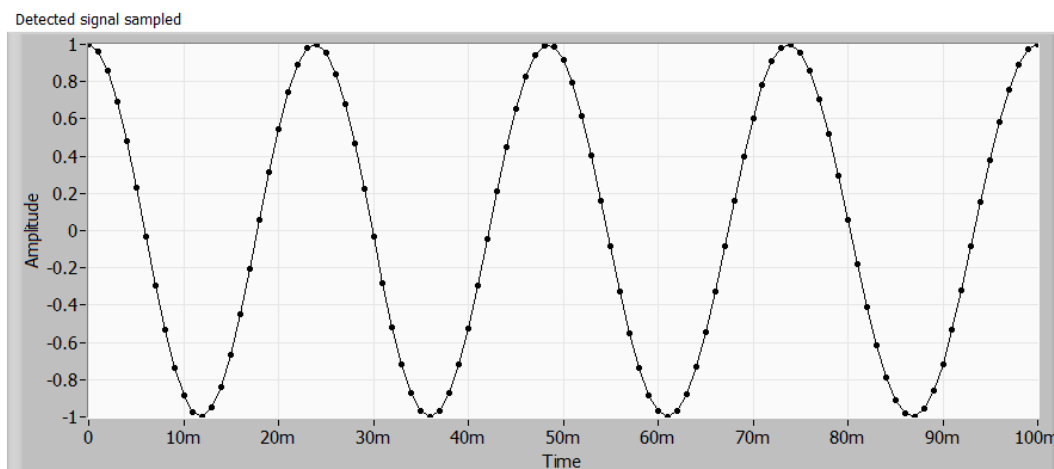


Figure 4.14 - The beat signal from a single reflector and a reference. Constant wavelength sweep rate.

And even the A-line seems the same as the one in Figure 4.3 for the constant sweep rate.

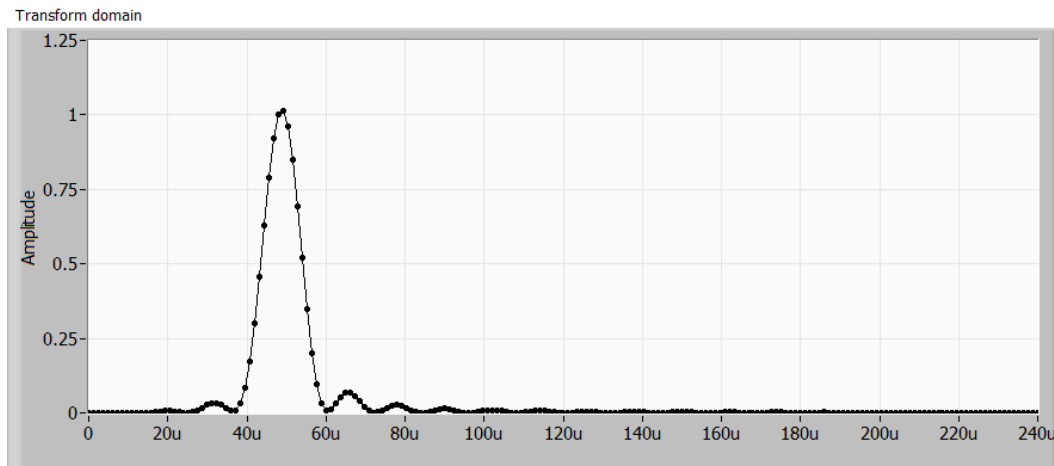


Figure 4.15 - The FFT after windowing and zero-padding. The FFT of the beat signal has only a single peak and appears very similar to the result from the constant sweep rate shown in Figure 4.3 on page 106.

As it turns out this is a little misleading as the effect is proportional to the distance of the peak. Small change from constant and a close-in peak and you will not see much change.

The reason we saw effects in the first few examples was because the non-linearity was exaggerated.

At further distances the effects of the even this modest non-linear sweep show themselves. After a few milli-meters the effects grow dramatically as the A-line peaks shrink and grow wider. At 9mm of distance the peaks are so wide that they merge with the peaks from 8mm. The loss in amplitude of the peak is a serious hit to signal to noise ratio as well.

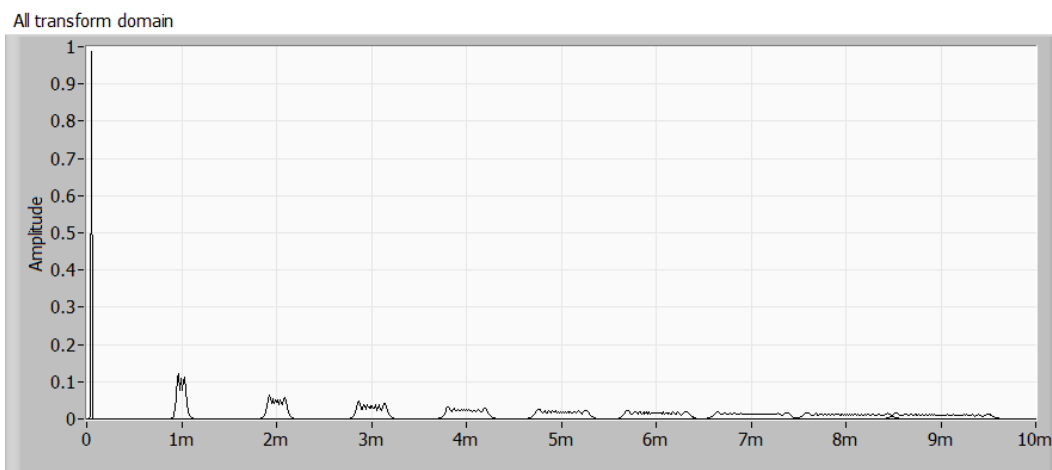


Figure 4.16 - FFT peaks as the measured interface is moved from 48 μ m to 9mm. The sweep rate is a constant nm/s (wavelength rate) which produces a non-constant optical frequency sweep rate. The width of the peak widens and the amplitude shrinks with relative distance from the reference.

The width of the peaks grow past 1mm by only 9mm of distance.

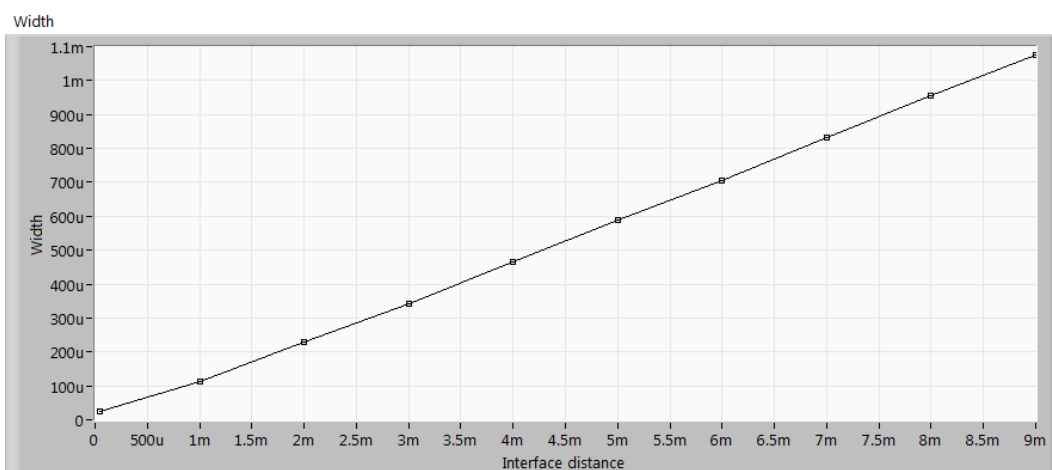


Figure 4.17 - Excess spreading in A-line peaks as the measured interface is moved from 48 μ m to 9mm. The sweep rate is a constant nm/s (wavelength rate) which produces a non-constant optical frequency sweep rate.

The amplitude drops off by almost two orders of magnitude in the same time.

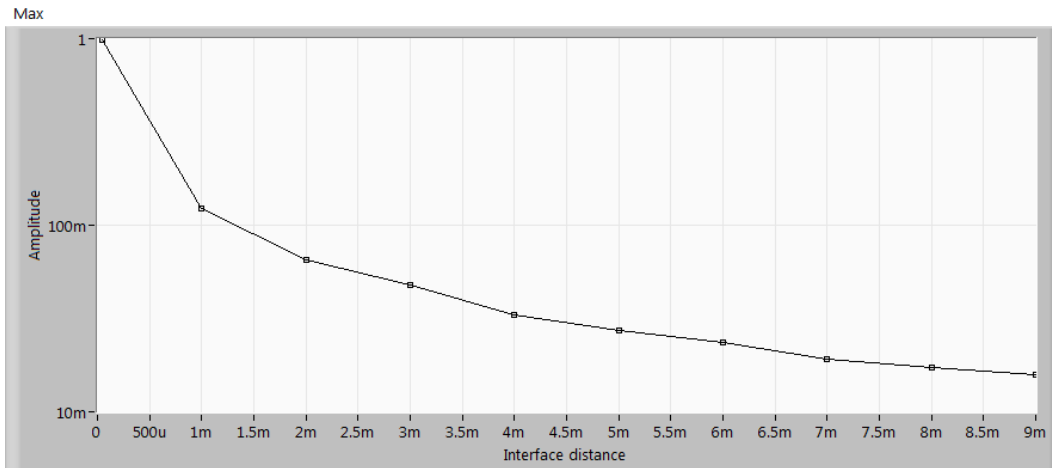


Figure 4.18 – Excess amplitude loss in A-line peaks as the measured interface is moved from 48um to 9mm. The sweep rate is a constant nm/s (wavelength rate) which produces a non-constant optical frequency sweep rate.

On the other hand, if we return to the constant sweep rate case, A-lines taken at different distances will neither grow wider nor lose amplitude. Thus maintaining both accuracy in location and signal to noise ratio.

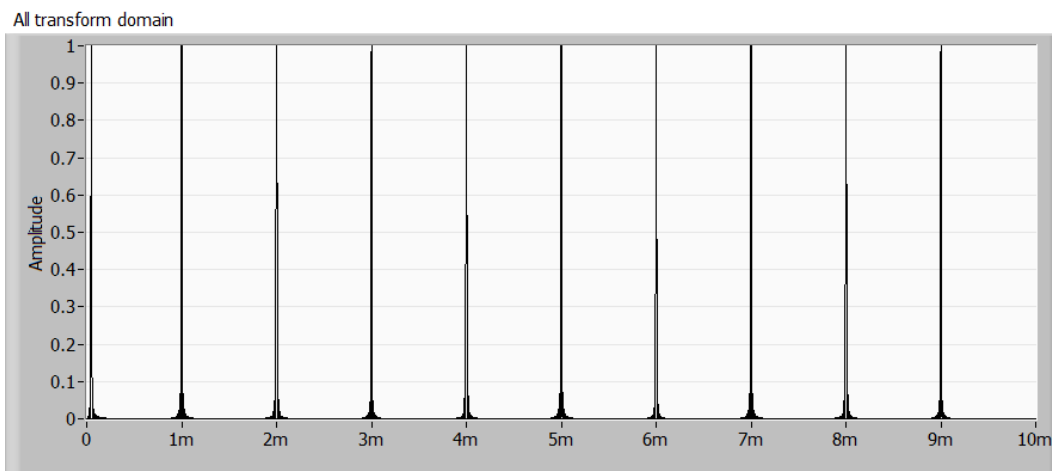


Figure 4.19 – A-lines of interfaces at distances from 48um to 9mm. The sweep rate was a constant optical frequency rate. There will be no excess spreading or loss of amplitude.

4.2. Compensating for non-linear sweeps

We have seen that even modest deviations away from a constant sweep rate can very seriously affect the A-line results. Therefore we will develop the means to compensate for the non-linear sweep.

First we should define what it is that we are interested in seeing.

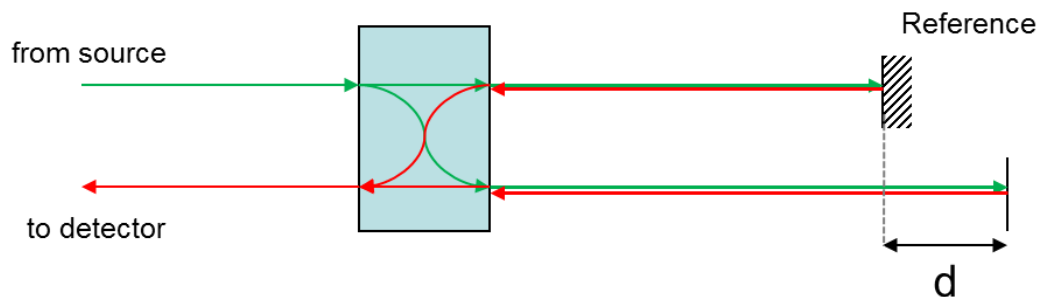


Figure 4.20 – SSOCT interferometer

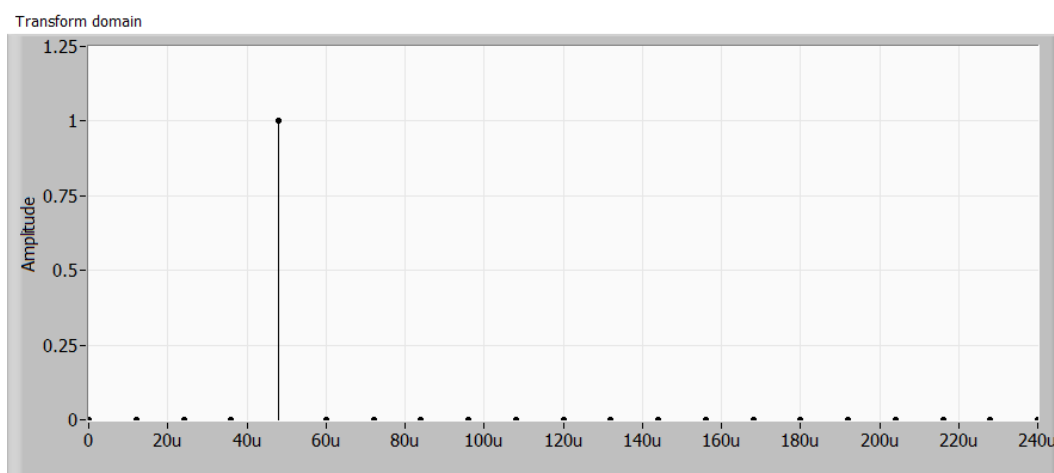


Figure 4.21 – Idealized A-line

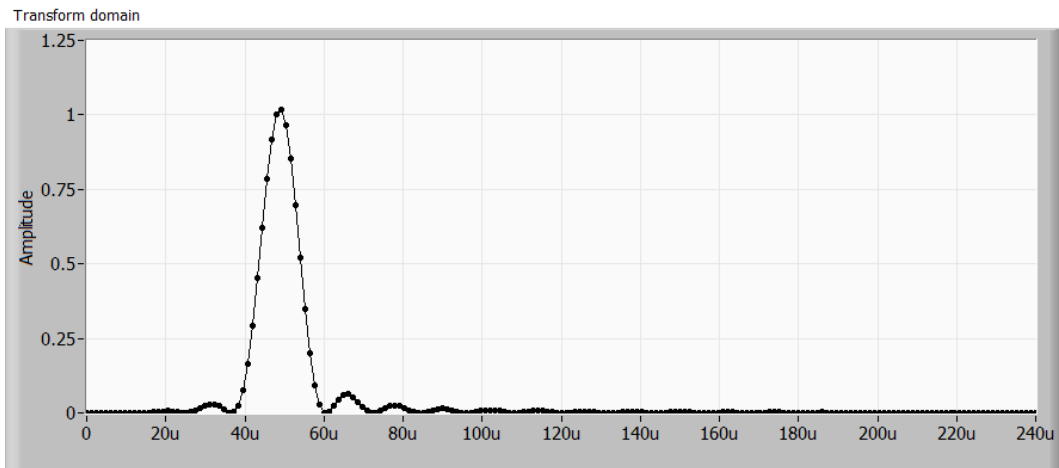


Figure 4.22 – Best A-line possible.

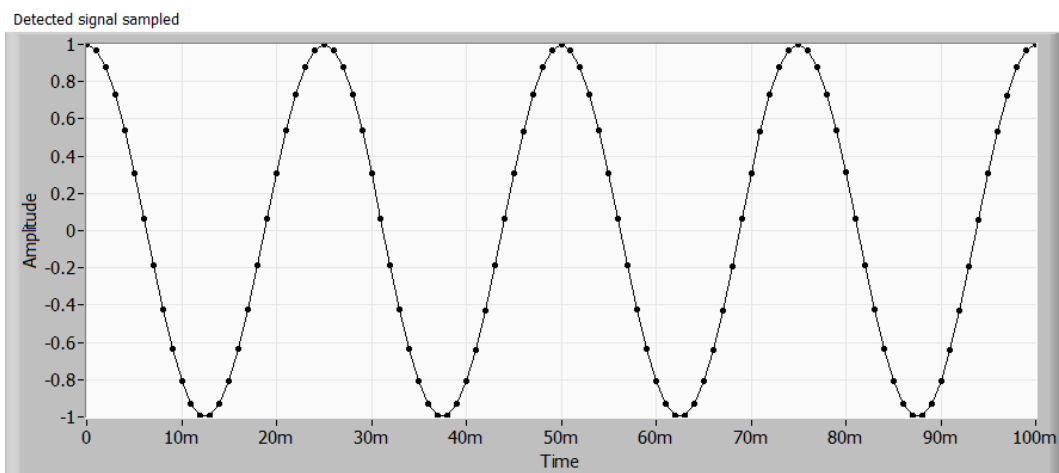


Figure 4.23 – Beat signal required to obtain the best possible A-line.

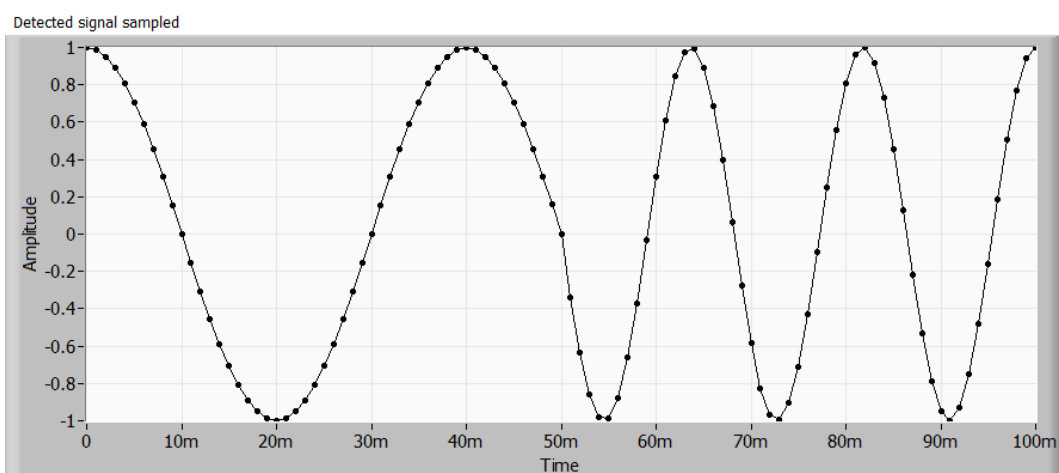


Figure 4.24 – Beat signal from a non-linear sweep. Specifically the sweep rate with square wave variation.

If we look closely at the optimal signal in Figure 4.23 we see that it had four complete cycles during the sweep. This is shown in Figure 4.25.

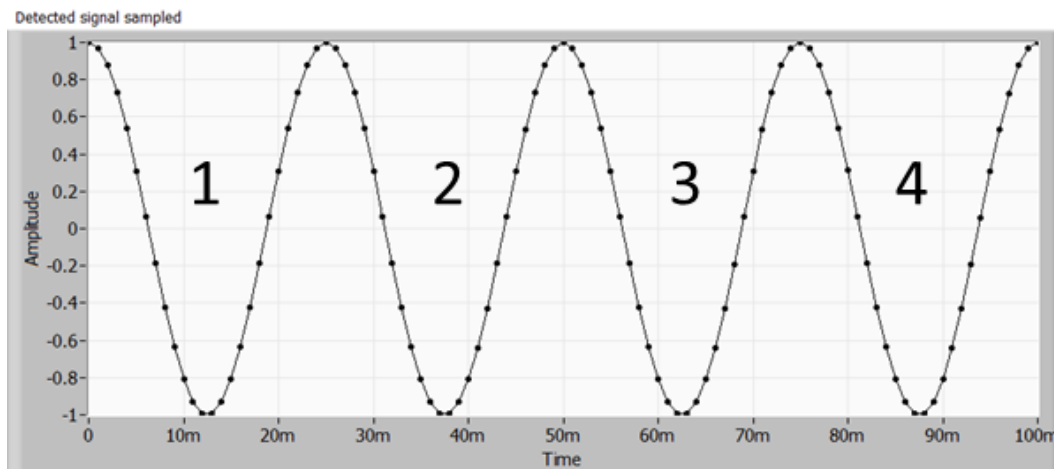


Figure 4.25 – Idealized beat signal had four cycles

Despite the square wave sweep rate, the beat signal in Figure 4.24 also completes exactly four complete cycles as shown in Figure 4.26.

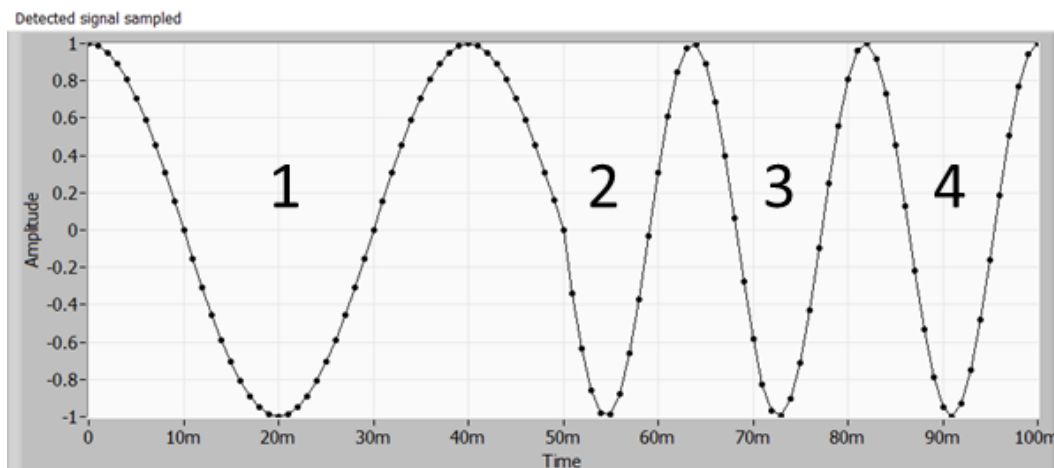


Figure 4.26 – Beat signal from highly non-linear sweep also has four cycles.

The difference is that the cycles were sampled an equal number of times in the case of the constant sweep rate as shown in Figure 4.27 but the number of samples in the square wave sweep rate vary depending on how fast the laser was sweeping during each cycle as shown in Figure 4.28.

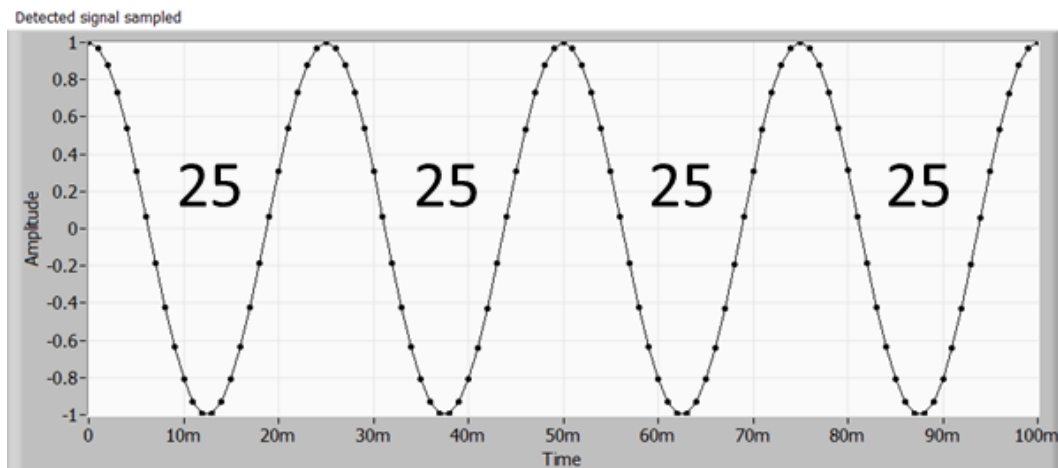


Figure 4.27 – The number of samples in each cycle is constant when the laser is swept at a constant sweep rate.

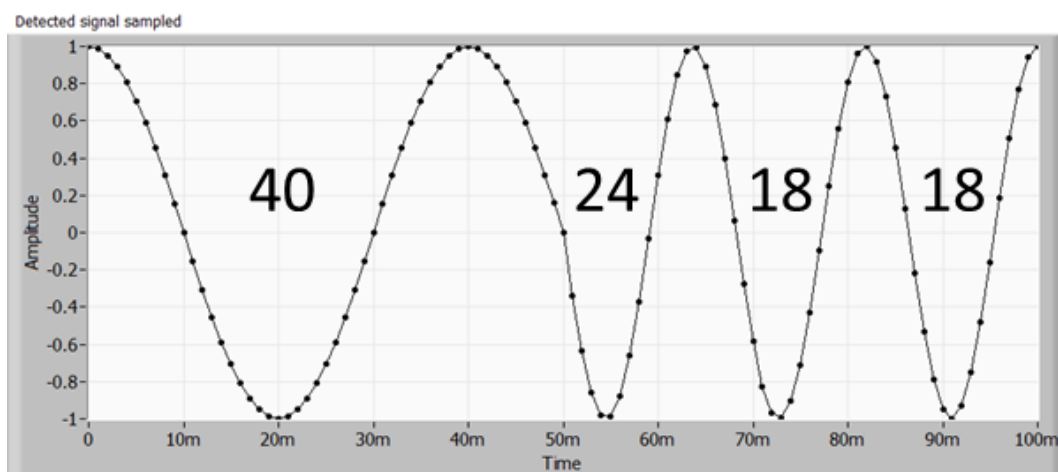


Figure 4.28 – The number of samples in each cycle varies depending on the sweep rate if the sweep rate is not constant.

If we sample each of the cycles with the constant number of samples as in the constant sweep rate case we would have the waveform shown in Figure 4.29. The samples would be spaced more widely when the sweep rate was slower and closer together when the sweep rate is faster.

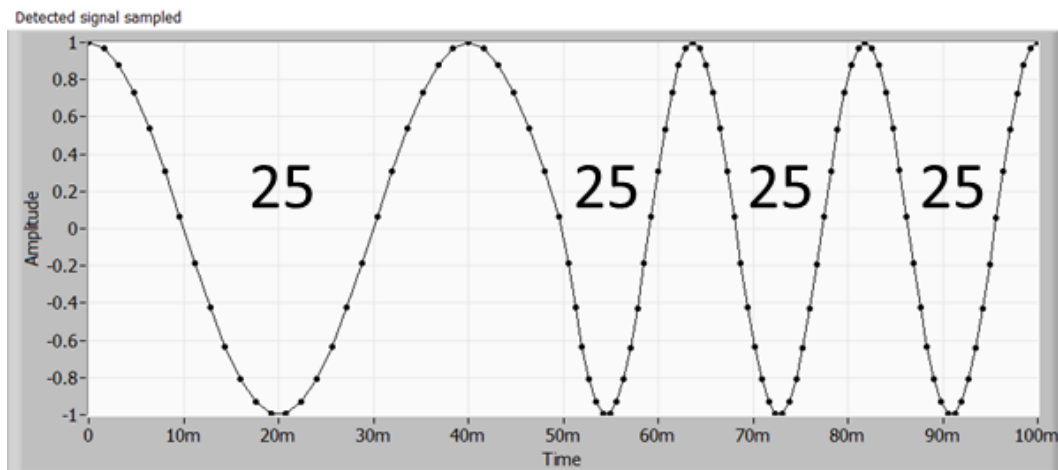


Figure 4.29 – Sampling the cycles using the same number of samples per cycle.

If we then plot the samples versus sample number rather than versus time, the waveform will look exactly the same as in the constant sweep rate case as shown in Figure 4.30.

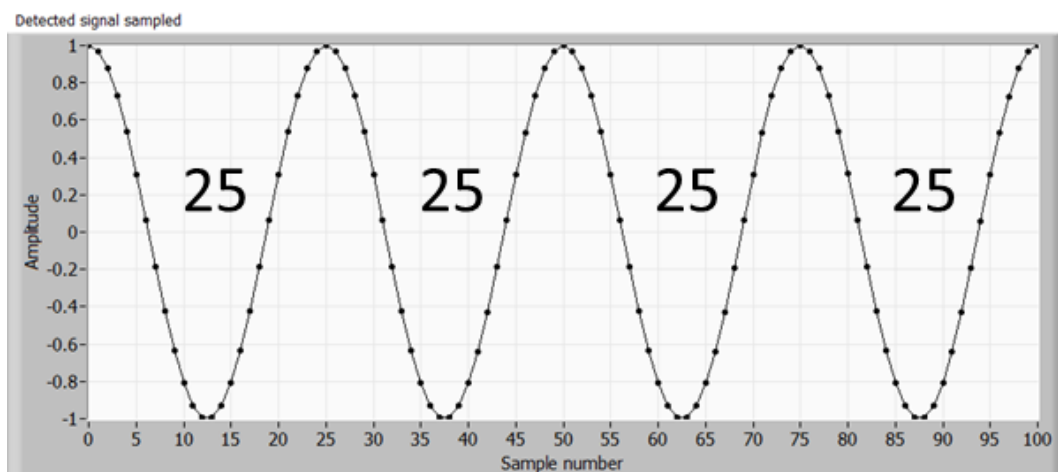


Figure 4.30 – Plotting the same data versus sample number rather than time.

Now we can window, zero-pad and take the FFT to find the single peak we were interested in finding.

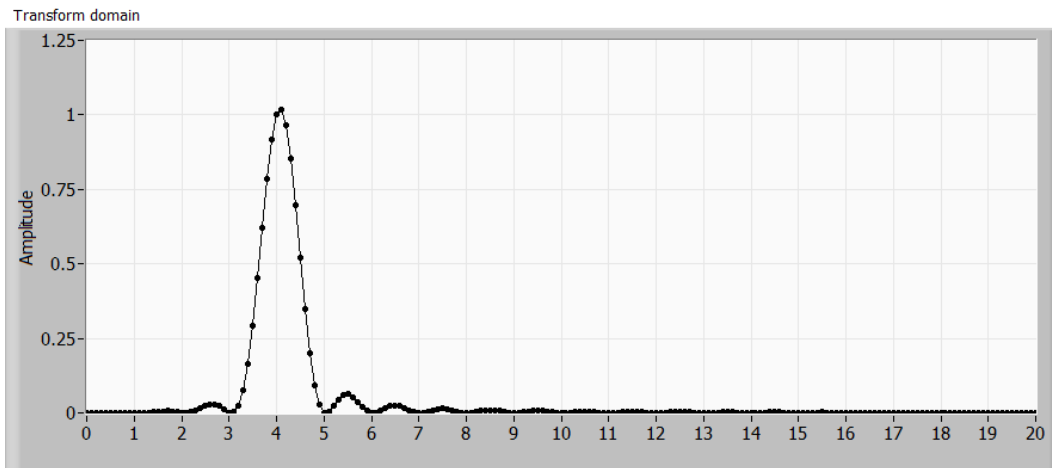


Figure 4.31 – Windowing, zero-padding and FFT gives the A-line we desired. Note that the scale is no longer distance. We will need to set the distance scale later.

4.3. Constant Optical Frequency Sampling

Let's revisit what we just did. We started with the results of sampling the non-linear sweep at a constant sampling rate. While the number of cycles across the sweep remained the same as in the constant sweep rate case, the number of samples that landed on each cycle varied with the sweep rate.

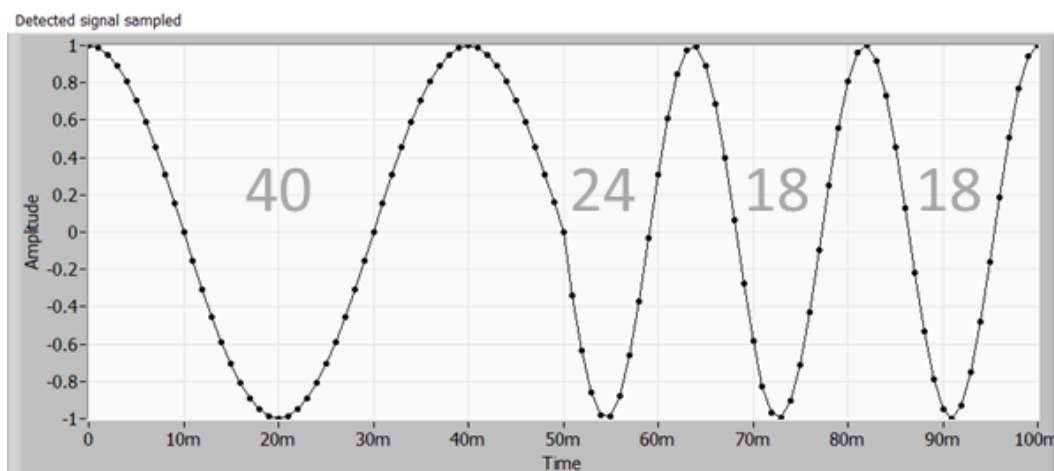


Figure 4.32 – The number of samples in each cycle depends on the sweep rate at the time.

If we plot the phase of the cycles as a function of time we get the two sectioned plot in Figure 4.33. The plot has two slopes as the sweep rate had two values during the sweep. The phase varies from 0 to 25 radians.

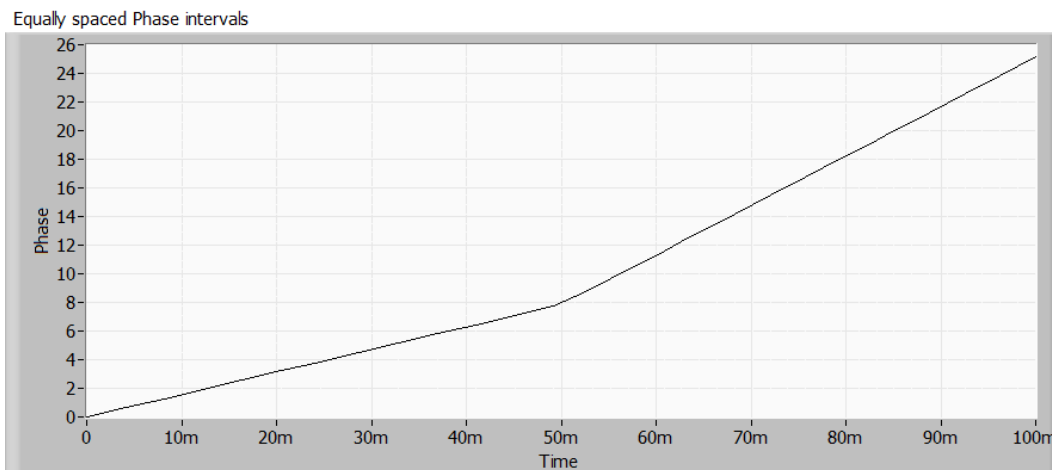


Figure 4.33 – Phase vs time.

Earlier we sampled the waveforms a constant number of times per cycle. In fact we were sampling at constant phase intervals. We divided the range of phases into sections of equal sized deltas as shown in Figure 4.34.

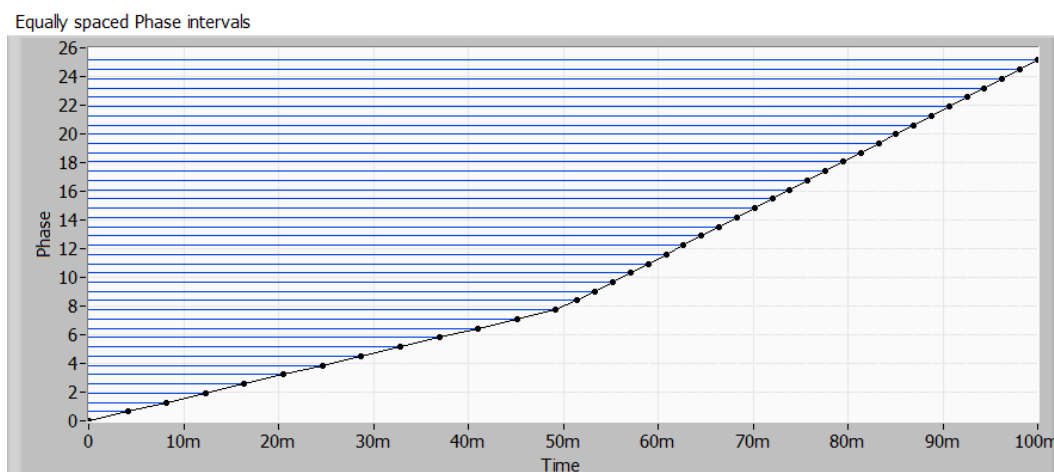


Figure 4.34 – Dividing the phase range into constant sized phase deltas.

Now we can use the plot of phase versus time to find the times which correspond with the constant phase deltas as in Figure 4.35

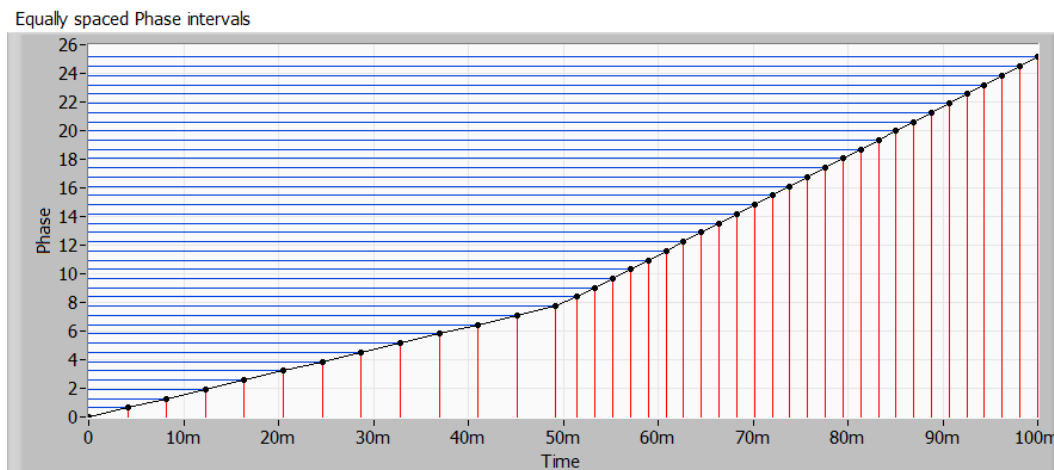


Figure 4.35 – The phase vs time curve is used to map the constant phase deltas into time values at which they occurred.

Now that we have the times corresponding to the constant delta phase points we can sample the beat signal at these times and obtain the equal number of samples per cycle we were looking for (Figure 4.36).

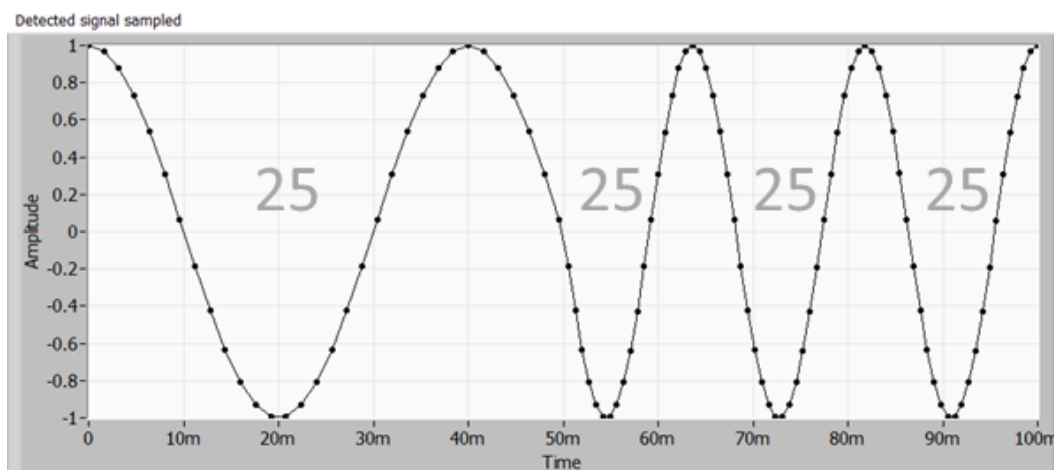


Figure 4.36 – Resampling at the times corresponding to the constant delta phase values gives us the constant number of samples per cycle we were looking for.

Now we can drop the time scale and plot the data versus sample number and we have our nice clean sine wave as in Figure 4.37.

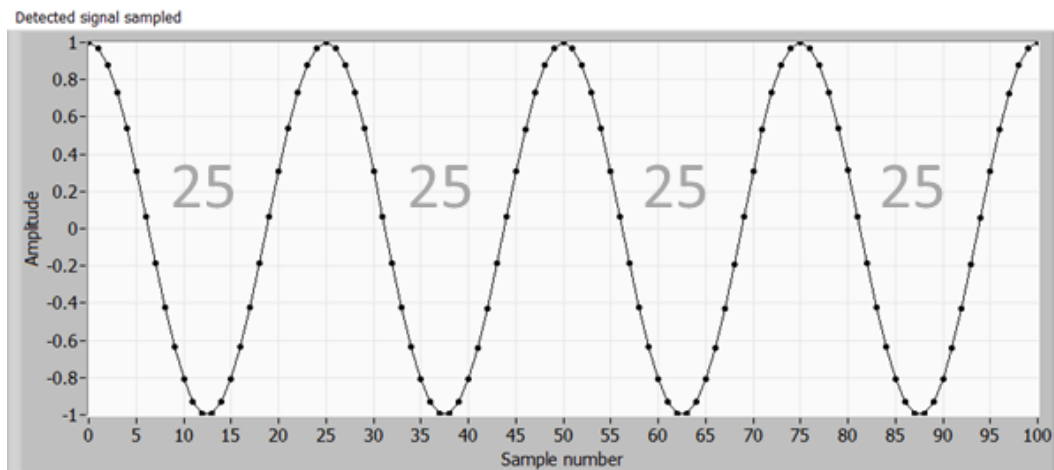


Figure 4.37 – Replotting the data vs sample number rather than vs time gives us a clean sine wave.

Now we window, zero-pad and take the FFT to achieve the single peak shown in Figure 4.38. The scale is not distance yet however.

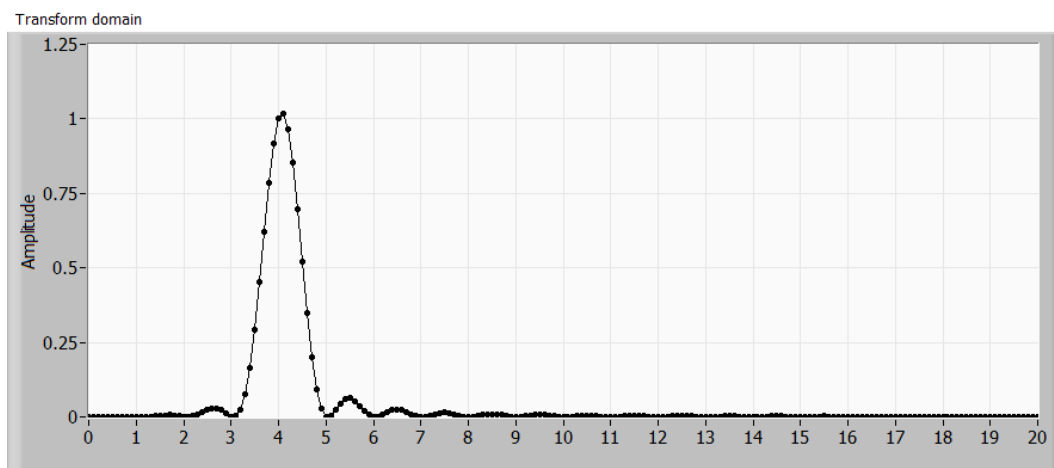


Figure 4.38 – FFT of the new sinewave is an unambiguous peak. The scale is not a distance scale yet.

Let's examine how optical frequency comes into this. It seems clear how the dividing the phase into equally spaced sections can result in the in a clean FFT but how do we get access the phase?

Let's go back to the beat signal from the square wave sweep rate sampled at the constant sample rate.

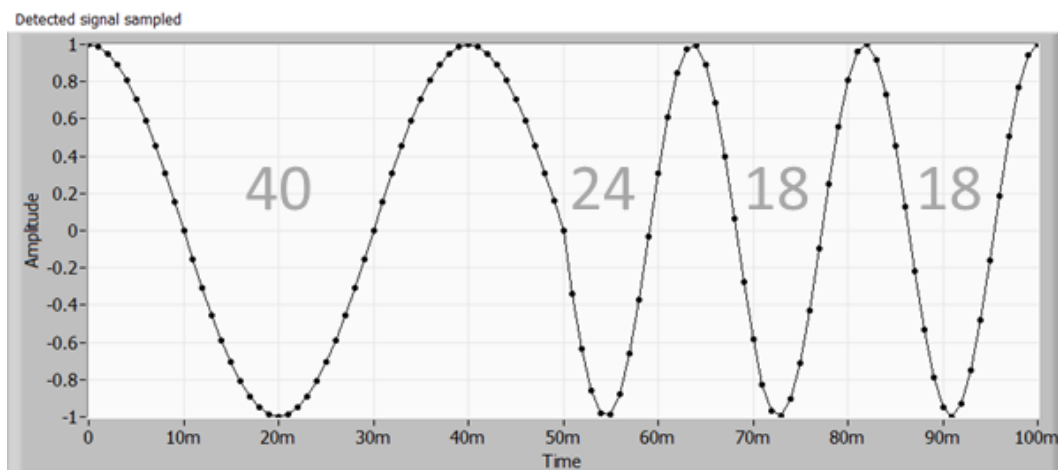


Figure 4.39 – Once again the beat signal from the square wave sweep rate.

Once again here in Figure 4.40 is the plot of the phase versus time.

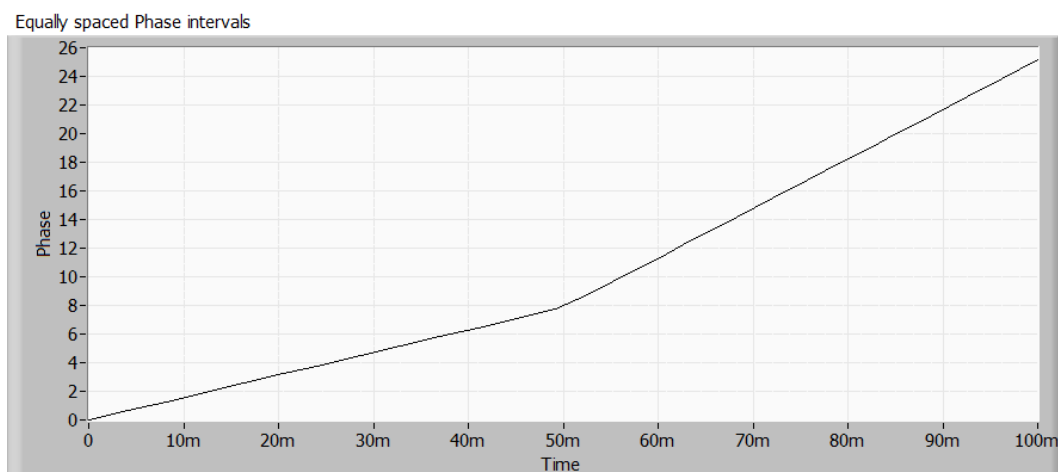


Figure 4.40 – Phase versus time.

The optical frequency is plotted versus time in Figure 4.41. Note the similarity in shape to the phase in Figure 4.40.

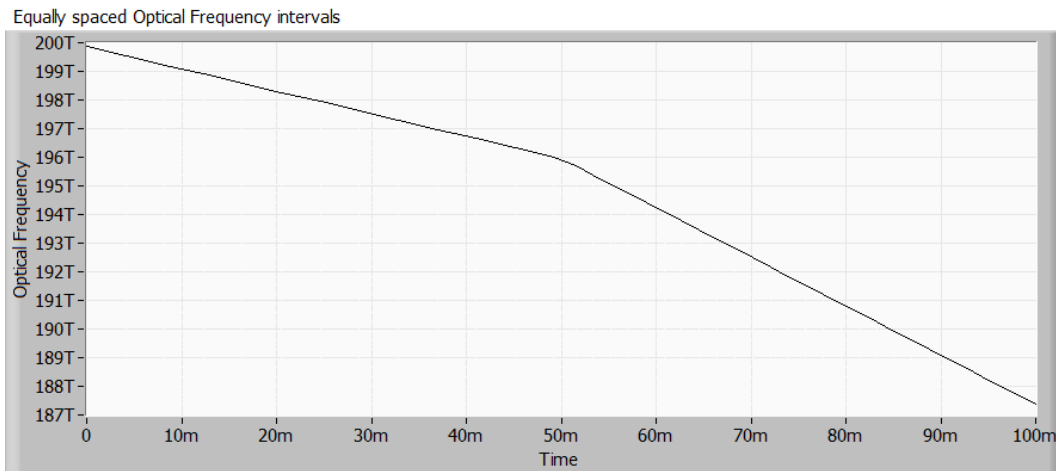


Figure 4.41 – Optical frequency of source vs time

If we plot phase versus optical frequency we see an interesting result. The phase appears to be a linear function of the optical frequency.

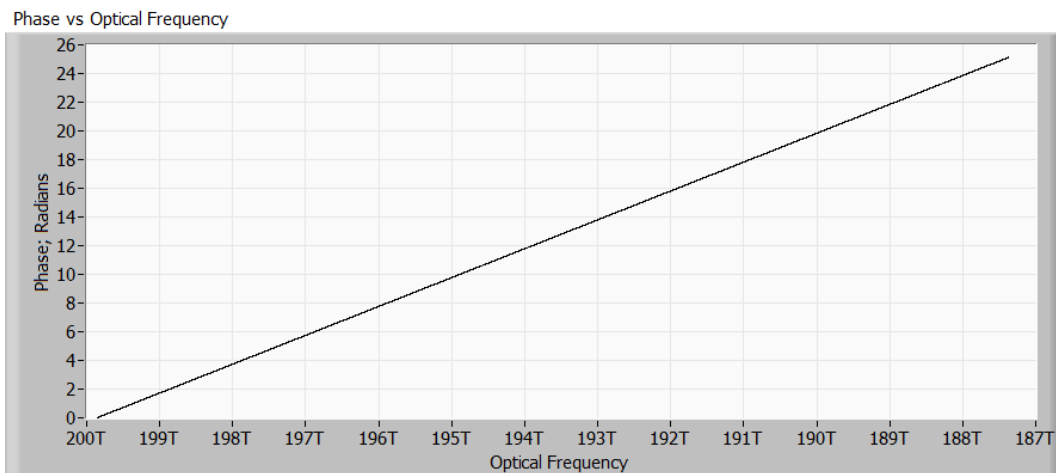


Figure 4.42 – Phase versus optical frequency.

In fact, as shown in Figure 4.43, the slope of the line is $2\pi\tau$, where τ is the roundtrip time in the interferometer.

$$\Phi(\nu) = 2\pi\tau\nu + \Phi(0) \quad \text{Eq. 4.4}$$

The fact that phase is proportional to optical frequency is sufficient to allow us to use ν in the place of Φ , the phase of the beat signal, when calculating equally spaced intervals.

$$\Phi \propto \nu \quad \text{Eq. 4.5}$$

slope (rad/hz)	intercept	residue
-2.01202p	402.1	616p
2 Pi Tau	slope / 2PiTau	
2.01201p	-1.0000055	
Reflection (d)	Delay (Tau)	
48u	320.222f	
2nd/c		

Figure 4.43 – Best linear fit of optical frequency versus time.

Let's see that in action.

Returning to the beat signal from the square wave sweep rate sampled at the constant sample rate, repeated once again in Figure 4.44

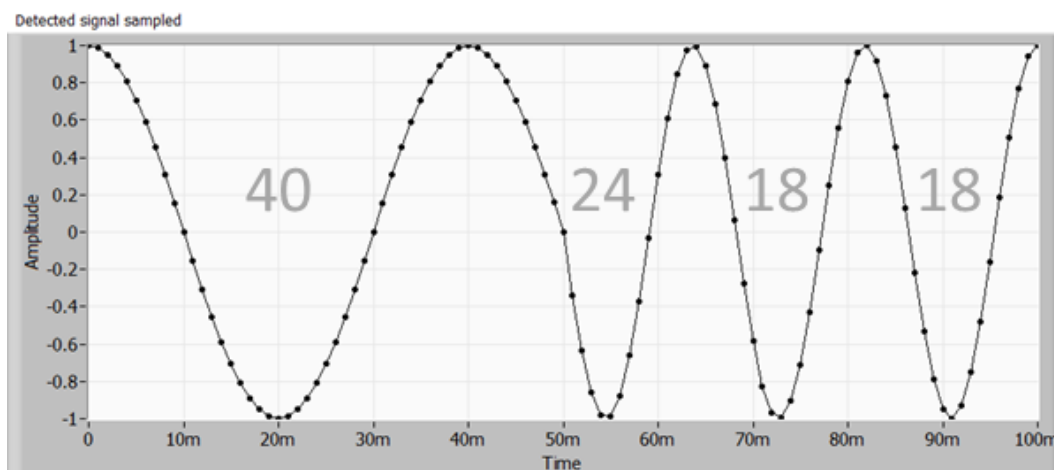


Figure 4.44 - Once again the beat signal from the square wave sweep rate.

In the place of phase as a function of time Figure 4.45 shows the optical frequency as a function of time.

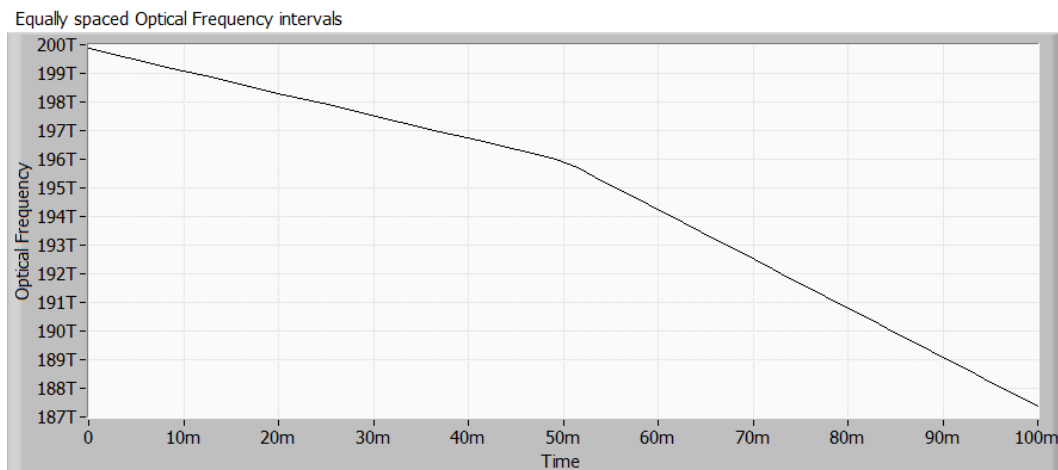


Figure 4.45 – Optical frequency as a function of time.

In Figure 4.46 we have divided up the optical frequency span into an integer number of equal sized intervals.

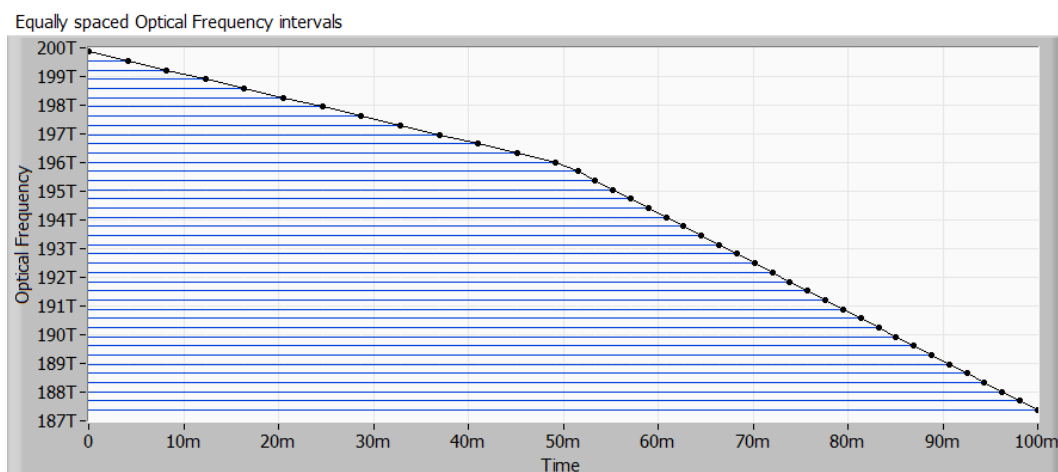


Figure 4.46 – Equally spaced optical frequency intervals.

We use the optical frequency as a function of time curve to find the points in time corresponding to these optical frequencies as shown in Figure 4.47.

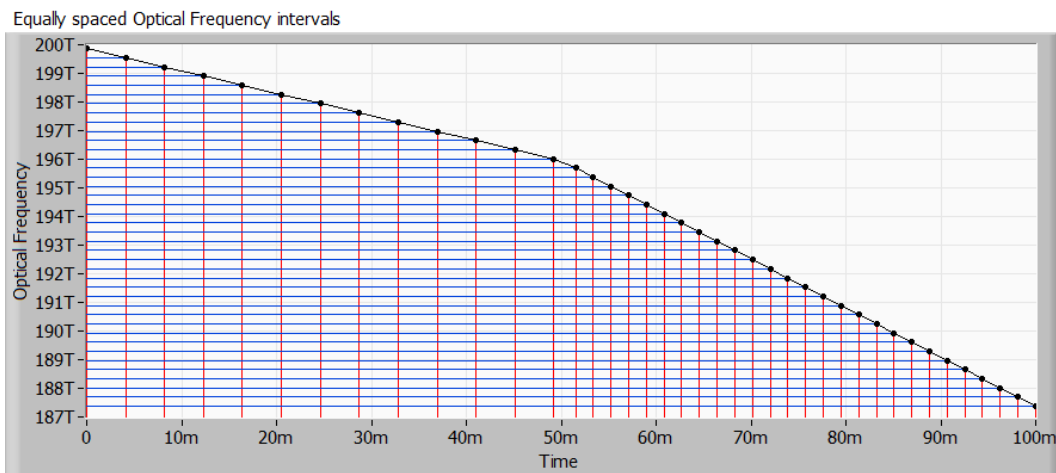


Figure 4.47 – The optical frequency versus time curve is used to find the times associate with the equally spaced optical frequencies.

Figure 4.48 shows the beat signal from Figure 4.44 resampled at these new times which results in a constant number of samples per cycle.

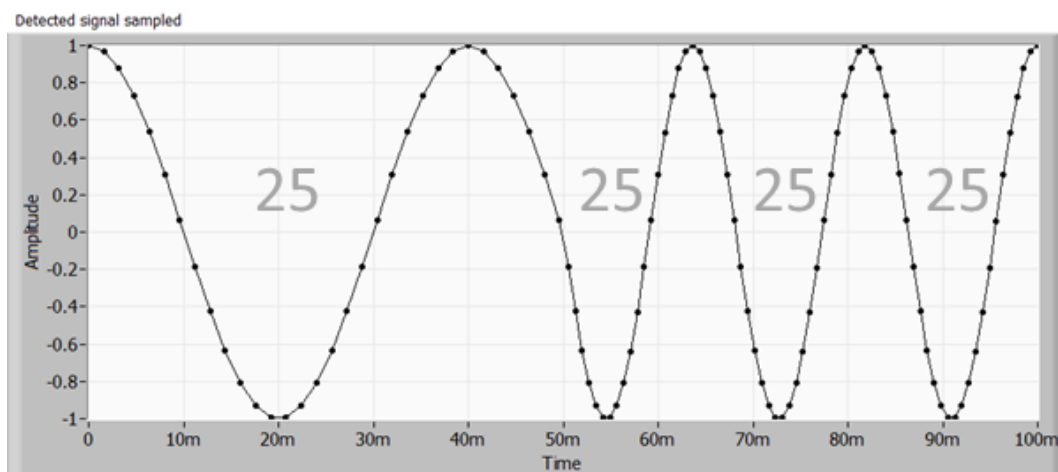


Figure 4.48 – Resampling at the times corresponding to the equally spaced optical frequencies puts equal numbers of samples on each of the cycles of the beat signal.

Now we can replot versus sample number as shown in Figure 4.49.

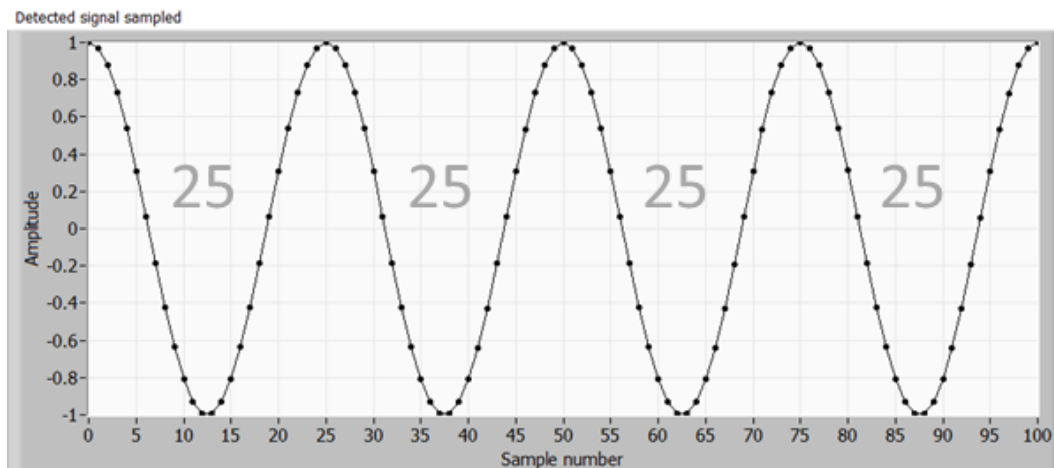


Figure 4.49 – The data is replotted versus sample number giving a clean sinewave.

Now we window, zero-pad and take the FFT to achieve the single peak shown in Figure 4.50. As mentioned before, the scale is not distance.

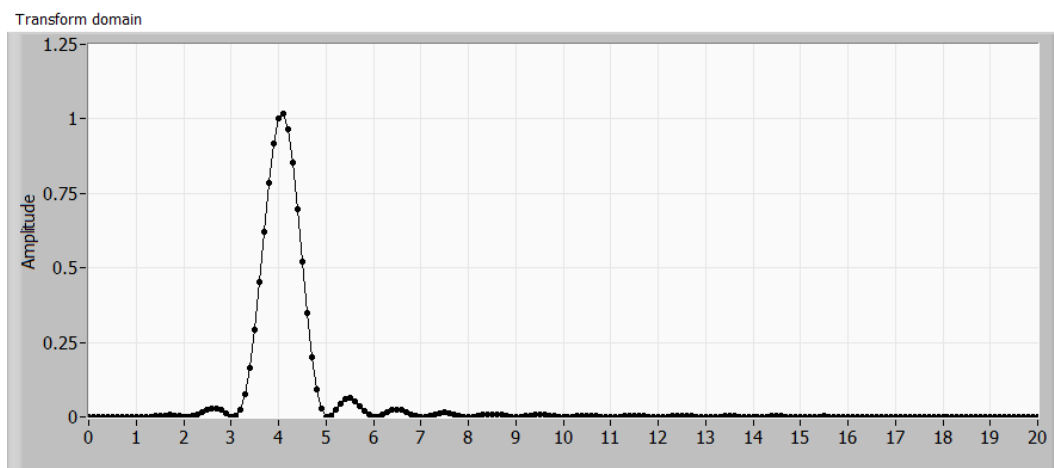


Figure 4.50 - FFT of the new sinewave is an unambiguous peak. The X-scale is not a distance.

This result is somewhat empirical but valuable from an intuition perspective. A mathematical treatment leading to the same result is in the next section.

4.4. Optical Frequency Sampling

The optical frequency and phase relationship was pointed out by Brinkmeyer in 1993 [Glombitza; Brinkmeyer (1993)].

The phase of the optical waveform can be approximated by its Taylor expansion. The current phase in terms of the phase at time τ seconds earlier is shown in Eq. 4.6.

$$\varphi(t) = \varphi(t-\tau) + \tau d\varphi(t-\tau)/dt + \frac{1}{2} \tau^2 d^2\varphi(t-\tau)/dt^2 + \text{HOT} \quad \text{Eq. 4.6}$$

It is just as valid and more useful for us to instead calculate the phase at the time τ seconds earlier in terms of the current phase as shown in Eq. 4.7.

The first and second order derivatives are taken at the current time rather than at the earlier time since we are working from the current time now.

$$\varphi(t-\tau) = \varphi(t) - \tau d\varphi(t)/dt - \frac{1}{2} \tau^2 d^2\varphi(t)/dt^2 + \text{HOT} \quad \text{Eq. 4.7}$$

Optical frequency is related to the phase as in Eq. 4.8.

$$\nu(t) = d\varphi(t)/dt \quad \text{Eq. 4.8}$$

Therefore we can put Eq. 4.7 in terms of the optical frequency as in Eq. 4.9.

$$\varphi(t-\tau) = \varphi(t) - 2\pi\tau \nu(t) - \frac{1}{2} (2\pi) \tau^2 d\nu(t)/dt + \text{HOT} \quad \text{Eq. 4.9}$$

The difference in optical phase over τ is shown in Eq. 4.10.

$$\varphi(t) - \varphi(t-\tau) = 2\pi\tau \nu(t) + \frac{1}{2} (2\pi) \tau^2 d\nu(t)/dt + \text{HOT} \quad \text{Eq. 4.10}$$

If we let τ be the round trip time in our interferometer, then this difference in phase becomes the instantaneous phase of the beat signal $\Phi(t)$ from the two signals leaving our interferometer as shown in Eq. 4.11.

$$\Phi(t) = \varphi(t) - \varphi(t-\tau) \quad \text{Eq. 4.11}$$

This means the instantaneous phase of the beat signal can be written in terms of the optical frequency as in Eq. 4.12.

$$\Phi(t) = 2\pi\tau \nu(t) + \frac{1}{2} (2\pi) \tau^2 d\nu(t)/dt + \text{HOT} \quad \text{Eq. 4.12}$$

The HOT (higher order terms) terms will have increasing powers of τ which is on the order of 10^{-12} and so we will ignore them.

We would also like to simplify the Eq. 4.12 to our results in Eq. 4.4 which we can do if the second term can be ignored as in Eq. 4.13.

$$\Phi(t) = 2\pi\tau \nu(t) \text{ if } \frac{1}{2} (2\pi) \tau^2 d\nu(t)/dt \text{ can be ignored} \quad \text{Eq. 4.13}$$

Brinkmeyer in '93 puts the criterion for 'ignorable' as shown in Eq. 4.14.

$$\tau^2 dv(t)/dt \ll 1 \quad \text{Eq. 4.14}$$

Most authors have cited Brinkmeyer in the years since which is reasonable since τ is small and sweep rates have been moderate.

However newer sources have much higher sweep rates which causes us to revisit the critereon.

For example, Table 2 shows this critereon evaluated for three lasers. The first laser is the laser used by Brinkmeyer in their OFDR studies in 1993. The laser is slow and so despite the inteferometric distances (τ) being relatively large the critereon evaluates to 0.1u, safely satisfying the critereon. The second laser is a modified New Focus 8700 series ECDL which sweeps much faster but the application space is such (OCT) that the interferometric distances are much smaller. The two offset each other and the critereon evaluates to 35u which still satisfies the critereon. The third laser is constructed from a Santec Ultra-wideband femtosecond pulsed laser. The sweep rate is very very fast and so despite being used with smaller interferometric distances the critereon evaluates to 1.25. Not just not much less than one but not even less than one. So this critereon has broken down.

Table 2 – Brinkmeyer critereon for Brinkmeyer’s laser, our New Focus laser and our Stretched Pulse Santec laser. The critereon still is reasonable for the New Focus laser as despite the sweep rate increasing by a factor of 1000 the time scale has decreased. The stretched pulse Santec laser on the other hand is so fast that the critereon breaks down despite the smaller time scale.

	Brinkmeyer 1993	New Focus Laser	Stretched Santec
τ	1ns	66ps	66ps
dv/dt	100Ghz/s	124.9Thz/s	287M Thz/s
1993 Critereon should be $\ll 1$.	0.1u	35u	1.25

And this shows only a few lasers. To get a better sense of the limits of the critereon we can plot the critereon vs a parameter space of τ and sweep rate (dv/dt) as shown in Figure 4.51.

The critereon is the vertical scale. Critereon values less than 100u are considered much less than one and are green. Critereon values over this are black.

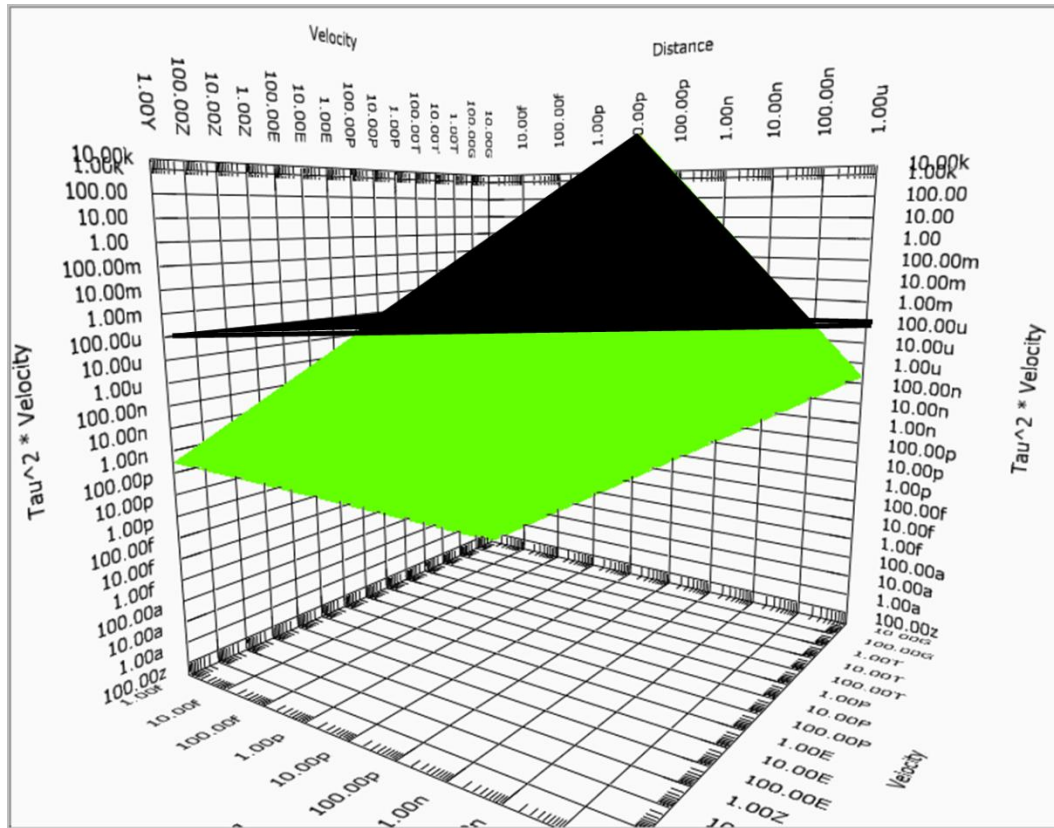


Figure 4.51 – Brinkmeyer critereon vs dv/dt (sweep rate or velocity) and τ . The green / black demarkation is at the $\ll 1$ being set to 100u (one part in 10,000).

Looking from the top we can see the sweep rate – τ pairs which satisfy the critereon (green) and which fail (black). The locations of the three lasers mentioned in Table 2 are shown in different colors.

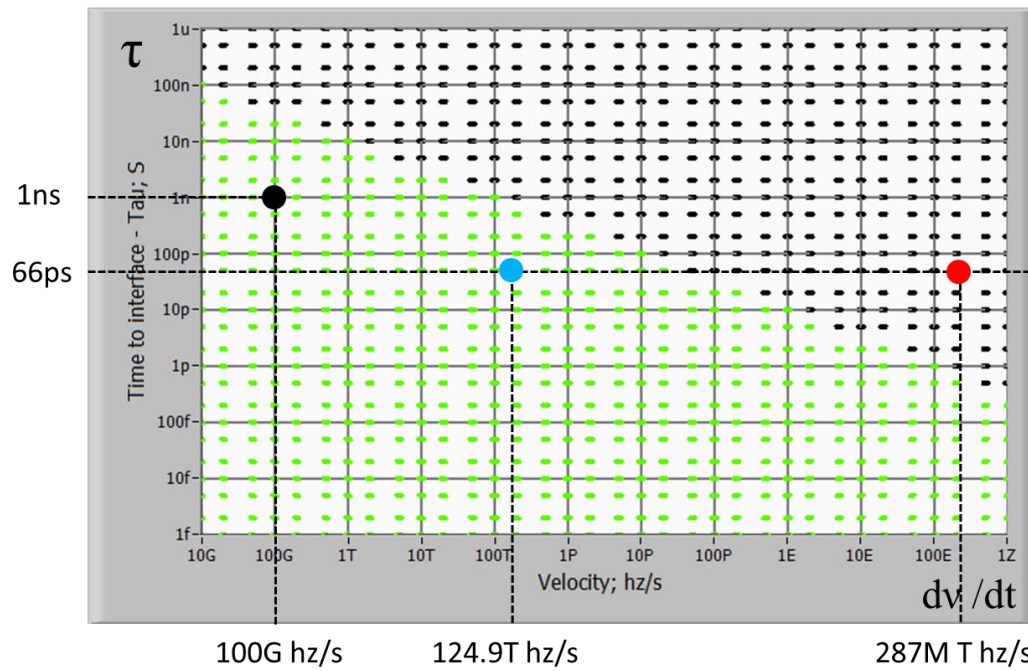


Figure 4.52 – From above the green area shows sweep rate and τ combinations which are acceptable. The black area is not allowable by the Brinkmeyer critereon.

The sum total of this is that the critereon breaks down for very high sweep rates. Our source is so fast that despite working over small distances there is too much change.

However if we look closer at the Taylor expansion you can see that the critereon of Eq. 4.14 is overly restrictive.

The term which is to be ignored doesn't have to be much less than 1, it can be ignored if it is much less than the term which is kept.

Or in other words:

$$\pi \tau^2 \, dv/dt \ll 2 \pi \nu \tau \quad \text{Eq. 4.15}$$

or

$$1/2 \tau \, (dv/dt) / \nu \ll 1 \quad \text{Eq. 4.16}$$

which is now a restriction that the amount of change of optical frequency is “relatively” small – small relative to the optical frequency itself. It is a little more inconvenient in that the optical frequency itself comes into play – hinting that there may be optical frequencies below which it is difficult to achieve this.

Table 3 shows the new critereon values for the three lasers, evaluated at 1500nm. The first laser, the laser used by Brinkmeyer in 1993 over OFDR distances now evaluates to less than .1p. The New Focus laser to 65p and the high speed laser fashioned from the ultra-wideband Santec laser evaluates to 48u. All are safely much less than 1.

Table 3 – The new critereon – under which all three lasers are acceptable.

	Brinkmeyer 1993	New Focus Laser	Stretched Santec
τ	1ns	66ps	66ps
dv/dt	100Ghz/s	124.9Thz/s	287M Thz/s
v	200T	200T	200T
New Critereon should be $\ll 1$.	786f	65p	48u

The new adherence map, plotted for 1500nm (200Thz) is shown in Figure 4.53. The green zone now includes all three lasers indicating that they satisfy the critereon.

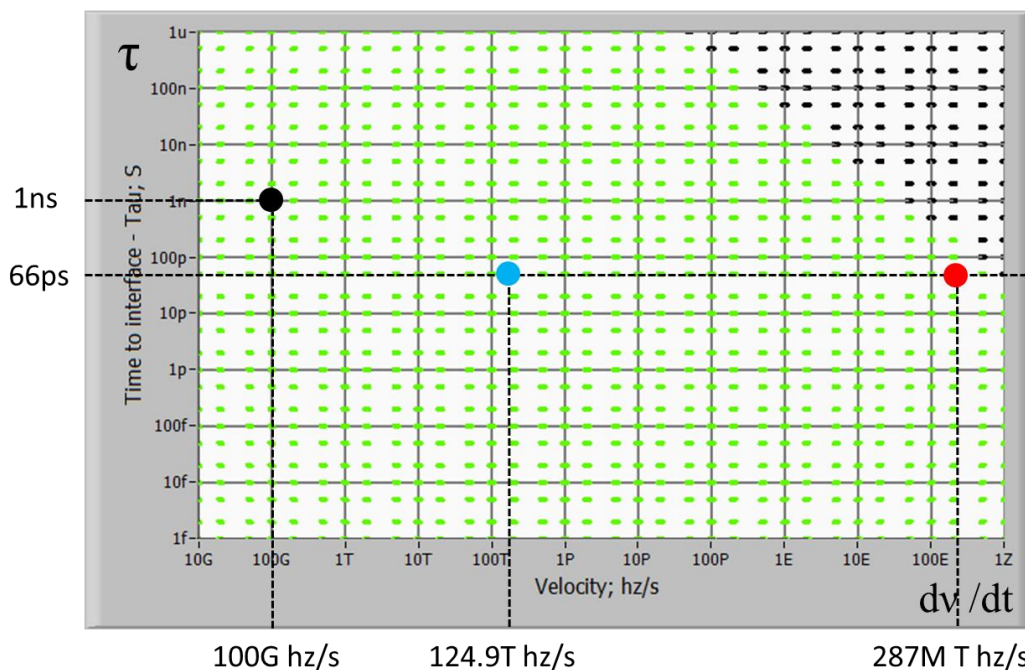


Figure 4.53 – The new critereon, plotted at 1500nm (200Thz), expands the acceptable sweep rates and τ 's to include the new laser.

4.5. Distance scale

The A-line distance scale was lost in the process of compensating for the non-linear sweep. As seen in Figure 4.50 and repeated here in Figure 4.54, the A-line now has only FFT bins.

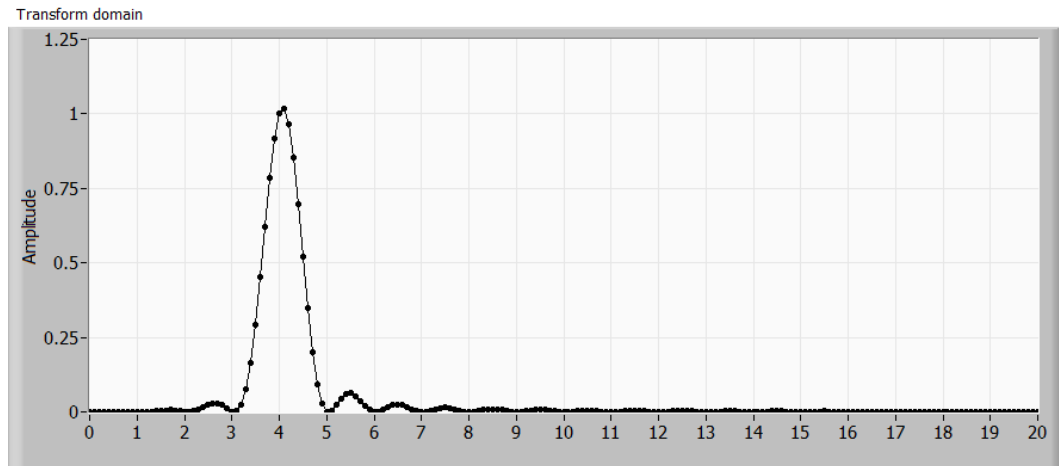


Figure 4.54 – After compensating for the non-linear sweep the A-line has only FFT bins to which need to be assigned distances.

There are several ways to assign the distance scale. The four we will discuss are:

1. Perfect standard
2. Differential standard
3. Perfectly known sweep rate
4. Perfectly known optical frequency extent

4.5.1. Perfect Standard

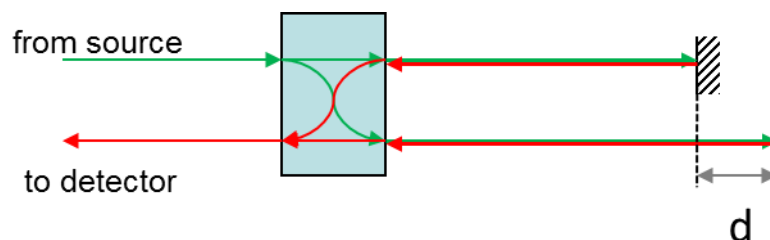


Figure 4.55 – A perfect standard has a distance d which is known.

When the distance from the reference to measurement plane is known ahead of time, the distance scale calibration is trivial. The FFT bin is assigned the distance and the rest of the scale falls into place.

$$\text{Distance scale} = d / \text{bin}(d) \quad \text{Eq. 4.17}$$

Example 1

If $d = 48u$ and the FFT after linearization falls onto bin 4 then the scale would be $48u / (4 \text{ bins}) = 12u/\text{bin}$.

The problem with this technique is that construction of an absolute reference can be complicated or expensive.

4.5.2. Differential Standard

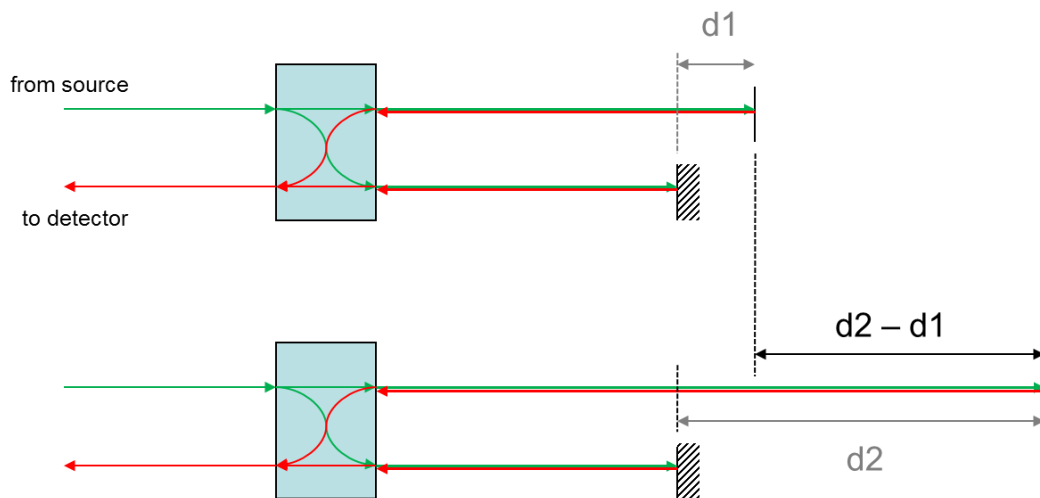


Figure 4.56 – The differential standard requires exact knowledge of neither of the two distances, only of the difference in distances.

It may be difficult to acquire a reasonable calibration standard. In many cases it may be easier or more convenient to do the calibration by a differential method. This is because while absolute measurements and constructions are difficult, high precision differential measurements are quite trivial.

If the FFT of the linearized beat signal from the d_1 plane maps to $\text{bin}(d_1)$

and that of d_2 maps to bin_{d2} then the FFT scale to distance scale is $(d_1 - d_2) / (\text{bin}(d_1) - \text{bin}(d_2))$.

$$\text{Distance scale} = (d_1 - d_2) / (\text{bin}(d_1) - \text{bin}(d_2)) \quad \text{Eq. 4.18}$$

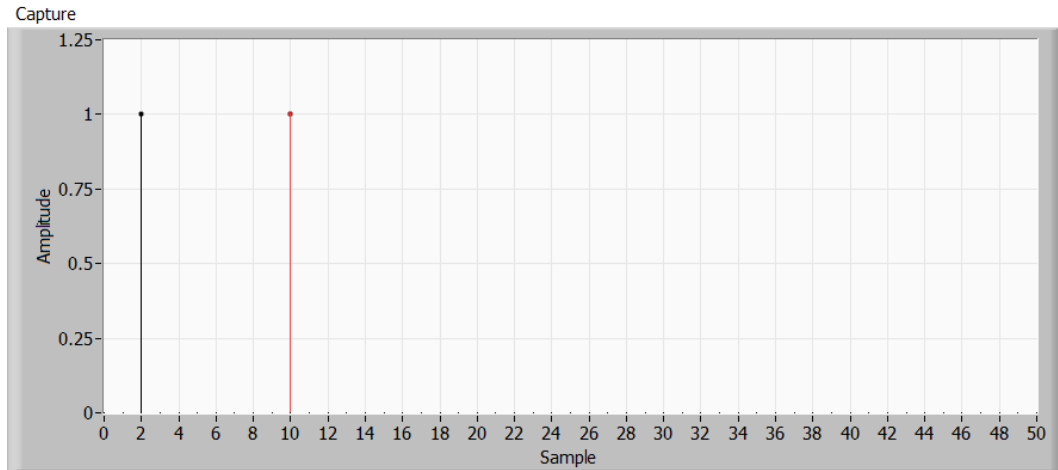


Figure 4.57 – FFT data from two measurement planes. One mapped to bin 2 and the other to bin 10.

Example 2

Let us assume that the measurement planes which produced the data in Figure 4.57 were separated by 96u. According to Eq. 4.18 the distance scale will be $96u / (\text{bin } 10 - \text{bin } 2) = 96u / 8 \text{ bins} = 12u/\text{bin}$.

Table 4 – Separation required to achieve a desired %error if encoder has 67nm resolution.

% error desired	Separation needed
1%	6.7um
0.1%	67um
0.01%	670um

Table 5 – Percentage error in distance scale from not knowing index of refraction

Material	Actual	Assumed (free space)	% error
Glass	1.5	1.0	50%
Skin	1.3	1.0	30%

4.5.3. Perfectly Known Sweep Rate

If dv/dt , the sweep rate, is exactly known and is a constant then the distance scale can be calculated from the frequency of the beat signal and applied to the FFT scale.

$$d = f_c / (2 n dv/dt) \quad \text{Eq. 4.19}$$

Example 3

Assume that dv/dt is 124.9Thz/s and the beat signal is as shown in Figure 4.58. The FFT in Figure 4.59 shows that the signal is 40hz. If we assume the material has an index of refraction of 1 then the distance scale will be $40\text{hz} * 3\text{E}8\text{m/s} / (2 * 1 * 124.9\text{Thz/s}) = 48\mu\text{m}$ as shown in Figure 4.60.

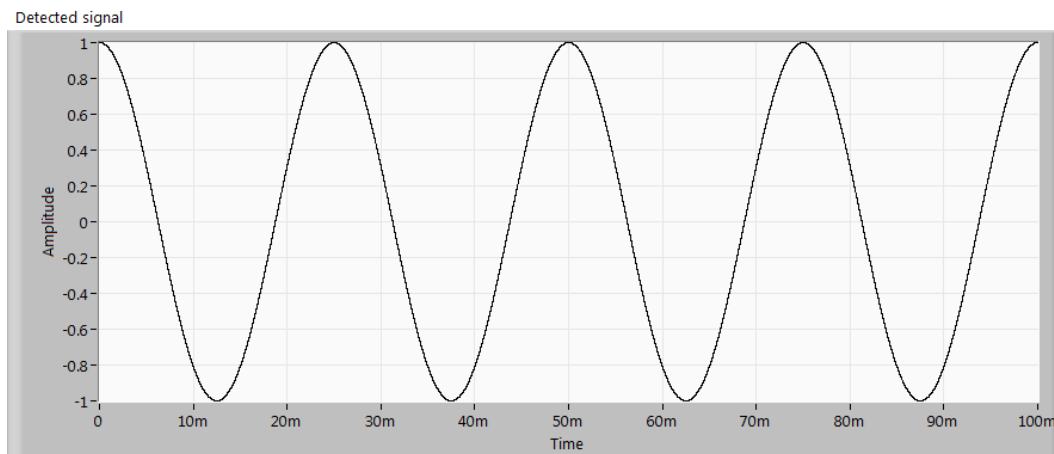


Figure 4.58 – Beat signal a calibration surface.

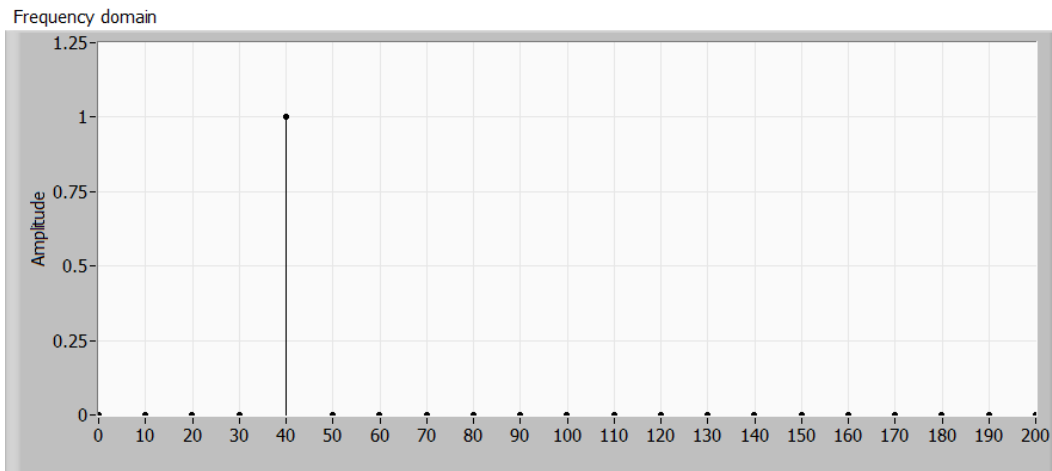


Figure 4.59 – FFT of beat signal showing 40hz.

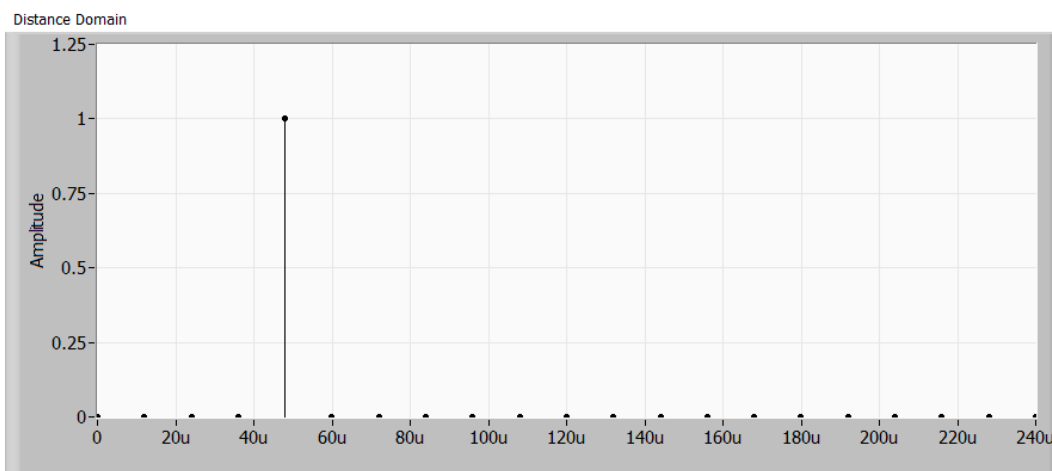


Figure 4.60 – Distance scale calculated from the frequency.

4.5.4. Perfectly Known Optical Frequency Extent

Let us assume again that dv/dt , the sweep rate, is known and a constant. Now, if exactly one cycle of the beat signal is traversed during the sweep then we have a waveform which defines the first bin of the FFT.

$$T_{\text{bin1}} = v_{\text{total}} / dv/dt \quad \text{Eq. 4.20}$$

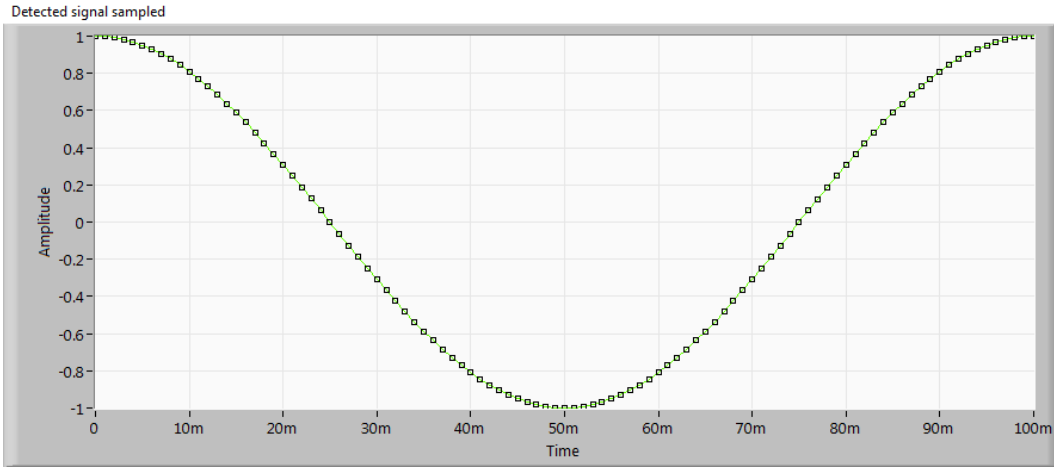


Figure 4.61 – T_{bin1} is the time taken for one complete cycle of the beat signal.

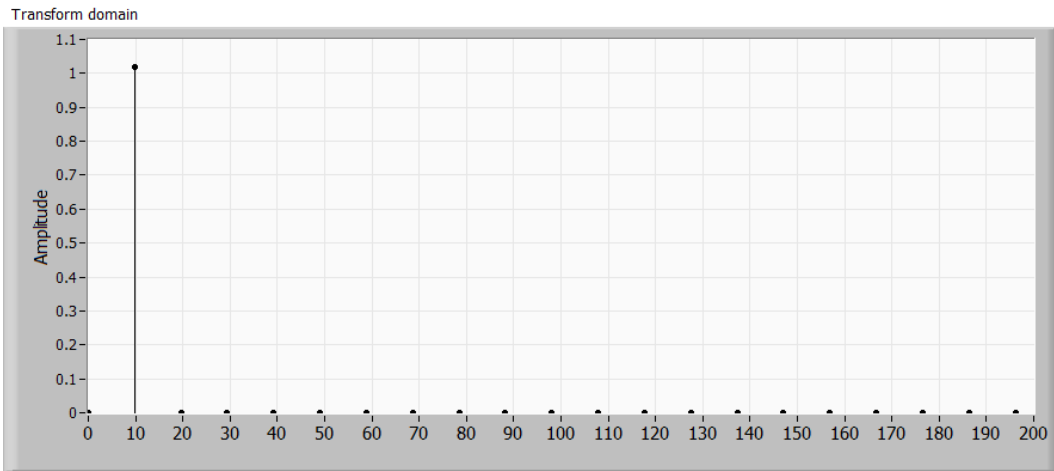


Figure 4.62 – FFT of fundamental beat signal (in this case 10Hz).

This will define the frequency of the first bin of the FFT.

$$f_{\text{bin1}} = dv/dt / v_{\text{total}} \quad \text{Eq. 4.21}$$

But this frequency can be calculated from the measurement plane to reference plane separation d .

$$f_{\text{bin1}} = dv/dt * 2 n d_{\text{bin1}}/c \quad \text{Eq. 4.22}$$

If we combine these equations we can eliminate dv/dt , the sweep rate, and obtain immediately an equation for the distance scale in terms of the total optical frequency covered in the sweep.

$$d_{\text{bin1}} = c / (2 n v_{\text{total}}) \quad \text{Eq. 4.23}$$

This equation doesn't depend on the sweep rate, only on the total optical frequency covered and so can be applied to the non-linear sweep cases as well (once the non-linearity has been compensated for).

Example 4

The total optical frequency covered in Figure 4.61 at our typical dv/dt of 124.9Thz/s was 12.49Thz. Thus $d_{bin1} = 299.8\text{Mm/s} / (2 * 1 * 12.49\text{Thz}) = 12\mu\text{m/bin}$.

4.6. Distance Limitations

There are some system aspects which limit the lengths at which the SSOCT signal can be measured.

1. Bandwidth.
2. Sampling rate
3. Coherence length

4.6.1. Bandwidth

The further a measurement plane the higher the frequency of the beat frequency. The bandwidth of the system will limit the highest frequency that can be detected. It is convenient to take as a limit the 3dB frequency of the system. Thus as $f = 2 d dv/dt / c$ we can write

$$d_{\max} = \frac{1}{2} f_{3\text{db}} * c / (dv/dt)_{\max} \quad \text{Eq. 4.24}$$

4.6.2. Sampling rate

The further an interface is removed from the reference the higher the frequency of the beat signal. The sampling rate of the system must be capable of sampling at least 2x the highest frequency in order to prevent aliasing [Shannon (1949)].

Aliasing will cause the beat signal to appear to be of a different frequency and the FFT will reflect this.

4.6.2.1.

Reducing the number of samples to induce aliasing

The Nyquist rate can be restated as placing two samples on each cycle of the highest frequency sinewave. Figure 4.63 to Figure 4.72 illustrate the effects of aliasing on the beat signal in time and frequency domain as the number of samples on each cycle are reduced from 25 to 1.75. The final case results in the number of samples per cycle to drop below two and causes aliasing.

The beat signal is chosen so that an integer number of cycles appear across the time duration so that the FFT's will map to an integer bin number and appear very clean. This way the effects of sampling less and less will be more obvious.

Figure 4.63 shows the beat signal sampled at 25 samples per cycle. There are so many samples that a straight line interpolation between samples (green) follows the actual beat signal (blue) so well that you can't make out the actual beat signal.

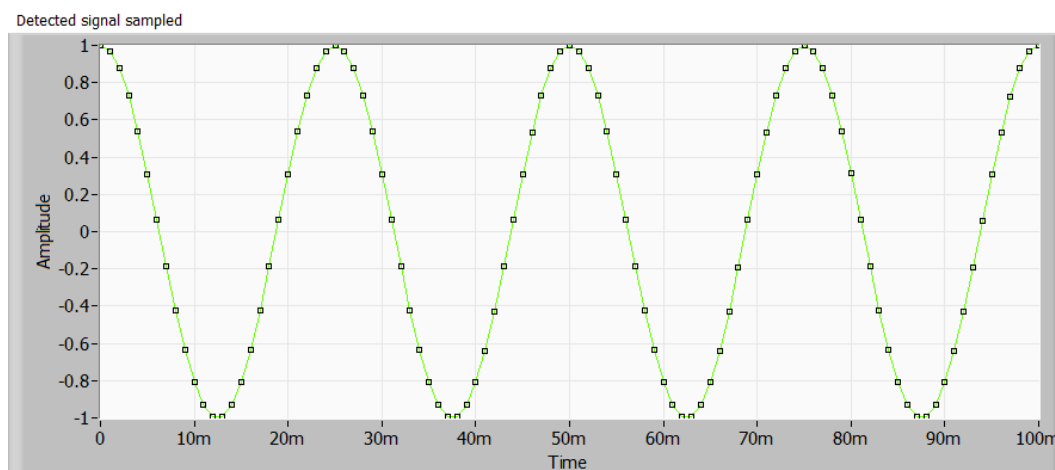


Figure 4.63 – Sampling rate 25 samples/cycle. Time domain.

Figure 4.64 shows the FFT of beat signal in Figure 4.63 which has 25 samples per cycle. The FFT is very sharp.

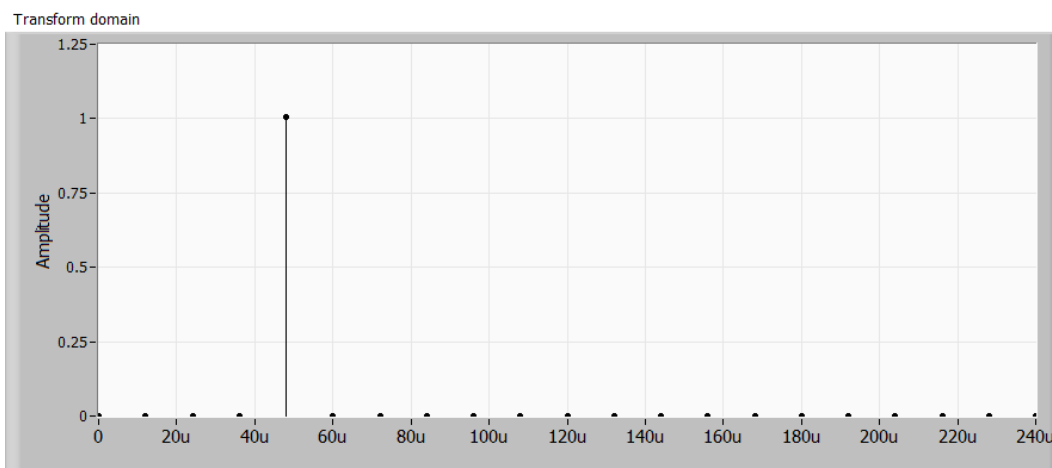


Figure 4.64 – Sampling rate 25 samples/cycle. FFT domain.

Figure 4.65 shows the beat signal sampled at 12 samples per cycle. A straight line interpolation between samples (green) still follows the actual beat signal (blue) very well. However it is possible to make out the beat signal since the straight line interpolation can't follow the tighter curves perfectly.

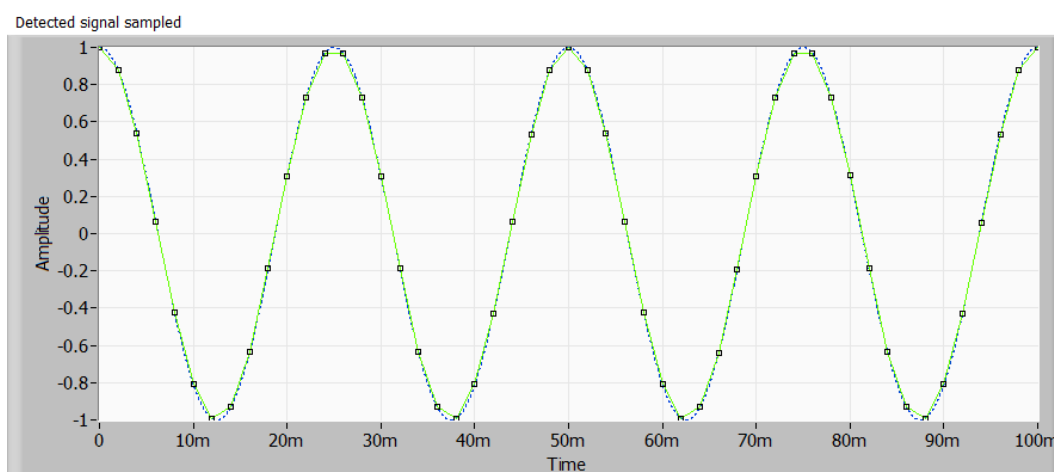


Figure 4.65 – Sampling rate 12 samples/cycle. Time domain.

Figure 4.66 shows the FFT of beat signal in Figure 4.65 which has 12 samples per cycle. The FFT is still very sharp.

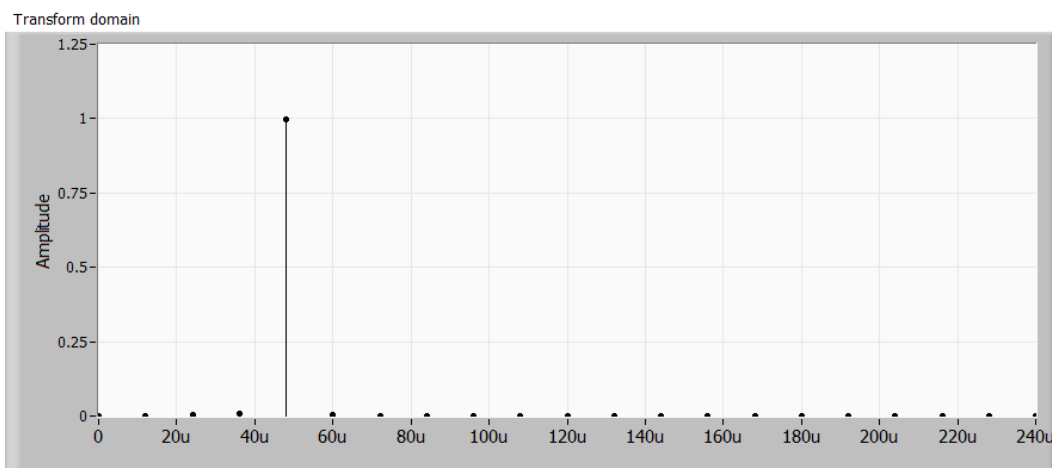


Figure 4.66 - Sampling rate 12 samples/cycle. FFT domain.

Figure 4.67 shows the beat signal sampled at 6 samples per cycle. A straight line interpolation between samples (green) now clearly deviates from the actual beat signal (blue).

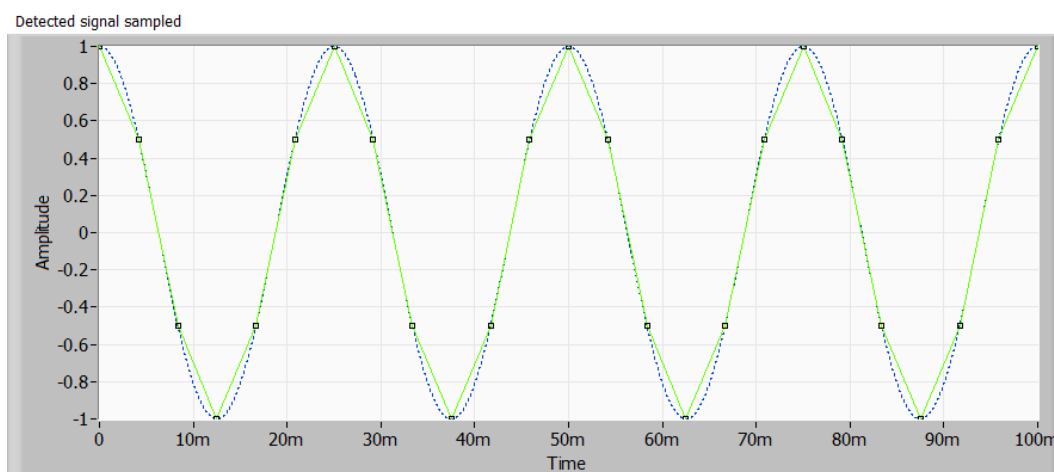


Figure 4.67 – Sampling rate 6 samples/cycle. Time domain. Note that the straight line interpolation in green between samples starts to visually deviate from the actual signal in blue.

Figure 4.68 shows the FFT of beat signal in Figure 4.67 which has 6 samples per cycle. Even though the samples of the time domain signal seem few by the eye the FFT is still very sharp and in the correct location.

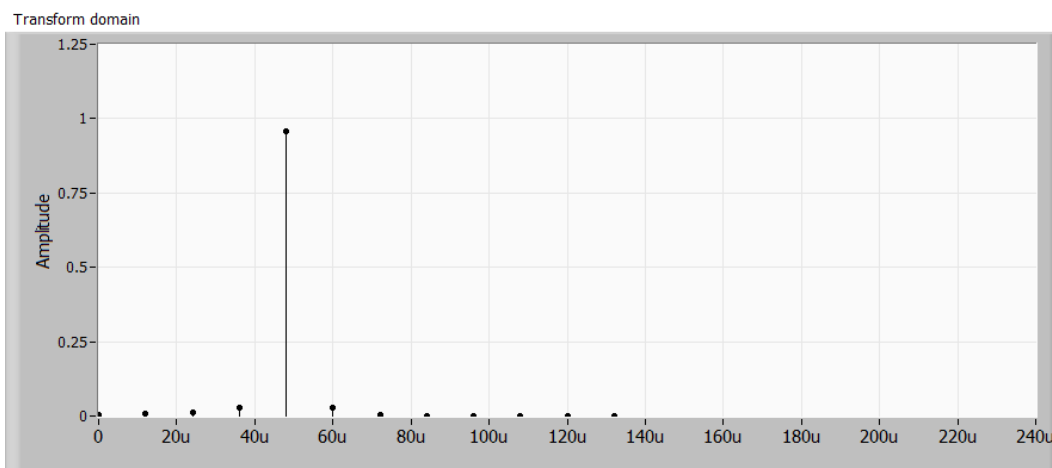


Figure 4.68 – Sampling rate 6 samples/cycle. FFT domain. The distance domain still shows the correct location. Some ‘noise’ in the sidebands is starting to become apparent.

Figure 4.69 shows the beat signal sampled at 3 samples per cycle. A straight line interpolation between samples (green) now resembles the actual beat signal (blue) only in its basic repetitivity.

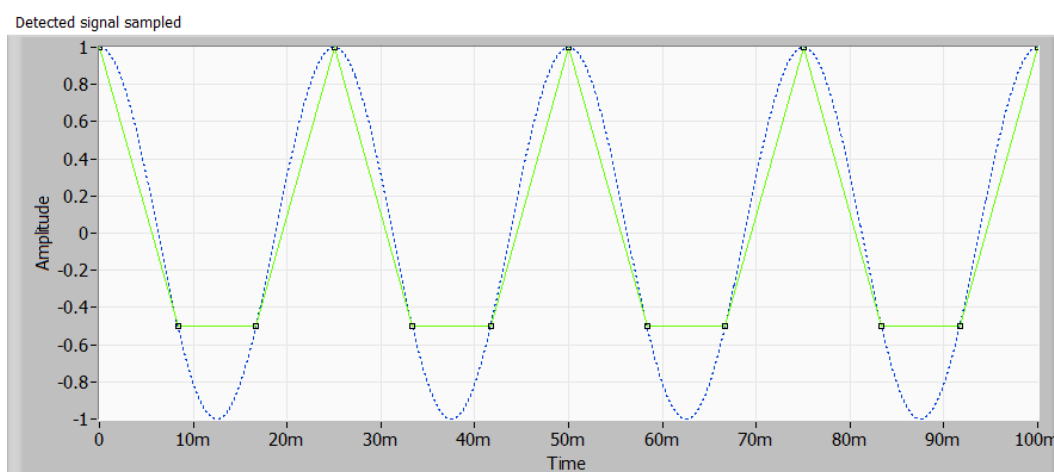


Figure 4.69 – Sampling rate 3 samples/cycle. Time domain. The straight line interpolation is now obviously different than the blue signal.

Figure 4.70 shows the FFT of beat signal in Figure 4.69 which has 3 samples per cycle. Once again, almost against intuition, the FFT is still quite sharp and in the location of the peak is not in doubt. This reflects the fact that the samples in the time domain satisfy Nyquist and so still follow the basic cycle pattern as the beat signal.

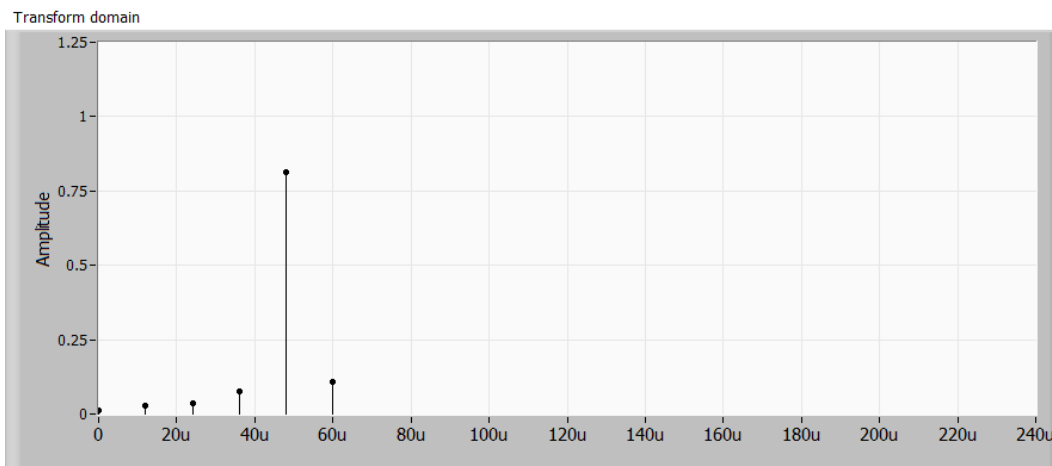


Figure 4.70 – Sampling rate 3 samples/cycle. FFT domain. Despite being sampled at barely above Nyquist the FFT still clearly marks the correct distance.

Figure 4.71 shows the beat signal sampled at 1.75 samples per cycle. This is fewer than the minimum two required for Nyquist. A straight line interpolation between samples (green) no longer resembles the actual beat signal (blue). In fact the straight line approximation seems to be of a different frequency. This is the effect known as Aliasing.

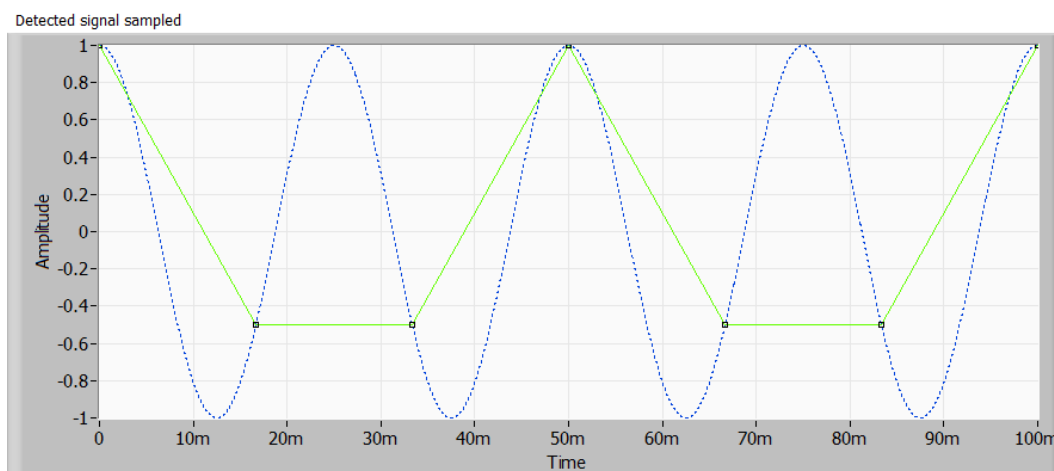


Figure 4.71 - Sampling rate 1.75 samples/cycle. Time domain. This is just under the 2 samples/cycle Nyquist limit. The straight line interpolation between points completely misses whole half cycles and no longer represents the actual signal in blue.

Figure 4.72 shows the FFT of beat signal in Figure 4.71 which has 1.75 samples per cycle. As this is not enough to satisfy Nyquist the peak is shifted to a

new location reflecting the fact that the samples no longer represent the true beat signal.

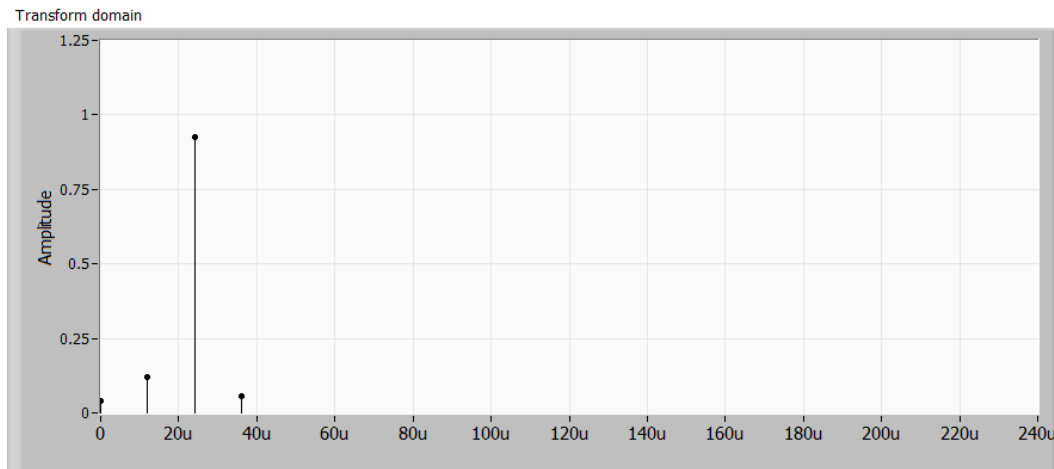


Figure 4.72 – Sampling rate 12 samples/cycle. FFT domain. The time domain being undersampled results in aliasing - the FFT has shifted away from the true location.

4.6.2.2. Effects of aliasing on an A-line

To see how aliasing would affect an A-line we take as an example the A-line from the material with 10 interfaces separated by 1mm as shown in Figure 4.73. The frequency of the beat frequency increases with the distance of the interface. The A-line shown was sampled at a sufficiently high rate for all the interfaces.

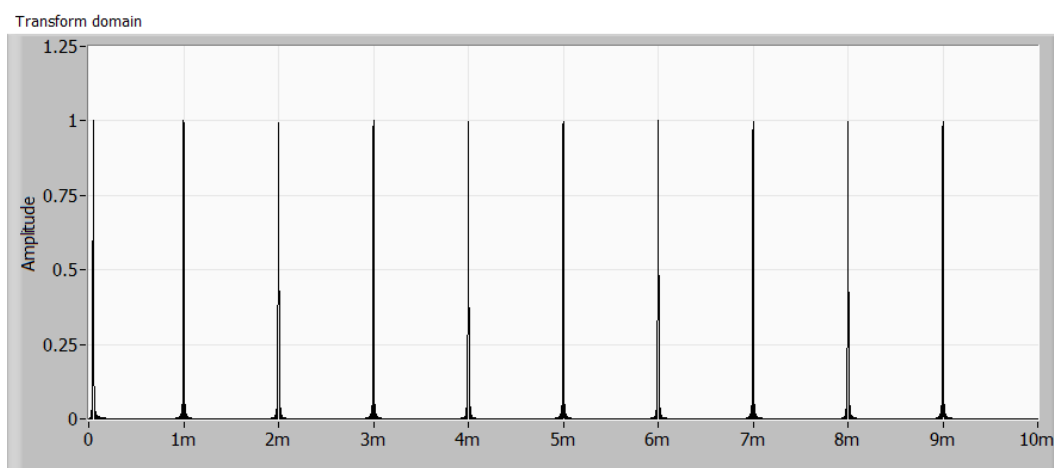


Figure 4.73 – A-line of 10 interfaces separated by 1mm each. The further the distance the higher the frequency and the higher the sampling rate has to be maintained to avoid aliasing.

In Figure 4.74 the sampling rate was still maintained at the same value. However a new sampling rate will be applied. The furthest interface that will be supported by the new sampling rate is shown as the vertical line.

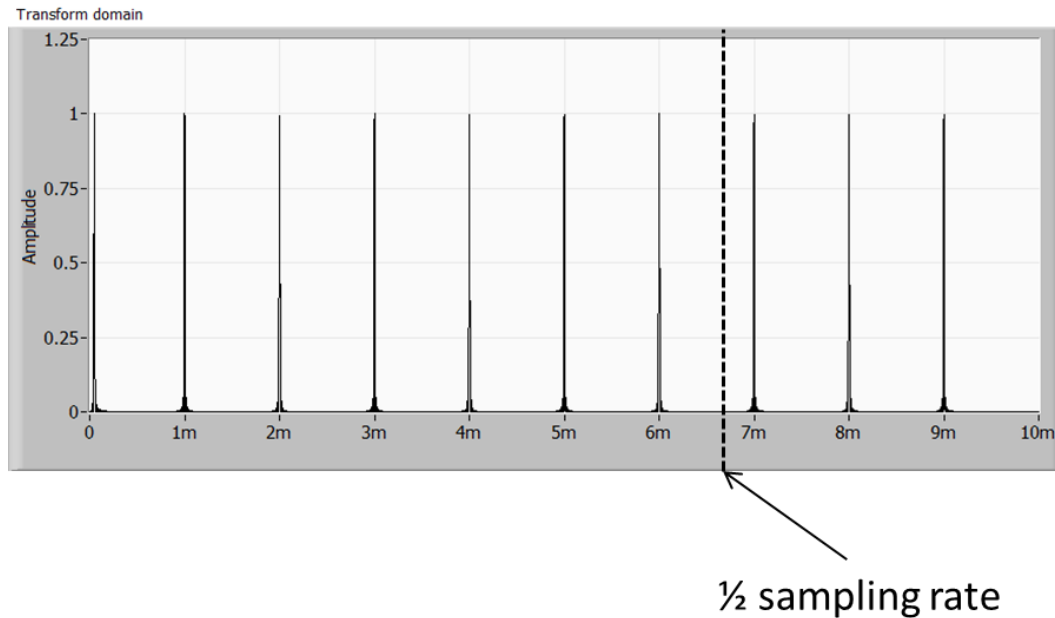


Figure 4.74 - FFT domain of measurement planes at various distances. The further the distance the higher the frequency and the higher the sampling rate has to be maintained to avoid aliasing. The dashed line shows one half the sampling rate that will be applied.

In Figure 4.75 the same set of interfaces were measured but sampled at the new sample rate. The peaks that used to appear at 7mm, 8mm and 9mm now appear in new positions. They have been ‘folded back’ across the $\frac{1}{2}$ sampling point. This is the effect of aliasing on an A-line. The effect would be subtle and is irreversible in an actual measurement so care must be taken to insure that either the rate is high enough for the material being measured.

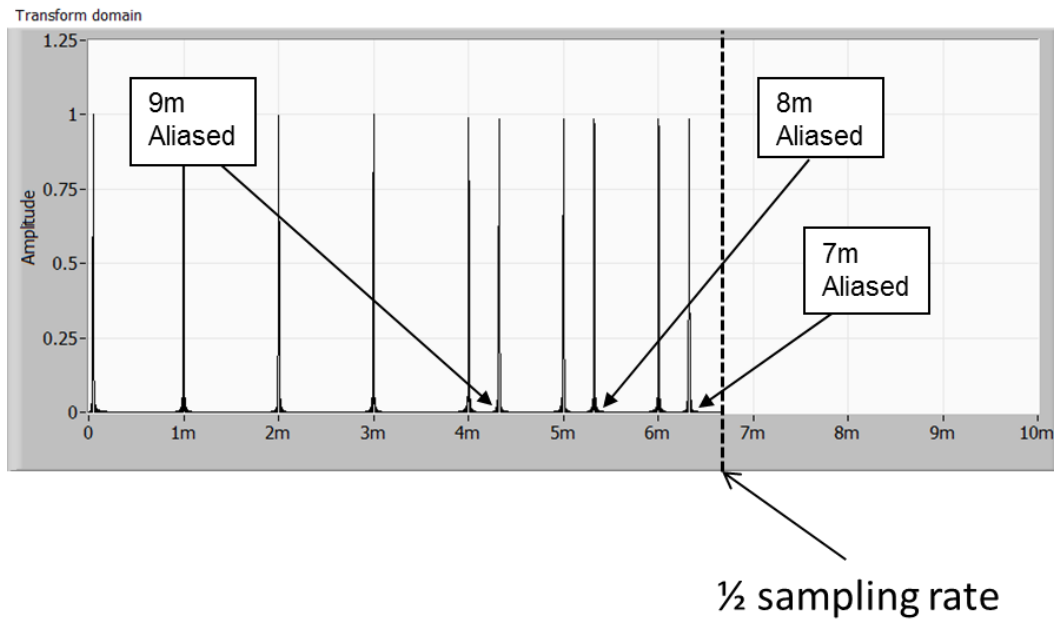


Figure 4.75 – Effect of aliasing on the A-line with interfaces more distant than the Nyquist rate allows folded back into the good data. This mixing of good and bad in an unseparable manner is what makes aliasing such a dangerous issue.

4.6.3. Coherence length

The coherence length of the laser also limits the maximum distance to the measurement plane [Passy et al. (1994)].

The signal-to-noise ratio as determined by the phase jitter is

$$\text{SNR} = \exp[-|\tau|/\tau_c] / (1 - \exp[-|\tau|/\tau_c]) \quad \text{Eq. 4.25}$$

where τ_c is the coherence length of the laser.

If we set the maximum distance to be bounded by a SNR of 1; the point at which the signal disappears into the noise, then we have an equation that includes τ_{\max} the maximum round trip time.

$$1 = \exp[-|\tau_{\max}|/\tau_c] / (1 - \exp[-|\tau_{\max}|/\tau_c]) \quad \text{Eq. 4.26}$$

and simplifying

$$\exp[-|\tau_{\max}|/\tau_c] = 1/2 \quad \text{Eq. 4.27}$$

or

$$\tau_{\max} = \log(2) \tau_c \quad \text{Eq. 4.28}$$

or in terms of distance

$$d_{\max} = \log(2) \tau_c n/c \quad \text{Eq. 4.29}$$

In practical cases, this limitation will not typically affect OCT applications as the measurement distances are more often limited to 10mm or less by absorption and scattering losses within the medium.

4.7. Topologies

Up to this point we have been concerned with the individual pieces of a Swept Source OCT system; the laser, with its inevitably non-linear sweep, the interferometer with reference and measurement planes, the A/D with its sampling rate and finally the post processing FFT and application of calibrations.

There are some common ways to construct systems of these components given what we have learned about non-linear sweeps and how to normalize them.

We will look at the four topologies outlined in Table 6. Two compensate for non-linear sweeps in real time by adjusting their sampling rates in synchrony with the varying laser sweep rate. The other two sample both the measurement and an optical reference at a fixed high rate and post process the data to first glean the equally spaced optical frequency intervals and second to resample the measurement data at these intervals.

Table 6 – Four topologies for realizing a basic Swept Source OCT system.

Topology	Linearization	Description
1	Real time	The laser provides the optical frequency triggers
2	Real time	Optical frequency triggers derived from an external optical reference.
3	Post process	Optical reference is measured each time
4	Post process	Optical reference is measured one time only

4.7.1. Laser provides optical frequency triggers

The most simple configuration starts with a laser which provides triggers at precise moments corresponding to equally spaced optical frequencies.

This leaves only windowing, zero-padding, FFT and application of depth scale.

In Figure 4.76 the laser passes its light into the measurement interferometer consisting of a 50/50 splitter, the reference mirror on one arm and a launching mechanism into the object under test. The reflections are recombined in the splitter and passed on to the detector where the beat signal is created. The beat signal is sampled by the A/D according to the triggers received from the laser. The samples are windowed, zero-padded and passed through an FFT after which the distance scale is applied to form the A-line.

A working example of this topology is given in 5.1 starting on page 158.

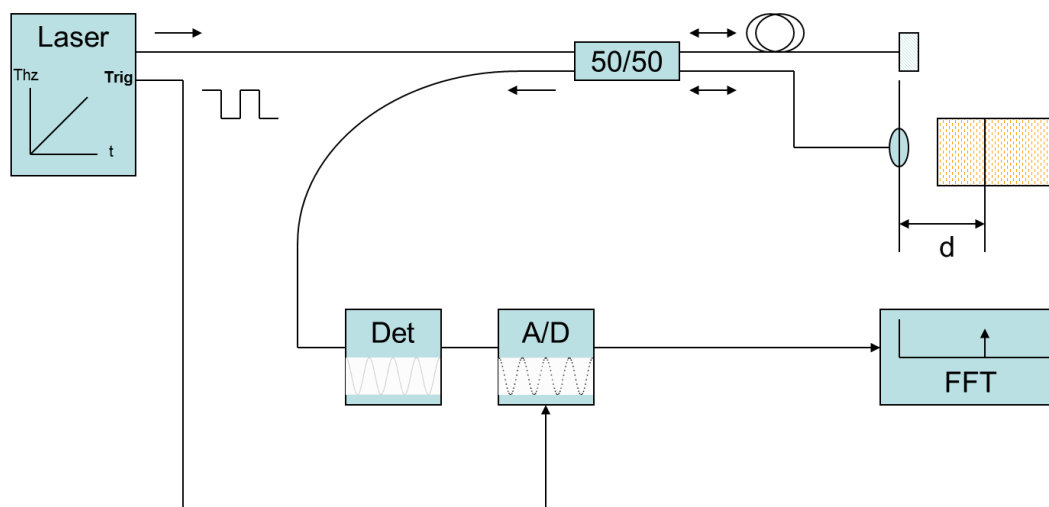


Figure 4.76 – Topology 1. Laser provides equally spaced optical frequency triggers to the A/D.

4.7.2. Optical frequency triggers derived from output of laser

This configuration is very similar to that in 4.7.1. In this case, rather than the laser providing triggers at the moments corresponding to the equally spaced optical frequencies, the triggers are created external to the laser by tapping a small percentage of the laser's output and running it through an etalon or other periodic

optical component such as a mach zender or michelson interferometer. After detection the electrical waveform is sharpened up by a zero-crossing detector or differentiator to provide good triggers for the A/D.

This system is a little more complex than before since we have to tap the laser output, add an optical element, another detector and the trigger sharpening apparatus.

The light is tapped after leaving the laser, a small percentage being routed to be used to generate the optical frequency triggers and leaving the majority of the light going on to the measurement interferometer. This majority enters the measurement interferometer through the 50/50 splitter. The reflections from the reference arm and measurement arm are recombined in the 50/50 splitter and detected to produce the beat signal. The beat signal is sampled by the A/D according to the triggers created from the small percentage of the laser's output which was passed through an optical component such as an etalon or machs zender or michaelson interferometer. The output of the optical component is an optical intensity which varies with optical frequency. This varying intensity is detected and sharpened to produce the sampling triggers for the beat signal. The beat signal samples are windowed, zero-padded and passed through an FFT after which the distance scale is applied to form the A-line.

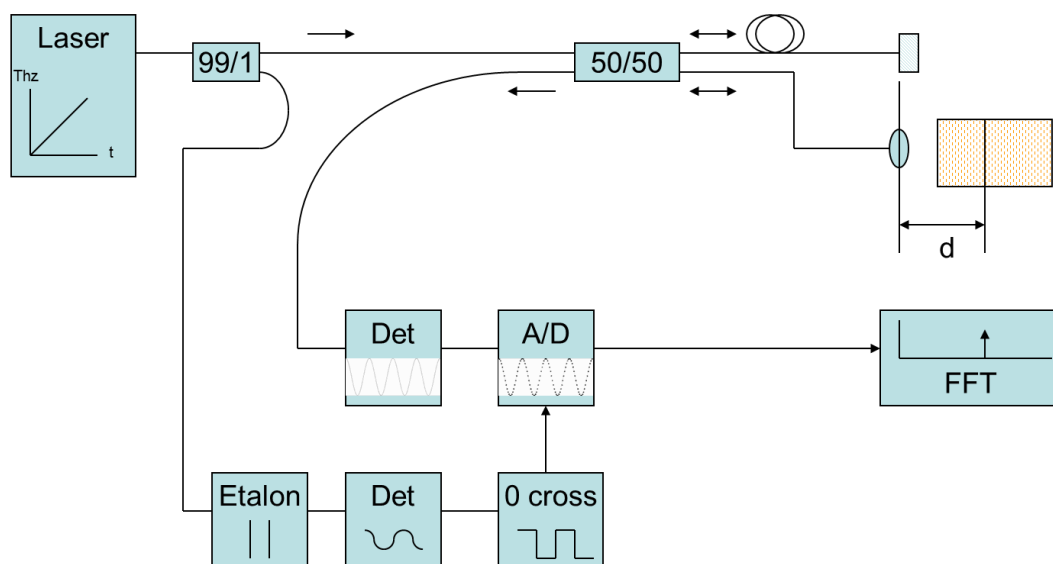


Figure 4.77 – Topology 2. Equally spaced optical frequency triggers are created by passing a portion of the output of the laser through an etalon. The

resulting periodic waveform is detected and trigger pulses for the A/D generated from zero crossings in the mean of the AC coupled detected signal.

4.7.3.

Optical data resampled using sample numbers recalculated each sweep

This configuration is much different than the two previous. The two previous topologies sampled the beat signal at the precise moments of equally spaced optical frequencies. This configuration simultaneously oversamples both the beat signal and an optical frequency reference. The optical frequency reference data is analyzed for optical frequency versus time which is then applied to the beat signal to resample at equally spaced optical frequency intervals. Thus the linearization takes place as an additional two post-processing steps.

The light is tapped after leaving the laser, a small percentage being routed to be used as an optical frequency reference leaving the majority of the light going on to the measurement interferometer. This majority enters the measurement interferometer through the 50/50 splitter. The reflections from the reference arm and measurement arm are recombined in the 50/50 splitter and detected to produce the beat signal. Meanwhile the small percentage passes through an optical element such as an etalon or machs zender or michaelson interferometer producing an optical intensity which varies with optical frequency. This varying intensity is sampled along with the beat signal by A/D at a sampling rate approximately 10x the Nyquist frequency as determined by the sweep rate and the longest delay in the measurement interferometer. The optical frequency reference data is analyzed The samples are windowed, zero-padded and passed through an FFT after which the distance scale is applied to form the A-line.

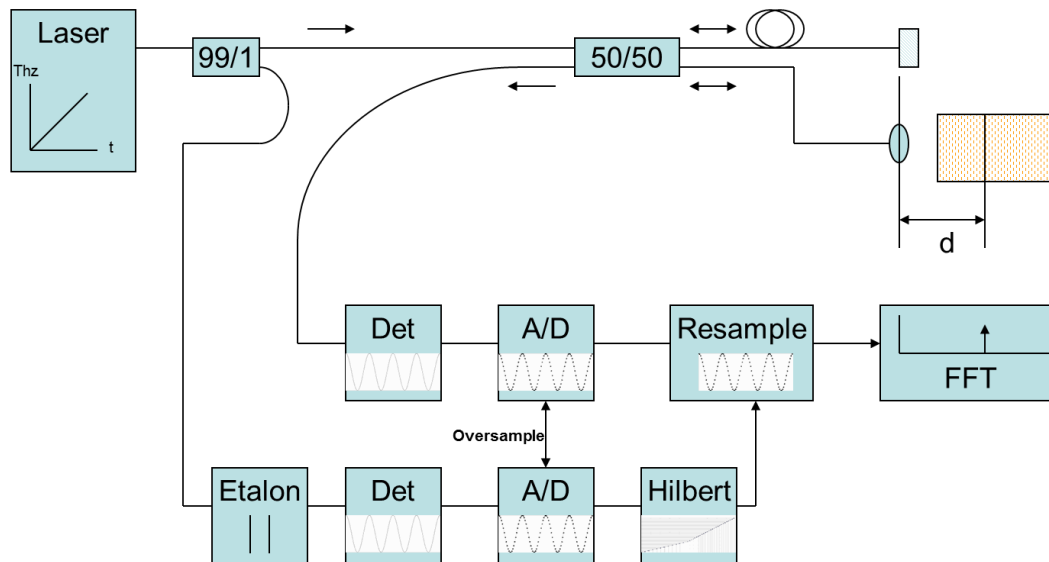


Figure 4.78 – Topology 3. The OCT optical data is oversampled along with data from an optical reference. The sample numbers associated with equally spaced optical frequencies are calculated from the optical reference data and used to resample the OCT data.

4.7.4.

Optical data resampled using sample numbers calculated once and reused

This configuration assumes that the laser is very repeatable. This is not to say that the sweep is linear, but rather that the sweep repeats well for a reasonable period of time.

This repeatability allows us to break the process of 4.7.3 into two steps. First an optical frequency reference is oversampled and analyzed to obtain the optical frequency versus time characteristics of the laser. Second the output of the measurement interferometer is oversampled and the time scale converted to optical frequency via the data which was the results of step 1. This second step can be repeated for as long as the data from step 1 remains valid.

The separation lets the measurement interferometer be used for the calibration of the optical frequency scale. Either the perfectly known standard of 4.5.1 on page 136 or the differential standard of 4.5.2 on page 137 can be used to acquire the distance scale for the A-line.

The optical frequency calibration is shown in Figure 4.79. The output of the laser is passed into the measurement interferometer through a 50/50 splitter. The reflection from the reference mirror and the calibration arm are recombined in the

splitter and passed on to the detector where the beat signal is created. The beat signal is over sampled by the A/D and analyzed in some manner such as the Hilbert transform to acquire the optical frequency vs time. This data is saved away for use in the runtime step. As was shown in 4.3 on page 121 optical frequency is proportional to the phase of a single reflector, so it is possible to use the Hilbert transform to acquire the phase of the beat signal and extract the equal spaced optical frequency times from it. It is not necessary that the distance d of the calibration arm of the measurement interferometer be known. If it is known then this data can be used to calibrate the A-line depth scale. If it is not known then the A-line depth scale must be calibrated by other means.

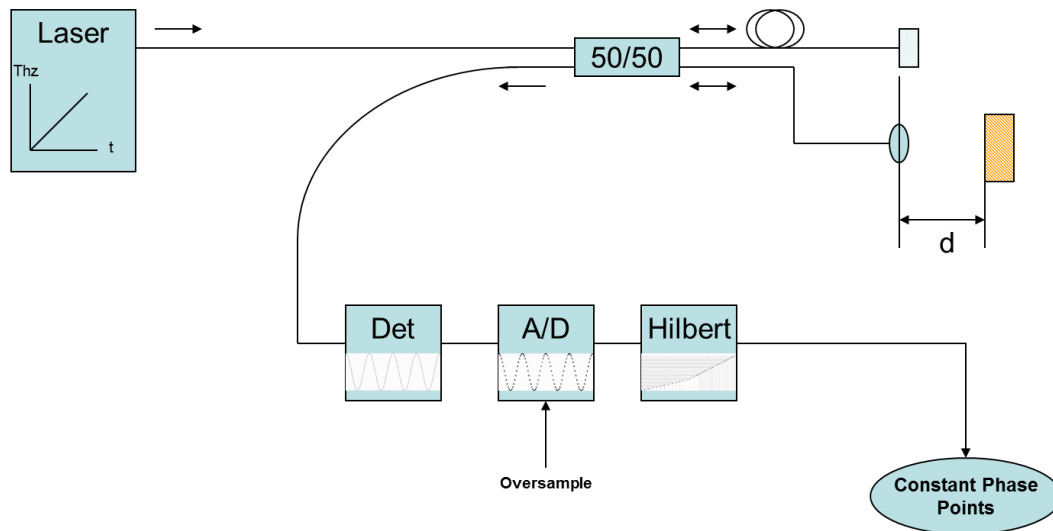


Figure 4.79 – Topology 4. Calibration step. A fixed distance is used to generate a periodic optical signal. The constant phase sample number are stored away.

The runtime configuration is shown in Figure 4.80. The laser enters the measurement interferometer through the 50/50 splitter. The reflection from the reference and measurement arms are combined in the 50/50 splitter and passed on to the detector where the beat signal is created. The beat signal is oversampled at the same rate as the calibration was performed at. The oversampled data is resampled at the equal spaced optical frequency points saved in the calibration step. This data is windowed, zero-padded and passed through an FFT. The distance scale is applied to form the A-line.

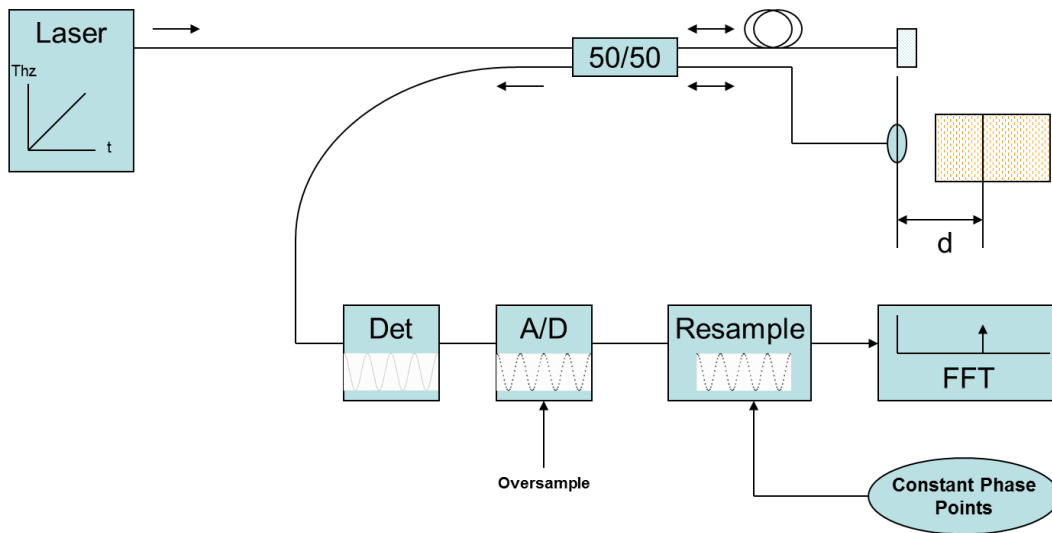


Figure 4.80 – Topology 4. Runtime. The constant phase sample numbers are used to resample the data from the actual measurement.

5 Working systems

We created two very different sources for Swept Source OCT. One was a New Focus External Cavity Tunable Diode Laser modified to provide realtime optical frequency markers which were used to clock the A/D [Cordes, A.H. et al. (2010)]. The other was a stretched pulse tunable laser formed by dispersively stretching the ultra-wideband output of a Santec Ultra-Wideband laser [Cordes, A.H. et al. (2009)].

The two sources were very different as to sweep rates, optical frequency extent, sweep stability and system topology supported. Despite this the two systems were able to share the OCT interferometer which allowed us to repeat measurements with systems built up around each source.

We will discuss:

1. The modified New Focus laser and an SSOCT system built around it.
2. The swept source built by stretching the Santec pulse and an SSOCT system built around it.
3. Comparisons of measurements taken with each.

5.1. New Focus Laser

New Focus has been making external cavity tunable diode lasers since the early 1990's. The PXI based 8700 was released in 2004 as a telecom component test laser and has mode hop free tuning from 1520nm to 1620nm. The motion is achieved with a voice coil motor. The maximum sweep rate is 2000nm/s. [New Focus (2004)]



Figure 5.1 – New Focus 8700 External Cavity Tunable Diode Laser

The optical cavity is a modified Littman-Metcalf external cavity as shown in Figure 5.2 where the wavelength is selected by the pivot angle ϕ which controls both the cavity length and the wavelength selection via the angle of the tuning mirror with respect to the diffraction grating [Liu, K.; Littman (1981)]. In the case of the 8700, the end mirror is the back facet of the diode laser and the gain medium is also that of the diode laser.

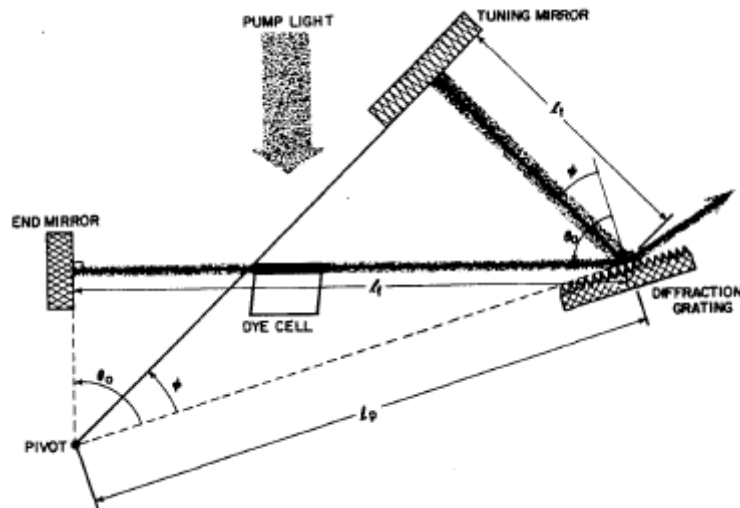


Figure 5.2 – The optical cavity is a Litmann-Metcalf external cavity. The pivot point is specially chosen so that only a single mode is supported as the cavity changes size. [Liu, K.; Littman (1981)]

The 8700 provides trigger signals via the TriggerA output shown in Figure 5.1 to clock an A/D [Pritchett et al. (Pending)]. This allows it to be used in the very simple Topology 1 as shown in Figure 5.3 and discussed in more detail in 4.7.1 on page 152.

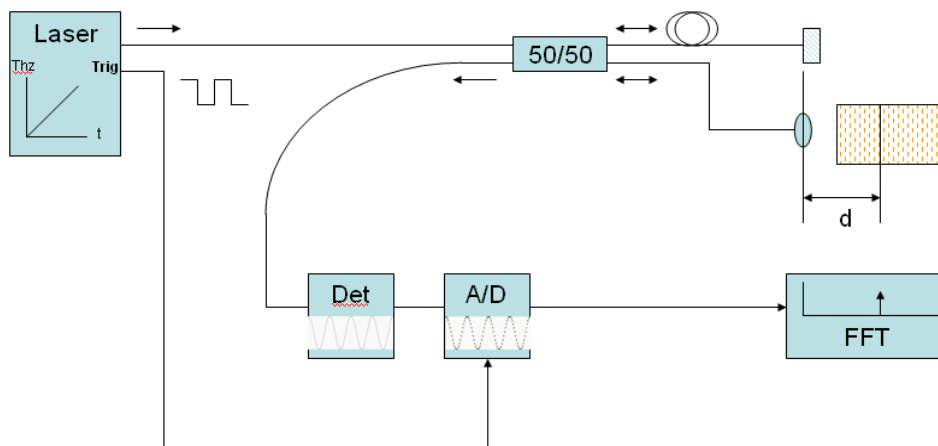


Figure 5.3 – Topology for the 8700 based SS OCT system. Trig A outputs triggers for the A/D.

The Trigger A signal from the standard 8700 provides a rising edge every 0.1nm during a sweep. This is useful for spectroscopy where the scientists tend to

work with wavelength and desire a nm scale. However it is not as useful for SS OCT. As we saw in 4.1.5 on page 111, sampling at constant wavelength intervals leads to A-line peaks which degrade rapidly with distance, both in amplitude and width as shown in Figure 5.4.

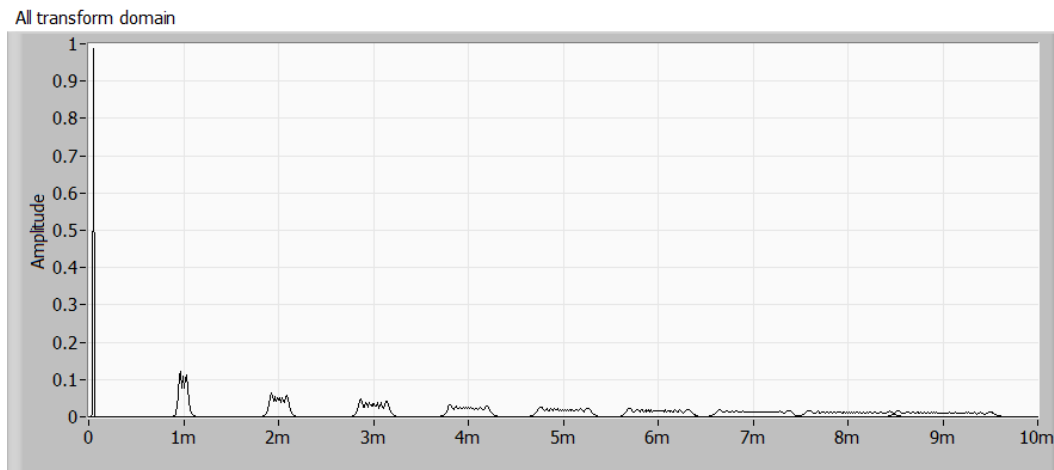


Figure 5.4 – The standard New Focus laser Trig A outputs triggers at 0.1nm intervals – constant wavelength intervals. The effect of constant wavelength sampling on the A-line is spreading and attenuation of the peaks.

What is desired are A-line peaks which retain their sharpness and amplitude with distance as shown in Figure 5.5. From chapter 4 we saw that this requires us to sample at equally spaced optical frequency intervals during the sweep. For this work the firmware of the 8700 was modified so that the Trigger A signals provided a rising edge at 10Ghz intervals.

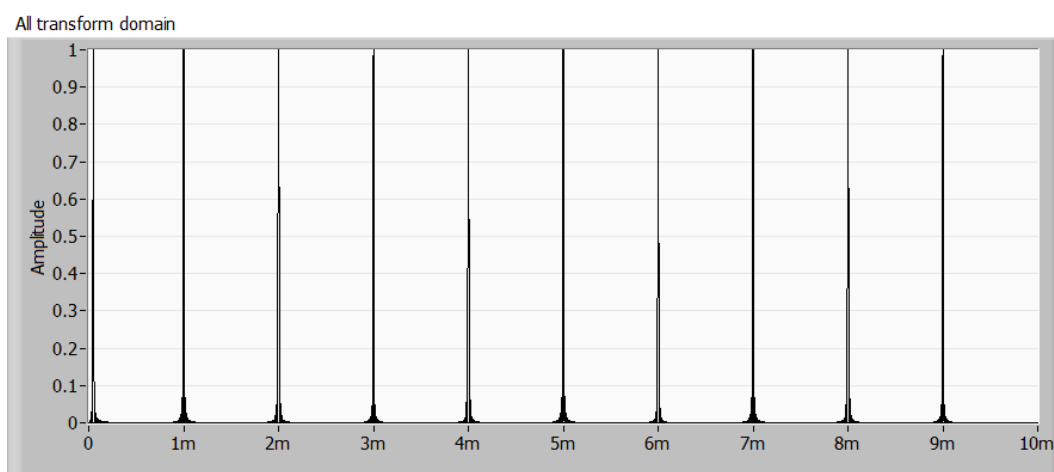


Figure 5.5 – The modified laser Trig A puts out triggers at constant Optical Frequency intervals. The effect on the A-line data is to preserve sharp peaks with distance.

The modified firmware includes three new commands to support the optical frequency triggers.

Table 7 – New commands for modified 8700

SCPI Command	Legacy	Units	Description
SOURce:FREQuency:SWEep:START	STRF	Thz	Start of sweep
SOURce:FREQuency:SWEep:STOP	STOPF	THz	End of sweep
VROM 73	VROM 73	GHz	Trigger spacing

The LabView interface in Figure 5.6 shows how the sweep is controlled in terms of optical frequency.

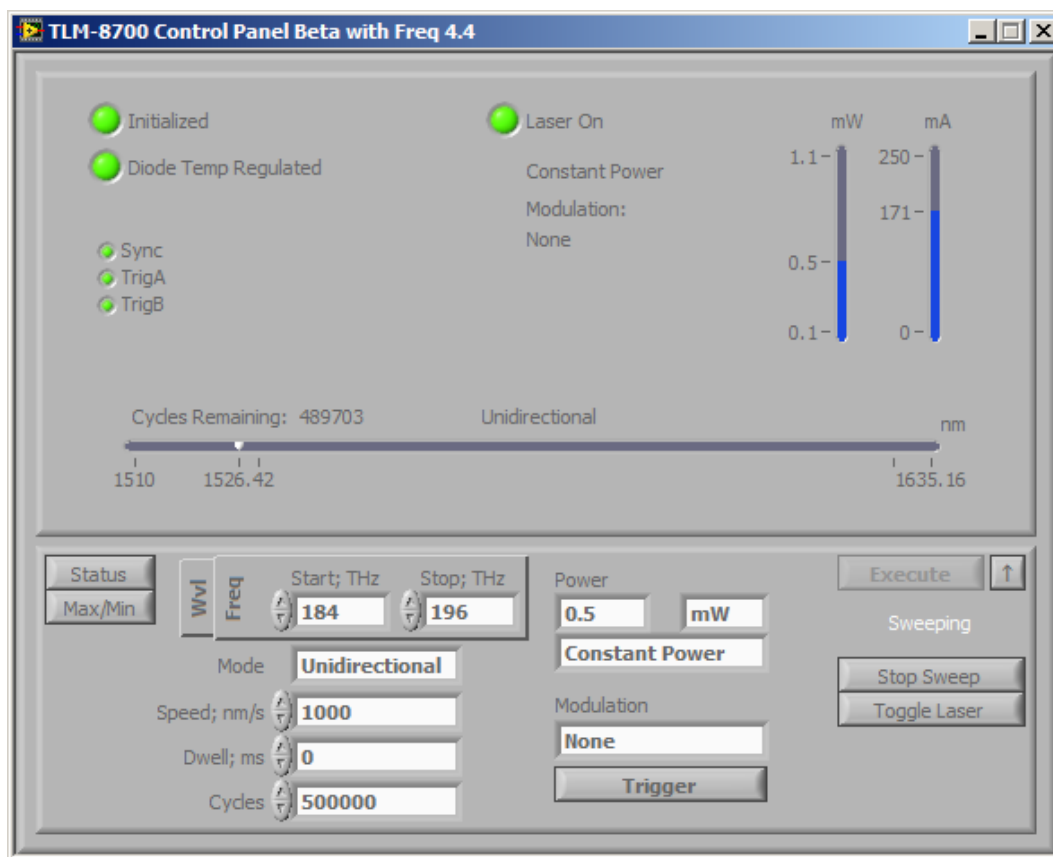


Figure 5.6 – Software to control optical frequency sweeps.

The LabView interface in Figure 5.7 shows the control over the Trigger A signal.

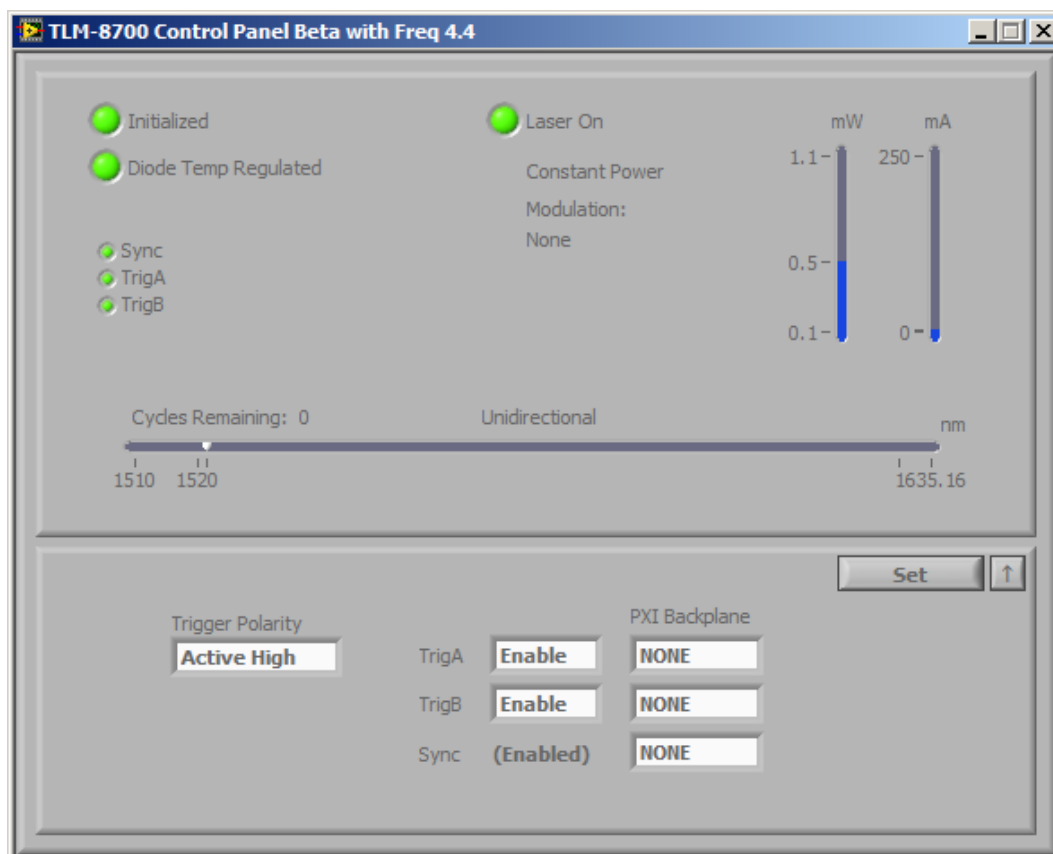


Figure 5.7 – Software to enable Trig A.

Figure 5.8 shows five complete sweeps at 1000nm/s. The SYNC signal, which brackets the sweep, is shown in red. The Trigger A signals are in green. There are very few of the Trigger A markers in the plot. This is because the markers are very narrow and don't show up in the oscilloscope trace. The black values are the detected signal of the laser after passing through an etalon which provides a periodic reference with optical frequency. The etalon values are for reference only and are not used to generate the Trigger A signals.

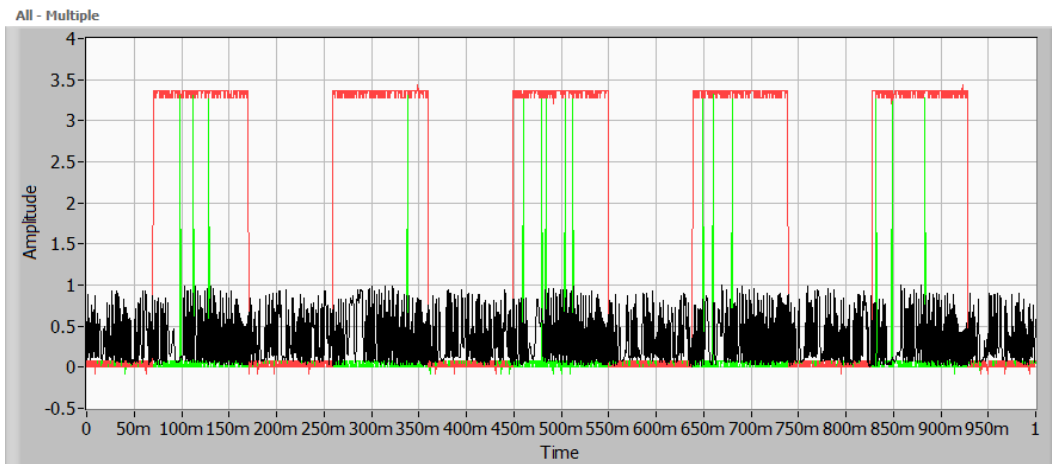


Figure 5.8 – Sync signals in red show the extent of a sweep. Trig A optical frequency markers are in green. Only a few show due to the limitations of the scope. In black are a periodic optical element.

One complete sweep is shown in Figure 5.9. The SYNC signal (red) is used to gate data acquisition. It rises with the first optical frequency marker (green) and falls with the last one. The optical frequency markers appear sparse because of limitations of the scope used for this measurement.

The etalon signal (black) provides an optical frequency reference and is present on the reverse sweep as well. The gap in the etalon data before and after the sweep are the turn-around points where the laser comes to a stop.

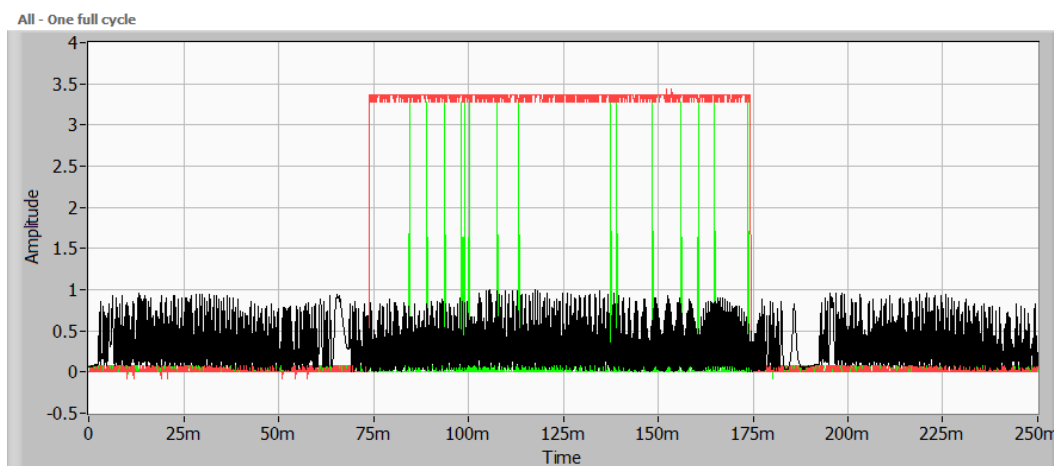


Figure 5.9 – One sweep cycle. Sync in red shows extent of the sweep. Trig A optical frequency markers are in green. The optical element is in black.

The first 23 optical frequency markers are shown in Figure 5.10 and the final 23 in Figure 5.11. The first and thirteenth markers match the first and eighth etalon cycles. Also the last and the thirteenth from the last markers match the last and eighth from last etalon cycles. This indicates the etalon spacing is 12/7 the optical frequency marker spacing of 10Ghz or 17.1Ghz.

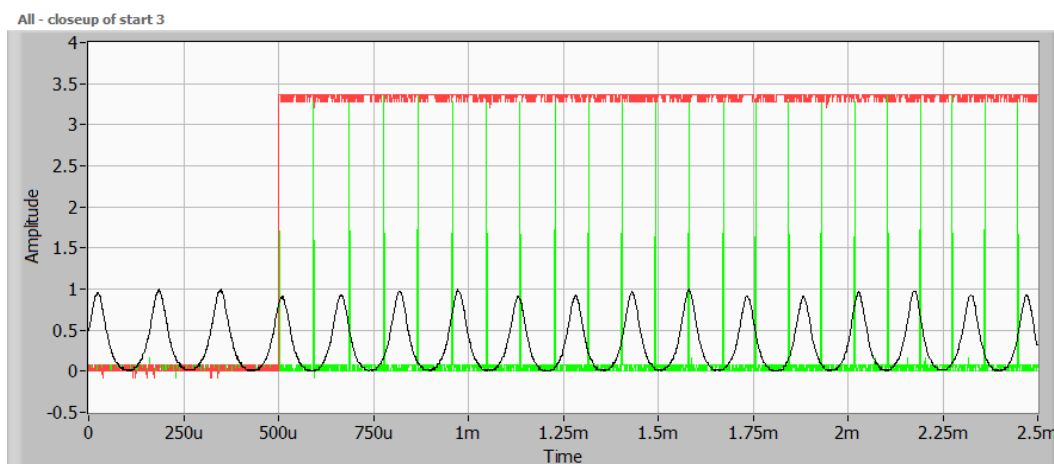


Figure 5.10 – The first 23 optical frequency markers (TrigA).

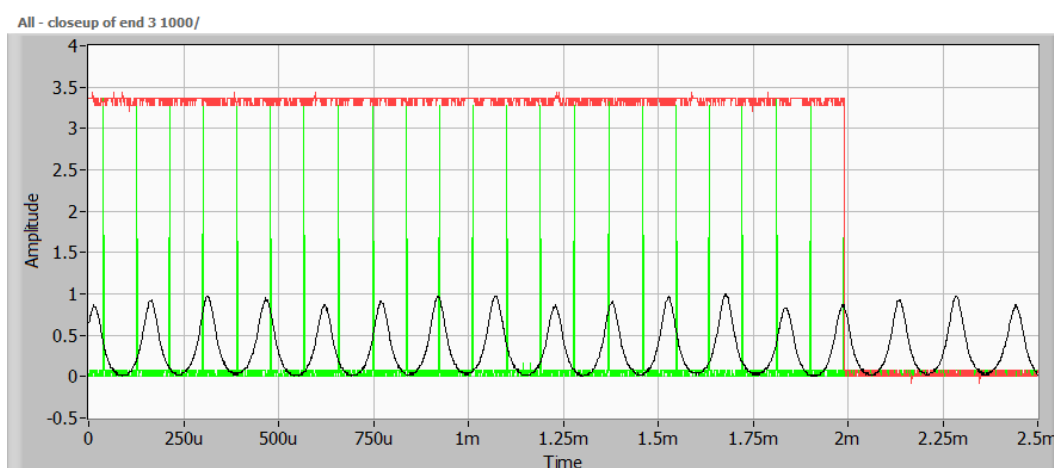


Figure 5.11 – The last 23 optical frequency markers (TrigA).

Figure 5.12 shows the first optical frequency marker. The rising edge comes as the laser sweeps across the first optical frequency of the sweep which is also marked by the rising edge of the SYNC signal.

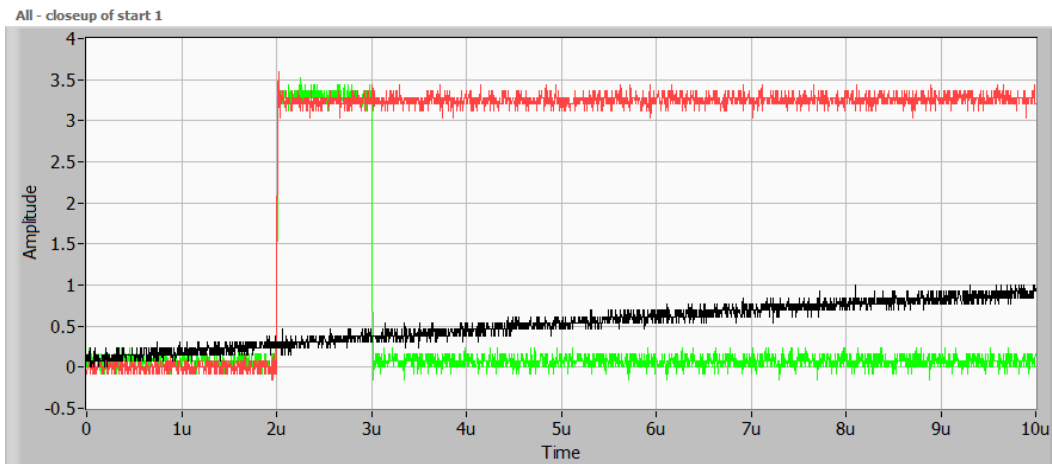


Figure 5.12 – The first optical frequency marker. The rising edge comes as the start optical frequency is reached and lasts for 1uS.

Figure 5.13 shows the end of the sweep. The rising edge of the final optical frequency marker comes as the laser sweeps past the stop optical frequency of the sweep. This stop optical frequency is also marked by the falling edge of the SYNC signal.

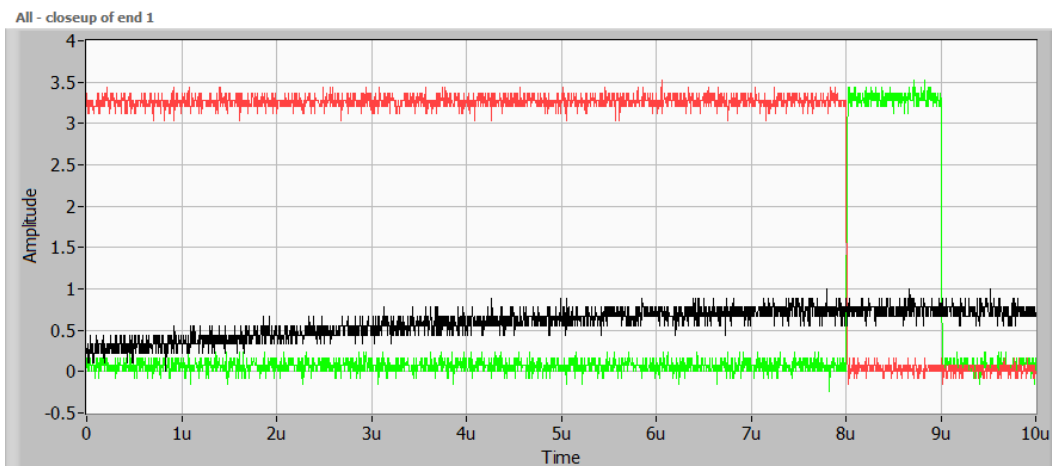


Figure 5.13 – The last optical frequency marker. The rising edge comes as the stop optical frequency is reached and lasts for 1uS.

The repeatability of the triggers is demonstrated in Figure 5.14. In this test a gas cell line was measured using wavelength markers adjusted to 1pm separation and the marker width reduced to 0.1uS as the original marker width of 1uS didn't allow any time between markers when sweeping at 1000nm/s.

The standard deviation of the peak location was taken as a measure of the frequency marker uncertainty. Two different lines were measured with the one-

sigma deviation being 12 MHz in one case and 20 MHz in the other. This indicates a repeatability of 1.7ppm across the 12THz scan range.

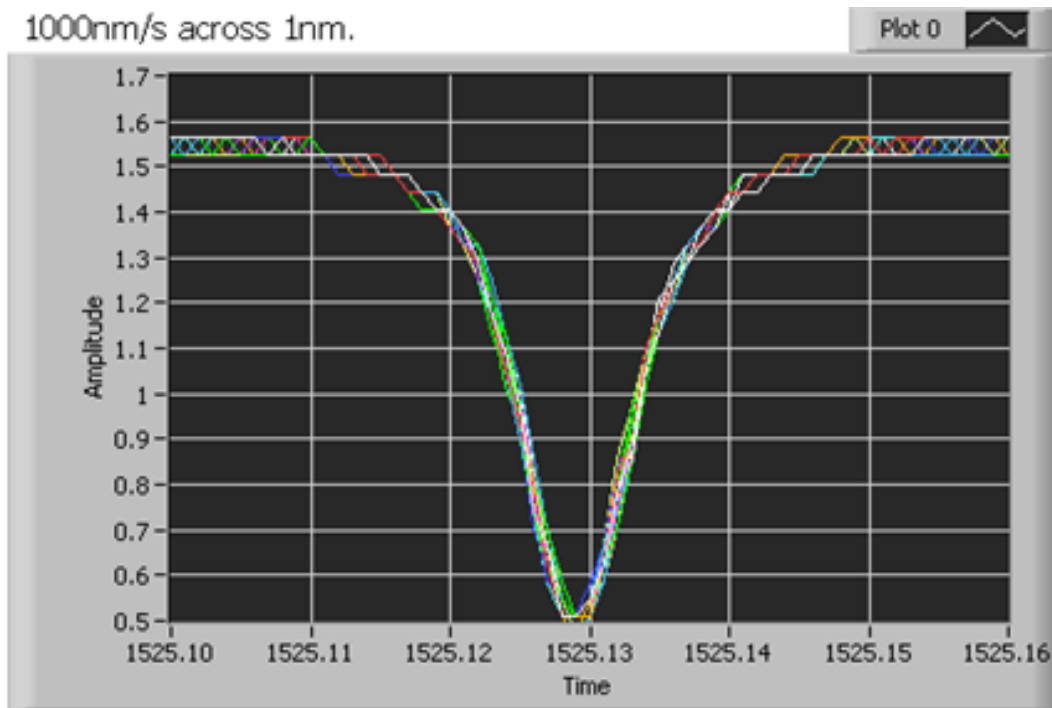


Figure 5.14 – Multiple scans of a gas-cell line using 1pm wavelength markers to clock the data acquisition. One sigma deviation of 12 – 20 MHz indicates 1.7ppm repeatability across the 12THz sweep range.

The assertion of Figure 5.4 that using the wavelength markers in an SS OCT system would result in a degraded signal as the distance between reference and measurement is increased is confirmed with the measurement shown in Figure 5.15. Thirteen different measurements were taken and the results plotted in the same graph. The peaks increase in width and decrease in amplitude with distance as predicted.

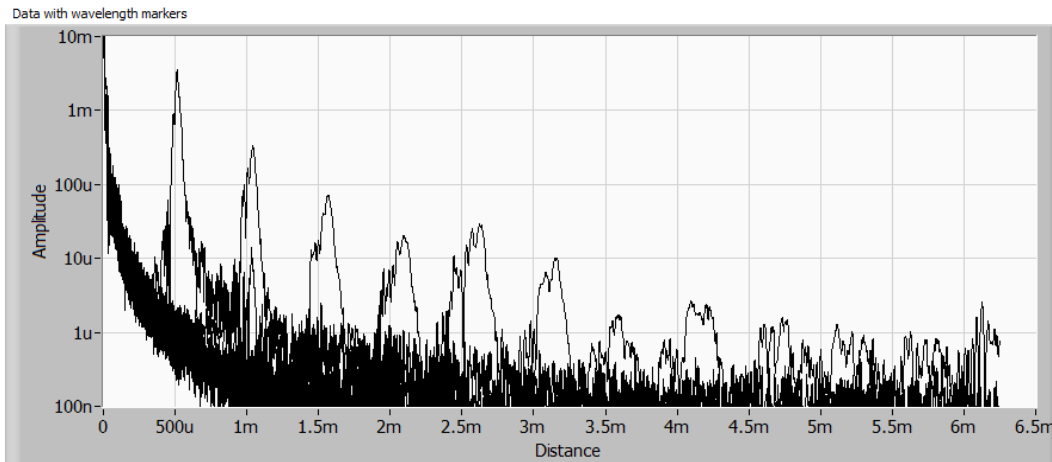


Figure 5.15 – Data at various distances measured with standard wavelength markers. Note the characteristic broadening.

The assertion of Figure 5.5 that using optical frequency markers instead is confirmed in the measurement data shown in Figure 5.16 where the same thirteen measurements of Figure 5.15 are repeated using optical frequency markers instead of the wavelength markers. The peaks no longer increase in width with distance. There is still attenuation but this is due to lack of collimation in the optical signal which is not taken into account in Figure 5.5.

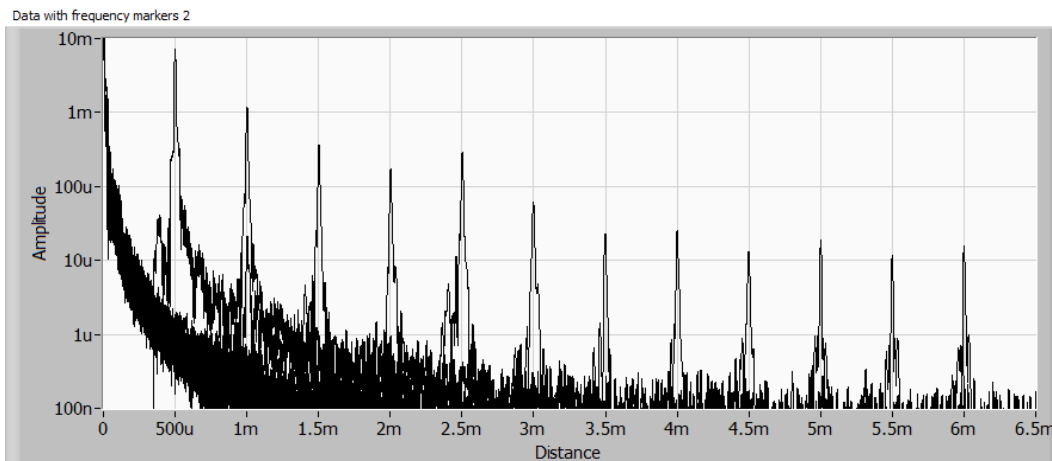


Figure 5.16 – Data at various distances measured with optical frequency markers. Note that the peaks remain sharp across the range.

A measurement was taken of a piece of scotch tape taped to a microscope cover glass or dioptré. An A-line is shown in Figure 5.17. From left to right are the reflections from the top of the tape, the bottom of the tape, the top of the glass and finally the bottom of the glass. The resolution in glass of the measurement is 8.3 μ m.

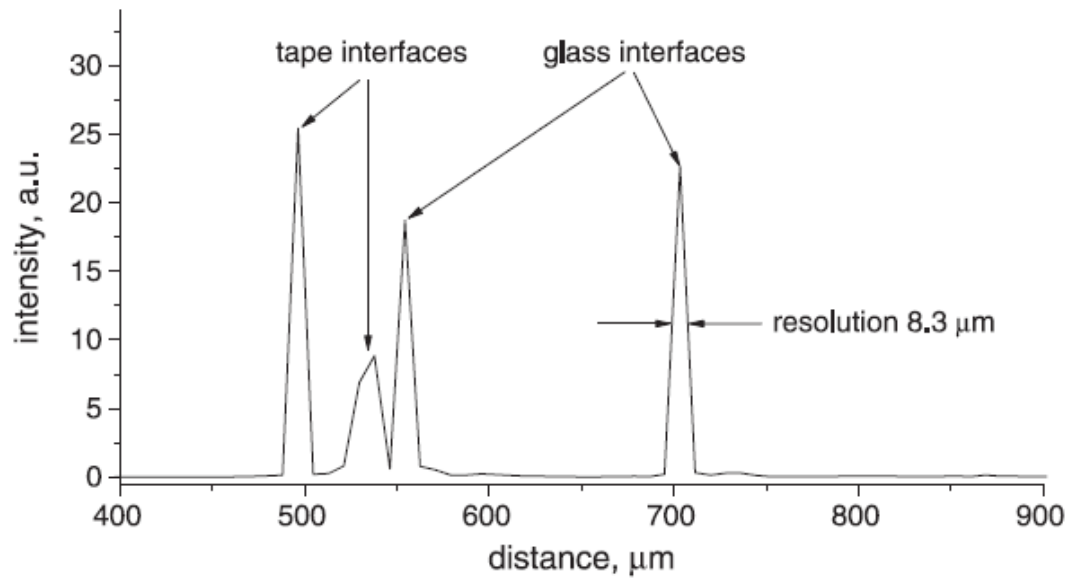


Figure 5.17 - A-scan for plastic tape glued to microscope dioptré. Distance calibrated in glass. [Cordes, A.H. et al. (2010)]

The B-scan of the same sample is shown in Figure 5.18. The location of the A-scan in Figure 5.17 is shown as a vertical white line. The location of a hair which was pinned under the tape is also shown. The hair caused the tape to lift enough so air was present between the tape and the glass in the A-line. Without this gap the glue of the tape acts to index match the tape and the glass making that the boundary between the bottom of the tape and the top of the glass indistinct.

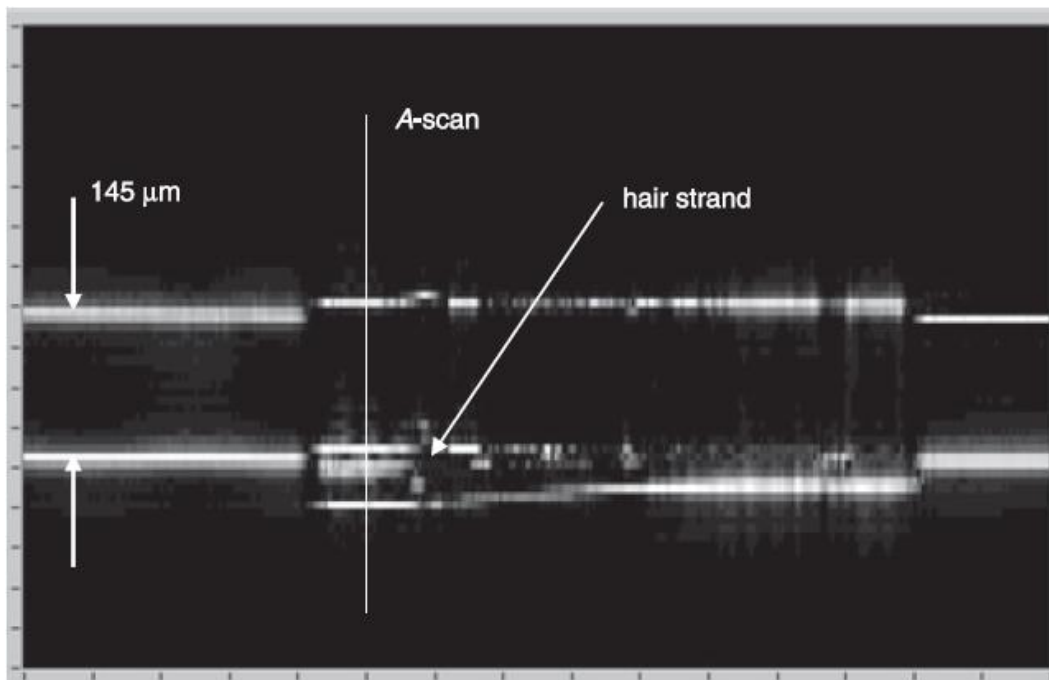


Figure 5.18 - B-scan for plastic tape and dioptré. Light enters from bottom. Spacing between tape and glass surface on left hand side of tape due to presence of hair strand indicated by arrow creating air bubble to the left. Position of Figure 5.17 A-scan is also indicated. [Cordes, A.H. et al. (2010)]

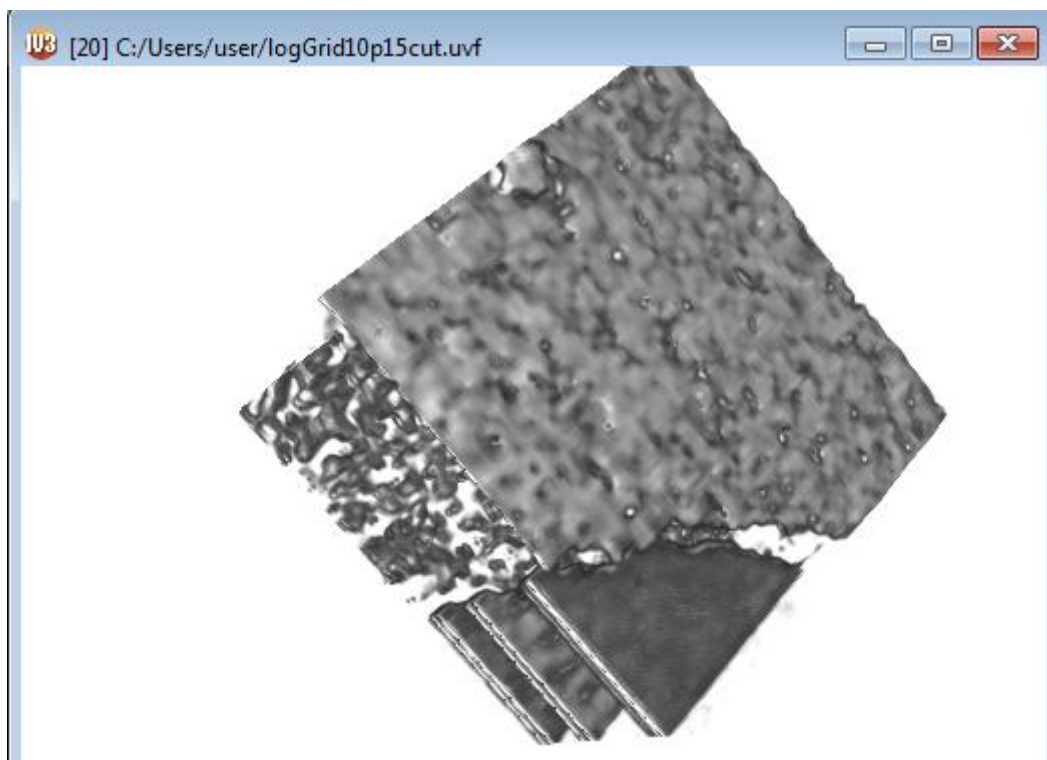


Figure 5.19 – C-scan of multiple slide dioptrés with scotch tap covering the majority of the area scanned.

5.2. Stretched Pulse Santec Laser

A stretched pulse tunable laser starts with the output of a very narrow impulse laser. This pulse is stretched and the optical frequencies chirped by a dispersive element. The result is a very fast swept laser. [Moon; Kim (2006) e Park et al. (2007) e Moon; Kim (2007) e Ahn et al. (2008)]

As the effective scan rates are much much higher, the equipment changes dramatically and presents some practical limitations. The New Focus laser scanned at 25THz / s which produced frequencies on the order of 1Khz from 1mm. These stretched pulse lasers scan 100's of nms in 100's of ns and can generate frequencies from a 1mm depth of on the order of 1Ghz. This immediately raises the bar as to the data acquisition which now must sample at 10Ghz type levels and takes us out of the National Instruments range. We used a 40Gs/s Tektronics oscilloscope with a 3.5Ghz bandwidth.

In our case the dispersive element is 8km of Corning DS fiber. As the dispersion for the DS fiber turns over at 1550nm this places a practical limit to the bandwidth and thus the resolution of an OCT system built around it. Non-linear effects (Raman) are taken advantage of to help filter the spectrum before the zero dispersion point.

We reported the results of a similar system at IMOC in 2009 [Cordes, A.H. et al. (2009)].

5.2.1. Components

The elements of the stretched pulse swept laser are shown below. The Santec UWS-1000H shown in Figure 5.21 puts out a sub-picosecond pulse which is dispersed by the Corning DS fiber in Figure 5.22. The two bending loss filters in Figure 5.23 and Figure 5.24 shape the spectrum by combining to attenuate the power near and past the 1550nm dispersion break as discussed in 5.2.2 beginning on page 174. The first filter is 12 turns of single mode jacketed fiber around a 0.5" diameter cylinder. The second filter is 9 turns of single mode jacketed fiber around a 0.75" diameter cylinder. The last element is a splitter which is the entrance to the OCT interferometer.

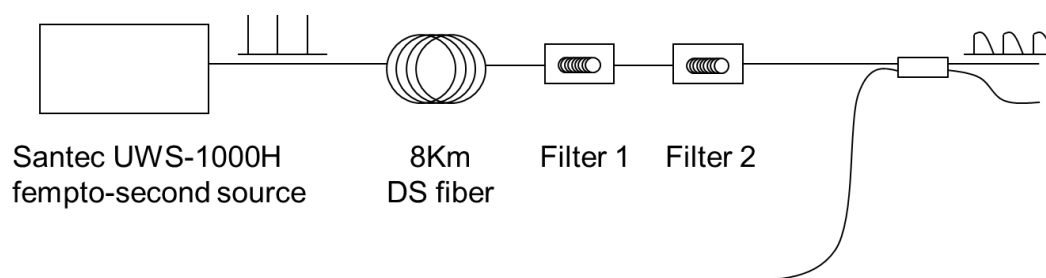


Figure 5.20 – Components.



Figure 5.21 – Santec Ultra-wideband Source

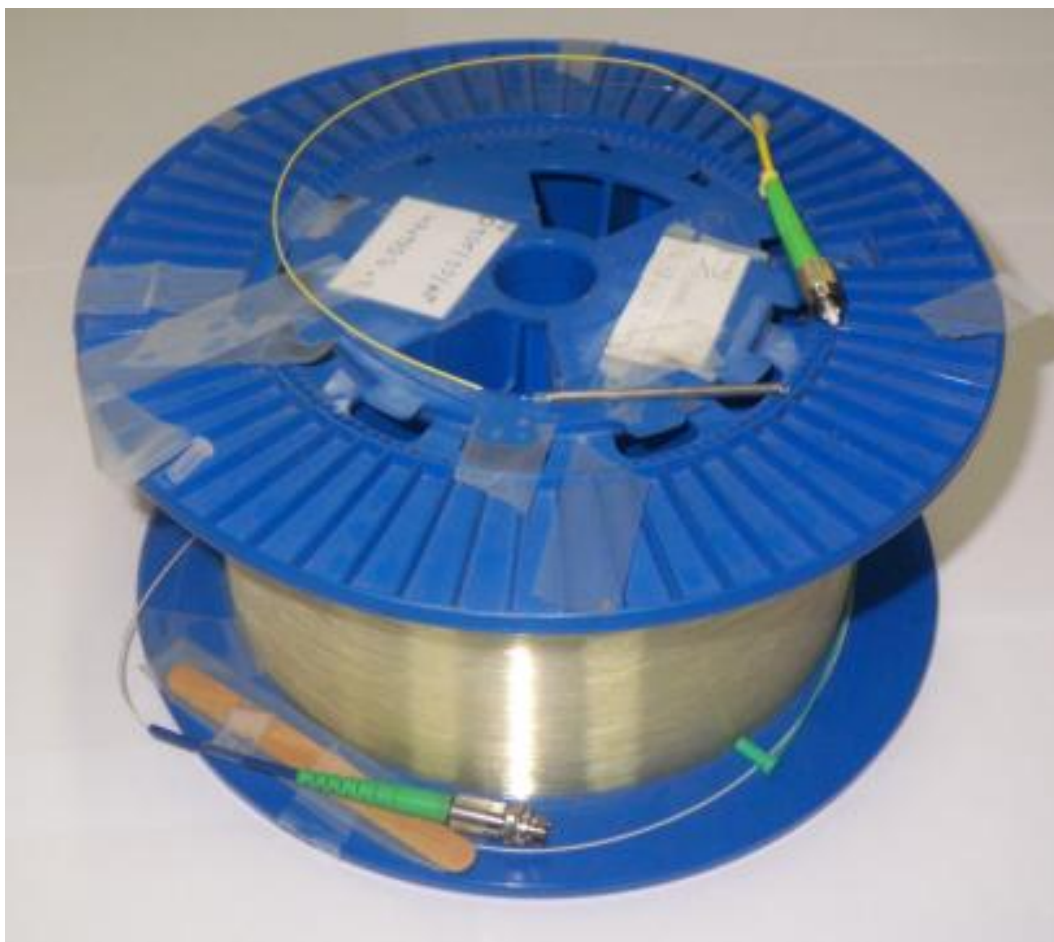


Figure 5.22 – DS fiber. Used for dispersion

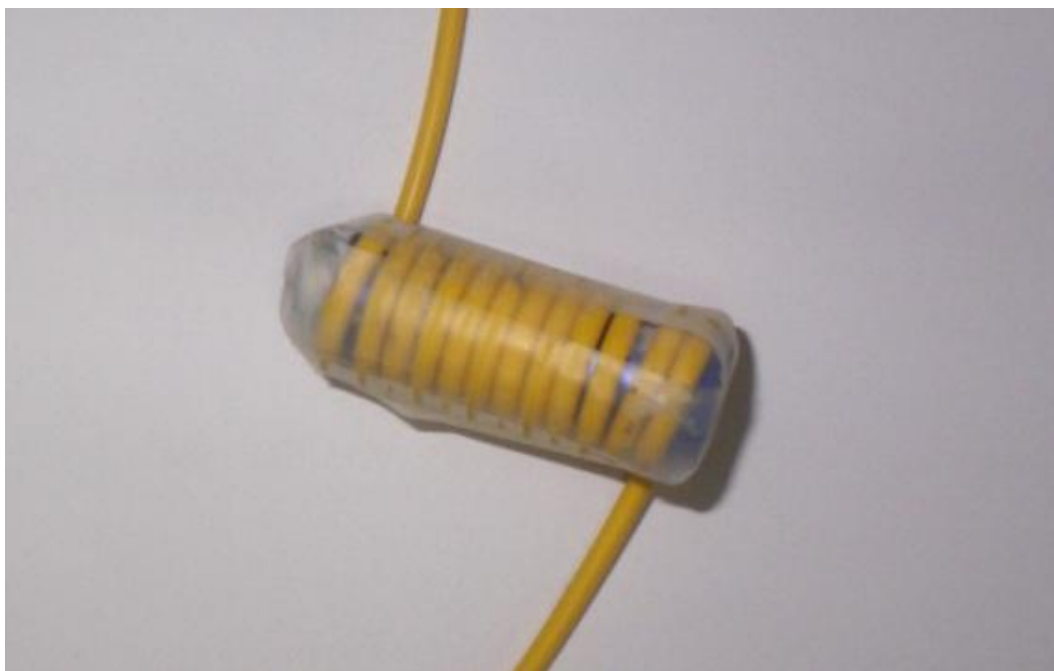


Figure 5.23 – Filter 1



Figure 5.24 – Filter 2

5.2.2. Time and Spectrum

The spectral content of the Santec laser shown in Figure 5.28 is very broad, stretching from below 1200nm to above 1700nm. We had two choices as to dispersion material, standard single mode (SM) fiber with a zero dispersion around 1300nm or dispersion shifted (DS) fiber with zero dispersion around 1550nm. In either case the dispersion curve has a minimum and then rises, causing two wavelengths at equal distances on each side of the minimum to experience the same delay. Having two wavelengths experience the same delay would kill the interferometer, so spectral content either below 1300nm (in the SM case) or above 1550nm (in the DS case) would have to be filtered out somewhere before the signal was detected. We decided to use the DS fiber for several reasons. First, there is a peak at 1550nm in the otherwise relatively flat power curve, so removing spectrum at 1550nm results in a flatter spectrum. Second, filtering higher wavelengths is relatively easy using cladding mode attenuation. Third, having the spectral peak on top of the zero dispersion caused RAMAN amplification to push energy from the 1550nm region into higher wavelengths even before the filters, making the filtering easier and the spectrum's edge sharper.

Figure 5.25 below shows the group delay curve for the DS fiber. The zero dispersion point is the minimum of the curve and is marked with a vertical dashed line. Spectral content above this dashed line will have to be removed from our system.

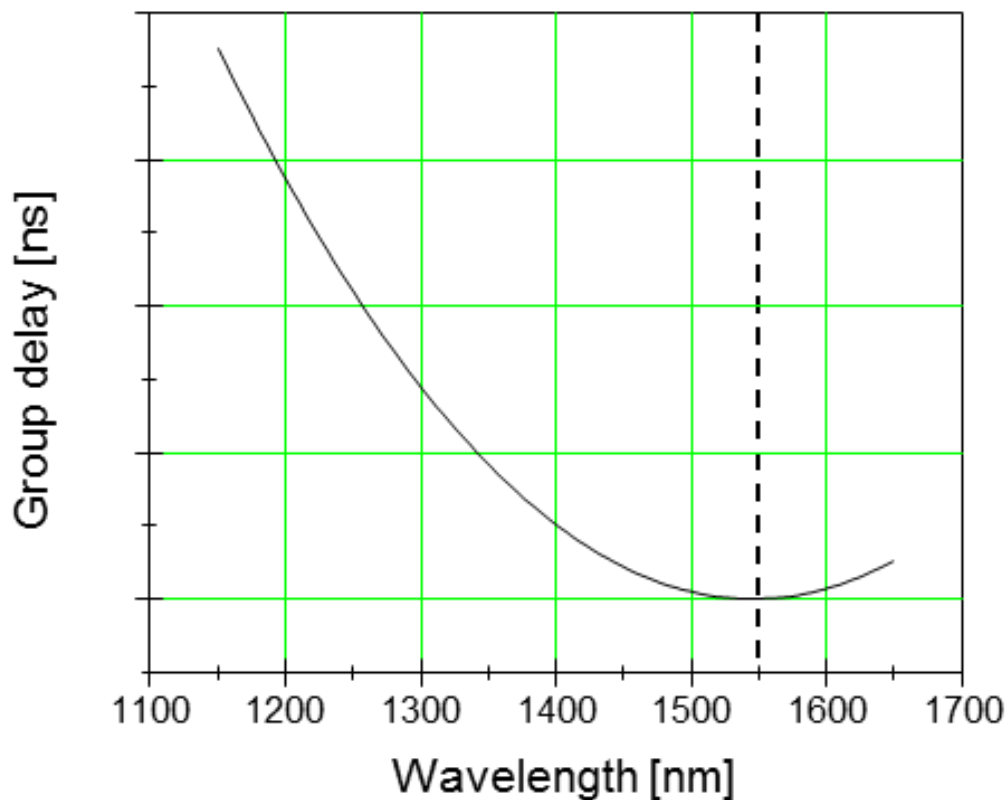


Figure 5.25 – Dispersion curve for DS fiber. Zero dispersion is at 1550nm.

The following sections will detail this process. The time and spectral characteristics after each component in the system will be shown and discussed. Each spectrum will have the vertical dashed line at the zero dispersion point to assist in tracking the progress of controlling the spectrum. A grey dot will mark the location in the system being discussed.

5.2.2.1. Output of the laser

The output of the Santec is very broadband. This would be excellent from a resolution standpoint but the power on the right side of the zero in the dispersion

(dashed line) is unusable. At this point it is less than a ps wide in time domain. Our autocorrelator was broken so we don't have data for the exact pulse shape here.

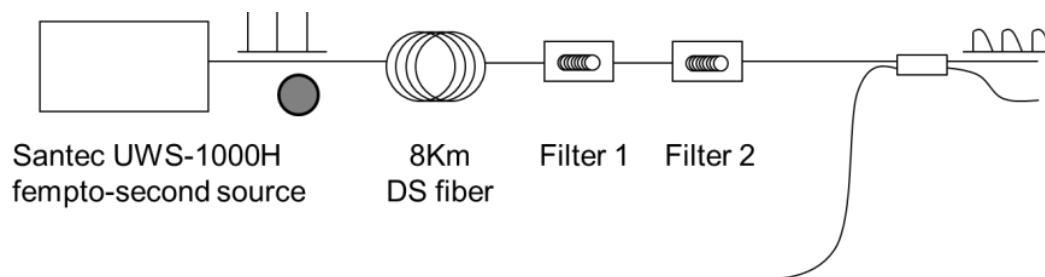


Figure 5.26 – Output of the laser

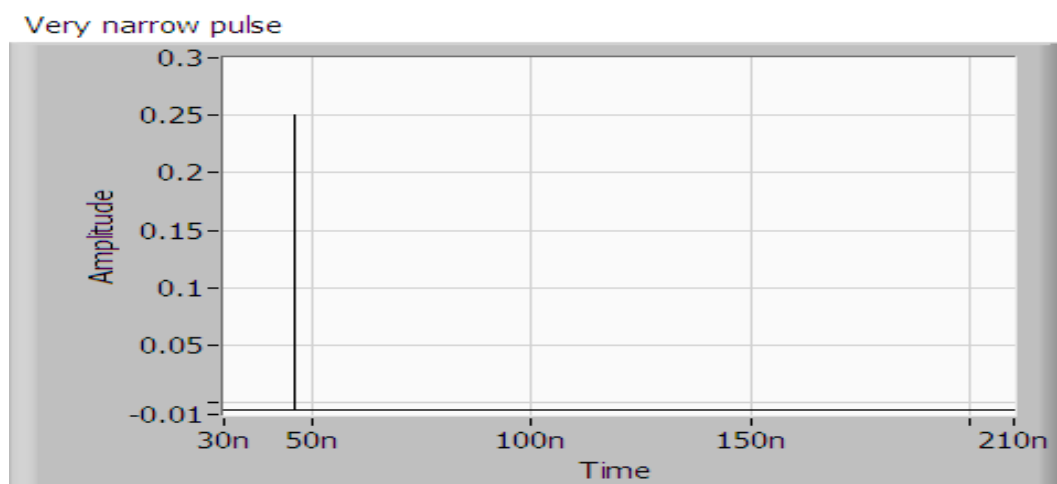


Figure 5.27 – Output of the laser. Time domain (drawing).

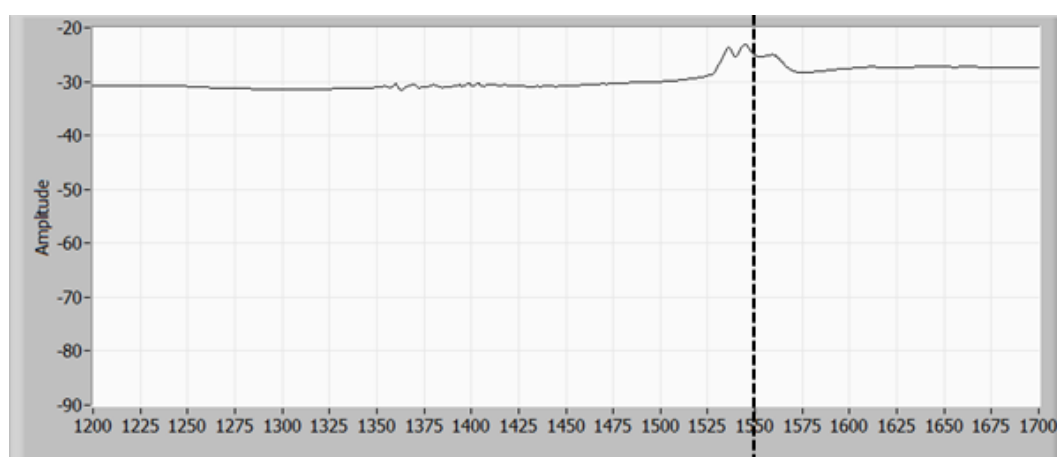


Figure 5.28 – Output of the laser. Spectrum. It covers an enormous range including optical frequencies above the turnaround point of the DS dispersion curve (dashed line at 1550nm).

5.2.2.2.

After the dispersive fiber

The fiber spreads the pulse and attenuates the signal. In addition, there is a Raman dip at 1475nm. The energy goes to 1575 and above which can be seen from the fact that there is less apparent attenuation at the higher wavelengths.

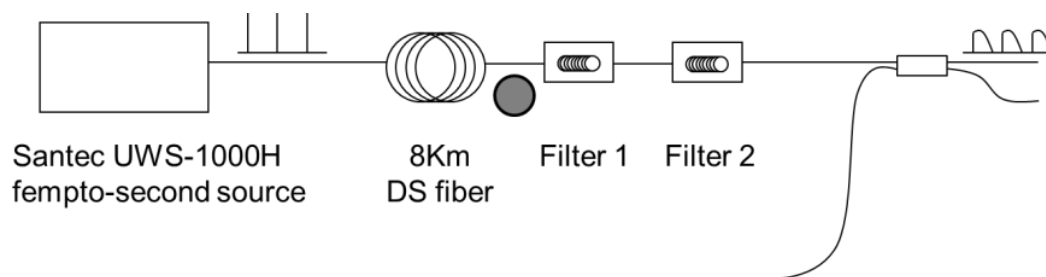


Figure 5.29 – After the fiber.

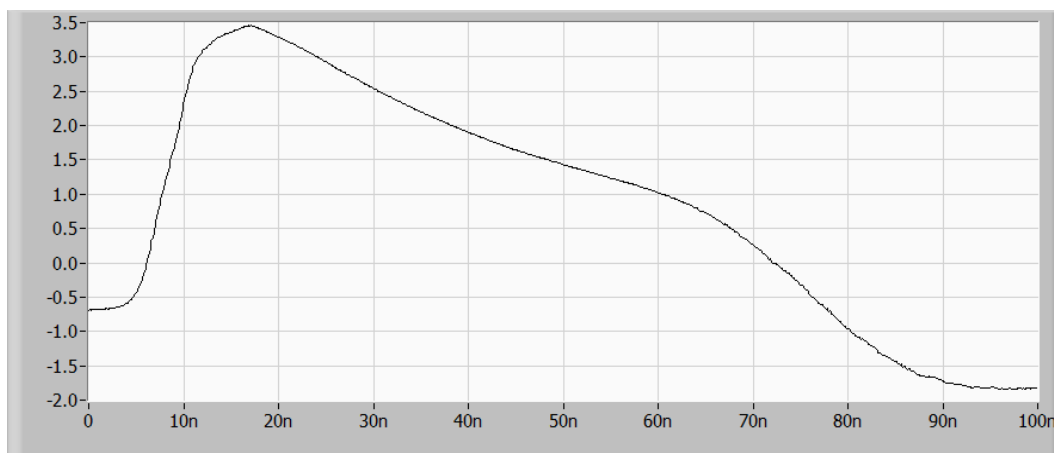


Figure 5.30 – After the fiber. Time domain. The pulse has been stretched out.

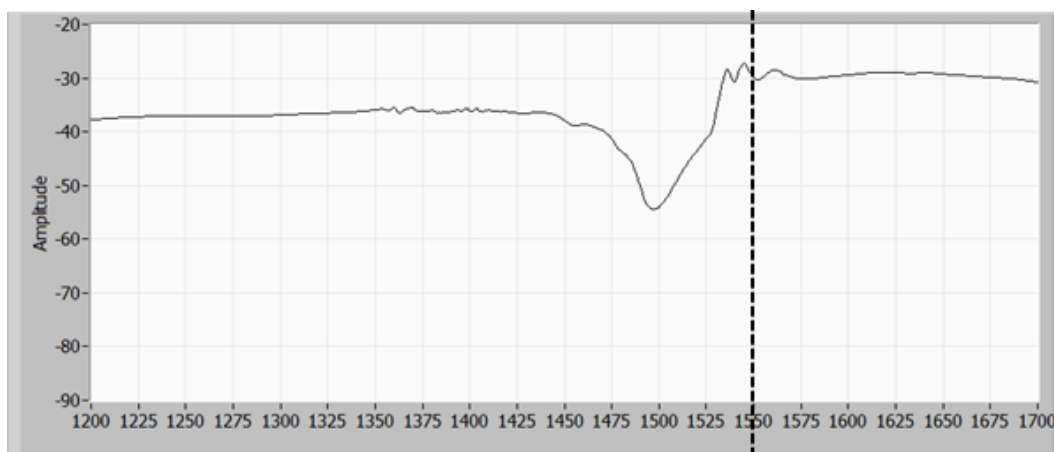


Figure 5.31 – After the fiber. Spectrum. There has been loss through the fiber and some Raman amplification moving energy from the 1500nm region to higher wavelengths.

5.2.2.3. After Filter 1

The first filter drops the spectrum above 1550nm by 20dB. There is still a lot of energy in the spectrum above zero dispersion.

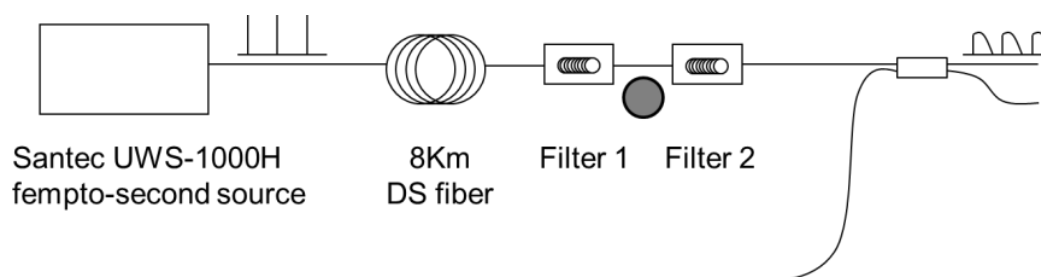


Figure 5.32 – After filter 1.

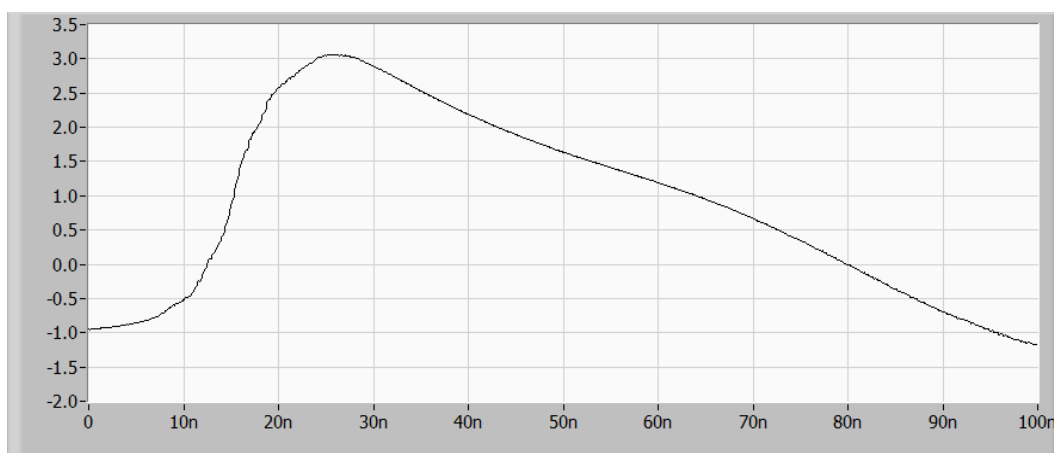


Figure 5.33 – After filter 1. Time domain.

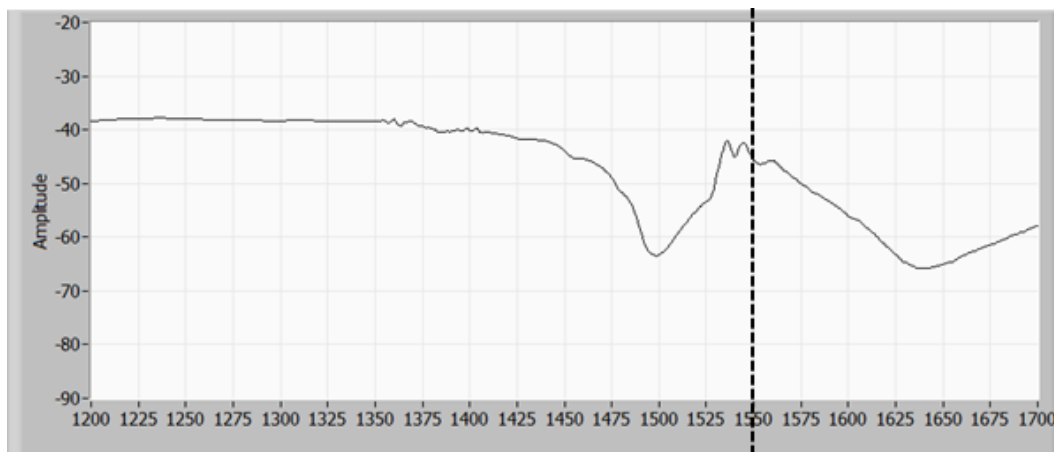


Figure 5.34 – After filter 1. Spectrum.

5.2.2.4. After Filter 2

The second filter drops the spectrum above the zero dispersion point into the noise.

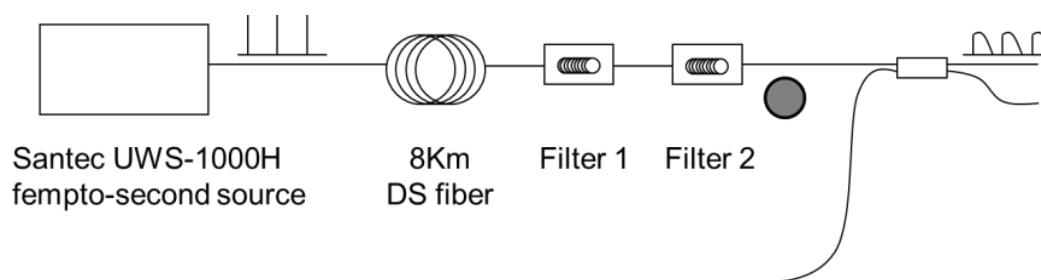


Figure 5.35 – After filter 2.

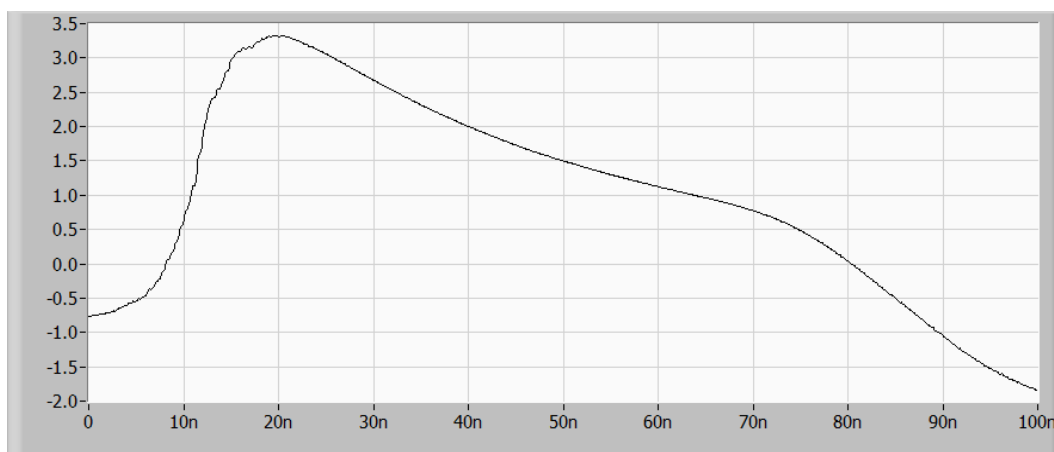


Figure 5.36 – After filter 2. Time domain.

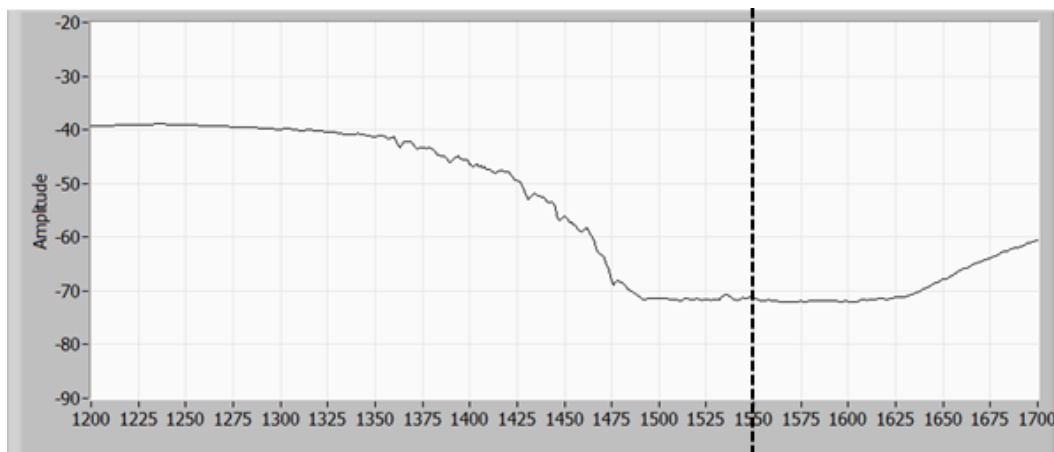


Figure 5.37 – After filter 2. Spectrum.

5.2.2.5.

At Reference / Measurement plane

The signal passed into the interferometer loses three more dB from the splitter. In our case we are using the Fresnel reflection from the tip of the fiber as our reference and without the need for a second arm could have used a circulator rather than a splitter to save 3dB in both directions. However we didn't have an appropriate wideband circulator available.

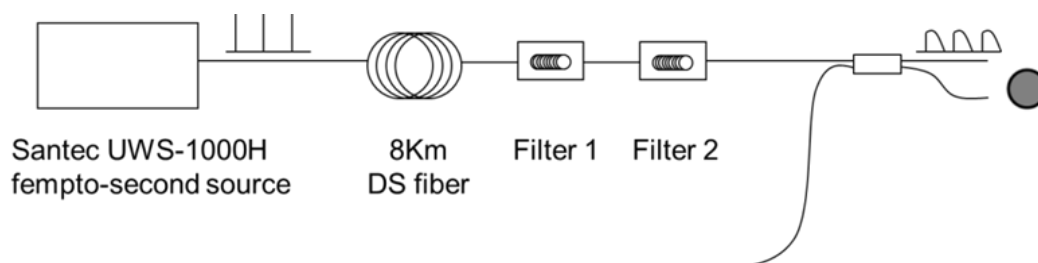


Figure 5.38 – At reference / measurement.

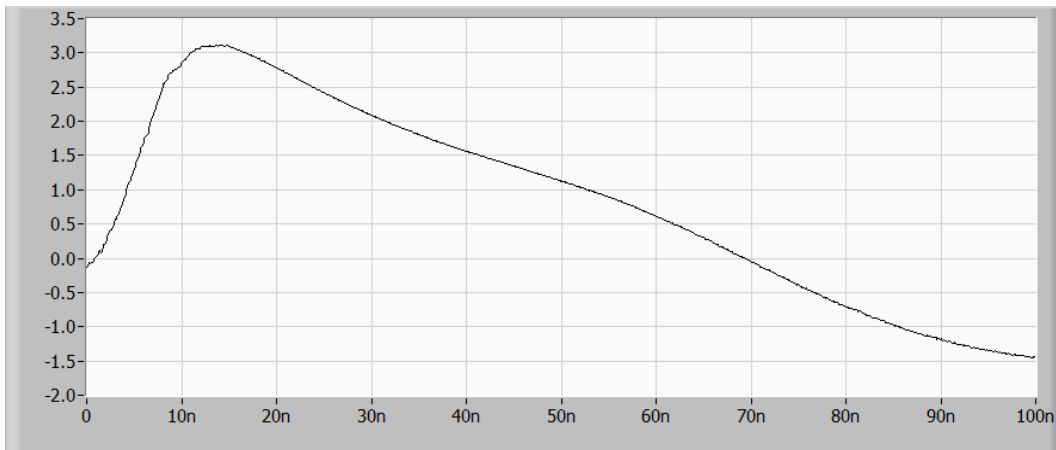


Figure 5.39 – At reference / measurement. Time domain.

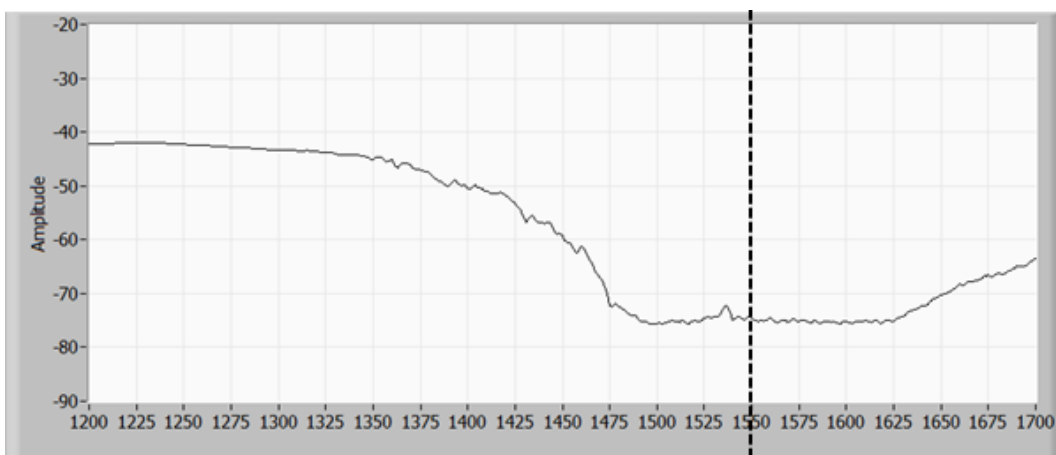


Figure 5.40 – At reference / measurement. Spectrum.

5.2.2.6. At the detector

The combined signal returned through the splitter is quite low. A zoomed scale is provided as the reflection is almost imperceptible on the original scale. In the first plot case only the reference reflection is shown. In the second plot there is a reflection to beat against the reference reflection. Note that the beat signal is obvious in the spectrum as well as in the time domain.

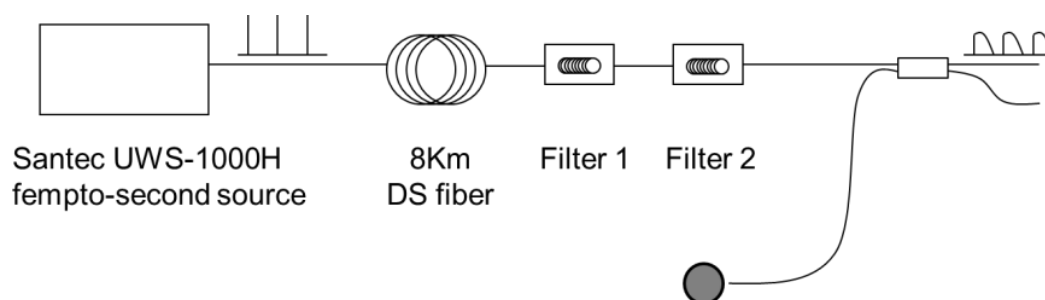


Figure 5.41 – At the detector

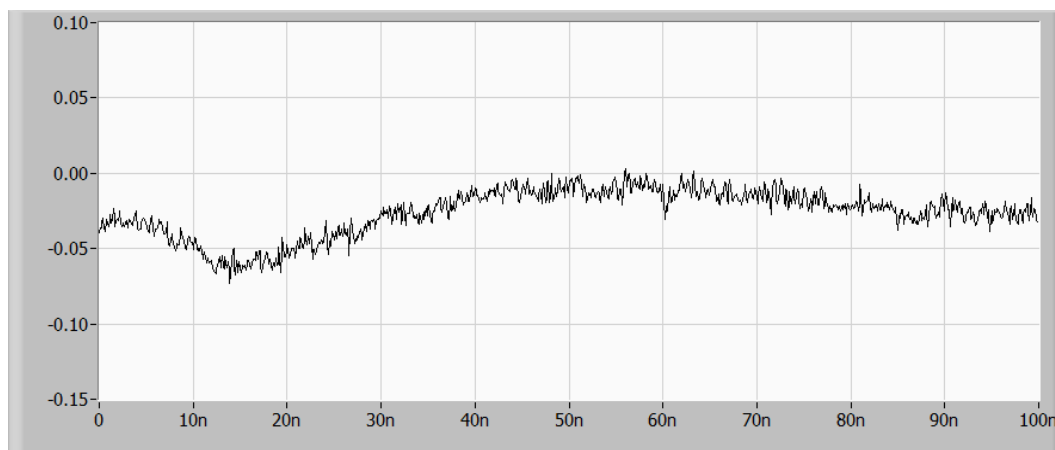


Figure 5.42 – At the detector. Reference reflection only. Time domain.

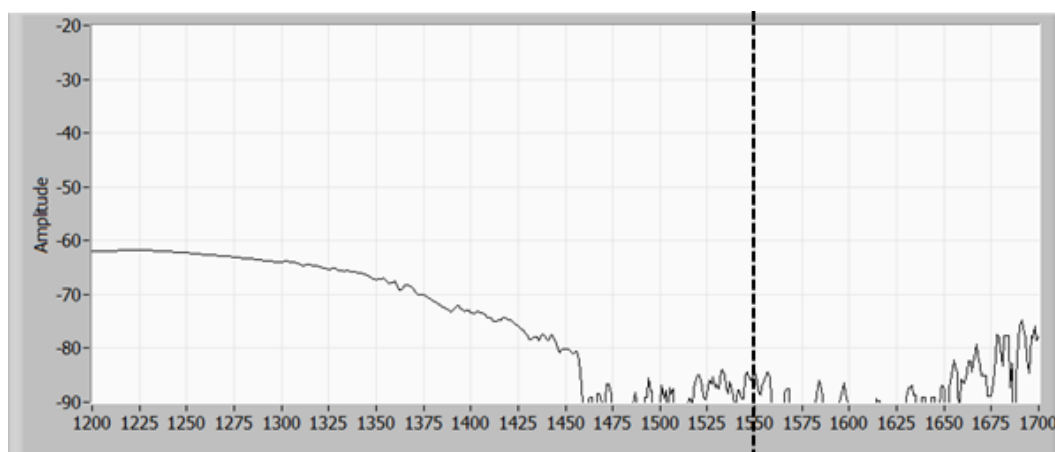


Figure 5.43 – At the detector. Reference reflection only. Spectrum.

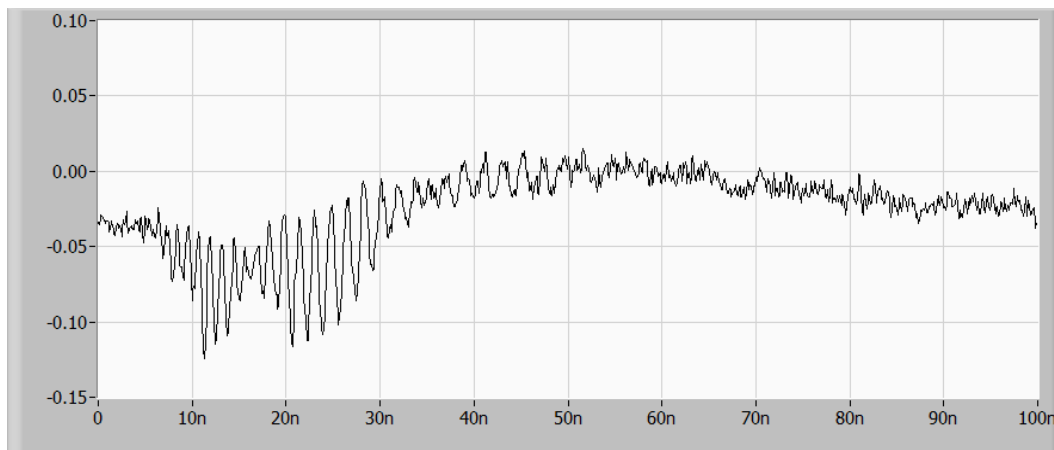


Figure 5.44 – At the detector. Beat signal. Time domain.

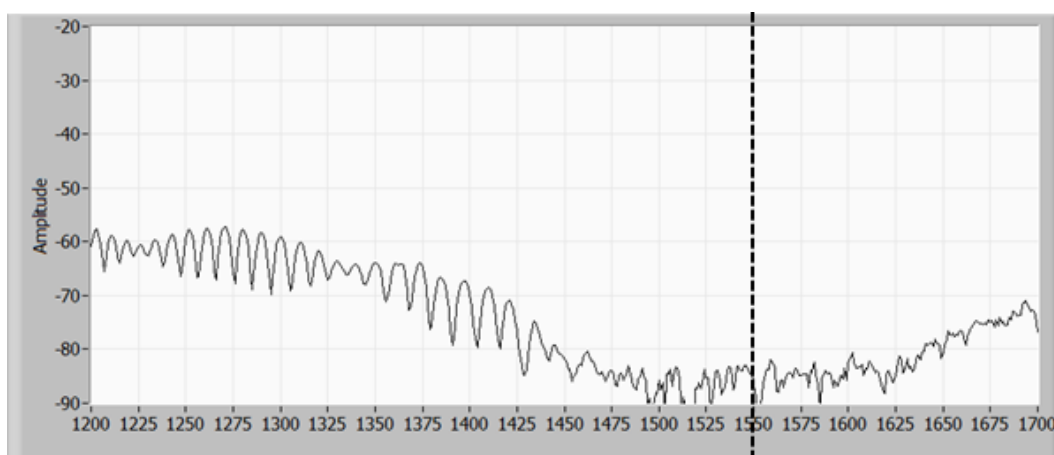


Figure 5.45 – At the detector. Beat signal. Spectrum.

5.2.3. Calibration

As the sweep of this source is generated by a passive component (the dispersion of the 8km of fiber) the optical frequencies carved out as a function of time are very repeatable.

We can use a single calibration from an arbitrary reflector to get the optical frequency scale. We use the Hilbert transform to get the phase scale for this reflector and use that to construct an arbitrary optical frequency scale as detailed in 4.2, 4.3 and 4.4 startin on page 116.

The distance scale is calibrated from two relative points as detailed in 4.5.2 on page 137.

5.2.3.1. Calibration of sweep

We start with the beat frequency from a reflector at an arbitrary distance. We don't really care what the distance is at this point since we will calibrate for distance later. This first step is just to linearize the scale with optical frequency.

Since this trace includes data before the sweep, during the sweep and after the sweep we have to select just the data from the sweep itself. This time section relative to the trigger has to be maintained throughout the time this calibration is to be used. If the trigger changes or the scale changes then the calibration would have to be done again.

Figure 5.46 shows the entire trace of the beat signal from the arbitrary distance.

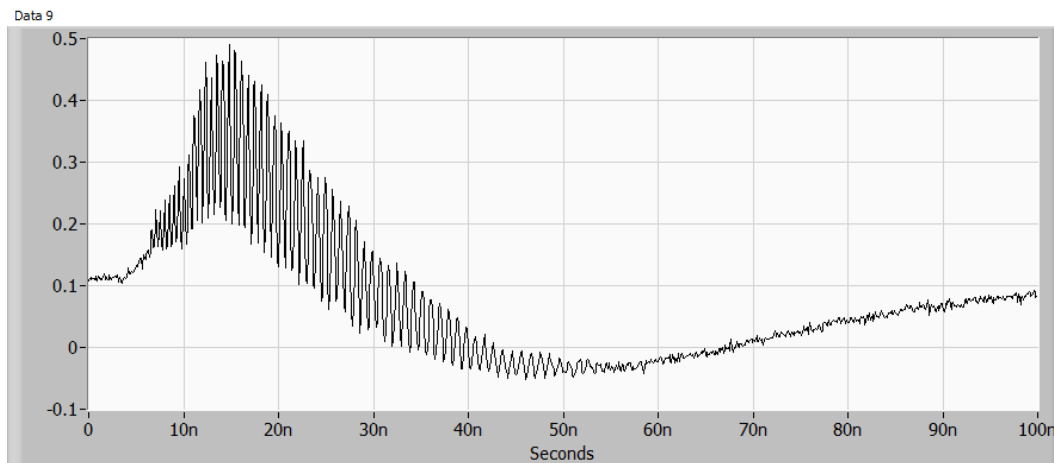


Figure 5.46 – Raw data

Figure 5.47 shows the section of the data chosen. This section includes only that part of the trace which has sweep data.

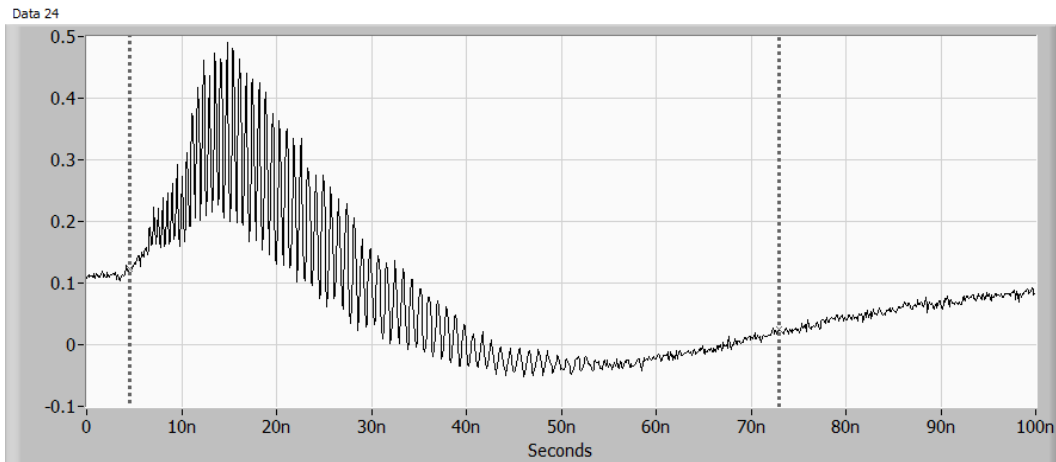


Figure 5.47 – Selected section. This same selection needs to be made on the actual data in order for the calibration to remain valid.

Figure 5.48 shows the sweep data only on a scale of samples in time. As the sweep was non-linear the time scale doesn't have any meaning for us anyway.

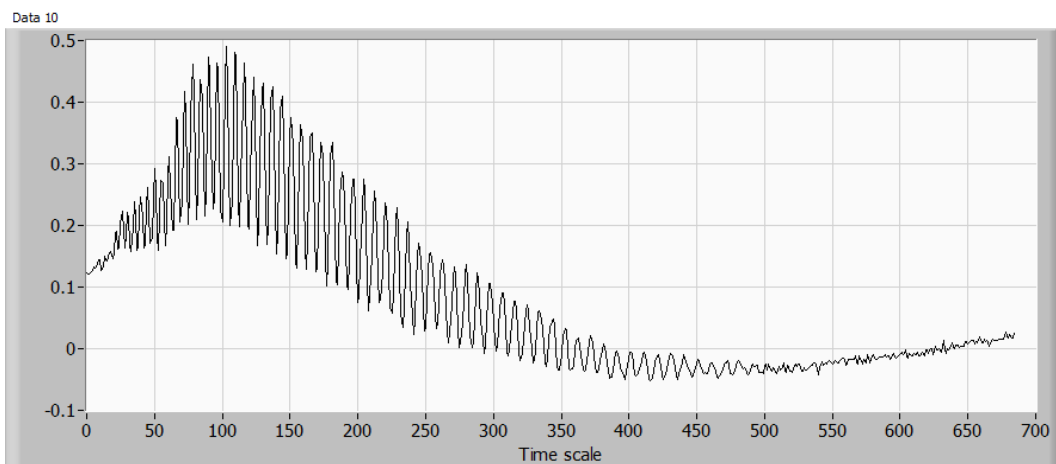


Figure 5.48 – Cut-data only with sample scale.

In Figure 5.49 we move to the frequency domain. We use a Blackman-Harris window to reduce the effects of neighboring frequency content. Our calibration requires a monotonic phase so we have to clean out the frequency content due to the envelope of the waveform. The windowed data maintains its sampling size. Zero padding in this domain could be useful for interpolation in the time domain but that is not being used here.

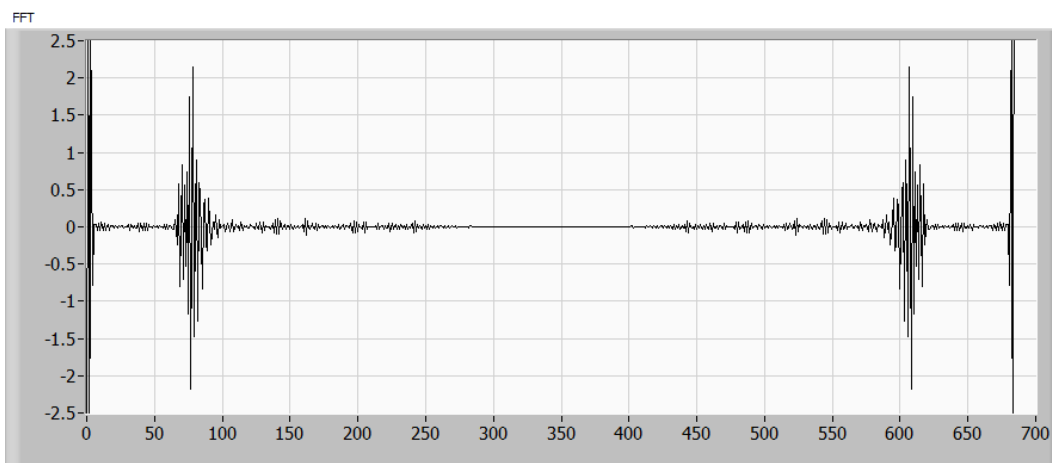


Figure 5.49 – FFT of cut-data

Figure 5.50 shows the selected portion of the spectrum, well away from the lower frequencies of the envelope. The section is taken to be symmetrical about the beat signal's frequencies in order to preserve as much as possible when windowing. The section is shown on the left side but is also symmetrically applied to the right side as well.

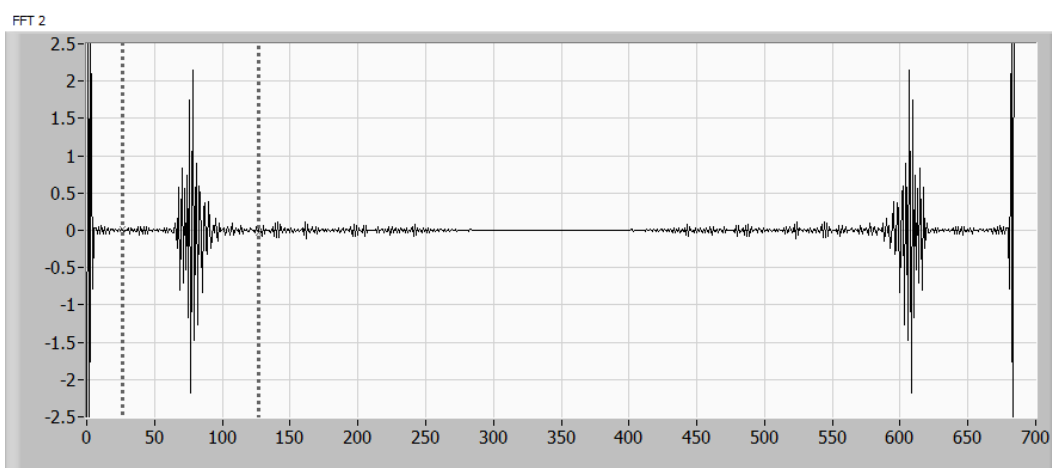


Figure 5.50 – Chosen area of FFT (choice is mirrored to the other data area).

Figure 5.51 shows the selected spectrum after it has been windowed with a Hamming window and the rest of the spectrum set to zero.

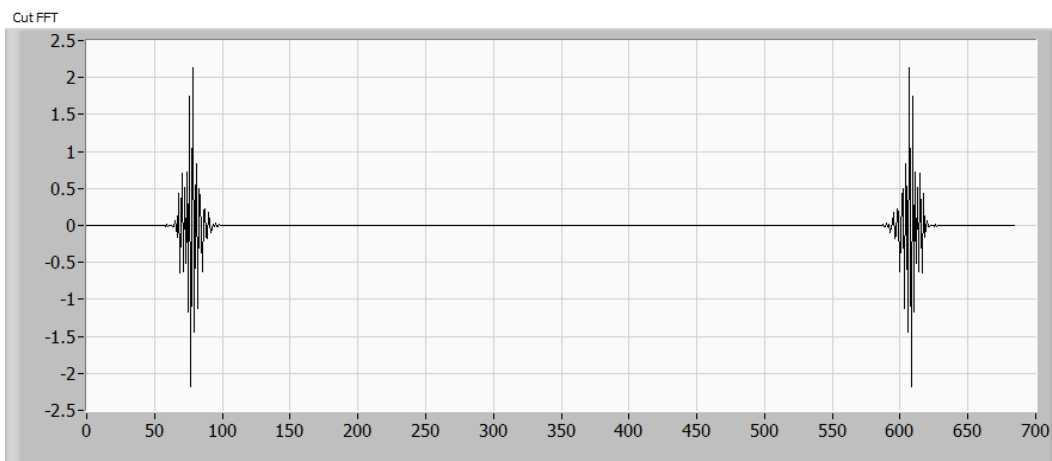


Figure 5.51 – Windowed with Hamming window

Now we move back to the time domain. Figure 5.52 shows the results of the IFFT.

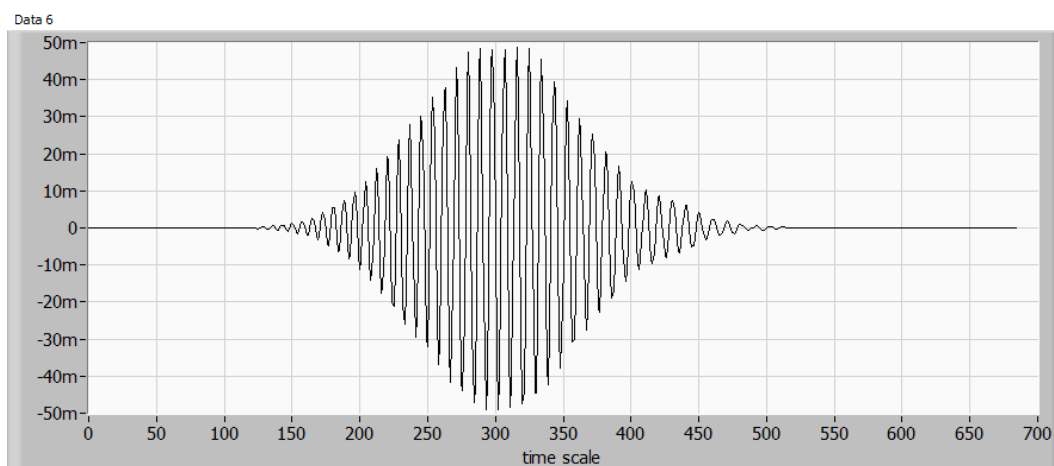


Figure 5.52 – IFFT

Figure 5.53 shows the Hilbert transform of the IFFT. The Hilbert transform will be used to obtain the instantaneous phase [Johansson (1999) e Feldman (2011) e Ahn et al. (2005) e Ahn; Kim (2007)].

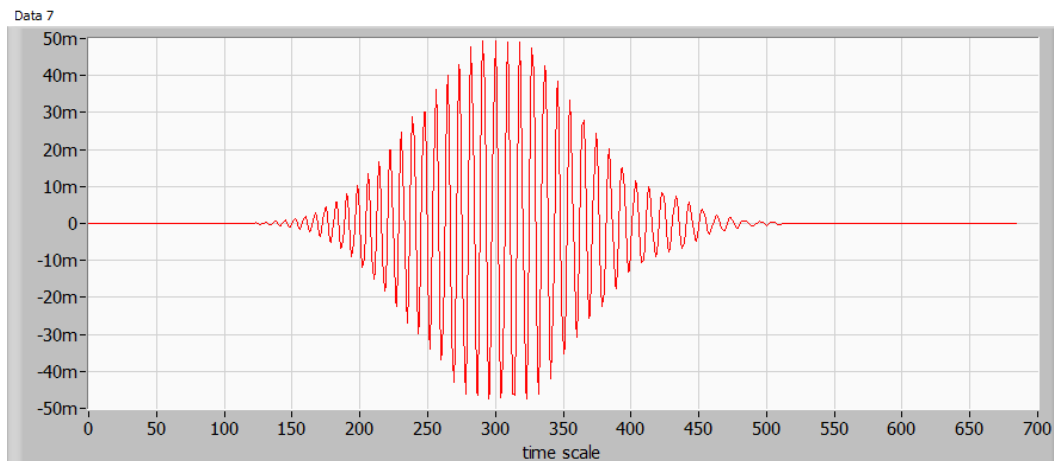


Figure 5.53 – Hilbert transform

Figure 5.54 shows a zoom of the IFFT and the Hilbert transform together in order to show the phase relationship between the two signals. The two are 90° out of phase.

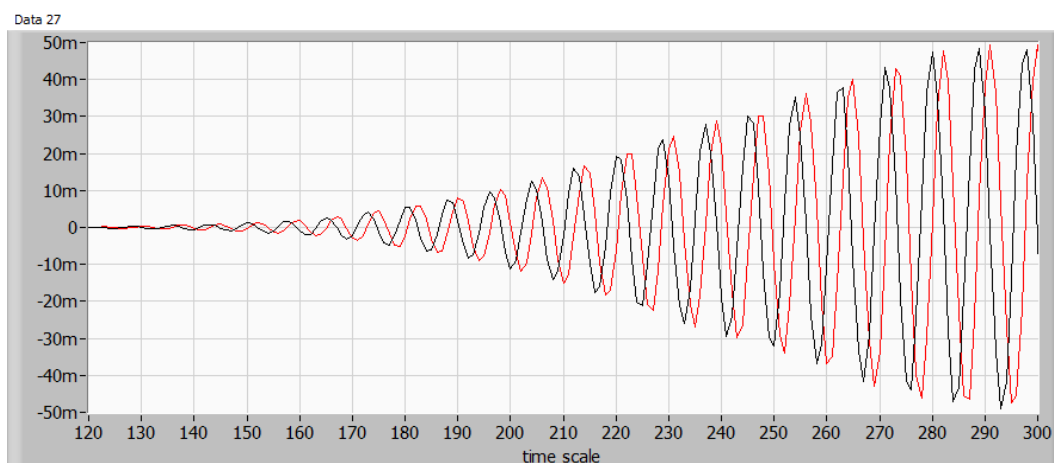


Figure 5.54 – Zoom of IFFT and Hilbert transform together

The instantaneous phase as a function of time is the arcTangent of the ratio of the Hilbert transform to the original data. The arcTangent produces values between $-\pi/2$ and $\pi/2$ as shown in Figure 5.55.

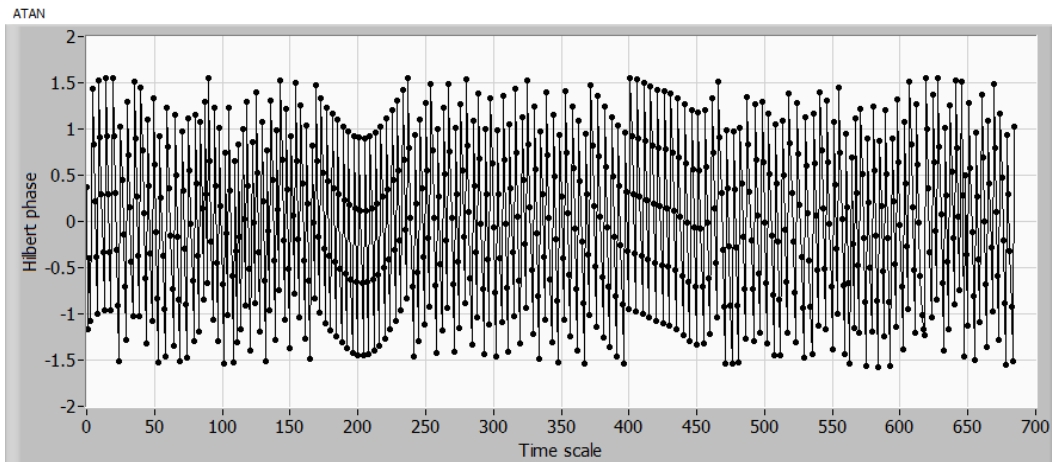


Figure 5.55 – ATAN(Hilbert / IFFT)

We unwrap the phase to get the phase to time sample mapping that we will use from here on out. As we showed in sections 4.3 and 4.4 starting on page 130 that this phase is well approximated by the optical frequency then Figure 5.56 is a mapping of the optical frequencies to the time samples and so can be used for all other reflective distances.

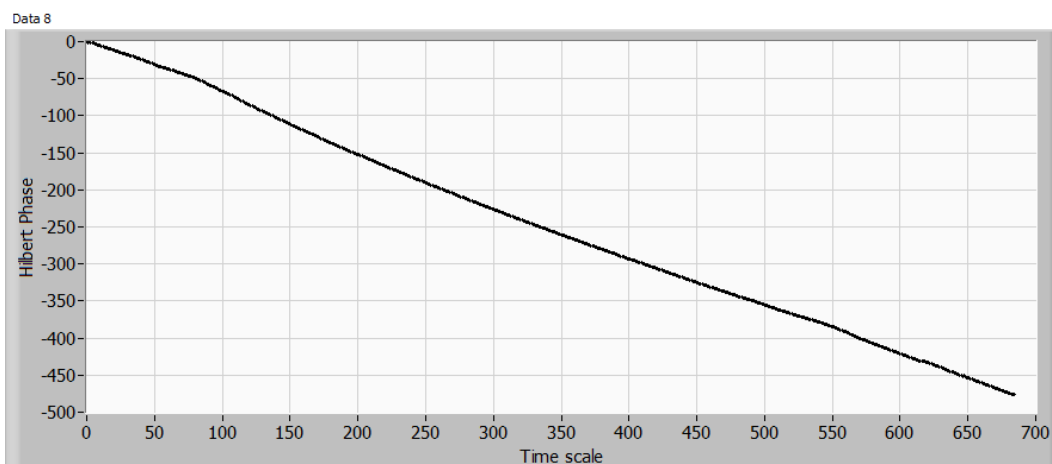


Figure 5.56 – Unwrapped phase

5.2.3.2. Applying the sweep calibration

Once again we collect the reflected and combined data from the sample and the reference. The data has to be sampled at the same sampling rate and cut at the same places as before in order for the sweep calibration to be valid.

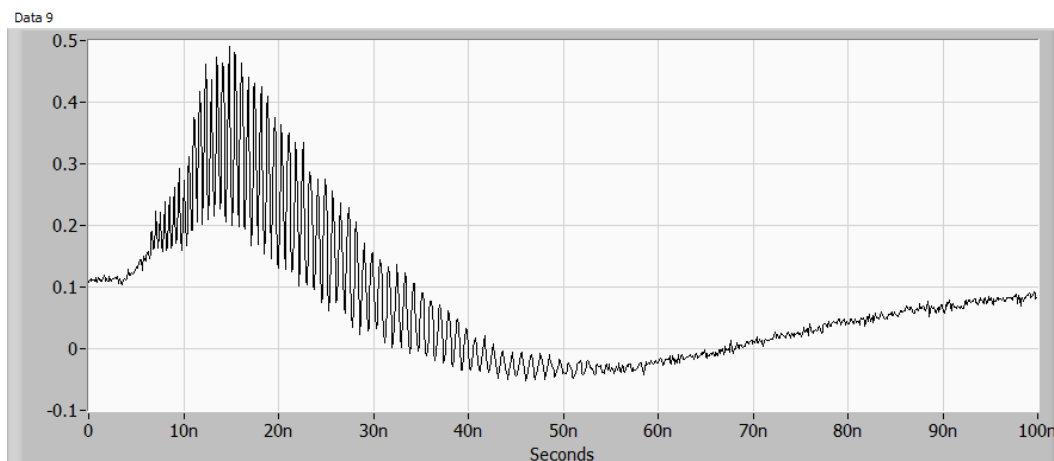


Figure 5.57 – The raw measurement data must be taken in the same way as the calibration – same triggering, same number of samples, same samplerate.

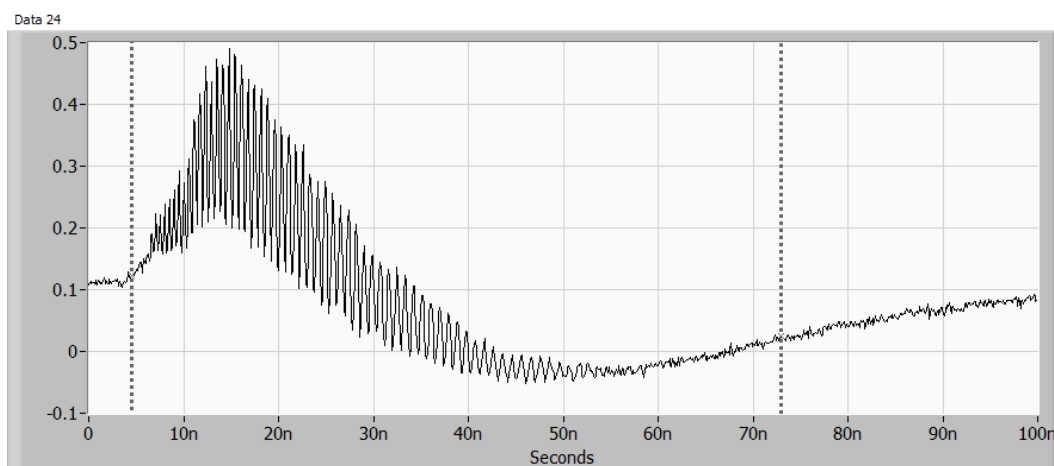


Figure 5.58 – The data must be cut in the same way as the calibration.

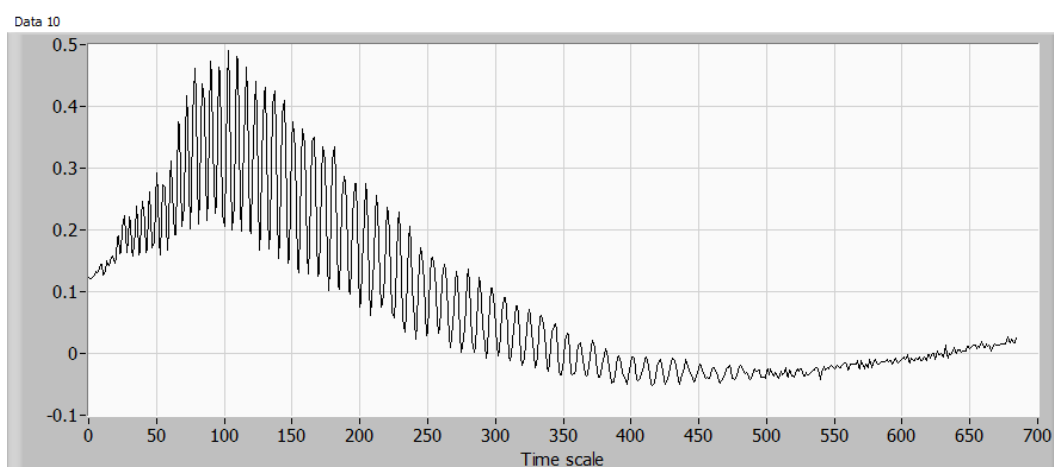


Figure 5.59 – The cut-data

Now, since we have the transformation from time scale to optical frequency scale we can apply it here. The exact value of the scale is still arbitrary since we didn't know the exact distances when we did the linearization calibration. But this isn't important since we will calibrate the distance scale in the transform domain directly. All we need at this moment is a scale which is proportional to the optical frequency, and that we have.

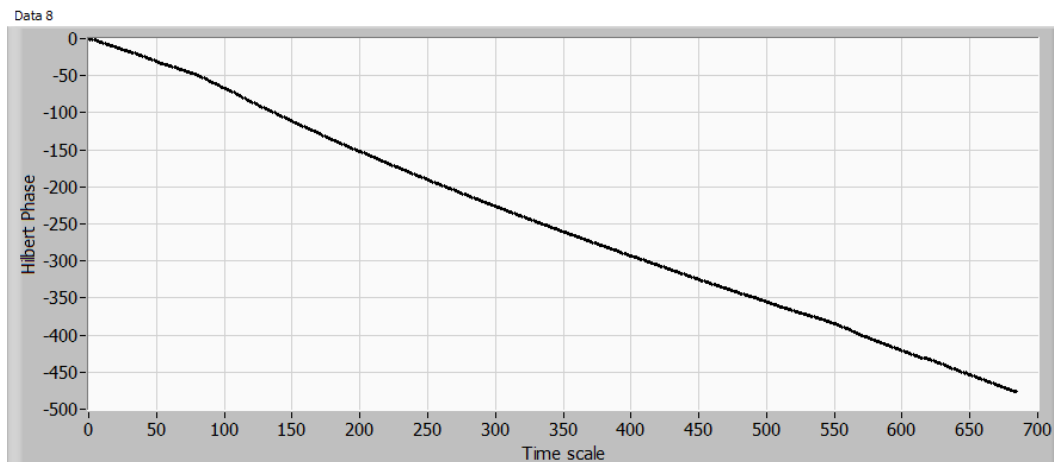


Figure 5.60 – Now we use the phase / time data we generated in the calibration phase to cast the time scale to phase (or optical frequency if you prefer).

Figure 5.61 shows Figure 5.59 after the Hilbert scale has been applied. An arbitrary optical frequency scale was applied as well to make the data appear more intuitive but it is manufactured.

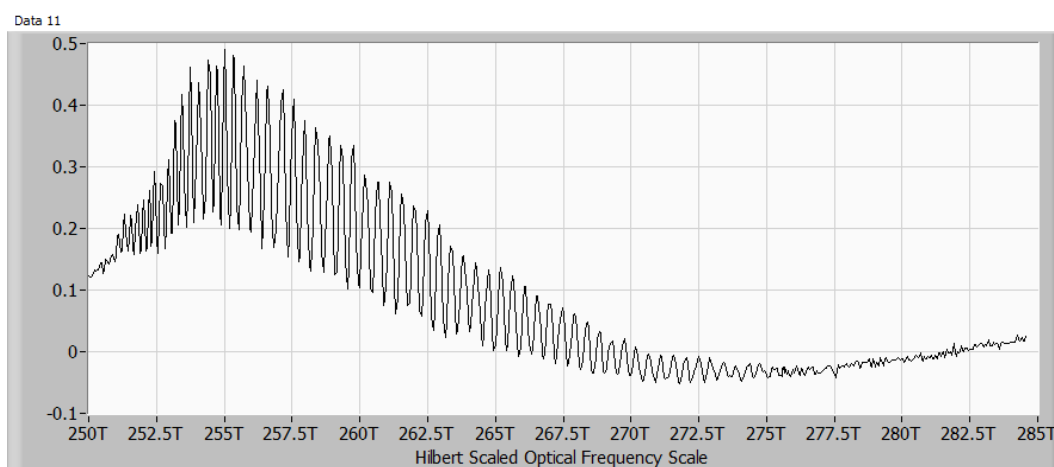


Figure 5.61 – Hilbert scale

While the scale is optical frequency, the samples are not at equal optical frequency intervals since the samples were taken at equal time intervals.

The next step then is to resample this data at equal optical frequency intervals, which is required for the FFT to the transform domain.

Figure 5.62 shows the resampled data.

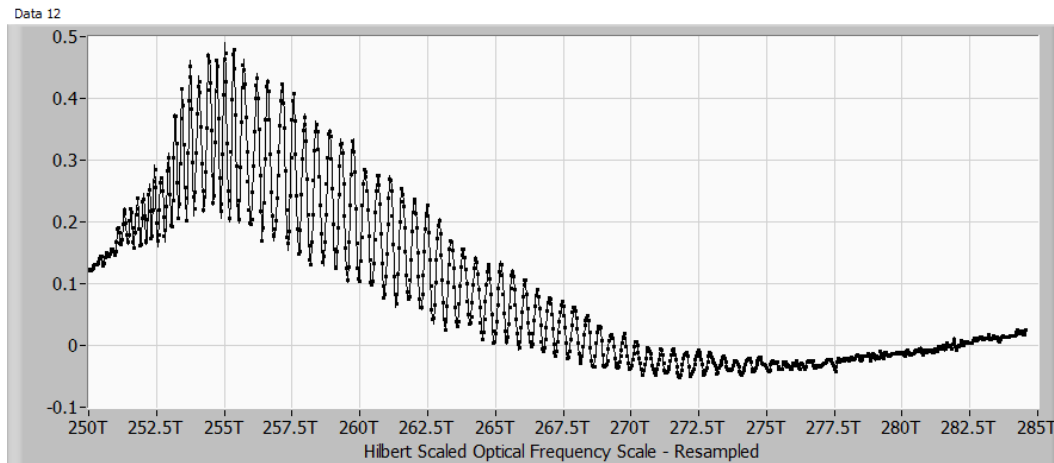


Figure 5.62 – The scale must have equally spaced samples for the FFT so we resample to a convenient number of points.

Now we can window and pad and take the FFT to the transform domain as discussed in section 3 starting on page 41. The window you use depends on the purpose of the measurement. If you have a single reflection and are interested in a narrow peak you might use a rectangular window. If you have multiple peaks you might use a Blackman-Harris in order to reduce the effects of one peak on the other at a distance. If there are multiple peaks which are close together and location of those peaks is important then you might use the rectangular window again since the effects of the initial phase will be held off longer as was seen in section 3.5 starting on page 86.

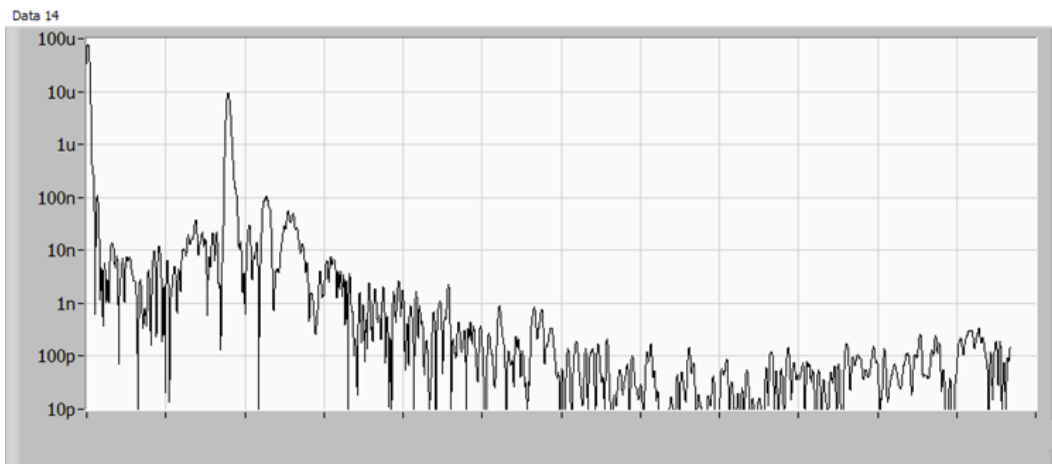


Figure 5.63 – The FFT gives us the A-line with the single peak expected. However the scale is not yet calibrated to distance.

5.2.3.3. Calibrating the distance scale

Since neither the sweep speed is constant nor the optical frequency range known and since the calibration reflection for the linearization of the frequency scale was at an arbitrary distance, the distance must be calibrated using the differential technique.

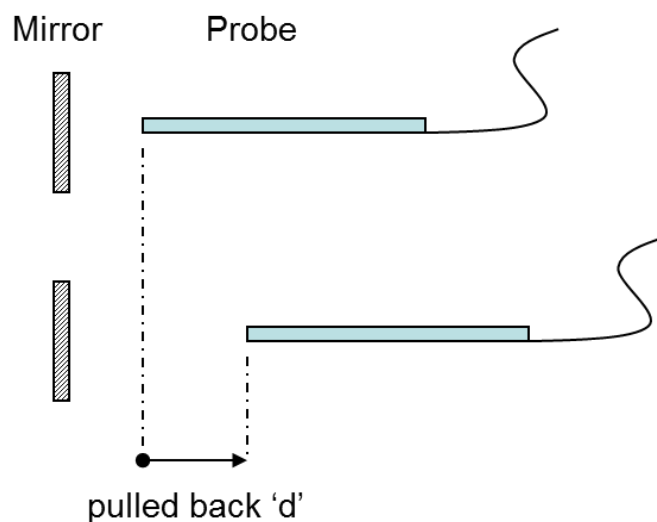


Figure 5.64 – A differential calibration will be used.

Taking linearized data at the two distances and plotting on the same graph we immediately see that the 150um of motion resulted in the peak moving 62.41 bins. The scale is then 2.34um / bin.

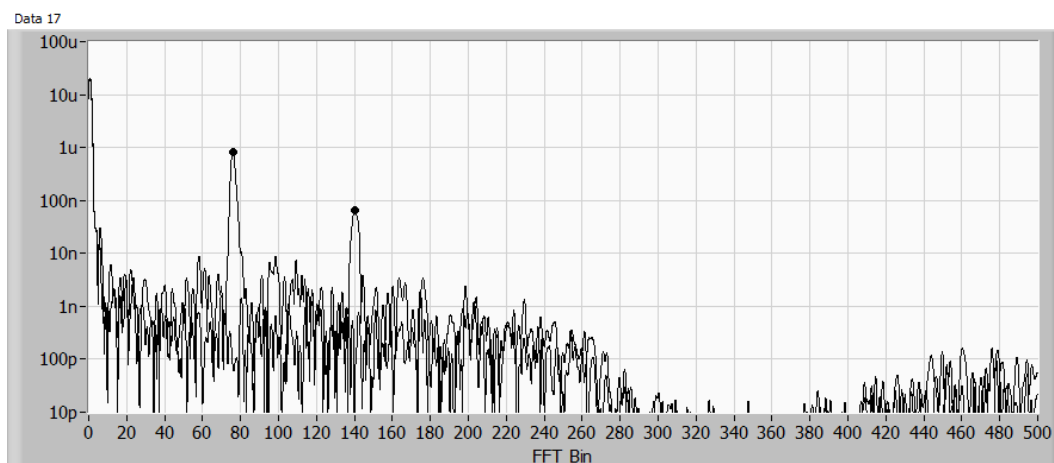


Figure 5.65 – Two measurements with a differential distance of 150 μ m. Peak detection tells us that the two peaks are separated by 64.21 bins. The scale calibration is thus 2.34 μ m/bin.

5.2.3.4. Application of distance calibration

Both the sweep calibration and the distance calibration are one time measurements in this topography as described in section 4.7.4 starting on page 155.

Figure 5.66 shows Figure 5.63 with the distance scale from Figure 5.65.

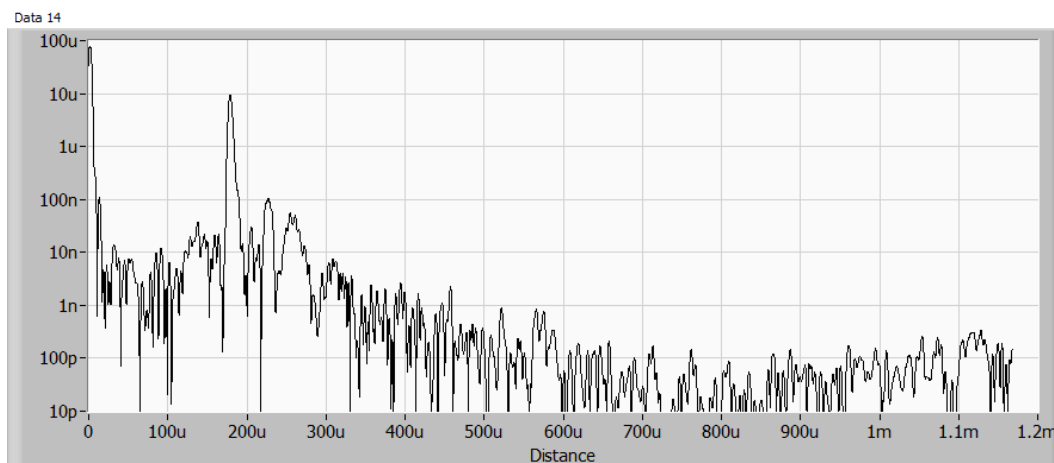


Figure 5.66 – Applying the distance scale to the previously measured data gives the final A-line. .

5.2.4. Resolution

We can evaluate the effect of the linearization and calibration by comparing the transform data with and without the linear optical frequency being applied.

The resolution of the system is considered to be the FWHM of the A-line peak from a single reflection.

To measure this we isolate the peak in Figure 5.66 as shown in Figure 5.67 and normalize to a peak value of 1 as shown in Figure 5.68.

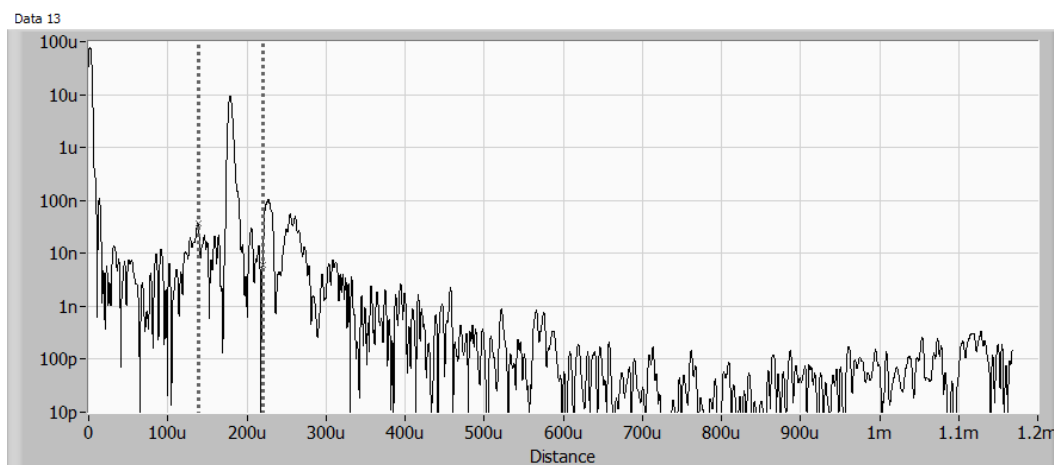


Figure 5.67 – Zoom into the peak to measure the width

The FWHM point on this normalized scale appears at the 0.5 amplitude and is 4.95 μ m in air or 3.3 μ m in glass.

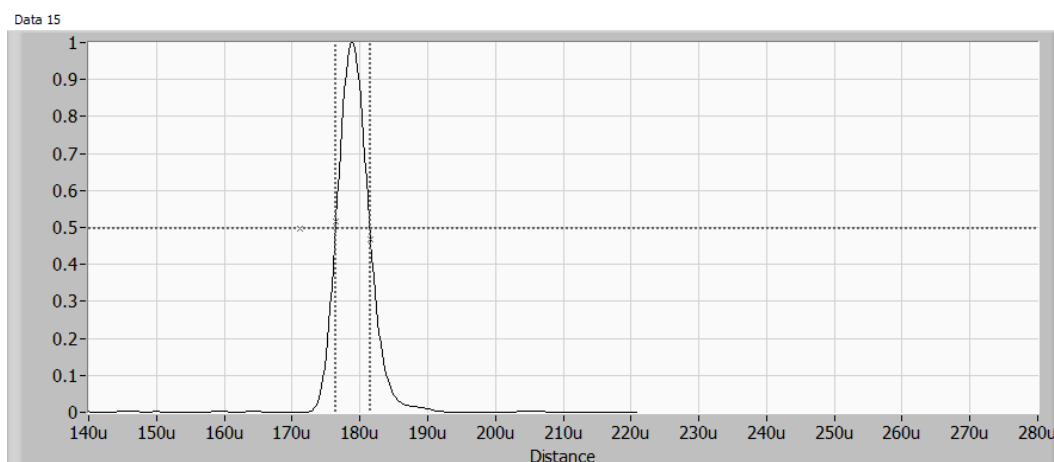


Figure 5.68 – On a linear scale the full width half max can be seen to be 4.95 μ m air (3.3 μ m glass).

Data taken from the same reflection but not linearized is shown in Figure 5.69. The data is cut as shown by the dashed lines and normalized to produce Figure 5.70.

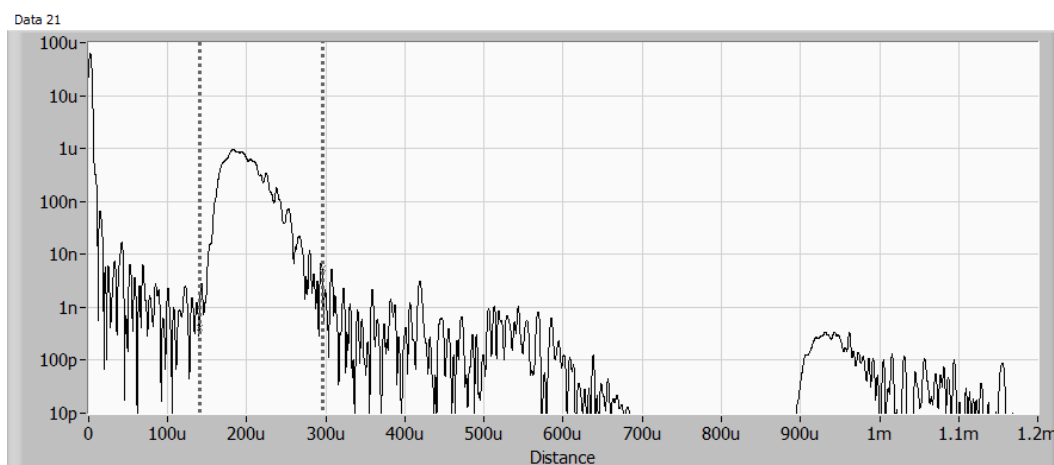


Figure 5.69 – Unlinearized peak

The FWHM of the unlinearized peak is taken at the 0.5 value in this normalized data and is 44.4 μ m in air or 29.6 μ m in glass.

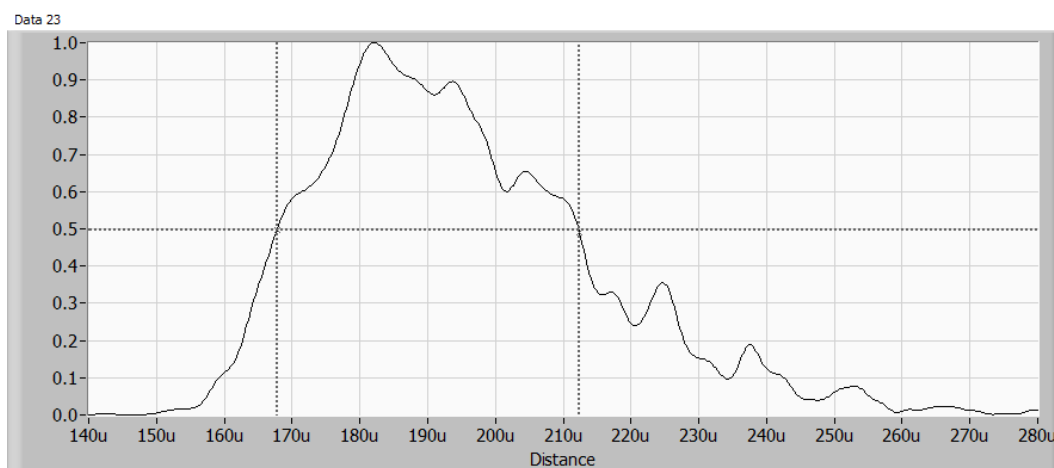


Figure 5.70 – FWHM of unlinearized peak is 44.4 μ m air (29.6 μ m glass).

Figure Figure 5.71 shows the linearized and unlinearized data together illustrating again the improvement in resolution as described in section 4.2 starting on page 50.

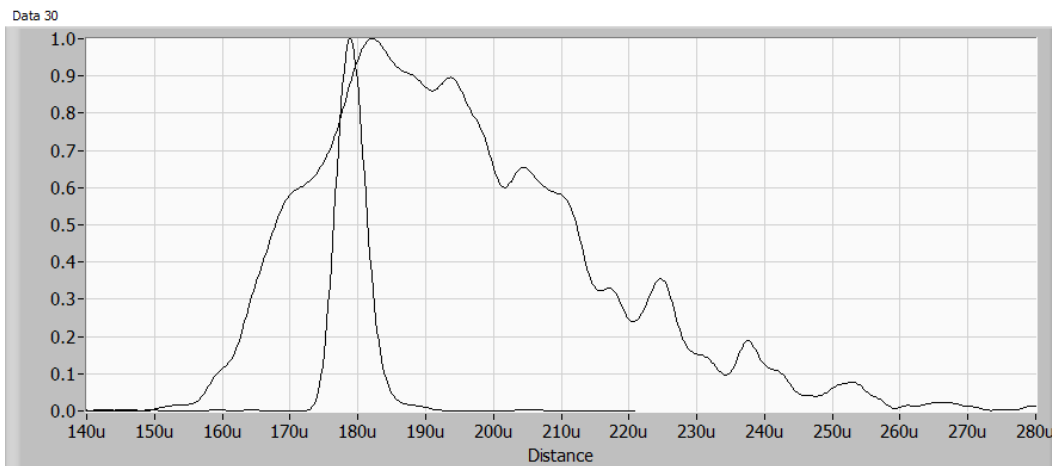


Figure 5.71 – Linearized and un-linearized data together.

5.2.5. Handywrap scans

Some measurements of handywrap were taken by both systems. Handywrap (shown in Figure 5.72) is a common household item whose thickness of 10um to 14um is a reasonable challenge for the stretched pulse system with its 5um axial resolution (Figure 5.68).



Figure 5.72 – Handywrap. 10um to 14um thick.

Figure 5.73 shows an A-line with the two peaks separated by 10um.

XY Graph

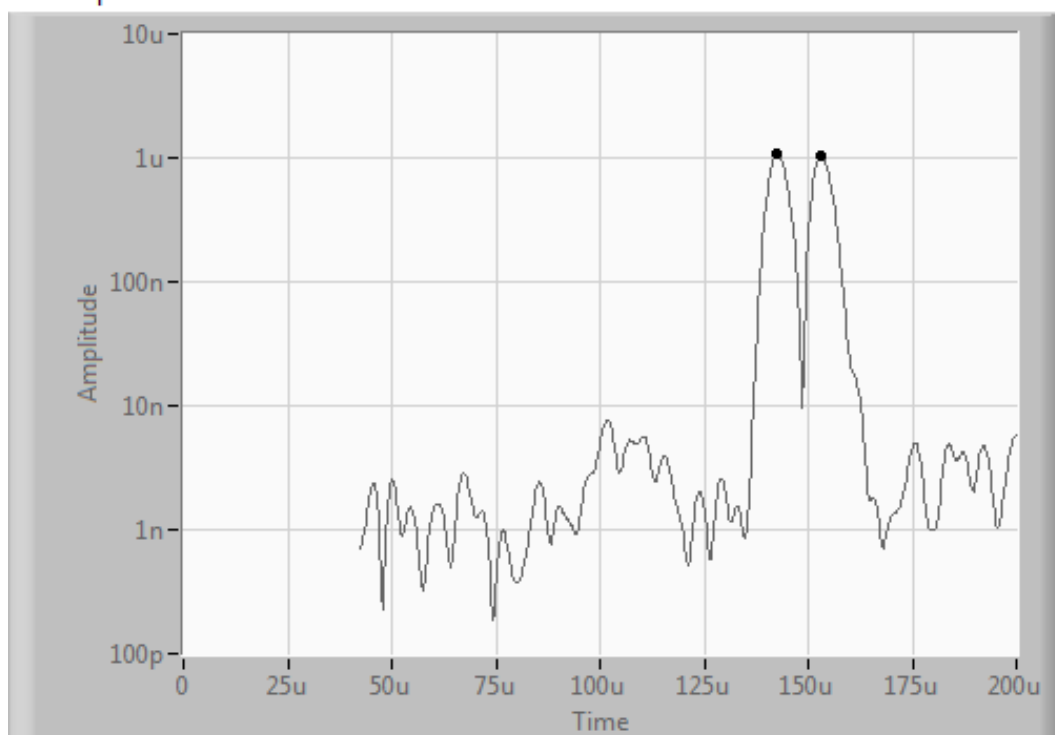


Figure 5.73 – A-line of handywrap. The two peaks are separated by 10um.

Figure 5.74 shows a 2mm B-scan of the Handywrap.

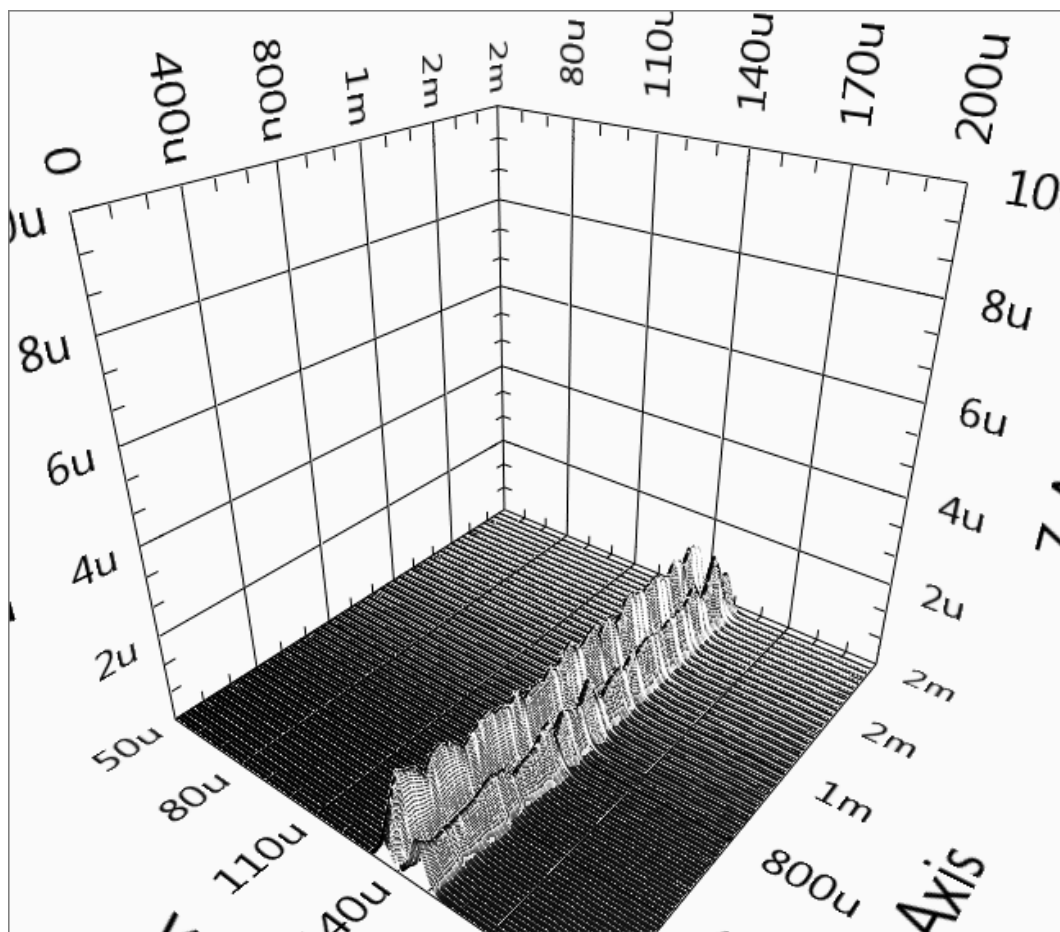


Figure 5.74 – B-scan of Handywrap. 2mm long.

Figure 5.75 shows a $2 \times 2 \text{ mm}^2$ C-scan of the handywrap.

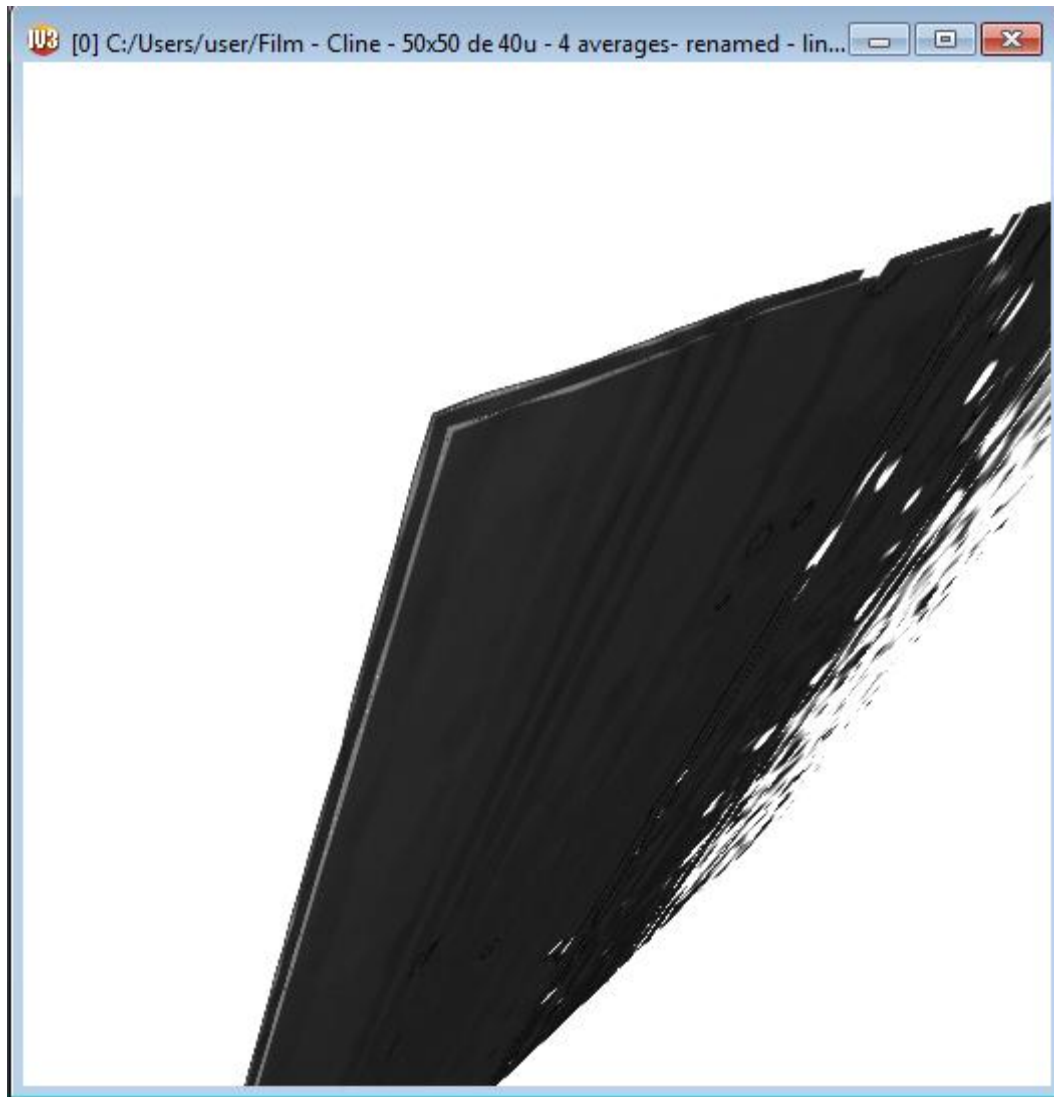


Figure 5.75 – C-scan of Handywrap. $2 \times 2 \text{ mm}^2$.

Figure 5.76 shows the locations of the peaks from a 2mm long B-scan of unstressed handywrap.

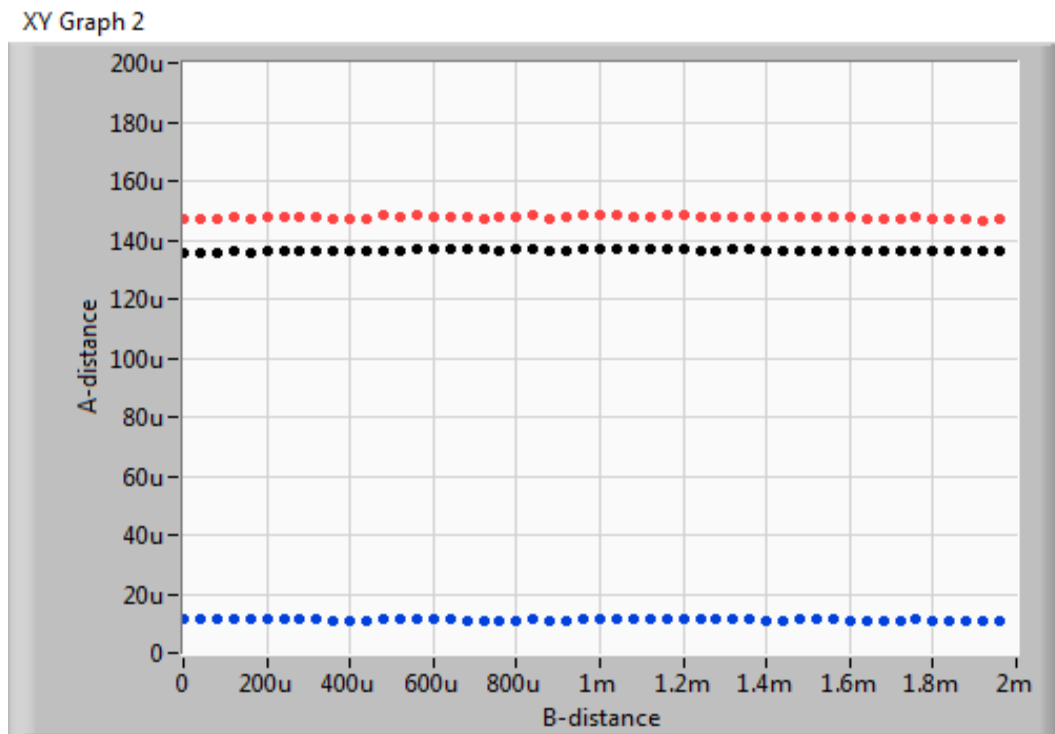


Figure 5.76 – Peaks from B-line of unstressed handywrap and delta showing thickness.

Figure 5.77 shows a 2mm long B-scan of stressed handywrap. The handywrap was stressed by puncturing the handywrap. The measurement started near the hole and moved radially away. Overall the handywrap was thinner ($<10\mu\text{m}$) and some very thin stress spots on the order of $5\mu\text{m}$ are visible.

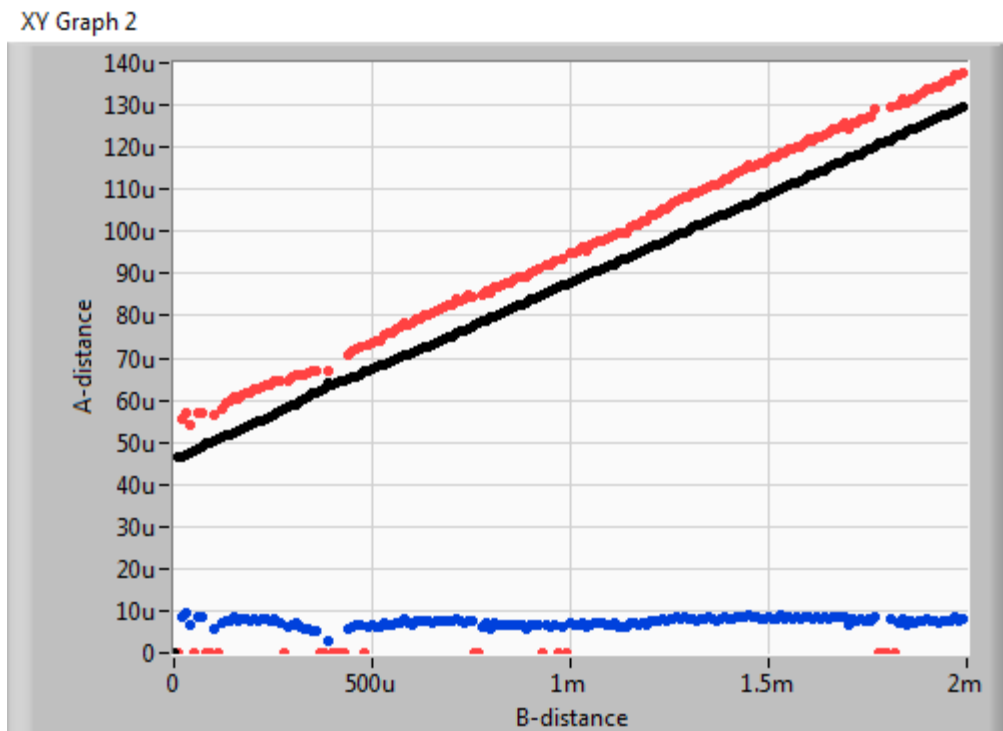


Figure 5.77 – Peaks from B-line of handywrap starting near puncture. Stress points can be seen where the two peaks combine into one.

5.3. Comparison of the two systems

The two systems were compared by measuring the same single reflector and double reflector.

The single reflector was the stage itself from an area between holes. The double reflector was a single location on a piece of handywrap.

Figure 5.78 shows the two A-lines using rectangular windows. The slight deviation in peak location is real and is related to temperature variations changing the location of the stage in relation to our measurement fiber output.

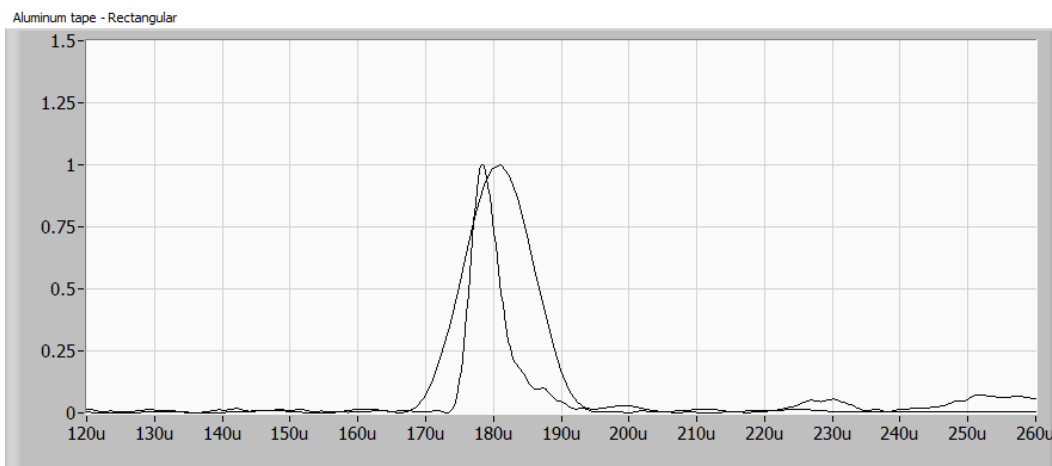


Figure 5.78 – One reflection, rectangular window.

Figure 5.79 shows the same point measured this time using a Blackman-Harris window.

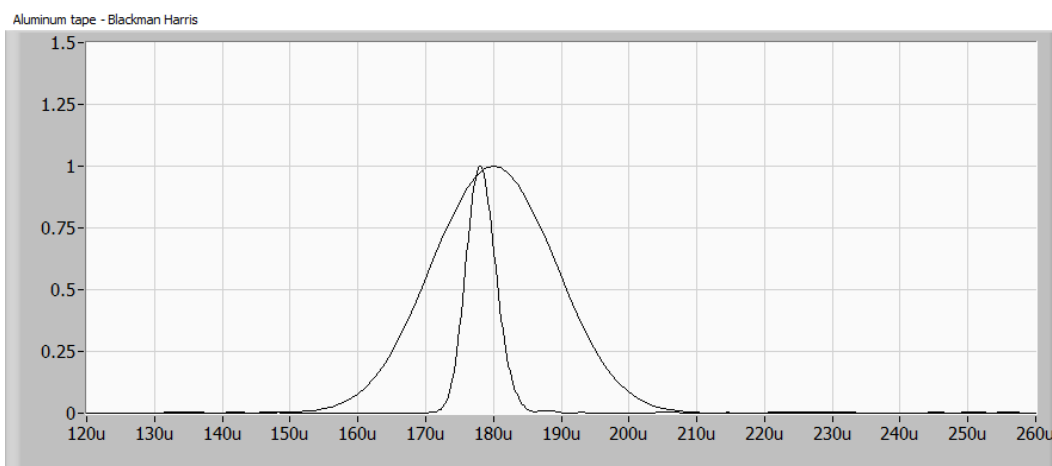


Figure 5.79 – One reflection, Blackman-Harris window.

Figure 5.80 and Figure 5.81 show measurements of handywrap using the two systems. The fact that the two measurements are slightly displaced is due to the temperature and vibration affecting the distance between the handywrap and the measurement fiber during the time it took to remove one system and prepare the other.

The fact that both systems show two peaks is interesting in that only the stretched pulse system has enough resolution to resolve the two peaks. The New Focus system sees two peaks because of the phenomenon described in detail in section 3.5 starting on page 86.

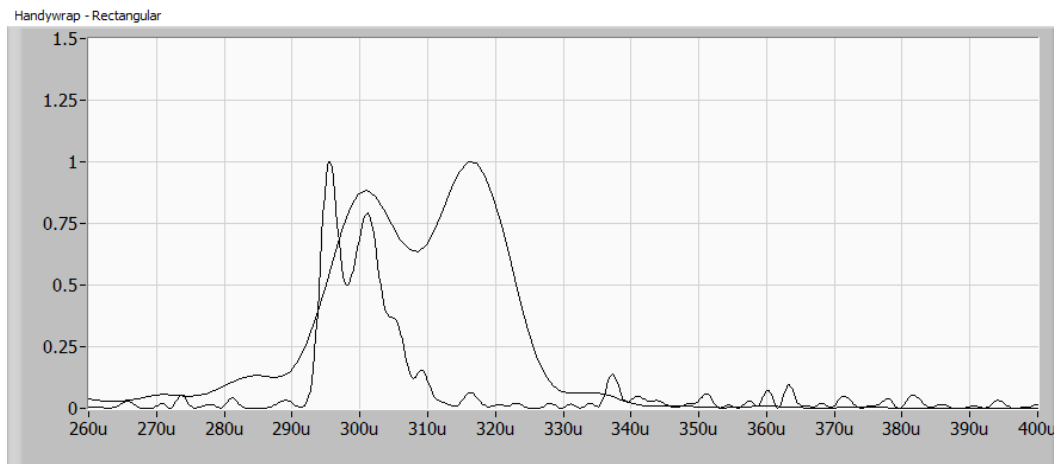


Figure 5.80 - Handywrap as seen by both systems – Rectangular windows. Again the slight difference in positions is due to temperature and vibration. The higher resolution data shows the actual separation (8um – 10um). The lower resolution data also has two peaks due to phase effects in the beat signals.

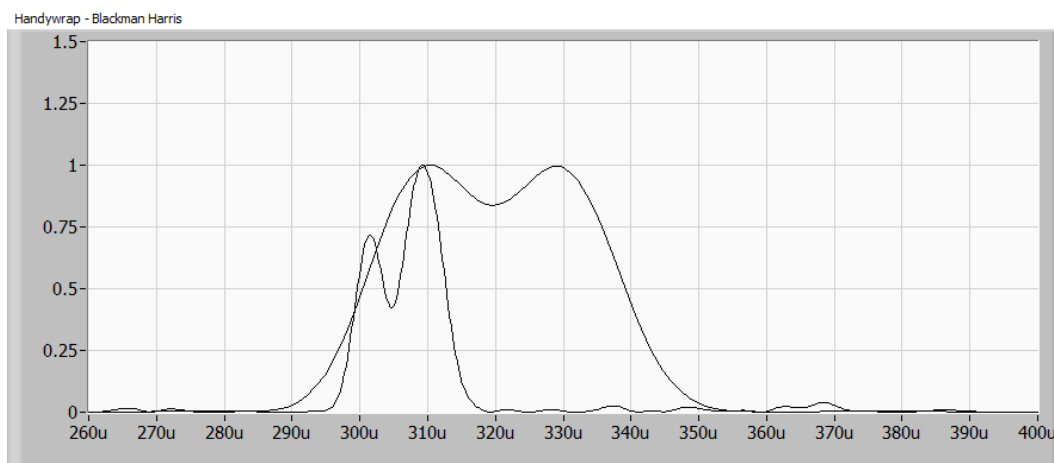


Figure 5.81 – Handywrap as seen by both systems – Blackman-Harris windows. Again the slight difference in positions is due to temperature and vibration. The higher resolution data shows the actual separation (8um – 10um). The lower resolution data also has two peaks due to phase effects in the beat signals.

6 Model

It was desired to model the OFDR Swept Source OCT system starting with the instantaneous sweep rate dv/dt .

Sweep rate was chosen as a starting point rather than optical frequency as the sweep rate is the controllable parameter of a tunable optical source and it was desirable to observe the effects of changing it as a function of time.

Optical frequency is the basic property of a laser, however, a tunable laser adds this one level above the optical frequency – direct control over the rate of change.

Given knowledge of the sweep rate $dv(t)/dt$, the optical frequency at time t can be written as the integral from $t=0$.

$$v(t) = v_0 + \int_0^t \frac{dv(t)}{dt} dt$$

This integral follows $dv(t)/dt$ in all its twists and curves in order to accumulate to the proper $v(t)$ at time t .

In a model we could limit ourselves to a $dv(t)/dt$ which can be described by a function but that is potentially limiting as it takes away the possibility of defining arbitrary functions.

Instead we have chosen to create a numerical $dv(n\Delta t)/dt$ where Δt is considered to be the model time and is kept much smaller than whatever timescale the model is asked to calculate in order that the granularity not be significant.

Rather than calculate the integral for each t starting from zero each and every time, the integral is calculated in a piecemeal fashion across each Δt and the integral accumulated.

The integral from point to point is estimated using the trapezoidal rule in Eq. 6.1 which has the nice result of providing reasonable results even across discontinuous functions.

$$\int_a^b \frac{dv(t)}{dt} dt = 1/2 \left(\frac{dv(b)}{dt} + \frac{dv(a)}{dt} \right) (b - a) \quad \text{Eq. 6.1}$$

This allows to calculate N samples of the optical frequency from 0 to N-1.

$$v(0) = v_0 \quad \text{Eq. 6.2}$$

$$v(\Delta t) = v(0) + \frac{1}{2} \left(\frac{dv(\Delta t)}{dt} + \frac{dv(0)}{dt} \right) \Delta t \quad \text{Eq. 6.3}$$

$$v(2\Delta t) = v(\Delta t) + \frac{1}{2} \left(\frac{dv(2\Delta t)}{dt} + \frac{dv(\Delta t)}{dt} \right) \Delta t \quad \text{Eq. 6.4}$$

$$v(3\Delta t) = v(2\Delta t) + \frac{1}{2} \left(\frac{dv(3\Delta t)}{dt} + \frac{dv(2\Delta t)}{dt} \right) \Delta t \quad \text{Eq. 6.5}$$

$$v(4\Delta t) = v(3\Delta t) + \frac{1}{2} \left(\frac{dv(4\Delta t)}{dt} + \frac{dv(3\Delta t)}{dt} \right) \Delta t \quad \text{Eq. 6.6}$$

$$\begin{aligned} v((N-1)\Delta t) &= v((N-2)\Delta t) \\ &+ \frac{1}{2} \left(\frac{dv((N-1)\Delta t)}{dt} \right. \\ &\left. + \frac{dv((N-2)\Delta t)}{dt} \right) \Delta t \end{aligned} \quad \text{Eq. 6.7}$$

To reiterate, Δt has been made very small in order that the trapazoidal rule estimate the integral even if the sweep rate were changing fast. In order to cover a time period T the number of points $N = T/\Delta t$ will become large. This affects how long the model takes to run and if the model crashes or not (lack of memory or just generic Labview problems with large data sets).

With $v(t)$ in hand, or more specifically $v(n \Delta t)$ $n=0..N-1$, we can calculate the instantaneous beat frequencies in an OFDR interfometer arising from the interactions of reflections from interfaces in the sample and reflections from the reference.

Each interface i in the sample will have a pathlength i which is different from that of the reference.

First the delay is calculated from the difference in path lengths, giving $2\tau_i$. Next, as time marches through $n \Delta t$, the reference optical frequency is $v(n \Delta t)$ while the delayed signal is taken as $v(n \Delta t + 2\tau_i)$ which is obtained from the model data by linear interpolation between whatever two known values happen to bracket $(n \Delta t + 2\tau_i)$. This works until the point that $(n \Delta t + 2\tau_i)$ leaves our model's time space which ends at $(N-1) \Delta t$.

With these two values in hand the instantaneous beat frequency for interface i is calculated as the difference.

$$freq_i(n \Delta t) = |v(n \Delta t) - v(n \Delta t + 2\tau_i)|$$

Eq. 6.8

$$n = 0 \text{ to } N-1$$

As we have the beat frequency for the duration of the sweep, we can accumulate the phase of the beat signal. The phase is the integral of the frequency plus initial conditions. This integral is estimated using the trapazoidal rule in the same way as before.

$$phase_i(0) = 0$$

Eq. 6.9

$$phase_i((n + 1) \Delta t)$$

$$= phase_i(n \Delta t) + \frac{1}{2} (freq_i(n \Delta t) + freq_i((n + 1) \Delta t) \Delta t)$$

Eq. 6.10

$$n = 1 \text{ to } N-1$$

Finally the amplitude of the beat signal is calculated from the phase.

$$signal_i(n \Delta t) = \cos(phase_i(n \Delta t))$$

Eq. 6.11

$$n = 0 \text{ to } N-1$$

Once we have the beat signal for each of the interfaces they are summed.

$$signal_{total}(n\Delta t) = \sum_i signal_i(n\Delta t)$$

Eq. 6.12

$n = 0$ to $N-1$

After this point all the processing follows in exactly the same way as it does for raw data from an OCT system; ie transformation of the time scale to an optical frequency scale, equal sampling in optical frequency domain, windowing, zero-padding and FFT to transform domain.

Because we have access to all the intermediate values; time, optical frequency, beat frequency, beat phase, we can observe first hand the relationships between them, including the optical frequency to beat phase relationship which is so interesting and key.

The majority of the figures in this work were created from this model in order to illustrate the details and relations between the various speeds, transforms phases and frequencies which are quite straight forward once you see them in action.

7 Conclusion

In this work we discussed swept sources for OFDR based OCT.

We discussed the terminology, the concepts and various system approaches. We then applied them to two systems, one based on a New Focus ECDL and the other on a Santec ultra-wideband laser whose sub-picosecond pulse was stretched to give us our swept source.

The operating regions for the two laser systems were very different and the the system requirements were very different too.

We modified the New Focus laser to create its own optical frequency markers, eliminating the need for external optical elements or calibrations. The frequencies generated by this swept laser were quite moderate, in the Khz region for up to 10mm of operating distance.

The stretched pulse laser resulted in a sweep whose sweep parameters were very stable but unknown. Thus we had to calibrate both the sweep linearity and the distance domain. We used our split calibration to do this, calibrating the linearity with the Hilbert transform method to a fixed reference of unknown dimensions and then calibrating the distance domain with the differential technique. The frequencies of this laser were much higher, on the order of 1Ghz per mm so the data acquisition here resembled something from a microwave lab.

7.1. Interesting things.

It was all very interesting but these are some items that may be new contributions, at least in this context.

1. We created a methodology which separates the calibration of a non-constant sweep into two pieces; first, linearization of the sweep and second

calibration of the distance domain. By treating the two steps separately the overall process can be simplified.

2. Rather than use a calibration reference of known dimensions we created a calibration method for the distance domain which is differential and does not require a known reference.
3. As our laser was so fast, we had to revisit a criterion proposed in 1993 [Glombitza; Brinkmeyer (1993)] which allowed for the mathematical substitution of optical frequency for the phase of the beat signal. We proposed a new criterion in light of our laser which no longer fell under the original criterion.
4. A derivation of the initial phase of the beat signal.
5. An improvement to the patented wavelength marker system developed by New Focus for spectroscopic applications. The improvement is to produce optical frequency markers for use in interferometric applications such as SSOCT.
6. In working to control the spectrum of the laser with respect to the zero dispersion point in the Corning DS fiber we found that using the non-linear effects (Raman) in the laser and a two stage cladding filter allowed us to build a simple low pass filter with a very sharp edge. The Raman is a double edged sword as since it is a non-linear effect, using it allowed any amplitude fluxuations in the Santec pulse to affect the spectrum.

7.2. In the future

It would be interesting to:

1. Move the OCT setup to a true optical table in a temperature controlled environment. The current location has issues both with vibration and temperature which limit the ability to do micron level measurements both in the short and long time frames.
2. The data acquisition train for the stretched pulse system needs better amplifiers and balanced detectors appropriate for the frequency region. Funny enough, the amplifiers and detectors we had to borrow were set for

too high a frequency, coming from telecommunications experiments at 40 GHz.

3. Improve the data acquisition to exploit the full 6 MHz of the laser.
4. Add new lateral motion control for faster B and C scans. The laser is fully capable of volumetric movies if the data acquisition and the motion control were up to it.
5. Improved computation. The models and the image processing and visualization were severely restricted by the computers and graphics available.
6. Other dispersive elements such as a chirped fiber Bragg grating might be available for the very broad wavelength range which would open up using even more of the spectrum and increasing the resolution. This would also increase the power available since there would be less attenuation.

8

Referências bibliográficas

AHN, T.-J.; KIM, D. Y. Analysis of nonlinear frequency sweep in high-speed tunable laser sources using a self-homodyne measurement and Hilbert transformation. **Applied Optics**, v. 46, n. 13, p. 2394-2400, 2007. Acesso em: 18/7/2012.

AHN, T.-J.; LEE, J. Y.; KIM, D. Y. Suppression of nonlinear frequency sweep in an optical frequency-domain reflectometer by use of Hilbert transformation. **Applied Optics**, v. 44, n. 35, p. 7630-7634, 2005. Acesso em: 18/7/2012.

AHN, T.-J.; PARK, Y.; KIEFFER, J.-C.; AZAÑA, J. Real-Time Optical Coherence Tomography Based on Linearly Stretched Pulse Interference. Conference on Lasers and Electro-Optics/Quantum Electronics and Laser Science Conference and Photonic Applications Systems Technologies. **Anais...**, OSA Technical Digest (CD).. p.CFM4, 2008. Optical Society of America. Disponível em:
<<http://www.opticsinfobase.org/abstract.cfm?URI=CLEO-2008-CFM4>>. Acesso em: 18/7/2012.

CHINN, S. R.; SWANSON, E. A.; FUJIMOTO, J. G. Optical coherence tomography using a frequency-tunable optical source. **Optics Letters**, v. 22, n. 5, p. 340-342, 1997. Acesso em: 23/7/2012.

CHOMA, M. A.; SARUNIC, M. V.; YANG, C.; IZATT, J. A. Sensitivity advantage of swept source and Fourier domain optical coherence tomography. **Optics Express**, 2003. Disponível em:
<<http://resolver.caltech.edu/CaltechAUTHORS:CHOoe03>>. Acesso em: 18/7/2012.

CORDES, A.H.; DE FARIA, G. V.; VON DER WEID, J. P. Fast broadband swept source for optical coherence tomography. Microwave and Optoelectronics Conference (IMOC), 2009 SBMO/IEEE MTT-S International. **Anais...** p.148 -151, 2009.

CORDES, A.H.; XAVIER, G. B.; VILELA DE FARIA, G.; VON DER WEID, J. P. High axial resolution swept source for optical coherence tomography. **Electronics Letters**, v. 46, n. 1, p. 27 -29, 2010.

DANIELSON, B. L.; WHITTENBERG, C. D. Guided-wave reflectometry with micrometer resolution. **Applied Optics**, v. 26, n. 14, p. 2836-2842, 1987. Acesso em: 23/7/2012.

EICKHOFF, W.; ULRICH, R. Optical frequency domain reflectometry in single-mode fiber. **Applied Physics Letters**, v. 39, n. 9, p. 693 -695, 1981.

FELDMAN, M. Hilbert transform in vibration analysis. **Mechanical Systems and Signal Processing**, v. 25, n. 3, p. 735-802, 2011. Acesso em: 18/7/2012.

GLOMBITZA, U.; BRINKMEYER, E. Coherent frequency-domain reflectometry for characterization of single-mode integrated-optical waveguides. **Journal of Lightwave Technology**, v. 11, n. 8, p. 1377 - 1384, 1993.

GOLUBOVIC, B.; BOUMA, B. E.; TEARNEY, G. J.; FUJIMOTO, J. G. Optical frequency-domain reflectometry using rapid wavelength tuning of a Cr4+:forsterite laser. **Optics Letters**, v. 22, n. 22, p. 1704-1706, 1997. Acesso em: 18/7/2012.

HARDING, S. P.; YALIN, Z. DIABETICS, RETINOPATHY, ISCHAEMIC MACULOPATHY, DIAGNOSIS, RETINAL IMAGE OPTIMISATION. **Research Intelligence**, v. Spring 2009, n. 37, p. 14-16, Spring. 2009. Acesso em: 20/7/2012.

HARRIS, F. J. On the use of windows for harmonic analysis with the discrete Fourier transform. **Proceedings of the IEEE**, v. 66, n. 1, p. 51 - 83, 1978.

HUANG, D.; SWANSON, E. A.; LIN, C. P. et al. Optical coherence tomography. **Science**, v. 254, n. 5035, p. 1178-1181, 1991. Acesso em: 23/7/2012.

JOHANSSON, M. **The Hilbert Transform**, 1999. Vaxjo University. Disponível em: <http://w3.msi.vxu.se/exarb/mj_ex.pdf>. .

LIU, K.; LITTMAN, M. G. Novel geometry for single-mode scanning of tunable lasers. **Optics Letters**, v. 6, n. 3, p. 117-118, 1981. Acesso em: 18/7/2012.

LIU, Y.-Y.; CHEN, M.; ISHIKAWA, H. et al. Automated macular pathology diagnosis in retinal OCT images using multi-scale spatial pyramid and local binary patterns in texture and shape encoding. **Medical Image Analysis**, v. 15, n. 5, p. 748-759, 2011. Acesso em: 20/7/2012.

MOON, S.; KIM, D. Y. Ultra-high-speed optical coherence tomography with a stretched pulse supercontinuum source. **Optics Express**, v. 14, n. 24, p. 11575-11584, 2006. Acesso em: 18/7/2012.

MOON, S.; KIM, D. Y. Normalization detection scheme for high-speed optical frequency-domain imaging and reflectometry. **Optics Express**, v. 15, n. 23, p. 15129-15146, 2007. Acesso em: 18/7/2012.

NEW FOCUS. New Focus OEM Tunable Laser Modules. Disponível em: <<http://pdf.directindustry.com/pdf/bookham/oem-tunable-laser-modules/55037-59489.html>>. Acesso em: 23/7/2012.

PARK, Y.; AHN, T.-J.; KIEFFER, J.-C.; AZAÑA, J. Optical frequency domain reflectometry based on real-time Fourier transformation. **Optics Express**, v. 15, n. 8, p. 4597-4616, 2007. Acesso em: 18/7/2012.

PASSY, R.; GISIN, N.; VON DER WEID, J. P.; GILGEN, H. H. Experimental and theoretical investigations of coherent OFDR with semiconductor laser sources. **Journal of Lightwave Technology**, v. 12, n. 9, p. 1622 -1630, 1994.

PRITCHETT, R.; WANG, W.; PIETERSE, J.-W. J.; CORDES, ANDREW H.; ABRIAM, R. O. Electronic wavelength marker system and method. ,Pending. Disponível em: <<http://www.google.com/patents?id=kf2bAAAAEBAJ>>. Acesso em: 18/7/2012.

SALEH, B. E. A.; TEICH, M. C. **Fundamentals of Photonics**. 2º ed. Wiley-Interscience, 2007.

SHANNON, C. E. Communication in the Presence of Noise. **Proceedings of the IRE**, v. 37, n. 1, p. 10 - 21, 1949.

SMITH, J. O. Mathematics of the Discrete Fourier Transform (DFT) with Audio Applications, Second Edition. Disponível em: <<https://ccrma.stanford.edu/~jos/mdft/>>. Acesso em: 23/7/2012.

TAKADA, K.; YOKOHAMA, I.; CHIDA, K.; NODA, J. New measurement system for fault location in optical waveguide devices based on an interferometric technique. **Applied Optics**, v. 26, n. 9, p. 1603-1606, 1987. Acesso em: 23/7/2012.

VON DER WEID, J. P.; PASSY, R.; MUSSI, G.; GISIN, N. On the characterization of optical fiber network components with optical frequency domain reflectometry. **Journal of Lightwave Technology**, v. 15, n. 7, p. 1131 -1141, 1997.